Dissertation

New and old entities in mitochondrial Ca^{2+} uptake

submitted by

Mag. rer. nat.
Claire Jean-Quartier
MSc

for the Academic Degree of

Doctor of Philosophy
(PhD)

at the

Medical University of Graz

Institute of Molecular Biology and Biochemistry

under the supevision of

Prof. Dr. Wolfgang F. Graier

2014

Declaration

Ich erkläre ehrenwörtlich, dass ich die vorliegende Arbeit selbstständig angefertigt und abgefasst, und jene Personen und Institutionen, die am Zustandekommen der Forschungsdaten beteiligt waren, namentlich gennant habe. Andere als die angegebene Quellen habe ich nicht verwendet und die den benutzten Quellen wörtlich oder inhaltlich entnommenen Stellen habe ich als solche kenntlich gemacht. Die Arbeit an der Dissertation und daraus entstandener Publikationen wurden gemäß den Regeln der "'Good Scientific Practice"' durchgeführt.

I hereby declare that this thesis is my own original work and that I have fully acknowledged by name all of those individuals and organizations that have contributed to the research for this thesis. Due acknowledgement has been made in the text to all other material used. Throughout this thesis and in all related publications I followed the guidelines of "Good Scientific Practice".

Graz, 25.08.2014

Claire Jean-Quartier

In thoughts of my MOM ...

Acknowledgements

First of all, I would like to thank my supervisor Wolfgang F. Graier for his guidance, patience and constant efforts for long-lasting discussions endeavoring to change my mind. All the same, I thank my thesis committee members Roland Malli, Klaus Groschner and Albin Hermetter for their excellent guidance. I also thank my project advisors Markus Deckers and Peter Rehling for their genial support upon my stay abroad.
Many thanks to the best colleagues one can wish for. Thank you for helping me with scientific discussions and technical assistance, Markus Waldeck-Weiermaier, M. Rizwan Alam, Oleksandr I. Bondarenko, M. Jadoon Khan, René Rost, Lukas Groschner, Felix Karsten, Florian Enzinger, Therese Macher, Anna Schreilechner and Sven Dennerlein. Just as well, many thanks to Corina Madreiter, Silke Grunau, Christiane Klec, David Pacheau, Marianne Fritz, Nicole Hofmann, Elisabeth Seles, Sandra Blass, Neelanjan Vishnu, Sonja Barth and Warisara Parichatikanond for mental next to scientific support and motivational encouragement throughout the years of my thesis.
I acknowledge support by the Austrian Science Funds (FWF, W1226-B18) and the Medical University of Graz, Karl Franzens University of Graz and the Graz University of Technology.

Summary

The process of mitochondrial Ca^{2+} sequestration across the inner mitochondrial membrane plays a central role in cell signal transduction and is pivotal for important cell and organelle function. The aim of this study is to identify proteins involved in this process and to assign their function. Very recently, the mitochondrial calcium uniport protein (MCU), mitochondrial Ca^{2+} uptake 1 and 2 (MICU1/2), mitochondrial Ca^{2+} uptake regulator (MCUR), essential MCU regulator (EMRE), uncoupling proteins 2 and 3 (UCP2/3) and leucine zipper EF hand-containing transmembrane protein (LETM1) have been described as contributors to the mitochondrial Ca^{2+} uptake machinery. Additionally, alternative proteins involved in mitochondrial Ca^{2+} uptake have been described including solute carrier protein SLC25A23, mitochondrial ryanodine receptors (RYR) and transient receptor canonical potential cation channels TRPC3, not exclusively targeted to mitochondria. We have confirmed previous observations that the MCU/MICU1 complex holds a primary role in mitochondrial Ca^{2+} accumulation and corroborated previous work on an engagement of UCP2/3 and Letm1 in mitochondrial Ca^{2+} sequestration. Notably, we have demonstrated that depending on SERCA activity, different mitochondrial Ca^{2+} uptake routes with molecularly distinct contributors are engaged upon IP3 mediated ER Ca^{2+} release. By applying electrophysiological measurements of the inner mitochondrial membrane at least three biophysically distinct Ca^{2+} currents could be verified, whose two essentially depend on the presence of MCU and UCP2/3, respectively. Finally, functional data highlight interdependency between these putative mitochondrial Ca^{2+} carriers and native proteomics disclose various complex formations of the individual proteins MCU, MICU1, UCP2/3 or Letm1. Our findings suggest multiple Ca^{2+} entry pathways based on a variable set of interacting proteins that result in the assembly of Ca^{2+} pores with distinct biophysical characteristics. In addition, using the example of MICOS, we demonstrate the impact of mitochondrial structure handling proteins on mitochondrial Ca^{2+} sequestration. Still, precise understanding of the mechanisms of mitochondrial Ca^{2+} uptake, molecular structure and function of mitochondrial Ca^{2+} channels is of particular importance for future therapeutic modulation of mitochondrial function a phenomenon linked to many severe human diseases.

Zusammenfassung

Die Aufnahme von Ca^{2+} durch Mitochondrien stellt einen elementaren Vorgang in der zellulären Signaltransduktion dar, der zahlreiche Funktionen der Zelle und der Organellen steuert oder beeinflusst. Diese Studie dient der Aufklärung der Identität und der Funktion von Proteinen, die diesem Prozess zugrunde liegen. In den letzten Jahren wurden verschiedene Proteine identifiziert, die am mitochondriellen Ca^{2+} Transfer beteiligt sind, dazu gehören der mitochondrielle Calcium Uniporter MCU, die Regulatoren MICU1 und MICU2 sowie MCUR und EMRE, zusÃ¤tzlich Uncoupling Proteine UCP2 und UCP3 sowie das Leucine-Zipper EF-Hand containing Transmembran-Protein (Letm1). Außerdem wurden auch andere Proteine beschrieben, welche die mitochondrielle Ca^{2+} Aufnahme beeinflussen, das Solute Carrier Protein SLC25A2 sowie der mitochondrielle Ryanodine Rezeptor (RYR) oder auch die TRPC3 Kanäle, welche nicht nur in Membranen von Mitochondrien sondern auch in der Plasmamembran zu finden sind. Wir konnten die bisherige Beobachtung bestätigen, dass ein Komplex aus MCU und MICU1 die grundlegende Rolle im mitochondriellen Ca^{2+} Transfer spielt. Weiters konnten wir die Beteiligung von UCP2/3 und Letm1 an diesem Vorgang nachweisen. Dahingehend haben wir gezeigt, dass unterschiedliche Wege des Ca^{2+} Transfer zu den Mitochondrien von der Aktivität der Sarko-/Endoplasmatischen Retikulum Calcium ATPase (SERCA) bestimmt werden. In Abhängigkeit des IP3-vermittelten Ca^{2+} Ausstroms aus dem endoplasmatischen Retikulum übernehmen die verschiedenen Komponenten ihre Rolle im mitochondriellen Ca^{2+} Einstrom. Mittels elektrophysiologischen Messungen an der inneren mitochondriellen Membran haben wir mindestens drei eigenständige Ca^{2+} Ströme nachgewiesen, wobei zwei von diesen mitochondriellen Ca^{2+} Strömen sowohl von MCU als auch UCP2/3 abhängig sind. Die Ergebnisse von funktionellen Messungen untermauern das Zusammenspiel zwischen diesen vermeintlich mitochondriellen Ca^{2+} Transportern und proteomische Analysen verweisen auf verschiedenartige Komplexe, die MCU, MICU1, UCP2/3 oder Letm1 beinhalten. Dies hat vielfache Signalwege des mitochondriellen Ca^{2+} Einstroms zur Folge, deren molekulare Bausteine sich an unterschiedliche Situationen anpassen. Des Weiteren zeigen wir am Beispiel des mitochondriellen Cristae organisierenden Systems (MICOS) die Bedeutung des strukturellen Aufbaus der Mitochondrien für den Prozess des mitochondriellen Ca^{2+} Transfers. Das Wissen über die genauen Mechanismen sowie die Struktur und die Funktion der molekularen Komponenten des mitochondriellen Ca^{2+} Aufnahme Komplexes wird zukünftige Therapien zahlreicher Krankheiten, die mit einer mitochondriellen Fehlfunktionen einhergehen, schaffen.

Contents

List of Figures

List of Tables

1. Introduction

1.1 Mitochondria

Mitochondria are complex organelles primarily known as the major site for energy production within cells. The endosymbiotic theory states mitochondria to have fused into former precessors of eukaryotes. Human cells usually contain thousands of mitochondria but the actual number varies between cell types, organs, organisms and by demand. Human blood cells are even devoid of mitochondria as they do not rely on respiration for ATP synthesis instead mainly relying on anaerobic glycolysis for energy production, whereas, muscle cells have an enormous energy demand and possess the highest number of mitochondria within the various human cell types [1, 2]. Next to the number there is the variable of size. Mitochondria are usually as small as 1 µm but vary in size, since they are under continuous movement and change in formation by means of mitochondrial plasticity.

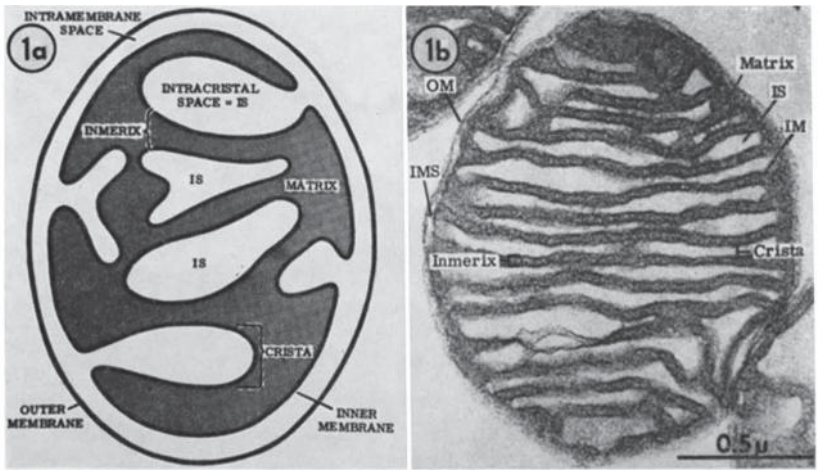

Figure 1.1: Structure of mitochondrial compartments: scheme on the left side, EM image of isolated beef heart mitochondria on the right side, taken from [3]

1.1.1 Mitochondrial structure

Mitochondria consist of two membranes and two compartments, the inter-membrane space (IMS) and the matrix. The matrix builds up the inner space of mitochondria enclosed by the two membranes. It comprises mitochondrial DNA and its translation apparatus as well as numerous proteins for metabolism including TCA cycle and fatty acid oxidation. The inter-membrane space between outer and inner membranes determines the ionic strength as basis for respiration and transport as well as signaling site for apoptosis. The outer and inner mitochondrial membrane (OMM, IMM) are structurally different as the OMM is flattened and the IMM exhibits grooves, the so-called cristae providing a large surface area through high membrane curvature. The OMM acts as barrier of the organelle as well as exchange and import site for proteins and other chemical substances. The IMM is impermeable for all solutes and requires carriers, exchangers and channels for transport across the membrane. The cristae, where ETS proteins are localized, are primary sites for energy production. Both membranes consist of lipid bilayers. Mitochondria possess a unique lipid backbone composition, which determines mitochondrial integrity but also influences protein transport across the membrane and regulates protein stability and activity [4, 5]. The lipid component cardiolipin (CL) is mainly present in mitochondrial membranes. Next to CL all common phospholipids, also found in other cellullar membranes, are present in mitochondrial lipid backbones, as most abundantly phosphatidylcholine (PC) and phosphatidylethanolamine (PE), phosphatidylinositol (PI) in moderate abundance, followed by phosphatidylserine (PS) and phosphatidic acid (PA). The lipid components PC, PS, PI are the three major lipids in mitochondrial membranes forming bilayers, while CL, PE and PA do not form bilayers and are more abundant at cristae sites as the basis for membrane curvature [6].

1.1.1.1 Mitochondrial associated ER membranes

Mitochondria respond to various signals from the cytosol but do also directly interact with the ER. For decades, groups failed to isolate intact mitochondria clean of ER-content. Microdomains of ER and mitochondria are tightly connected forming contact-sites, the so-called mitochondria associated membranes. These contact sites allow lipid exchange and are especially important for Ca^{2+} signaling involving the IP3-receptor (IP3R) for inter-organelle communication [7]. Mitochondrial distribution and morphology (Mdm) proteins as well as mitochondrial morphology maintenance

(Mmm) proteins reside either in the OMM or ER membrane as known from yeast. Together they form complexes and build up the ER-mitochondria encounter structures (ERMES).

1.1.1.2 Mitochondrial plasticity

Mitochondria are dynamic organelles, changing their form and size over time according to functional needs. They can fuse together and they can divide. Fusion and fission are processed by GTPases from the dynamin protein family. One such member the dynamin-related protein Drp1 is fundamental for OMM fission and two other known dynamin members Mitofusin 1 & 2 (Mfn) are involved in OMM fusion events [8]. Drp1 expression was pointed out to be regulated by free mitochondrial Ca^{2+} and manipulated by ruthenium red or spermine [9]. The optic atrophy / dynamin-like protein OPA1 was reported to be responsible for IMM fusion events [10, 11] and shown to affect mitochondrial Ca^{2+} handling [12] while fission 1 homolog Fis1 and mitochondrial fission factors (Mff) were shown to be involved in IMM fission [13, 14].

1.1.2 Mitochondrial function and physiology

Mitochondria are primarily known for oxidizing carbon sources in order to produce ATP, which is driven by a proton gradient across the IMM. This chemiosmotic process is based on the electron transport system involving a set of enzymes, producing energy as proton gradient effecting a pH and voltage gradient. Electrons are first transferred from reduced nicotin adenine dinucleotide (NADH) via the NADH dehydrogenase (complex I) or reduced flavin adenine dinucleotide (FADH) via succinate dehydrogenase (complex II) or through other electron transferring flavoproteins to the cytochrome c oxidoreductase (complex III) over coenzyme Q. Complex III then transfers electrons from the Q cycle further to the cytochrome c oxidase (complex IV) via cytochrome c. Complex IV oxidizes cytochrome c and produces H_2O out of molecular oxygen. The ATP synthase (complex V) utilizes the free energy produced along the complexes and pumps protons into the IMS. Then, the ATP synthase phosphorylates ADP to ATP using the released energy from protons reentering the matrix.

The net energy outcome of metabolized sugars through glycolysis, citric acid cycle (TCA) and aerobic respiration amounts to 38 ATP molecules per glucose compared to only 2 ATP molecules under anaerobic conditions where pyruvate, not entering the TCA, is broken down to lactic acid. Mitochondria also metabolize fatty acids to acetyl

CoA by β-oxidation, further processed by TCA, yielding a similar amount of ATP depending on the size of fatty acids.

Moreover, mitochondria in adipocytes are responsible for the production of heat via thermogenin (UCP1). This member of the uncoupling protein family acts as a proton carrier creating a proton leak from IMS to matrix and thereby converts the free energy to heat instead of using it for ATP production [15]. Activation of UCP1 by free fatty acids enhances respiration while uncoupling the ETS from the ATP synthase. The uncoupling proteins UCP2 and UCP3 are not involved in this process of thermogenesis [16] and their function will be discussed later. Moreover, mitochondria are a main source for the production of reactive oxygen species (ROS), important intracellular messengers as retrograde signal on mitochondrial state of activity and its components [17].

1.2 Mitochondrial Ca^{2+} transport is accomplished by a variety of proteins

Mitochondrial Ca^{2+} uptake regulates main functions of mitochondria as respiration up to apoptosis [18]. Mitochondrial Ca^{2+} homeostasis determines cell fate and has to be maintained accordingly. This basic concept involves a set of key players for ion transport as well as various kinds of regulators and additional proteins contributing to mitochondrial Ca^{2+} uptake that all lead to distinct levels of basal Ca^{2+}, capacity and speed of mitochondrial Ca^{2+} uptake. During the last few years, many proteins were identified to be involved in Ca^{2+} uptake. To begin with, our group firstly introduced uncoupling proteins UCP2 and 3 to be involved in mitochondrial accumulation of Ca^{2+} [19]. Soon afterwards, the mitochondrial Ca^{2+}/H^{+} exchanger LETM1 was introduced into this field of mitochondrial science [20] next to the mitochondrial $Na+/Ca^{2+}$ exchanger NCLX [21]. It did not last long until the next key player was found, an EF hand containing protein located to the inner mitochondrial membrane, the mitochondrial calcium uptake protein MICU1 [22]. One year later, the mitochondrial Ca^{2+} uniporter protein MCU was discovered [23]. However, this event did not stop the flood of newly discovered proteins involved in mitochondrial Ca^{2+} uptake [24, 25, 26, 27, 28, 29].

1.2.1 Core component of the mitochondrial uptake machinery in the inner mitochondrial membrane

For decades groups were searching for the assumed exclusive basic protein behind mitochondrial Ca^{2+} uptake since experiments on isolated organelles have shown mitochondria to take up large amounts of Ca^{2+} that was blocked by ruthenium red [30]. Patch-clamping of the inner mitochondrial membrane has later disclosed a Ca^{2+} selective ion channel [31]. Over the years though, people realized, that mitochondrial Ca^{2+} uptake is accomplished by multiple proteins. Recently, MCU was suggested to be the actual pore-protein [32]. Mootha group reported that only the proteins MICU1, MICU2, the negative MCU regulator MCUb and the essential mitochondrial regulator EMRE are part of the mitochondrial Ca^{2+} uniporter complex [26]. Reconstitution experiments of human MCU in yeast disclosed that MCU activity depends on EMRE, and moreover, an amoebazoa orthologue of MCU does not require EMRE for mitochondrial Ca^{2+} import [33]. However, other groups demonstrated additional interactions with this complex [28, 29, 34]. This fact supports the idea of a transient complex behind mitochondrial Ca^{2+} uptake, interacting and influencing MCU, while the underlying machinery can vary due to biochemical differences in preparation of the complex, variations throughout cells and tissues and most importantly due to different pathways in the regulation of mitochondrial Ca^{2+} uptake.

1.2.2 Proteins involved in mitochondrial Ca^{2+} uptake across the inner mitochondrial membrane

Upon MCU knockdown, mitochondrial Ca^{2+} uptake was shown to be significantly decreased but not completely diminished, and basal metabolism in MCU knock-out mice was unaffected [35], pointing to additional mitochondrial Ca^{2+} transporters. Next to individual Ca^{2+} transporting proteins, Ca^{2+} binding proteins as accessories such as sensors and regulators are imperative as it was shown for the MCU complex.
One of these accessories was recently shown to involve the Ca^{2+}/calmodulin dependent protein kinase CaMKII as regulator of MCU. MCU was demonstrated to have two phosphorylation sites for CaMKII and experiments on silencing or blocking CaMKII lead to a decrease in mitochondrial Ca^{2+} uptake as well as suppressed the formation of mitochondrial permability pore (MPTP) opening [36]. Another regulatory protein, the Ca^{2+} dependent proline-rich tyrosine kinase 2 (Pyk2), was recently pointed out to phosphorylate MCU and thereby promoting oligomerization of MCU to channel-

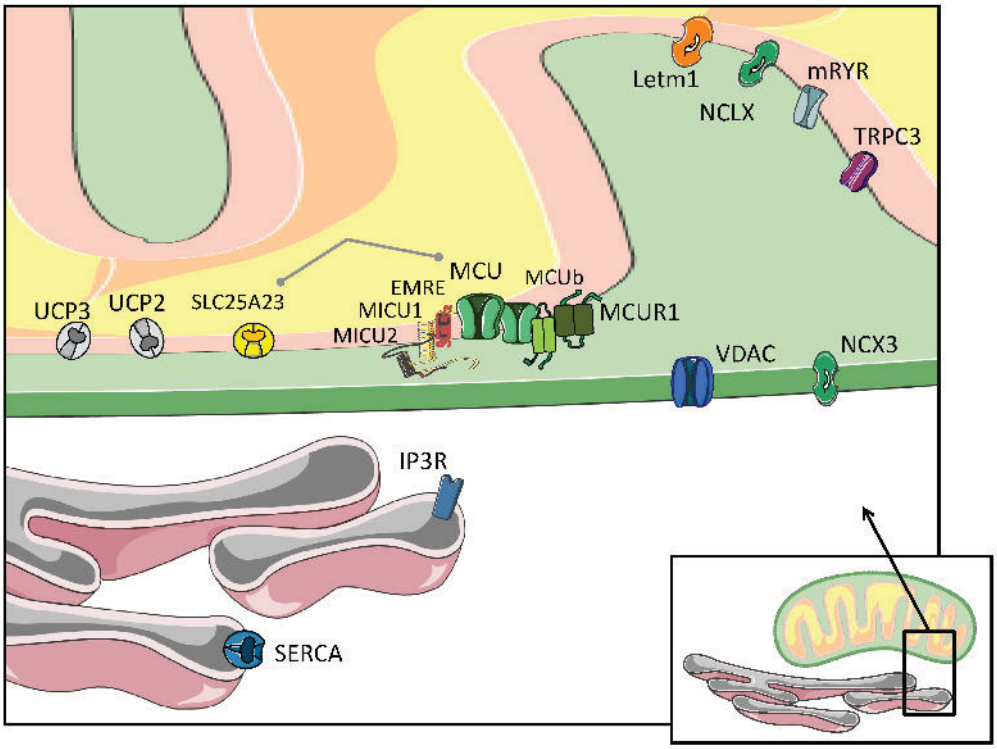

Figure 1.2: Complexes and proteins involved in mitochondrial Ca^{2+} uptake: core complex of MCU & MCUb within the IMM, EMRE1 associated with MCU in IMM, MICU1 associated to IMM with MICU2 in IMS, MCUR1 at IMM but mainly in matrix; solute carrier proteins UCP2/3 and SLC25A23 spanning through IMM with 6 transmembrane domains; Letm1 within IMM, TRPC3 in IMM next to plasma membrane, NCLX within IMM, mRYR in IMM, NCX3 and VDAC in OMM

tetramers [37].

UCP2 and 3 were demonstrated to play an important functional role in mitochondrial Ca^{2+} uptake machinery [19]. These UCPs belong to the large family of mitochondrial solute carriers of the SLC25 family exhibiting structural solute carrier features. The SLC25 family contains 46 members so far known, 5 isoforms are members of the UCP subfamily. Reconstituted UCP2 and 3 were reported to transport anions such as Cl^- and fatty acids as well as H^+ [38]. Additionally, UCP2 reconstituted in lipid vesicles, supported the exchange of malate, oxaloacetate and aspartate for PO_4^{3-} in exchange for a H^+ [39]. The protein was also suggested to be involved in ROS signaling [40]. Expression level analysis of UCP2 highlights its occurrence in undifferentiated stem cells that was lost during neuronal differentiation [41]. Polymorphisms of UCP2 and 3 were further linked to diabetes mellitus, obesity and lipid-metabolism associated disorders

[42].
The leucine zipper EF hand containing transmembrane protein (Letm1) is an integral membrane protein, located in the inner mitochondrial membrane and was first postulated to be a K^+/H^+ exchanger and was shown to be involved in Wolf-Hirschhorn syndrome [43]. Letm1 was later demonstrated to be Ca^{2+}/H^+ exchanger and characterized to be electroneutral, insensitive to MCU inhibitor ruthenium red and NCX inhibitor CGP-37157 [20, 44]. Additionally, Letm1 was reported to be involved in the biogenesis of respiration complexes I, III and IV [45].
Very recently, SLC25A23 also known as SCamC-3, another solute carrier protein, so far known to transport Mg^+-ATP/P_i, was shown to interact with MCU and MICU1 and to contribute to mitochondrial Ca^{2+} uptake. It is located in the inner mitochondrial membrane and contains EF-hand motives [29].
As the case may be, also the canonical transient receptor potential channel TRPC3, which mainly resides in the plasma membrane, was reported to be enriched in the IMM, contributing to cytosolic Ca^{2+} dependent mitochondrial Ca^{2+} uptake [27].

1.2.3 Mitochondrial Ca^{2+} transport across the outer mitochondrial membrane

The OMM was long believed to be freely permeable for small molecules as ions. It was later shown that the voltage dependent anion channel (VDAC1), also called porin, is the main transport protein in the outer mitochondrial membrane. There are additional two known isoforms in higher eukaryotes VDAC2 and VDAC3, which show both lower expression levels and are less characterized so far [46].
The anion channel VDAC1 opens at zero or low membrane potentials across the outer membrane. Upon voltages above 30-40 mV, VDAC1 changes its conformation into closed state and switches to cation selectivity, fascilitating Ca^{2+} import [47, 48]. VDAC1 was demonstrated to be further regulated by the antiapoptotic protein Bcl-xL in handling mitochondrial Ca^{2+} uptake [49].

1.2.4 Mitochondrial Ca^{2+} extrusion

Next to main routes for mitochondrial Ca^{2+} uptake, Ca^{2+} extrusion from the organelle is likewise fundamental for Ca^{2+} homeostasis. The release of Ca^{2+} from mitochondria was shown to be induced by Na^+ [52]. The underlying molecular identity of the characterized channel was solved decades later and introduced the sodium/lithium/calcium

protein	monomer/ complex (kDa)	structure	inhibitor	stimulant
MCU	40 / 450	multipass membrane, CCDC	minocycline	RuRed
MICU1	54 / 450	single pass membrane, 2 EF-hands		Ca^{2+}
MICU2	50 / 450	4 EF-hands		Ca^{2+}
MICU3	60 / $*$	single pass membrane, 3 EF-hands		
MCUR1	40 / $*$	multi-pass membrane, CCDC		
EMRE	10 / 450	single pass membrane		Ca^{2+}
MCUb	39 / 450	multi-pass membrane, CCDC		
Letm1	83 / 300, 550	single pass membrane, EF-hand		
UCP2	33 / $*$	multi-pass membrane, dimer, 3 Solcar repeats	genipin, FA	ATP, GTP
UCP3	34 / $*$	multi-pass membrane, 3 Solcar repeats	genipin, FA	ATP, GTP
TRPC3	96	multi-pass membrane, 4 ankyrin repeats	Pyr3, BTP2, voltage	voltage
SLC25A23	52 / $*$	multi-pass membrane, 3 EF-hands, 3 Solcar repeats		Mg-ATP/P_i, ROS_m
NCLX	64	multi-pass membrane	CGP-31757	Li^+
VDAC1	31 / 400	membrane spanning beta-barrel, dimer	voltage	voltage
$*$MPTP	$*$/ 400		minocycline, cyclosporin A	Ca_m^{2+}, ROS_m

Table 1.1: Proteins involved in mitochondrial Ca^{2+} transfer in non-excitable human cells [31, 50, 51, 18]; fatty acids (FA), coiled-coil domain (CCDC), ruthenium red (RuRed), alkyl-pyrazole-carboxylate (Pyr3), bis-trifluoromethyl-pyrazole (BTP2), adenosine triphosphate (ATP), guanosine triphosphate (GTP), reactive oxygen species (ROS)

exchanger NCLX (SLC24A6), a mitochondrial isoform of the Na^+/Ca^{2+} exchanger (NCX), which is located in the inner mitochondrial membrane and is inhibited by CGP-31757 [21].
The alternative isoform from the NCX superfamily, namely NCX3, was demonstrated to mediate Ca^{2+} extrusion from mitochondria within the outer mitochondrial membrane in neuronal mitochondria [53]. Furthermore, mitochondrial Ca^{2+} extrusion can occur via the MPTP. Upon induction of mitochondrial permeability transition VDAC1 forms a large transient complex with several proteins located in various mitochondrial compartments, including adenine nucleotide translocase ANT (SLC25A4) and cyclophilin D (CypD), leading to a pore, spanning through both mitochondrial membranes. MPTP formation can occur under physiological conditions [54] and pathophysiological conditions such as oxidative stress or Ca^{2+} overload. The MPTP is traversable for molecules up to a size of 1.5 kDa. Cyclophilin D facilitates Ca^{2+} transport through VDAC by desensitizing MPTP to Ca^{2+} [55].

1.2.5 Cell type specific Ca^{2+} uptake

There are various cells, distinct from each other, within one single but multi-cellular organism, though they are produced from the same DNA. Cells can express different sets of genes depending on their function and will possess distinct morphologic and phenotypic characteristics forming a cell type. During embryogenesis cell types derive from totipotent cells of germ-layers which can be summed up to three groups, the endoderm, ectoderm and mesoderm. Cells from endoderm differentiate into secretory cells. Ectoderm is basis for epithelial barrier cells and the nervous system. The large group of mesoderm derived cells includes cells for metabolism, contractility, barrier, immune system and reproduction. Various cells can not only express higher or lower amounts of proteins, they can also express different isoforms or feature different post-translational modifications that could mark the cell type specificity of certain processes within cells. Overall, mitochondrial fine-tuning of Ca^{2+} signaling is related to the regulation of cell type specific functions [56]. The distinct regulation as well as expression of the above listed proteins will be highlighted in the results section.

1.3 Structural dependence on mitochondrial Ca^{2+}

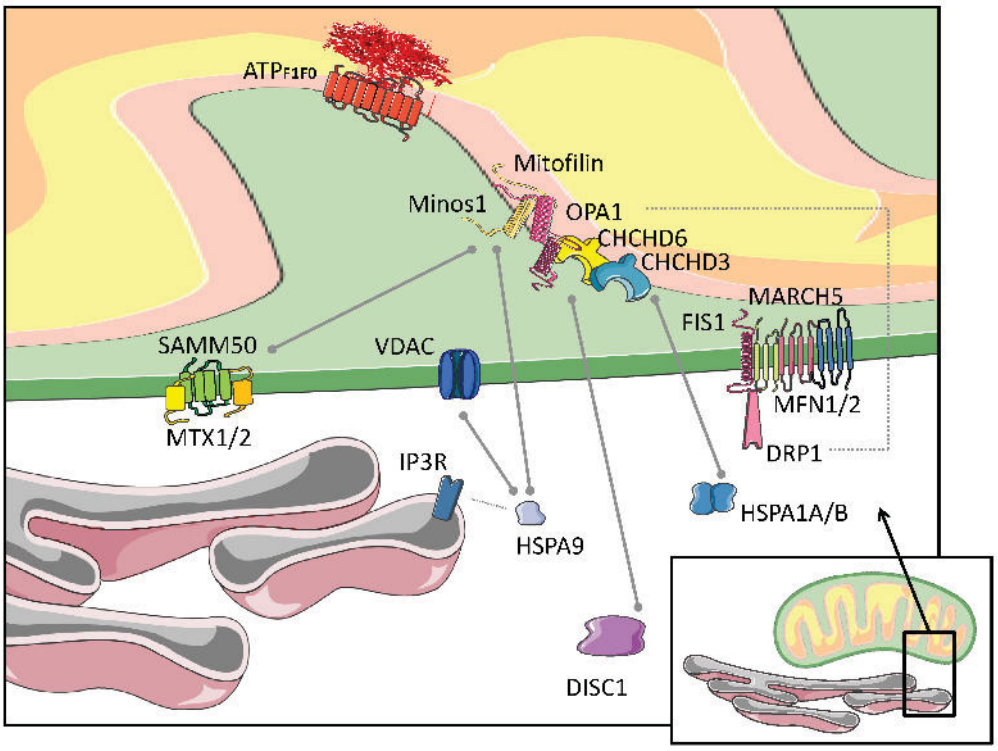

Figure 1.3: Complexes and interacting proteins in mitochondrial ultrastructure: main MICOS complex consists of Mic60 (former Mitofilin/IMMT), Mic27 (APOOL), Mic26, Mic25 (CHCHD6), Mic19 (CHCHD3), Mic12 and Mic10 (former Minos1), and OPA1 which further leads to Drp1 and Mfn1/2 interaction, amongst others, further interactions are described between MICOS with ATP synthase, HSPA9 or DISC1 [57].

Mitochondrial dynamics based on fusion and fission is connected to mitochondrial Ca^{2+} handling [9, 12, 58, 59]. Still, the question remains whether mitochondrial structure and morphology are directly regulated by mitochondrial Ca^{2+} or if structure determines mitochondrial function. To follow this lead, on the one hand, mitochondrial Ca^{2+} impacts respiration [60, 61], and on the other hand, proper inner membrane structure is linked to functional respiration [62]. To consider another view, the mitochondrial Ca^{2+} uniporter needs an intact membrane potential to be fully functional, and membrane potential is also affected by disturbed mitochondrial cristae structure.

Next to the above mentioned proteins involved in mitochondrial Ca^{2+} uptake, the inner mitochondrial membrane consists of several proteins arranging the architecture in curvature and invaginations of cristae membranes as well as interconnecting inner and

outer mitochondrial membranes. Under oxidative stress and apoptosis mitochondria can undergo remodeling and the inner membrane changes its morphology to a cubic-like form with decreased curvature and wider cristae junctions [63]. There is one large IMM complex called mitochondrial contact site and cristae organizing system (MICOS, former MINOS) fundamental for the cristae shape [64]. Furthermore, oligomerization of the ATP synthase from the respiration complex has been shown to largely contribute to the inner membrane curvature [65].
So far known, main subunits of the human complex are Mic60 (former Mitofilin/IMMT), Mic27 (APOOL), Mic26, Mic25 (CHCHD6), Mic19 (CHCHD3), Mic12 and Mic10 (former Minos1), interacting with ATP synthase and subunits of the respiratory complex, further interacting with HSPA9, DISC1, Opa1, Drp1 and mitofusins (Thapa et al., 2005; Alkhaja et al., 2012; Zerbes et al., 2012). There are also some putative interactions between MICOS and the translocase of the outer membrane (TOM) as well as the sorting and assembly machinery (SAM), that thereby interconnect the mitochondrial intermembrane space assembly machinery [66].
Notably, the dynamin-related GTPase protein Opa1, localized in the IMM and to the intermembrane space, contributes to the interconnection of inner membranes and mitochondrial fusion [67]. Recently, functional studies on Opa1 revealed its inverse impact on mitochondrial Ca^{2+} uptake by decreasing cristae permeability for Ca^{2+} ions. The impact of MICOS on mitochondrial Ca^{2+} accumulation highlights the importance of maintaining mitochondrial cristae formation and structural integrity.

1.4 Ca^{2+} signaling

There are numerous signaling pathways underlying the communication within cells based on second messenger generation in order to activate specific effectors. Ca^{2+} ions function as such internal messenger and are regulated by several kinds of proteins, such as voltage-operated and receptor-operated channels. In more detail, there are the inositol-1,4,5-triphosphate (IP3) cassette involving phospholipase C (PLC), the ADP ribosyl cyclase signaling involving cyclic-ADP and nicotinic-acid-ADP mobilization to ryanodine receptor (RYR) activation, the sphingomyelin pathway and possible cross-talk from various other signaling pathways [68]. Specific cell types feature various responses to Ca^{2+} signaling events, as e.g. endothelial cells and myocytes react with contractility, neurons produce signal transmission, immune cells are activated to immunity responses and secretory cells are rendered either active or inactive.

Ca^{2+} as signaling messenger is presented as transient signal which can be processed as brief bursts or continuous stimulation for prolonged signals which can be further compiled to periodic oscillations depending on the specific cell type. The Ca^{2+} concentration inside the cell at resting conditions adds up to 0.1 µM while outside up to 1.8 mM. No other ion has such huge variations in its concentration between inner and outer cell compartments. As for K^+ respective concentrations amount to 140 and 4 mM, 0.8 and 1.5 mM in case of Mg^{2+}, 12 and 145 mM for Na^+ as 4 and 116 mM for Cl^- (72). Thereby, small changes in subcellular Ca^{2+} presence can have dramatic effects on the cell's fate. Due to the difference in ion concentration between interior and exterior a voltage gradient of up to 70 mV is produced [69]. In case of polarized mitochondria there is a inner membrane potential of 180 mV due to a net outflow of H^+ ions along the inner membrane and additional 60 mV due to a pH gradient [70]. Mitochondria act on fine-tuning of cytosolic Ca^{2+} signaling and thereby determine all kinds of Ca^{2+} dependent processes, fundamental for the cell but also for the organelle itself. Various metabolic enzymes within mitochondria are regulated by Ca^{2+} ions, as FAD-glycerol-3-phosphate dehydrogenase, pyruvate dehydrogenase phosphatase, NAD-isocitrate dehydrogenase, oxoglutarate dehydrogenase, ATP synthase and cytochrome c oxidase [71, 72, 73].
However, Ca^{2+} signaling is not just an important mechanism in health solely, but also in disease. Ca^{2+} next to ROS signals are involved in several cell-death pathways (necrotic death as cell fate). For programmed cell death, apoptosis, ATP has to be present, otherwise a release of cytochrome C will ultimately lead to necrosis, the unregulated form of cell death. Next to apoptosis and necrosis, necroptosis comes into play as the alternative pathway of cell death dependent on extracellular Ca^{2+} influx. Ca^{2+} was also shown to trigger autophagy [74].

1.4.1 Mitochondrial Ca^{2+} signaling in cardiovascular disease

Mitochondrial Ca^{2+} handling is connected to endothelial function, whereas endothelial dysfunction implicates disturbed smooth muscle contractility, vasoconstriction, platelet adhesion and wound healing, inflammatory responses, proliferation and apoptosis, altogether phenomena linked to cardiovascular disease [75, 76].
To implicate the involvement of mitochondrial Ca^{2+} uptake in cardiovascular disease, therapeutic inhibition of MCU as well as of MPTP were suggested for treating ischaemic cell death [35]. In detail, targeting MCU alone was proposed [77] not to suffice for treatment and could even have a negative impact. The same group sug-

gested the combined targeting of MCU and MPTP as the "most effective approach to treatment" of reperfusion injury in the heart. However, MCU was reported to play an essential role in neuroprotection [78]. All the same, it was shown in hepatocytes, that during chemical hypoxia, CsA was not protective but cytoprotection occured with Ruthenium Red Ru360 and less potent but still present by minocycline and doxycycline [79]. Thereby, they assumed that the cytoprotective benefit comes from MCU inhibition and not from the inhibition of MPTP. These findings could also be translated as to cell-specific basics of mitochondrial Ca^{2+} response to hypoxia.

1.4.2 Mitochondrial Ca^{2+} signaling and cancer

Mitochondrial Ca^{2+} signaling regulates apoptotic events [80]. Oncogenes and tumor-suppressors were therefore suggested to impact mitochondrial Ca^{2+} homeostasis in order to suppress mitochondrial apoptosis [81, 82]. Ca^{2+} also plays an important role in angiogenesis and participates in the regulation of cell proliferation that are both fundamental factors in cancer [83]. Furthermore, cancerogenesis and tumor progression are influenced by small non-protein-coding RNAs (micro-RNA) that are involved in gene regulation [84]. The micro-RNAs miR25, miR92a and miR363 were demonstrated to down-regulate MCU, thereby reducing mitochondrial Ca^{2+} uptake and vulnerability to apoptosis [85], in particular, miR25 was shown to be over-expressed in several cancer cells, that highlights the important role of mitochondrial Ca^{2+} uptake in tumorigenesis. In a more detailed matter, the protein UCP2 was correlated for its expression levels with the cell's dependence on glycolytic metabolism and proliferation kinetics as UCP2 is mainly expressed in cancer cells as well as activated lymphocytes, macrophages and hematopoietic stem cells [41]. In a different study of cancer cell physiology UCP2 was correlated to adenosine monophosphate protein kinase (AMPK) activity and levels of hypoxia induced factor HIF-1, a biomarker for several cancer types [86]. for tumor therapy

1.5 Mitochondrial biosensors

Biosensors give the opportunity to detect analytes in vivo and even within biological compartments such as mitochondria. Such probes offer the opportunity to monitor various metals and ions, metabolites, ligands and enzyme activities in real-time. Next to a specific target of the sensor, there are some considerations when choosing a sen-

sor. Multiple sensors are available with different dissociation constants. Measuring e.g. Ca^{2+} outside or inside a cell or organelle requires sensor binding capacities at a completely different concentration range. Furthermore, fluorescent dyes with single emission intensity are non-ratiometric. Ratiometric sensors have to be applied for absolute quantification, which are independent on the sensor's concentration. They exhibit either two emission or excitation intensities, respectively, a spectral shift upon target binding, thereby presenting the final change in signal as ratio. Ratiometric measurement provides correction possibilities of background noise, bleaching or various fluctuations prone by the fluorimeter or microscope assembly.

1.5.1 Chemical sensors

There are numerous indicators which permeate the cell membrane and accumulate within organelles. These substances posses a fluorescent backbone, which is quenched upon either binding or non-binding to a specific target. Functional groups of acetoxymethyl or acetate esters are used for the sensor to permeate the cell as an uncharged molecule. The ester moiety is then cleaved by cellular esterases exposing cationic functional groups which cannot cross cell membranes and thereby do not leak out of the cellular compartment. Specifically, methyl and ethyl ester derivates are enriched in mitochondria upon an intact membrane potential. For indirect measurement of analytes within organelles, small molecular weight indicators can also be applied as hydrophilic salts, which cannot permeate cell membranes. Dye modifications of high molecular weight dextran conjugates, which are biologically inert and have to be inserted into a cell by electroporation or similar techniques, are also utilized for avoiding dye compartmentalization within organelles. Several compartmentalized indicators are usually washed out through loss of membrane potential. In case of immuno-fluorescence measurement thiol reactive chloromethyl moieties are used for fixation of samples, which covalently bind to cystein residues and thereby remain inside the organelle after permeabilization and aldehyde fixation treatment [87].

1.5.2 Genetically encoded sensors

Genetically encoded biosensors were engineered on the basis of the discovery on fluorescent proteins [88, 89]. One or two fluorescent proteins as reporters are bound to a sensing peptide which changes its conformation upon substrate binding. Some common examples for Ca^{2+} sensors consisting of one fluorescent protein are aequorins and

pericams [90]. Other types of biosensors are based on the principle of Förster resonance energy transfer (FRET), and possess a pair of fluorescent proteins with distinct fluorescence intensities, which change their position to each other upon binding to a target and thereby produce a ratiometric signal based on FRET [91, 92]. One or repeated targeting sequences for a specific organelle are fused to the sensor. For mitochondrial localization, the N-terminus of the sensor is equipped with various peptides commonly targeting the protein to subunits of the cytochrome C oxidase, pyruvate dehydrogenase, ATP synthase for matrix localization or glycerol phosphate dehydrogenase and mitochondrial import receptor TOM for IMS or OMM localization. Figure 1.4 lists some mitochondrial biosensors used for various target metabolites and ions.

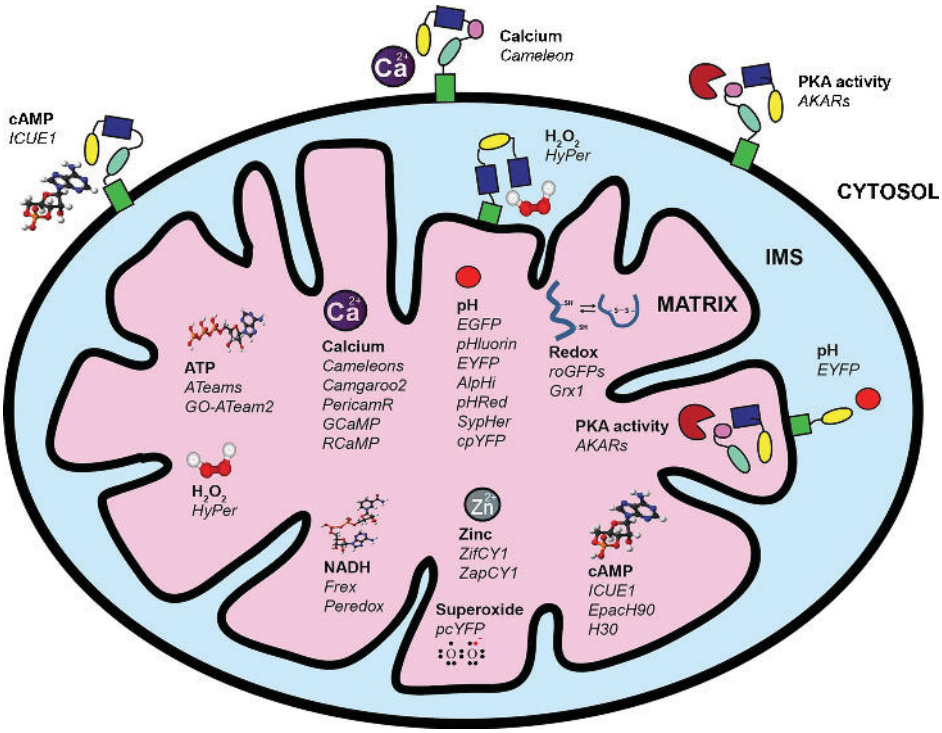

Figure 1.4: Genetically encoded biosensors targeted to mitochondria, scheme taken from [93]

1.5.3 Studying mitochondrial Ca^{2+} uptake

Due to complexity and number of proteins involved in mitochondrial Ca^{2+} uptake, it is crucial to include multiple views on the assessment of mitochondrial Ca^{2+} sequestration involving inter-organelle as well as stand-alone uptake modes [94, 95, 96]. There

are several direct and indirect approaches to measuring mitochondrial Ca^{2+} uptake including chemical substances and genetically encoded proteins targeted to organelles. These biosensors can be accumulated inside an organelle, peripherally to membranes, accumulated within the cytosol or rest in the cell surroundings. Next to biosensors, a completely different approach of assessing mitochondrial Ca^{2+} uptake can be accomplished by the patch clamping technique used on the isolated organelle, by means of measuring ion flux and channel conductance on single mitoplast level, which will be highlighted later.

In general, there are two main modes of Ca^{2+} uptake by mitochondria, IP3R mediated Ca^{2+} release from internal stores and a direct uptake from elevated cytosolic Ca^{2+} levels. First mode of uptake resembles the cellular response to various signals, therefore, it is crucial to be implemented into the various protocols of assessing mitochondrial Ca^{2+} uptake in single cells.

2. Materials and Methods

Chemicals in general were purchased from Roth (Lactan, Graz, Austria) and Sigma (Sigma Aldrich, Vienna, Austria) as well as PAA (PAA Laboratories, Pasching, Austria). Plastic-ware, if not otherwise indicated, were obtained from Corning (Szabo-Scandic, Vienna, Austria), Greiner (Greiner Bio-One GmbH, Kremsmünster, Austria), Sarstedt (Sarstedt GmbH, Winer Neudorf), Eppendorf (Eppendorf, Vienna, Austria) and VWR (VWR International, Vienna, Austria).

2.1 Cell culture

All cell-lines were grown in humidified environment enriched with 5% CO2 at 37°C. The human umbilical vein endothelial cell-line EA.hy926 [97] was grown on Dulbecco's modified eagle's medium (DMEM) supplemented with 10% fetal calf serum (FCS), 1% HAT (5 mM hypoxanthin, 20 µM aminopterin, 0.8 mM thymidine), 50 U/ml penicillin and 50 µg/ml streptomycin. HeLa S3 [98, 99] and HEK-293 [100] cells were grown on DMEM containing 10% FCS, 50 U/ml penicillin, and 50 U/ml streptomycin. HeLa control cells, HeLa MCU knockdown cells have been produced upon request and supplied by TeBu-bio (Tebu-bio SAS, Le Perray-en-Yvelines Cedex, France). HeLa cells with stable MCU knockdown and the respective scrambled control cells were produced by applying the SilenciX technology (Tebu-bio). HEK-293 cells stably overexpressing MIC10-Flag and UCP2-Flag were produced by using pcDNA5.1 and POG44 recombinase and selectively cultivated in 2 µM hygromycin (Sigma) containing medium over 3 weeks. The neuroblastoma cell-line SHSY5Y [101] was grown on DMEM/HAMS 1 : 1, supplemented with 50 µg/ml penicillin and 50 U/ml streptomcycin. The pancreatic beta cell-line INS-1 832/13 [102] was grown on RPMI medium containing 10 mM HEPES, 10 mM glucose, 2 mM glutamine, 10% FCS, 1 mM sodium pyruvate, 50 mM beta-mercaptoethanol, 50 U/ml penicillin and 100 µg/ml streptomycin.

target mRNA	sequences	
shMCU	GGTGCAATTTATCTTTATA	
scrambled	AGGUAGUGUAAUCGCCUUG	
siLetm1	UCCACAUUUGAGACUCAGU	AUGUUCCAUUUGGCUGCUG
siMICU1	GCAAUGGCGAACUGAGCAAUA	GCAGCUCAAGAAGCACUUCAA
siUCP2	UUGUAGGCAUUGACGGUGC	
siUCP3	GGAACUUUGCCCAACAUCA	
siMCU	GGAAAGGGAGCUUAUUGAA	GCCAGAGACAGACAAUACU
siMICU1	GCAGCUCAAGAAGCACUUCAA	UAUUGCUCAGUUCGCCAUUGC
siMIC10	GGAGGUGGUCUUAAAUAAA	
siSTIM1	GGCUCUGGAUACAGUGCUC	
siORAI1	GUUAUCAGUCUGAGCCAGG	

Table 2.1: siRNA sequences targeted against various mRNAs

2.1.1 Cell transfection

For transient overexpression of biosensors and/or knockdown, cells were grown to 60% confluency. Plasmids for 4mtD3CPV, 4mtPericam and siRNAs (Microsynth, Balgach, Switzerland), see table 2.1, were added to DMEM medium without serum, without antibiotics and antifungals, and mixed with the transfection reagent TransFast (Promega, Mannheim, Germany). Each 200 pmol/ml siRNA, 1.5 µg/ml plasmid DNA and 8 µl/ml TransFast were used. In case of overexpressing two different plasmids, DNA ratio was adjusted to 1 µg biosensor DNA and 3 µg of the target protein coding plasmid DNA. The transfection mix was mixed and incubated for 15 min to ensure complete formation of liposomes and then put on top of cells. After 1 h incubation time the transfection mix was diluted by adding the same volume of medium without supplements. For knockdown experiments, cells were incubated in the transfection mix over-night and afterward replaced with full medium. In case of overexpression, the transfection mix was removed after 4 h and replaced with full medium suited for the given cell-line.

2.1.2 Quantitative PCR

Knock-down efficiency of functional siRNAs was validated individually and in combination by real-time quantitative-PCR in comparison to scrambled siRNA as control as described previously [103]. RNA was isolated 48 h after cell transfection by peqGOLD Total RNA Kit S-Line (Peqlab, Erlangen, Germany). Corresponding cDNA was pro-

duced by reverse transcription of the isolated RNA using Applied Biosystems High Capacity cDNA Reverse Transcription Kit (Life technologies, Vienna, Austria). RTq-PCR was performed using GoTaq qPCR Master Mix (Promega, Mannheim, Germany) on the LightCycler 480 system (Roche, Basel, Switzerland).

2.2 Isolation of mitochondria

Mitochondria were freshly isolated from HeLa, HEK, EA.hy926 and INS-1 cells by differential centrifugation, based on the protocol of Frezza et al. [104]. Cells were harvested and washed with PBS. The cell pellet was suspended in 200 mM sucrose buffer containing 10 mM Tris-MOPS, 1 mM EGTA and protease inhibitor cocktail 1 : 50 (Sigma P8340) and the pH was adjusted to 7.4 using Tris. Cells were homogenized with a glass-teflon potter using 50 to 100 strokes. Nuclear remnants and cell debris were pelleted at 700 g for 10 min. The supernatant was centrifuged at 3000 g for 20 min giving a mitochondrial pellet with little ER contamination. Alternatively, for higher quantity of isolated mitochondria but lower quality, the mitochondrial fraction was pelleted at 10000 g resulting in a large enclosed content of other organelles within the fraction. The mitochondrial pellet was washed and centrifuged down at 10000 g for 15 min. All fractions were kept on ice until further utilization.

2.2.1 Preparation of mitoplasts

Mitoplasts were prepared from freshly isolated mitochondria, as previously described [96]. Mitoplast formation was achieved by incubation of isolated mitochondria in hypotonic solution (5 mM HEPES, 5 mM sucrose, 1 mM EGTA, pH adjusted to 7.4 with KOH) for 8 min. Thereafter, hypertonic solution (750 mM KCl, 80 mM HEPES, 1 mM EGTA, pH adjusted to 7.4 with KOH) was added to restore isotonicity.

2.2.2 Mitochondrial protein isolation

For native analysis, isolated mitochondria were solubilized in 1% digitonin, 2 mM Tris/HCl pH 7.4, 0.1 mM EDTA , 50 mM NaCl, 10% glycerol and 1 mM protease inhibitor. Protein content was determined by using the Bradford [105] reagent from Biorad protein assay (Biorad Laboratories GmbH, Vienna, Austria) or BCA [106] protein assay (Thermo Fisher Scientific Inc., Vienna, Austria). For sample lysis, the protocol is described in section 2.3.

2.2.3 Mitochondrial complex activity assays

Isolated mitochondria were dissolved in solubilization buffer, containing 1% digitonin, 0.1 M NaCl, 10 % glycerol, 1 mM EDTA, 2 mM PMSF, 20 mM Tris, pH7.4, and separated by blue native electrophoresis [107]. Gel slides were preincubated in the according buffer based on the in-gel activity staining protocol [108]. For complex I activity, gel slides were incubated in 5 mM Tris, pH 7.4 and substrates 0.5 mg/ml nitro blue tetrazolium chloride blue and 0.1 mg/ml NADH were added. Complex IV activity was determined in 50 mM KP_i, pH 7.2, containing 0.1 mg/ml diaminobenzidine and 0.16 mg/ml heart cytochrome c. Substrate incubation lasted for 2.5 h until complete staining.

2.3 Proteomics

Mitochondrial fractions were analyzed via size exclusion chromatography on an Amersham Frac-900 (GE Healthcare, Freiburg, Germany), equipped with a Superose 6 10/300 GL and an AKTA purifier, using System Control 1 software. Alternative size-dependent processing of mitochondrial fractions was carried out on a gradient mixing on a Gradient station ip BioComp (Science Services GmbH, Munich, Germany) follwed by ultra-centrifugation on a Optima L-90 (Beckman Coulter, Krefeld, Germany). Samples were post-processed by Western Blot [109] as described beneath.

2.3.1 Immunoprecipitation and pull-down experiments

Mitochondrial fractions were analyzed for interaction partners using anti-FLAG agarose (Sigma). 1 ml columns for immunoprecipitation were washed with 0.1 M KP_i and 50 µl Flag agarose was added, washed with KP_i once and twice with washing buffer (composition as solubilization buffer but 0.3% instead of 1% digitonin) [110], one time using solubilization buffer (composition see subsection 2.2.3 and collected by centrifugation at 100 g for 30 sec. Freshly isolated mitochondria from FLAG-tagged and WT cells were solubilized for 1 h at $4°C$ and cleaned from debris at 14000 rpm for 15 min. Solubilized mitochondria with 700 µg protein content were loaded onto prepared flag-agarose columns, closed and incubated overnight on a shaker wheel. Columns were centrifuged at 100 g for 1 min and the flow-throughs were collected separately. The immunoprecipitates in the columns were then washed 10 times using washing buffer and consecutively dried at 200 g for 2 min. Finally, the immunoprecipitate was eluted

by adding 100 µl 1:20 flag peptide in washing buffer, incubation for 30 min on a shaker, followed by centrifugation at 200 g. The elution step was repeated for left-over protein using 25 µl washing buffer. Protein lysates, eluates and flowthroughs were precipitated overnight.

2.3.2 Gel electrophoresis and Western Blot

Harvested cells or cellular fractions were lysed in RIPA buffer, containing 1% NP-40, 150 mM NaCl, 1 mM EDTA and 50 mM Tris, pH 7.4, and protease inhibitor. Protein content was precipitated in 14.4% TCA at $-20°C$ over-night. Precipitates were pelleted at $4°C$ at 160000 g, washed in aceton and dried at $37°C$ for 10 min. Either cell lysates or cell fractions from mitochondrial isolations were dissolved in solubilization buffer, see subsection 2.2.3 for native analysis or Laemmli sample buffer, which was diluted from the 5x concentrate containing 10% SDS, 20% glycerol, 0.2 M Tris-HCl, pH 6.8 and 10 mM dithiothreitol or beta-mercaptoethanol. 20 -60 µg of protein were loaded onto the gel and separated by SDS or Blue Native Page. The gel content was transferred to a PVDF or nitrocellulose membrane. The membrane was blocked in TBST with $5-10\%$ milk for 2 h and incubated with the primary antibody at $4°C$ overnight. The primary antigen-antibody complex was detected by incubating the blot with a horseradish peroxidase-conjugated secondary antibody at room temperature for 2 h. Membranes were developed with the ECL Plus Western blotting detection system (GE Healthcare, Vienna, Austria) or Immobilon Western Chemiluminescent HRP Substrate (Merck Millipore, Darmstadt, Germany). To control the equal amount of protein loading of whole cell lysates and isolated mitochondria, protein expression levels were densitometrically normalized to either MCU expression (sc-246071, Santa Cruz, Vienna, Austria), VDAC1 and VDAC2 (sc-32063 and sc- 32059) or beta-actin (sc-47778), respectively. Additional antibodies used against UCP2 (sc-6525), UCP3 (sc-7756), Letm1 (sc-271234), MICU1 (sc-160210), Orai1 (sc-68895). Antibodies against Taco1[110], Mitrac12[111], Tom70 and Mic10 (4853 and 4835) were provided by M. Deckers and P. Rehling, Department of Cellular Biochemistry, University Medical Center Göttingen, Germany).

2.3.3 Mass Spectrometry

Eluted proteins were separated on 14% SDS-Page gels and stained with colloidal coomassie blue and silver-nitrate. Each gel lane was cut into equal gel slices and di-

gested with trypsin (Promega), as described by Shevchenko et al. [112]. Peptides from each gel slice were analyzed by nano-flow high performance liquid chromatography Agilent 1100 (Agilent Technologies, Böblingen, Germany) coupled to a nano-electrospray LtQ-Orbitrap XL mass spectrometer (Thermo Fisher) as previously described [110].

2.4 Patch Clamp Recordings

Single channel measurements were performed in mitoplast-attached configuration by O. Bondarenko (Institute of Molecular Biology and Biochemistry, Medical University Graz, Austria) [113].

Patch pipettes were pulled from glass capillaries using a Narishige puller (Narishige Co. Ltd., Tokyo, Japan), fire-polished at a resistence of 8-12 MΩ. Mitoplasts were bathed in a cytosol-similar solution containing 145 M KCl, 1 M EGTA, 1 M HEPES, pH adjusted to 7.2 with KOH. For single channel recordings, the pipette solution contained 105 mM $CaCl_2$ and 10 mM HEPES, 10 µM cyclosporin A (Tocris Bioscience, Bristol, UK) and 10 µM 7-chloro-5-(2-chlorophenyl)-1,5-dihydro-4,1-benzothiazepin-2(3H)-one (CGP 37157, Ascent Scientific Ltd., Bristol, UK) to prevent opening of the permeability transition pore, and the activity of the mitochondrial Na^+/Ca^{2+} exchanger, respectively. pH was adjusted to 7.2 with $Ca(OH)_2$. Single channel currents were recorded at a fixed holding potential indicated in the respective figures. For whole-mitoplast recordings, pipette solution contained 120 mM cesium methanesulfonate, 30 mM CsCl, 1 mM EGTA, 110 mM sucrose, 2 mM gluconic acid, pH adjusted to 7.2 by tetraethylammonium hydroxide. For obtaining whole-mitoplast configuration, voltage steps of 300-600 mV and 20 to 50 ms duration were applied. Voltage ramps of 1 s duration from -160 to $+50mV$ were delivered every 5 to 10 s from the holding potential of 0 mV. Currents were recorded using a patch-clamp amplifier (EPC7, List Electronics, Darmstadt, Germany). Data collection was performed using Clampex software of pClamp V9.0 (Molecular Devices, Sunnyvale, CA, USA). Signals obtained were low pass filtered at 1 kHz using an eight-pole Bessel filter (Frequency Devices) and digitized with a sample rate of 10 kHz using a Digidata 1200A A/D converter (Molecular Devices, Sunnyvale, CA, USA). All measurements were performed at room temperature. For recording cationic currents via whole mitoplasts, bath solution containing 150 mM TRIS-HCl, 1 mM EGTA, 1 mM EDTA, 10 mM HEPES, pH 7.2. For I_{Na} recording, NaCl was substituted for TRIS-HCl. Ca^{2+}-containing bath solution for I_{Ca} recording containing 140 mM TRIS-HCl, 3 mM $CaCl_2$, 10 mM HEPES, pH 7.2.

2.5 Fluorometry in suspension

Chemical sensors were obtained from Molecular Probes (Molecular Probes Europe, Leiden, Netherlands), except for FURA-2/AM (TEFLabs, Austin, TX, USA). Intracellular assay buffer contained 125 mM KCl, 2 mM KH_2PO_4, 1 mM $MgCl_2$, 20 mM HEPES, 10 µM EGTA, 5 mM succinate, malate and glutamate, pH adjusted to 7.4 with KOH. Assay buffer for intact cells contained 135 mM NaCl, 5 mM KCl, 1 mM EGTA, 1 mM $MgCl_2$, 10 mM Hepes and 10 mM glucose, pH adjusted to 7.4 with NaOH. Measurement was performed at room temperature under stirring at 700 rpm.

2.5.1 Indirect mitochondrial Ca^{2+} measurement

Indirect measurement of free mitochondrial Ca^{2+} uptake was performed with Calcium-Green 5N or FURA-5K as previously described [96]. Either isolated mitochondria or harvested cells were washed with EGTA containing buffer. Cells were resuspended in assay buffer to a dilution of $10^6 cells/\ ml$ and digitonin was freshly added to 0.01%. Isolated mitochondria were resuspended in assay buffer with a protein content of 2 mg/ml. Calcium Green 5N dye was added to a final concentration of 2 µM and FURA-5K to 1 µM. Samples were excited at 506 nm or 430 and 480 nm and fluorescence collected at 532 nm or 510 nm on a Hitachi 4500 spectrofluorimeter (Metrohm Inula GmbH, Vienna, Austria), for Calcium Green or FURA measurement respectively.

2.5.2 Direct Ca^{2+} measurements in suspension

Intact cells were used for determination of cytosolic Ca^{2+} levels with FURA-AM and mitochondrial Ca^{2+} levels with RHOD-AM. Isolated mitochondria or permeabilized cells were loaded with either 3.3 µM FURA-2/AM or 5 µM Rhod-2/AM for 30 min at room temperature. For FURA measurement, samples were excited at 340 and 380 nm and fluorescence collected at 510 nm. The protocol for RHOD included an excitation at 550 nm and emission at 590 nm.

2.6 Microscopy of single cells

Loading buffer for intact cells on coverslips contained 135 mM NaCl, 5 mM KCl, 2 mM $CaCl_2$, 1 mM $MgCl_2$, 10 mM Hepes, 2.6 mM $NaHCO_3$, 0.44 mM KH_2PO_4, 0.34 mM Na_2HPO_4, 10 mM glucose, 0.1% vitamins, 0.2% essential amino acids and 1% peni-

cillin/streptomycin, pH adjusted to 7.4 with NaOH. Ca^{2+} containing assay buffer for intact cells contained 135 mM NaCl, 5 mM KCl, 2 mM $CaCl_2$, 1 mM $MgCl_2$, 10 mM Hepes and 10 mM glucose, pH adjusted to 7.4 with NaOH. Ca^{2+}-free assay buffer for intact cells contained 135 mM NaCl, 5 mM KCl, 1 mM EGTA, 1 mM $MgCl_2$, 10 mM Hepes and 10 mM glucose, pH adjusted to 7.4 with NaOH. Single-cell measurement of permeabilized cells were performed in intracellular assay buffer containing 120 mM KCl, 0.5 mM KH_2PO_4, 1 mM $MgCl_2$, 20 mM HEPES, 30 µM EGTA and 5 mM succinate and 10 mM glucose, pH adjusted to 7.4 with KOH.
For measurement, cells were mounted into an experimental chamber and perfused with the according assay solution at a flowrate of 1 ml/min. Fluorescence measurements were performed on two systems. The main system, the inverted microscope Zeiss Axiovert 200M (Zeiss Microsystems, Jena, Germany), was equipped with a 40x objective (Zeiss Microsystems), a Visichrome High Speed polychromator (Visitron Systems, Puchheim, Germany), a Photometrics Coolsnap HQ CCD camera (Photometrics, Tucson, AZ, USA) and a Ludl MAC 6000 filter wheel (Ludl Electronic Products, Hawthorne, NY, USA). Data was recorded using the software VisiView 2.0.6 (Universal Imaging, Visitron Systems). The second system, a Nikon Eclipse TE300 (Nikon corporation, Japan) was equipped with a Plan Fluor 40 x oil objective (Nikon), the polychromator lamp Opti Quip 770 (former OptiQuip, USA), an optical beam splitter Dual View Micro-imager (Optical Insights, Visitron Systems) and a liquid-cooled CCD camera Photometrics Quantix KAF (Roper Scientific, Tucson, AZ, USA). Data acquisition was done using the MetaFluor 4.0 (Molecular Devices, Sunnyvale, CA, USA).

2.6.1 Measurement of cytosolic Ca^{2+} with FURA2-AM

Cells were loaded with 3.3 µM Fura-2/AM for 45 min before mounting into perfusion chambers for experiments in loading buffer. Fura-2 was excited alternatively at 340 nm and 380 nm, using filters 340HT15, 380HT15 (Omega Optical, Brattleborough, VT, USA), and emitted light was collected at 510 nm, using 510WB40 filter (Omega Optical). $[Ca^{2+}]_{cyto}$ was expressed as F_{340}/F_{380} as mean fluorescence collected from 30 to 90 single cell measurements, performed at room temperature.

Sensor	Final c. (µM)	Kd (µM)	Excitation (nm)	Emission (nm)
Calcium Green 5N	2 (DMSO)	14	506 ± 10	532 ± 10
Fura-5K	1 (DMSO)	0.2	340/380 ± 5	510 ± 20
Fura-2-AM	3.3 (DMSO)	0.2	340/380 ± 10	510 ± 10
Rhod-2-AM	5 (DMSO)	0.6	550 ± 10	590 ± 10

Table 2.2: Description of chemical sensor properties and protocols

2.6.2 Measurement of mitochondrial Ca^{2+} with mitochondria targeted cameleon

Cells were transiently transfected with the FRET-based mitochondrial cameleon 4mtD3CPV. The sensor was excited at 440 nm by filter 440AF21 (Omega Optical) and emission was collected at 480 and 535 nm through emission filters 480AF30 and 535AF26 (Omega Optical). $[Ca^{2+}]_{mito}$ was expressed as F_{535}/F_{480} as mean fluorescence collected from 20 to 70 single cell measurements, performed at room temperature.

2.6.3 Measurement of mitochondrial Ca^{2+} and pH with mitochondria targeted ratiometric pericam

Cells stably expressing mitochondrial ratiometric pericam were used to simultaneously monitor $[Ca^{2+}]_{mito}$ and $[H^{+}]_{mito}$ as previously described [103]. mtRP was excited at either 430 nm or 485 nm with the filter 433DF15 (Omega Optical). Emitted light was recorded at 535 nm using a 535AF26 emission filter (Omega Optical). $[Ca^{2+}]_{mito}$ was expressed as $1 - F_{430}/F_0$. Changes in pH were expressed as $1 - F_{485}/F_0$, where F_{485} is the fluorescence at a given time and F_0 is the mean fluorescence of 20 to 70 single cell measurements collected at the beginning of recordings. Experiments were performed at room temperature.

2.6.4 Confocal Microscopy

High resolution imaging of cells was performed with a Nipkow-disc-based array confocal laser scanning microscope (ACLSM) as described previously [19]. The ACLSM consisted of a Zeiss Axiovert 200m including a Zeiss 100x/1.45 oil objective (Zeiss Microsystems), equipped with VoxCell Scan (VisiTech, Sunderland, UK), and an air-cooled argon ion laser system series 543 (CVI laser optics, Melles Griot, CA, USA). Emitted light was collected through the according filter-set (Omega Optical, Brat-

Sensor	Type	Excitation (nm)	Emission (nm)	Mitochondrial Targeting
mtRP	single-FP	430 ± 10 (Ca^{2+}), 480 ± 5 (H^+)	535 ± 10	COX4
4mtD3cpv	FRET	430 ± 10, 480 ± 5	535 ± 10	4xCOX8

Table 2.3: Description of genetically encoded mitochondrial targeted biosensors

tleboro, VT) using the high resolution CCD camera Photometrics CoolSNAPfx-HQ (Roper Scientific, Tucson, AZ, USA). Acquisition and analysis were performed with MetaMorph 7.7 (Molecular Devices, Visitron Systems).

2.6.5 Electron Microscopy of mitochondria

For ultrastructural analysis of mitochondria, Hek cells were grown to 90% confluency and fixed with 0.1% glutaraldehyde and 4% formaldehyde in DMEM containing 10% FCS for 15 min at RT and followed by further fixation in 2.5% glutaraldehyde in 0.1 M caccodylic buffer for 12 h at 4 $°C$. Afterwards, cells were incubated in 1% osmium tetroxide for 3 h and uranyl acetate for 30 min followed by incorporation into Agar 100 epoxid resin (Plano, Wetzlar, Germany) for 48 h at 80$°C$. Thin sections, counterstained with 1% uranyl acetate and lead citrate, were recorded with a CM120 transmission electron microscope (Philips, Eindhoven, Netherlands), equipped with a TVIPS 2k∗2k CCD camera (Tietz video and imaging processing systems, Gauting, Germany). Similar procedures described previously in [110, 114] .

2.7 Measurement of mitochondrial respiration

For measurement on oxygraph 2k (Oroboros Instruments, Innsbruck, Austria) [115], cells were grown in 10 cm plastic culture dishes until reaching 80% confluency, washed with PBS and then harvested and finally resuspended in 4.2 ml assay buffer. Half of the suspension was added to each of the two glass chambers, which were calibrated for 2 ml. Post-measurement, cells were counted in a Neubauer counting chamber (Marienfeld, Lauda-Königshofen, Germany). After transferring the cell suspension into the chamber, the chamber was closed and usually reached a stable signal after 10 min. A typical protocol ended with FCCP titration to measure the maximal oxygen consumption capacity and then 1 mM KCN was added to stop mitochondrial respiration and determination of residual oxygen consumption. Mitochondrial oxygen consump-

tion was expressed as O_2 flow per cells in $pmol/(sec * 10^6 cells)$. All experiments were conducted at $37°C$ at a stirring speed of 750 rpm.

High-throughput oxygen consumption measurement was accomplished using a XF96 extracellular flux analyzer (Seahorse Bioscience, MA, USA) as described previously [116]. Cells were plated in a XF96 polystyrene cell culture microplate (Seahorse Bioscience) at a density of 35000 cells/well. After 24 h incubation, cells were washed and incubated in unbuffered XF assay medium supplemented with 2 or 0 mM glutamine, 5.5 mM D-glucose and 1 mM sodium pyruvate for 30 min at $37°C$. Oxygen consumption rate (OCR) during consecutive addition of 1 µM oligomycin, 2 µM carbonyl cyanide, various concentrations of FCCP and 2.5 µM antimycin A.

3. Results

3.1 Multiple methods for the assessment of mitochondrial Ca^{2+} uptake are necessary

There are several methods for the assessment of mitochondrial Ca^{2+} uptake including the utilization of isolated organelles as well as cells. The method of isolating mitochondria has been used for mitochondrial characterization and general studies on mitochondrial function in-vivo since the mid of last century until today. Permeabilization procedures have been applied since two decades on tissue, fibers and cells in order to penetrate the plasma membrane, thereby gaining access to the cellular inside by keeping organelle integrity. Each method comprises its own benefits and drawbacks. The different preparations were utilized to study mitochondrial Ca^{2+} uptake and highlighted distinct modes and new insights into Ca^{2+} accumulation inside these organelles.

3.1.1 Preparations of isolated mitochondria and permeabilized cells revealed different mitochondrial Ca^{2+} uptake modes

Ca^{2+} uptake in mitochondrial preparations can be measured indirectly by applying boluses of Ca^{2+} to a bath containing a Ca^{2+} indicator. Ca^{2+} uptake is then measured by the clearance of Ca^{2+} from the bath, by means of a decline in signal intensity over time, after the addition of $CaCl_2$. Such Ca^{2+} boluses can be applied for several times. Ultimately, adding several drops of Ca^{2+} to the mitochondrial preparation leads to the phenomenon of permeability transition and a Ca^{2+} leak from the organelle through the opening of the mitochondrial permeability transition pore. This is highlighted as an increase of signal intensity after a certain number of additions (Figure 3.1).

First, we assessed Ca^{2+} uptake by isolated mitochondria indirectly by the Ca^{2+} indicator Calcium Green in the experimental buffer. Normalization of sample amounts

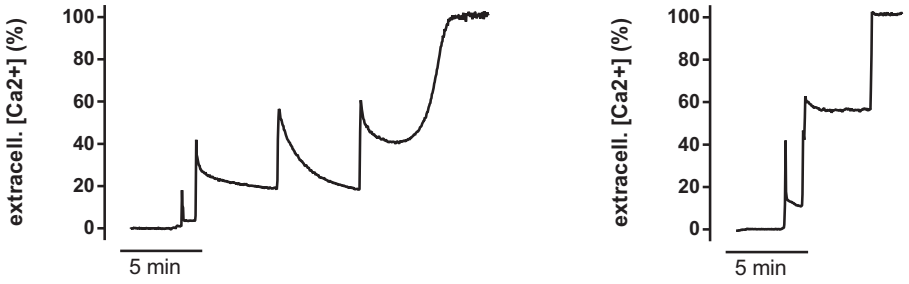

Figure 3.1: Indirect measurement of Ca^{2+} buffering by isolated mitochondria from HeLa cells (left panel) and INS-1 cells (right panel), using Calcium Green: spikes represent 10 µM Ca^{2+} additions and the subsequent decline in signal intensity is described as the uptake by the organelles; extracellular Ca^{2+} concentration as percent of sensor saturation; example tracings (n=2) of 2.8 and 2 mg mitochondrial protein content from HeLa and INS-1 cells.

was adjusted to protein content. The clearance of free extra-mitochondrial Ca^{2+} after several Ca^{2+} boluses reflects the capacity. This approach showed inhomogeneities most probably related to quality of the individual preparation including homogenization procedures and integrity of the isolated organelles. Figure 3.1 shows two Calcium Green measurements using isolated mitochondria from HeLa cells, on the left side, and INS-1 cells, to the right. In case of HeLa cells the organelle isolation resulted into 2.8 mg isolated protein and in case of INS-1 cells protein content of the mitochondria fraction accounted to 2 mg. The mitochondrial preparation from HeLa cells exhibited a higher Ca^{2+} uptake capacity compared to the collected INS-1 mitochondria.

In the next experiment, instead of using isolated mitochondria, cells were added to a bath containing the Ca^{2+} indicator Calcium Green and permeabilized via digitonin. Ca^{2+} accumulation within mitochondria, measured in permeabilized cells, occurred upon addition of Ca^{2+} to the bath for several boluses. The total sum of Ca^{2+} taken up by the organelles could be shown to depend on the sample amount. Permeabilized cells, in contrast to isolated mitochondria, were normalized to cell number. Figure 3.2 shows two Calcium Green measurements of permeabilized HeLa cells using $1.3 * 10^6$ cells on the left side and $5.9 * 10^8$ cells on the right side.

Mitochondrial Ca^{2+} uptake could be inhibited by the addition of ruthenium red to the bath containing permeabilized cells, shown in Figure 3.3.

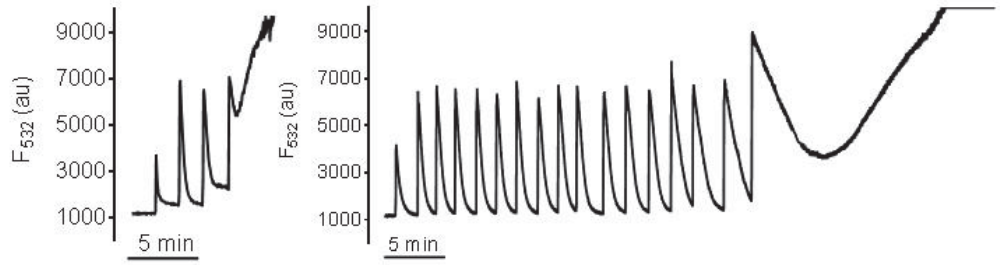

Figure 3.2: Indirect measurement of mitochondrial Ca^{2+} buffering in permeabilized HeLa cells, using Calcium Green: Spikes represent 50 µM Ca^{2+} additions to the bath containing digitonin-treated HeLa cells, mitochondrial buffering is shown to depend on cell number; Fluorescence of Calcium Green upon Ca^{2+} binding in arbitrary units, representative tracings for n=3-5, figure taken from [96].

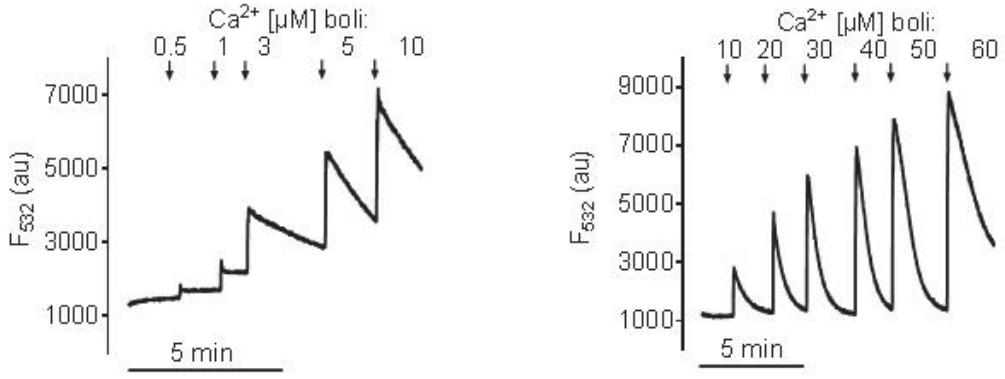

Figure 3.4: Sensor sensitivity and corresponding concentration dependent kinetics during indirect measurement of mitochondrial Ca^{2+} buffering using permeabilized cells and Calcium Green: spikes represent 0.5-60 µM Ca^{2+} additions, as indicated, to digitonin treated HeLa cells; Fluorescence of Calcium Green upon Ca^{2+} binding in arbitrary units, representative tracings (n=3), figure taken from [96].

Furthermore, $CaCl_2$ was titrated to the bath at increasing concentrations. Titration of Ca^{2+} at varying concentrations, to the bath containing permeabilized cells, exhibited

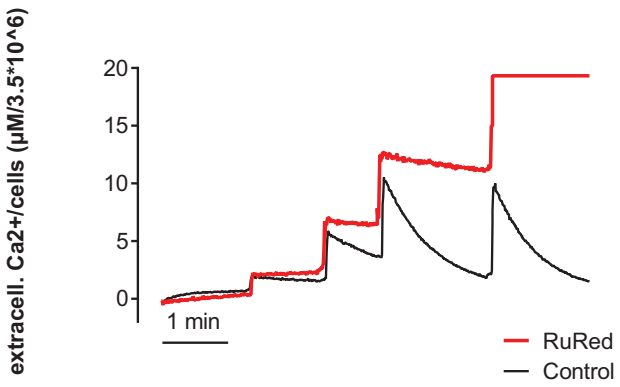

Figure 3.3: Effect of Ruthenium Red during indirect measurement of mitochondrial Ca^{2+} buffering using permeabilized cells and Calcium Green: Spikes or steps represent 20-50 µM Ca^{2+} additions to digitonin treated HeLa cells, representative tracings (n=3) of untreated (black) and 10 µM RuRed (red) treated cells; applied Ca^{2+} concentration normalized to cell number.

different kinetics in the clearance of free extra-mitochondrial Ca^{2+}. Significant Ca^{2+} uptake by mitochondria was shown only at concentrations higher than 3 µM (Figure 3.4). In order to neglect a possible impact by the indicator on Ca^{2+} accumulation, different Ca^{2+} indicators were compared, added to a bath containing permeabilized cells. FURA-5K possesses a higher sensitivity to Ca^{2+} of 0.2 µM instead of 14 µM for Calcium Green. The utilization of FURA-5K did not result in a more sensitive response than the experiments using Calcium Green and reflected the low Ca^{2+} affinity of mitochondrial Ca^{2+} uptake in permeabilized HeLa cells (Figure 3.5 left side).

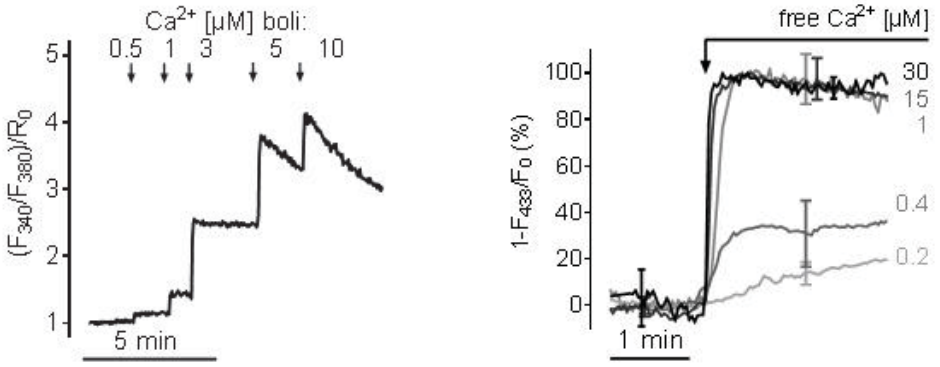

Figure 3.5: Sensor sensitivity during indirect measurement of mitochondrial Ca^{2+} buffering using permeabilized cells and FURA-5K or Pericam: Calcium Green and digitonin treated HeLa cells in repsonse to 0.5-10 µM Ca^{2+} additions (left panel), 4mtRP and digitonin treated EA.hy926 cells in response to perfusion with 0.2-30 µM Ca^{2+} (right panel); representative tracings for Calcium Green (n=3) and mean ± SEM (n=8−17), sensor fluorescence upon Ca^{2+} binding as ratio, figure taken from [96].

In order to go more into detail regarding capacity and affinity, mitochondrial Ca^{2+} uptake was further directly assessed on the single-cell level. Therefore, endothelial cells stably expressing the mitochondria targeted Ca^{2+} biosensor 4mt-pericam were permeabilized and perfused with buffers containing different Ca^{2+} concentrations. Ca^{2+} uptake was then evaluated on a fluorescence microscope. This approach revealed an even higher affinity of mitochondrial Ca^{2+} uptake and showed a response to Ca^{2+} concentrations lower than 1 µM (Figure 3.5 right side). Moreover, a detailed view on the kinetics of the different approaches, using various sensors to measure mitochondrial Ca^{2+} uptake either indirectly or directly, highlights distinct readings depending on the sensor and protocol chosen for one given model (Figure 3.6). In summary, the highly sensitive intra-mitochondrial biosensor pericam revealed a high affinity Ca^{2+} uptake with low capacity, since the signal got saturated at low Ca^{2+} concentrations above 1 µM, while the extra-mitochondrial indicators Calcium Green and Fura-5K revealed a high capacity Ca^{2+} uptake with low affinity.

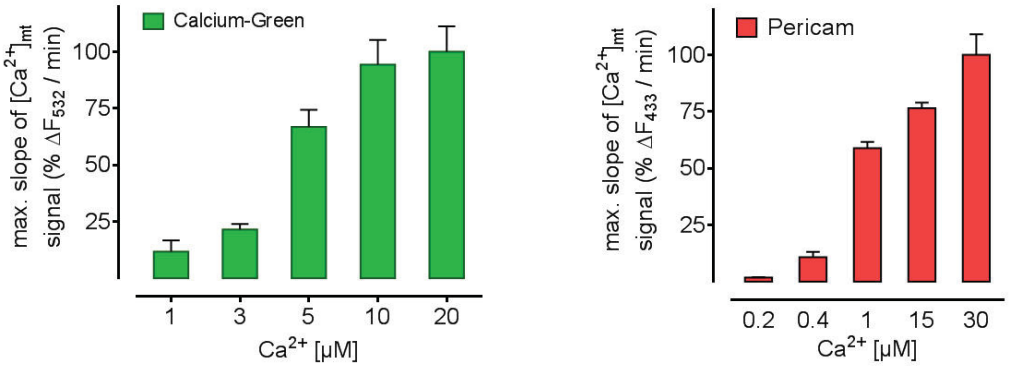

Figure 3.6: Sensor sensitivity during indirect measurement of mitochondrial Ca^{2+} uptake using permeabilized cells and Calcium Green (left panel, mean ± SEM, n=3-5) or direct by Pericam (right panel, mean ± SEM, n=8-17): maximal slope of Ca^{2+} uptake calculated from fluorescence at the sensor's individual wavelength, figure adopted from [96].

3.1.2 Various mitochondrial preparations respond differently to inhibitors

Mitochondrial Ca^{2+} uptake was measured in isolated mitochondria and permeabilized cells (Figure 3.7. Application of uncoupler FCCP diminished mitochondrial Ca^{2+} uptake as did MCU inhibitor ruthenium red. Ruthenium Red can not pass cell membranes and thereby is not employable on intact cells. Together with FCCP, both inhibitors are selective to mitochondria and could be easily utilized in permeabilized cells next to the isolated organelles. However, all preparations were differently affected by the inhibitors. Isolated mitochondria exhibited differing residual uptake rates in adherent (top right panel) and suspended organelles (top left panel). Permeabilized cells showed less than 10% response after application of the inhibitors (bottom left panel). The kinetic comparison in all preparations in terms of inhibition of mitochondrial Ca^{2+} uptake over time, is highlighted in the bottom right panel in Figure 3.7.

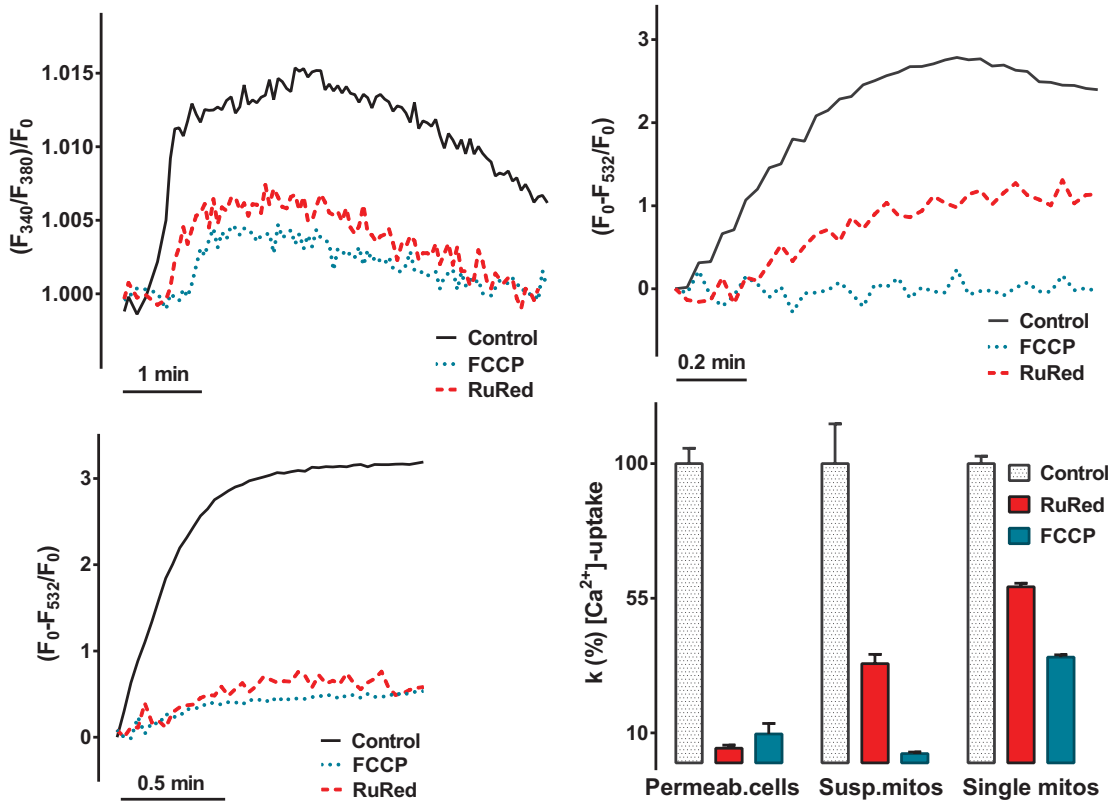

Figure 3.7: Application of inhibitors in measuring Ca^{2+} uptake using different mitochondrial preparations: uncoupler FCCP (1 µM) and MCU inhibitor RuRed (1 µM), in isolated mitochondria: Ca^{2+} measured by FURA (n=9-22, top left panel), and Calcium Green (n=3, top right panel), as well as in permeabilized cells: Ca^{2+} measured by Calcium Green (n=3-4, bottom left panel), representative tracings and overview of the according kinetic parameter shown as mean ± SEM (bottom right panel), fluorescence signal given as ratio, figure adopted from [96].

3.1.3 Assessing mitochondrial Ca^{2+} uptake via mitochondrial targeted biosensors

Mitochondrial Ca^{2+} uptake was measured in EA.hy926 cells using mtRP and 4mtD3cpv as different example biosensors. mtRP exhibits high targeting efficiency while 4mtD3cpv lead to a high degree of mistargeting and sensor accumulation within the cytosol. The response to Ca^{2+} of 4mtD3cpv was recorded from the excitation of CFP around 435 nm and collecting fluorescence of YFP and CFP at 535 nm and 480 nm. mtRP was excited at 430 nm and 480 nm and emission collected around 535 nm. Individual tracings are demonstrated in Figure 3.8 on the left side for mtRP in response to its two different

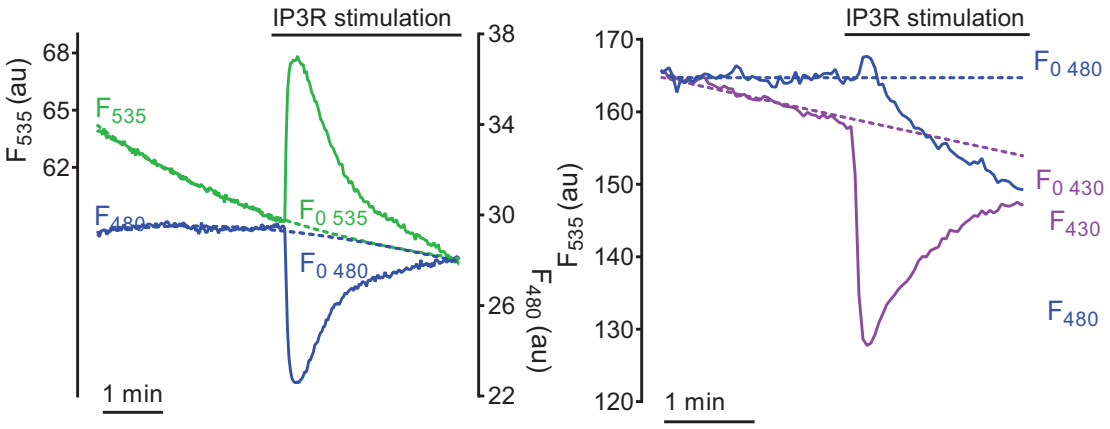

Figure 3.8: Individual fluorescence tracings of biosensors in response to Ca^{2+}: both emission wavelengths of cameleon at 480 and 535 nm (left side) and the responses to the two excitation wavelengths of pericam at 430 and 480 nm (right side), figure adopted from [96].

excitation wavelengths and on the right side for4mtD3cpv with its two emission wavelengths. In case of mtRP the higher excitation wavelength at 480 nm did result in a weak response to Ca^{2+} which was crucially affected by pH changes due to uncoupling through FCCP, shown in Figure 3.9 on the right side. On the other side, fluorescence of 4mtD3cpv was not distinctly changed by adding FCCP.

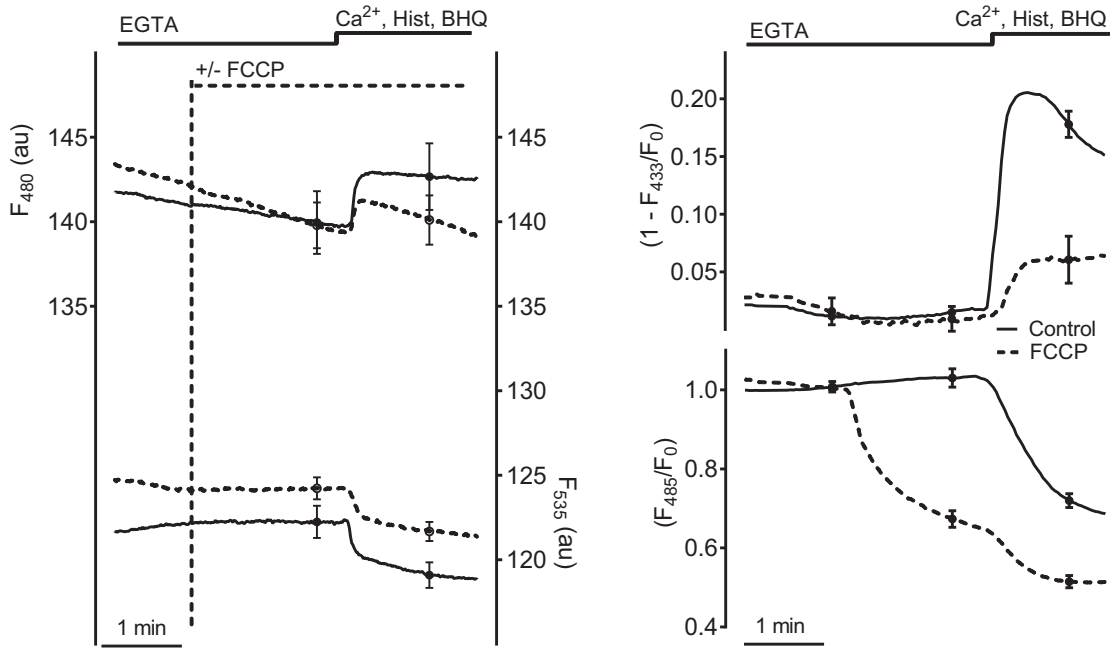

Figure 3.9: Fluorescence courses at individual wavelengths of pericam (mean ± SEM, n=3, 13-20 cells) and cameleon (mean ± SEM, n=3, 11-13 cells) in regard to their sensitivity to FCCP: addition of FCCP highlighted as dashed line, signal as fluorescence intensity or its ratio in arbitrary units, figure adopted from [96].

3.1.4 Assessment of the inner mitochondrial membrane via mitoplast preparations revealed multiple Ca^{2+} currents

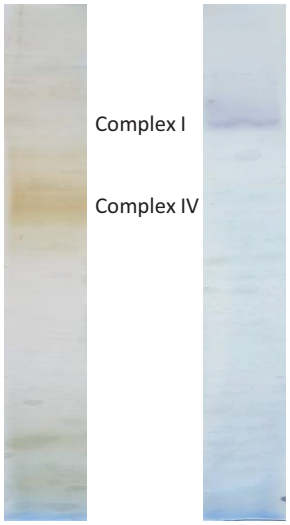

Figure 3.10: Complex I and IV activity in isolated mitochondria: complex activity staining of example membranes containing separated mitochondrial protein complexes isolated from Hek cells through blue native page.

First, isolated mitochondrial fractions were checked for their activity as measure for their integrity. Respiratory complex activity staining was determined for complex I and IV, shown in Figure 3.10. Positive activity was manifested as stained bands on the gel at the height according to size of the corresponding respiratory complex. Complex I indicator build up a blue stain and complex IV provoked an accumulation of yellow dye.

Mitoplast formation through incubation of isolated mitochondria in hypotonic medium was monitored over time in order to get the optimal time frame for swelling (Figure 3.11). The decline in optical density within the first 8 to 10 min points to an increase in sample volume which was due to water accumulation within the mitochondria. After this time-period, absorption values were stable and did not change for additional 30 min. This stage was assigned to rupture of the outer mitochondrial membrane and full mitoplast formation. Finally, after 40 min, optical density values increased slowly over time. This long-lasting incubation in hypotonic solution lead to rupture of mitoplasts, by means of breaking the inner mitochondrial membrane, and a volume decrease due to the leakage of the mitochondrial content through broken membranes. Therefore, incubation of mitochondria in hypotonic medium was adjusted to 8 min for

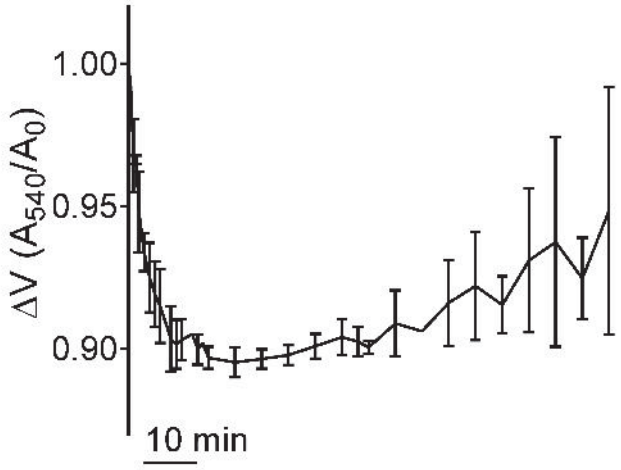

Figure 3.11: Optical measurement of mitochondrial swelling in hypotonic buffer by a decrease in absorption at 540 nm, signal ratio of absorption over time to initial absorption as mean ± SD (n=3), figure adopted from [113].

optimal swelling.

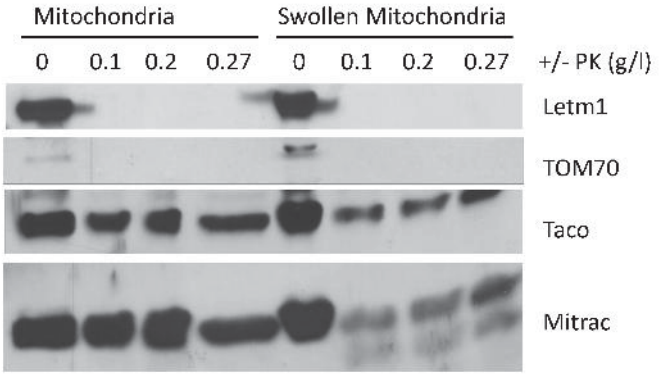

Figure 3.12: Western Blot analysis of mitochondria and mitoplast fractions after PK treatment: samples were incubated for 10 min with proteinase K at 0-0.27 g/l, blotted against Letm1 (IMM), TOM70 (OMM), Taco1 (matrix) and Mitrac12 (IMM).

Mitochondrial and mitoplast preparations were checked for their protein content and integrity. Swelling of mitochondria lead to rupture of the OMM and IMM proteins became vulnerable to digestion by proteinase K treatment. Mitochondrial as well as mitoplast fractions were incubated with different concentrations of PK. Samples were then analyzed for their levels of standard membrane and matrix protein TACO, shown in Figure 3.12. The translational activator of cytochrome C (TACO1) resides in the mitochondrial matrix and could not be digested by PK as long as the IMM

was intact. Both, mitochondria as well as mitoplast samples were not affected by PK treatments. The mitochondrial translation regulation assembly intermediate of cytochrome c oxidase (MITRAC12) poses an IMM protein and its antibody showed double bands upon degradation due to PK. Signals for the IMM protein Letm1 also disappeared upon PK treatment that pointed to its antibody binding from the IMS side. The mitochondrial import receptor on the OMM TOM70 was immediately digested by PK in isolated mitochondria and swollen mitochondria. Outer membrane proteins were still present as shown by this analysis, most probably as loose remnants stuck to the IMM.

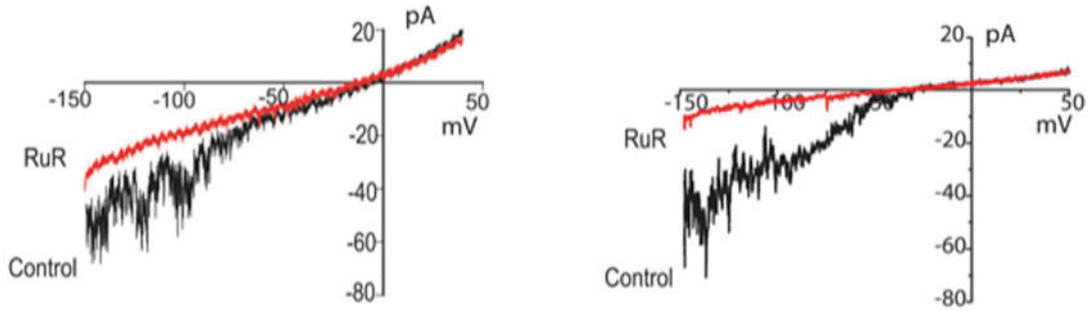

Figure 3.13: Current-Voltage analysis of patched mitoplasts from EA.hy926 and HeLa cells, inhibitory effect of Ruthenium Red: representative tracings (n=3-6) of mitochondrial currents of HeLa and EA.hy926 cells upon mitoplast-attached mode induced by voltage ramps of -150 to 50 mV, figure adopted from [96].

Mitoplasts isolated from HeLa as well as EA.hy926 cells were used for electrophysiological characterization of the inner mitochondrial membrane. Membrane currents were recorded in membrane-attached mode induced by voltage ramps from -150 up to 50 mV. Patch pipette solutions contained high levels of Ca^{2+}. During measurement mitoplasts were kept in high K^+ buffers containing cyclosporin A for inhibition of MPTP formation and CGP-37157 for inhibiting NCLX. Pipette solutions containing low chloride was used in control experiments in order to check for Cl^- outward currents which did not result in any differences compared to high Cl^- content. All the same, anion exchange inhibitors were applied in additional control experiments. Neither DIDS nor niflumic acid showed any differences in the recorded tracings. Ruthenium red was used to block mitochondrial Ca^{2+} uptake and lead to partial up to complete inhibition of Ca^{2+} currents in HeLa and EA.hy926 cells (Figure 3.13). The MPTP inhibitor cyclosporin A as well as the NCX inhibitor CGP-31757 did not show any effect on the currents observed, neither did Ca^{2+}-activated potassium channel (K_{Ca}) blocker

paxiline, nor K_{ATP} inhibitor gilbenclamide.

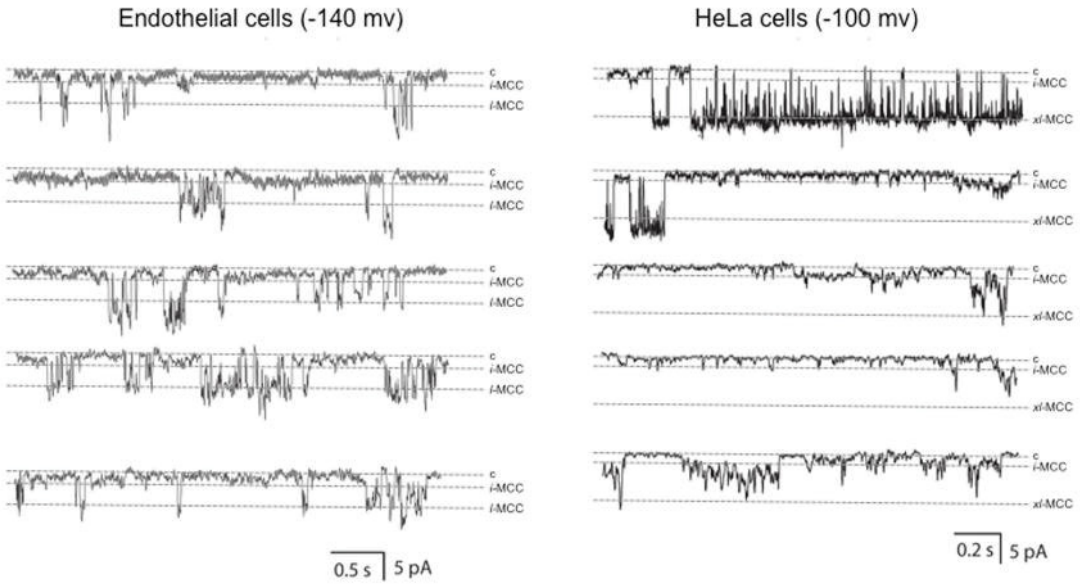

Figure 3.14: Patch Clamping of mitoplasts from EA.hy926 and HeLa cells demonstrates distinct Ca^{2+} currents: representative tracings of single channel events in mitoplasts from HeLa (right panel, n=10) and EA.hy926 cells (left panel, n=5) at indicated voltages, figure adopted from [96].

Strong inward currents were recorded within mitoplast-attached configuration under negative potentials. Mitochondrial Ca^{2+} currents measured were not stable and different single channel events within the same sample could be observed over time. Mitoplasts from wild-type cells exhibited multiple single channel conductances. In case of endothelial cells, three distinct conductances were recorded, referred to as small, intermediate and large mitochondrial Ca^{2+} current (s-MCC, i-MCC, xl-MCC) (Figure 3.14 left side). Two different Ca^{2+} currents could be shown for HeLa cells within this first comparison, referred to as intermediate and extra-large mitochondrial Ca^{2+} current (i-MCC, xl-MCC) (Figure 3.14 right side). Further analysis of Ca^{2+} currents in mitoplasts from HeLa cells presented a third distinct mode of current, namely the burst mitochondrial Ca^{2+} current (b-MCC) (Figure 3.15) which occurred at high amplitude of open and closed transitions and frequently interrupted recordings of i-MCC and xl-MCC. The channel behind i-MCC was most frequently observed in both cell types, followed by a much lower occurrence of either b-MCC or s-MCC and l-MCC. The least abundant current recorded was the xl-MCC in HeLa cells. In general, single channel

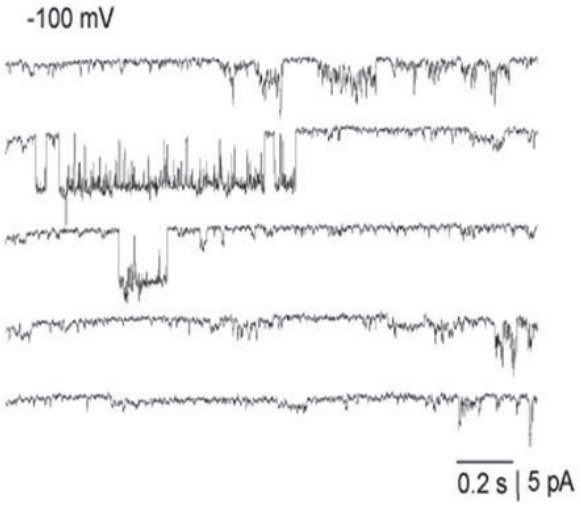

Figure 3.15: Burst mode current (b-MCC) in patched mitoplasts from HeLa cells, examplary tracings adopted from [113].

activity of all observed currents increased at higher voltage settings. Availability of the individual currents were calculated for their occurrence within active patches instead of density averaged from all experiments, since more than 50% out of all measured mitoplasts were silent. By that way the fact, that the rate of occurrence in channel activity also depended on patch pipette size, could be neglected. Biophysical parameters were normalized to activity, highlighted in table 3.1.

	OC (%)	**G (pS)**	**mT$_o$ (ms)**	**mT$_c$ (ms)**	**nP$_o$ (ms)**
EA.hy926					
s-MCC	30%	7.69 ± 1.42	2.44 ± 0.51	19.20 ± 15.88	0.88 ± 1.27
i-MCC	64%	13.37 ± 2.44	3.14 ± 0.58	11.26 ± 3.82	1.11 ± 0.64
l-MCC	21%	34.52 ± 4.65	4.57 ± 5.40	52.07 ± 35.87	0.70 ± 0.96
HeLa					
i-MCC	70%	11.7 ± 0.6	14.9 ± 2.4	3.5 ± 0.5	0.61 ± 0.14
xl-MCC	12%	80.2 ± 7.8	1.9 ± 0.88	6.08 ± 1.50	0.77 ± 0.06
b-MCC	35%	22.5 ± 1.7	22.6 ± 2.6	4.4 ± 0.9	0.34 ± 0.08

Table 3.1: Gating parameters of mitochondrial Ca^{2+} currents in mitoplasts from endothelial and HeLa cells: OC = occurrence within active cells, G = conductance mT$_c$ = mean closed time, mT$_o$ = mean open time, nP$_o$ = open probability, table adopted from [113, 95].

3.1.5 Indirect measurement of mitochondrial Ca^{2+} uptake via respiration

Several metabolic enzymes and proteins, important for the Krebs cycle, are regulated by Ca^{2+}. Therefore, respiration is also regulated by Ca^{2+}, and depends on intact mitochondrial Ca^{2+} uptake. By means of the relation between respiratory rates and mitochondrial Ca^{2+} signaling, Ca^{2+} uptake could be assessed indirectly by measurement of oxygen consumption.

Ca^{2+} elevating agonists induce an increased cellular demand of energy and thereby enhance mitochondrial respiration. Agonist induced ATP mobilization and accumulation within the ER leads to Ca^{2+} release from the ER and thereby stimulated citrate cycle, respiratory and glykolytic enzymes which enhance ATP production.

Mitochondrial Ca^{2+} uptake after IP3R activation resembles an important mechanism in Ca^{2+} signaling and IP3R activation is closely related to store operated Ca^{2+} entry (SOCE). Rapid Ca^{2+} release from the ER activates ORAI channels by STIM1 clustering to the plasma membrane. Knock-down experiments on ORAI1 and STIM1, the main proteins involved in SOCE, decreased extracellular Ca^{2+} entry, measured by FURA (Figure 3.16 right panel) and lead to a direct effect on mitochondrial oxygen consumption (Figure 3.16 left panel). Oxygen consumption was greatly decreased due to impaired Ca^{2+} mobilization. Uncoupling through FCCP increased oxygen consumption exclusively. This maximal respiratory activity is independent from the Ca^{2+} supply and could be used as control.

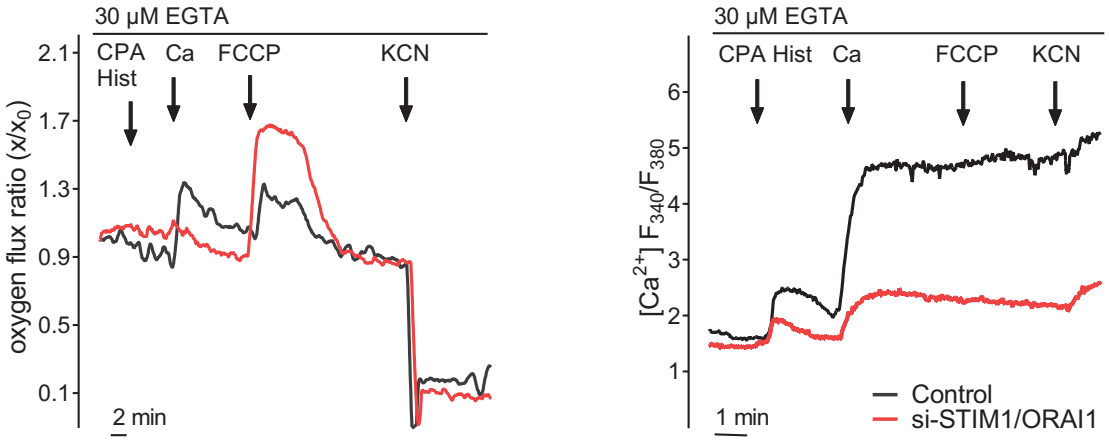

Figure 3.16: Oxygen consumption (left panel) and cytosolic Ca^{2+} levels measured by FURA (right panel) upon Stim1 and Orai1 knock-down: combined knock-down of ORAI and STIM diminish repiration induced by Ca^{2+} stimulation, representative curves for n=4.

3.2 Various proteins are involved in distinct mitochondrial Ca^{2+} uptake pathways

In order to assess the individual role of the various proteins, so far suggested to be involved in mitochondrial Ca^{2+} uptake, experiments on siRNA or shRNA-mediated knock-down as well as overexpression of untagged and tagged constructs were conducted and analyzed by the multiple methods described before.

3.2.1 Letm1 and UCP2/3 achieve distinct mitochondrial Ca^{2+} transfer modes

Both, Letm1 and UCPs were highlighted to be involved in Ca^{2+} transfer into mitochondria. In order to evaluate their individual roles various protocols of fluorescence microscopy were carried out. In case of Letm1 knock-down, mitochondrial Ca^{2+} uptake was primarily reduced upon readdition of Ca^{2+} to Ca^{2+}-starved cells, shown in Figure 3.17. Ca^{2+} affinity for the individual role of Letm1 was assessed using permeabilized cells. In Ca^{2+}-free buffer permeabilized cells were perfused with different Ca^{2+} concentrations triggering low and high affinity uptake. The actual intracellular concentration for low and high Ca^{2+} was set to around 175 nM and 920 nM by calculations from FURA-2 as described in [117]. Mitochondrial Ca^{2+} uptake under low Ca^{2+} addition was reduced in case of Letm1 knock-down.

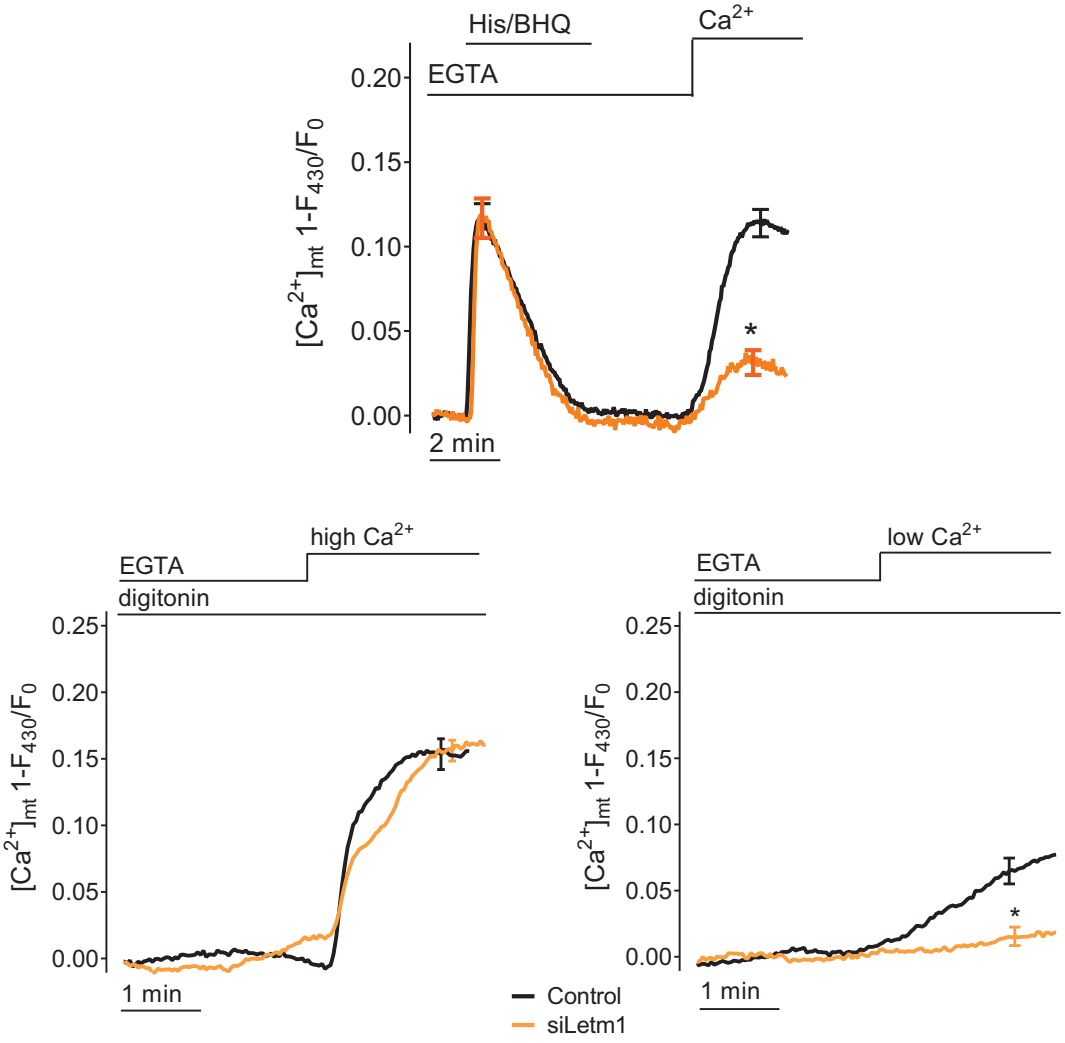

Figure 3.17: Mitochondrial Ca^{2+} uptake upon Letm1 knock-down (siLetm1) using intact cells stimulated with IP3R agonist followed by readdition of Ca^{2+} (upper panel), and permeabilized cells (lower panel) after perfusing samples with 20 µM (low Ca^{2+}) or 500 µM (high Ca^{2+}): Fluorescence of mtRP at 430 nm upon Ca^{2+} binding as ratio in arbitrary units, n=4-6, 12-17 cells, * for significant differences using ANOVA and Dunnet as individual t-tests, $p < 0.05$, adopted from [103].

The role of UCPs in human cells was assessed by knock-down of UCP2 and UCP3. As both proteins share over 70 % identity and share common features and domains, single knock-down of only one UCP family member could result into functional compensation by its homolog. Therefore, in case of knock-down of UCP2 and UCP3, siRNAs against both uncoupling proteins, noted in table 2.1, were used at the same time. Mitochondrial Ca^{2+} uptake after induced Ca^{2+} release from the ER by IP3R agonists was reduced upon knock-down of UCP2/3 compared to control conditions

(Figure 3.18). Furthermore, permeabilized cells at knock-down of the two UCPs did take up less Ca^{2+} after perfusing them with high Ca^{2+}.

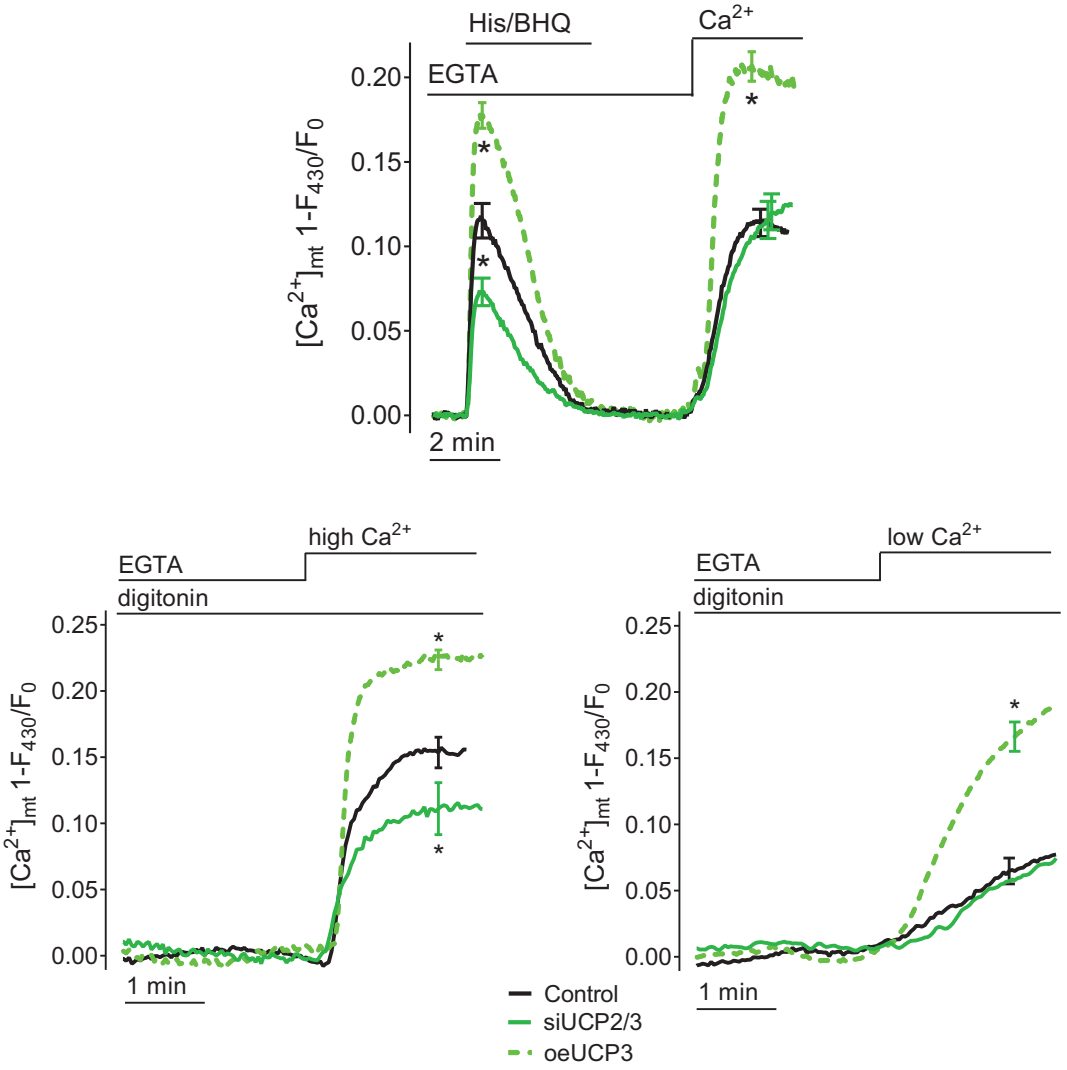

Figure 3.18: Mitochondrial Ca^{2+} uptake upon UCP2/3 knock-down (siUCP2/3) and UCP3 overexpression (oeUCP3) using intact cells stimulated with IP3R agonist followed by read-dition of Ca^{2+} (upper panel), and permeabilized cells (lower panel) after perfusing samples with 20 µM (low Ca^{2+}) or 500 µM (high Ca^{2+}): Fluorescence of mtRP at 430 nm upon Ca^{2+} binding as ratio, n=4-6, 12-16 cells, * for significant differences using ANOVA and Dunnet as individual t-tests, $p < 0.05$, adopted from [103].

3.2.2 Isolated mitoplasts show MCU-independent currents

Mitochondrial Ca^{2+} accumulation in mitochondria is decreased upon transient (Figure 3.19 left panel) and stable (Figure 3.19 right panel) knock-down of MCU.

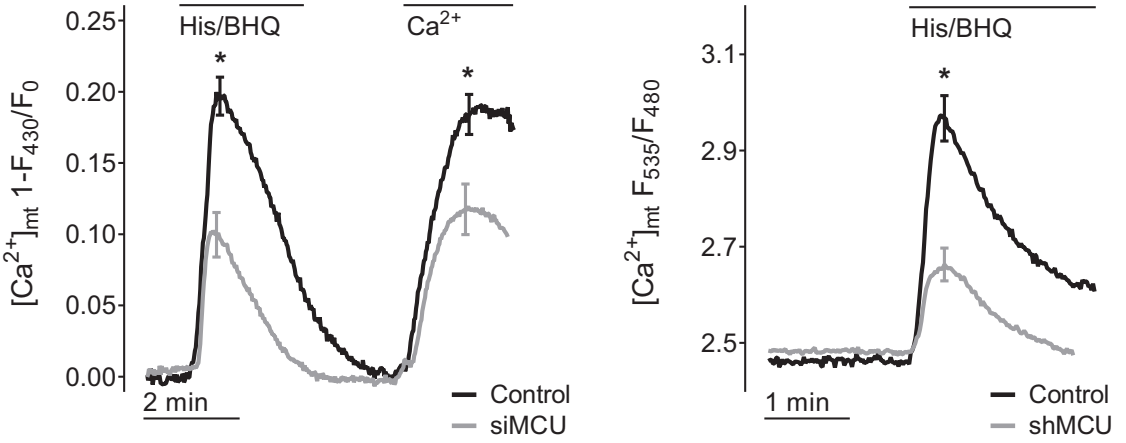

Figure 3.19: Mitochondrial Ca^{2+} uptake upon transient (siMCU left panel) and stable (shMCU right panel) knock-down of MCU: Fluorescence of mtRP at 430 nm (right, n=6, 20-27 cells) and 4mtD3cpv (left, n=9, 103-115 cells) as ratio, * for significancant differences using t-test, $p < 0.01$.

In order to refine the different previously recorded mitochondrial currents for the mitochondrial Ca^{2+} current underlying MCU acitivity, mitochondria were isolated from cells with stable knock-down of MCU. Mitoplast therefrom were used for mitoplast-patch clamping experiments. General acitivity was decreased in mitoplasts from the artificial cells (Figure 3.20 left panel). Additionally, activity of the individual observed currents was also altered with decreased levels in i-MCC and higher levels of xl-MCC upon MCU knock-down (Figure 3.20 right panel).

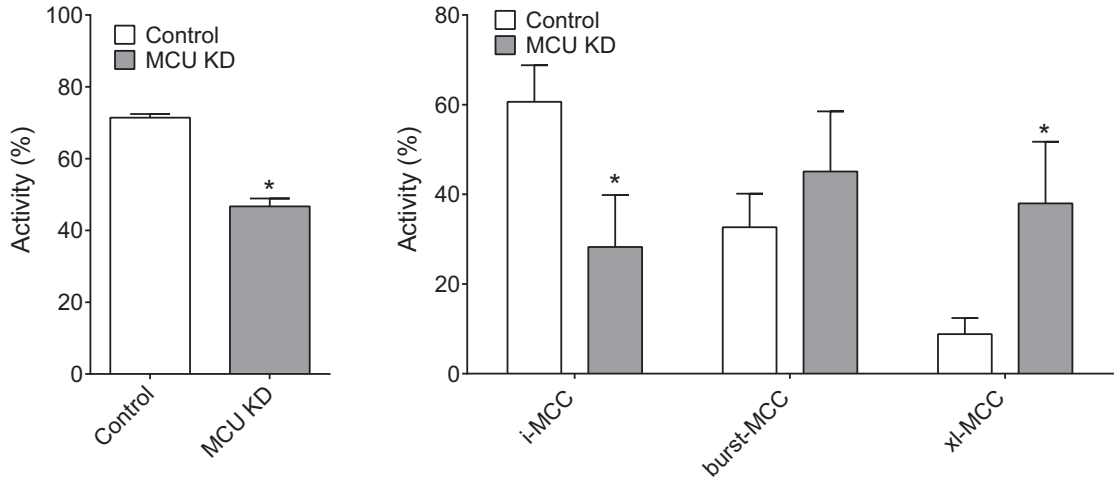

Figure 3.20: Mitoplast Ca^{2+} currents upon MCU knock-down (shMCU): total active patches out of control and shMCU cells and individual activity of intermediate (i-MCC) burst (b-MCC) and extra large (xl-MCC) mitoplast Ca^{2+} currents, * for significance tested using t-test, $p < 0.01$, adopted from [95].

3.2.3 Mitochondrial Ca^{2+} uptake is regulated by MICU1

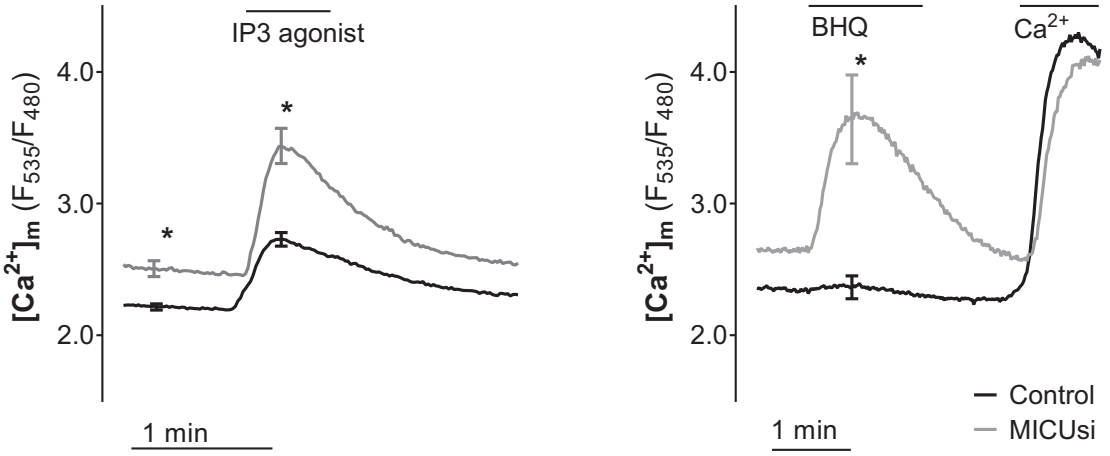

Figure 3.21: Mitochondrial Ca^{2+} uptake measured upon knock-down of MICU1: fluorescence signal of 4mtD3cpv given as ratio YFP/CFP, n=5-6, 33-38 cells, * for significant differences using t-test, $p < 0.05$.

MICU1 was discovered a year before the finding of the actual mitochondrial calcium uniporter protein. And still, the role of MICU1 was not characterized until recently.

In order to identify MICU function as a gatekeeper, ratiometric biosensors have to be utilized without consequent calculations of ratios based on initial fluorescence signals. A comparison of basal levels of mitochondrial Ca^{2+} content between different samples was rendered possible by skipping such correction calculations, demonstrated in Figure 3.21. Upon knock-down of MICU1, basal levels of mitochondrial Ca^{2+} were higher than in wild-type cells. Maximal accumulation of Ca^{2+} within mitochondria corresponded to maximal mitochondrial Ca^{2+} capacity, and therefore, mitochondrial Ca^{2+} uptake was decreased in MICU1 knock-down cells. Moreover, upon inhibition of SERCA by the application of 2,5-di(tert-butyl)-1,4-benzohydroquinone (BHQ), which provokes passive Ca^{2+} efflux from the ER, Ca^{2+} accumulated in mitochondria upon MICU1 knock-down but not in wild-type cells.

3.2.4 Mitochondrial Ca^{2+} handling proteins affect mitochondrial respiration

Since respiratory activity is regulated by mitochondrial Ca^{2+}, we assessed oxygen consumption after Ca^{2+} mobilization related to decreased expression levels of the investigated proteins. Knock-down of MCU, Letm1 or UCP2/3 lead to decreased respiratory rate after SOCE dependent IP3 mediated Ca^{2+} mobilization, shown in Figure 3.22.

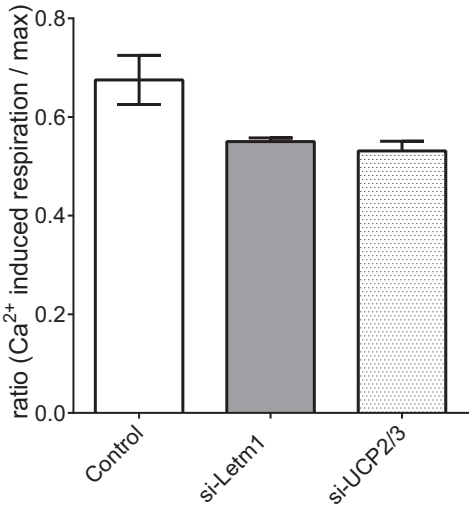

Figure 3.22: Oxygen consumption after mitochondrial Ca^{2+} uptake upon Letm1 or UCP2/3 knock-down: ratio between oxygen consumption rate (OCR) after Ca^{2+} mobilization and subsequent mitochondrial Ca^{2+} uptake as ratio to maximal OCR after uncoupling, mean of n=3-4, significance tested using ANOVA as individual t-tests with $p > 0.05$.

3.2.5 Distinct mitochondrial Ca^{2+} uptake in various example cell-lines on the example role of UCP2/3

UCP2 and UCP3 have been shown before (3.18) to affect mitochondrial Ca^{2+} uptake. However, knock-down of the individual proteins in various cell-lines yields different results. Various cell-lines were tested for mitochondrial Ca^{2+} uptake upon IP3 mediated Ca^{2+} release from intracellular stores, shown in figure 3.23. UCP2/3 Knock-down resulted into an significant decrease of Ca^{2+} accumulation within mitochondria of EA.hy926 cells. INS-1 cells were not similarly impacted but still exhibited reduced uptake levels. In the second case of excitable cells, SHSY5Y cell-line, knock-down of UCP2/3 did not result in reduction of mitochondrial Ca^{2+} uptake levels. Thus, the individual proteins differently contribute to mitochondrial Ca^{2+} uptake in distinct cell-lines. Still, the different behaviour of HeLa S3 and HeLa Tebu cells demonstrates the fact, that even in the same cell type protein expression levels could be different and/or protein complexes and interactions could be differently regulated.

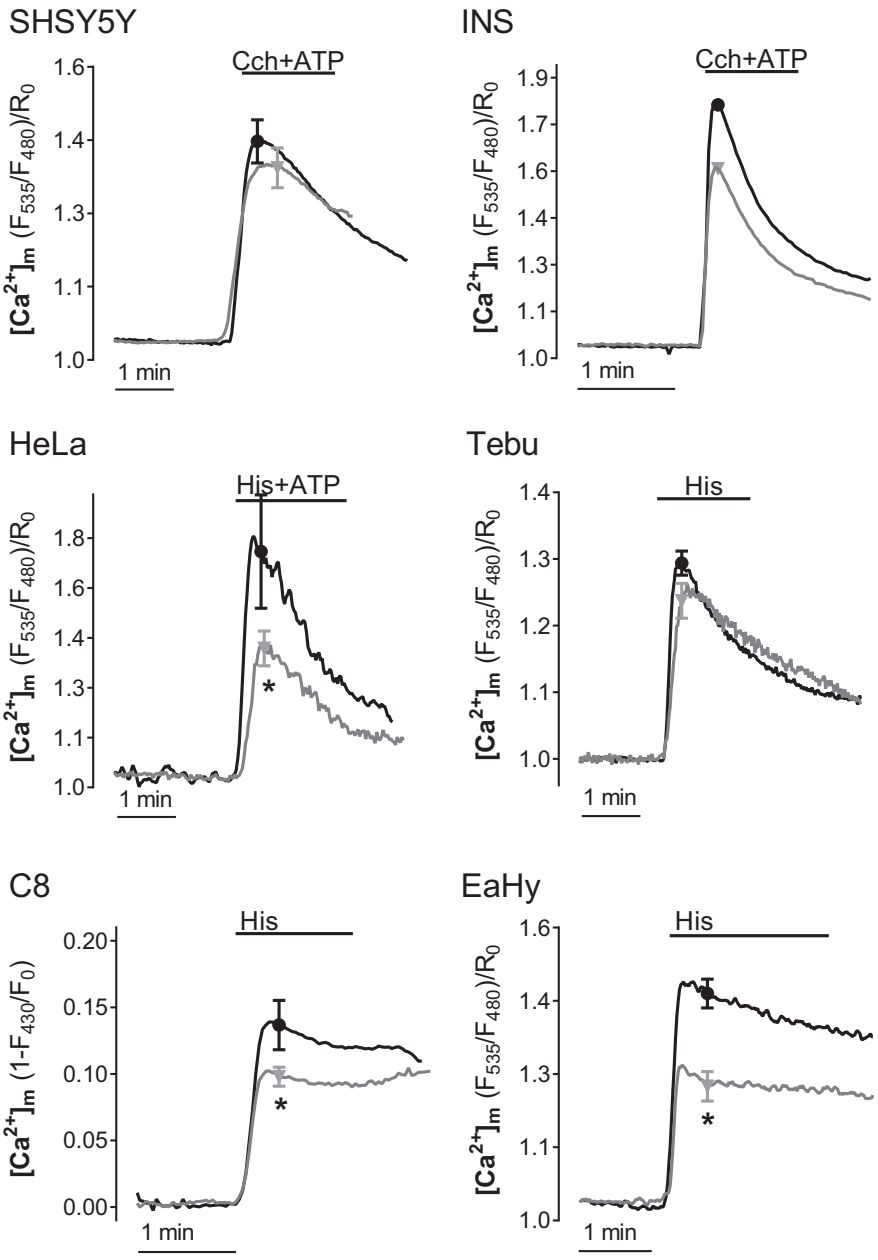

Figure 3.23: Mitochondrial Ca^{2+} uptake measured upon knock-down of UCP2/3 in various cell-lines: fluorescence signal of mtRP or 4mtD3cpv given as ratio, n=3-8, 9-45 cells; abbreviations Ea for EA.hy926 as well as C8 for EA.hy926 cells stably expressing mtRP, Tebu for a distinct type of HeLa cells, acquired from tebu-bio, other than HeLa for HeLa S3 cells, significance t-test * for $p < 0.05$

3.2.6 Mitochondrial Ca^{2+} entry pathways are based on a variable set of interacting proteins

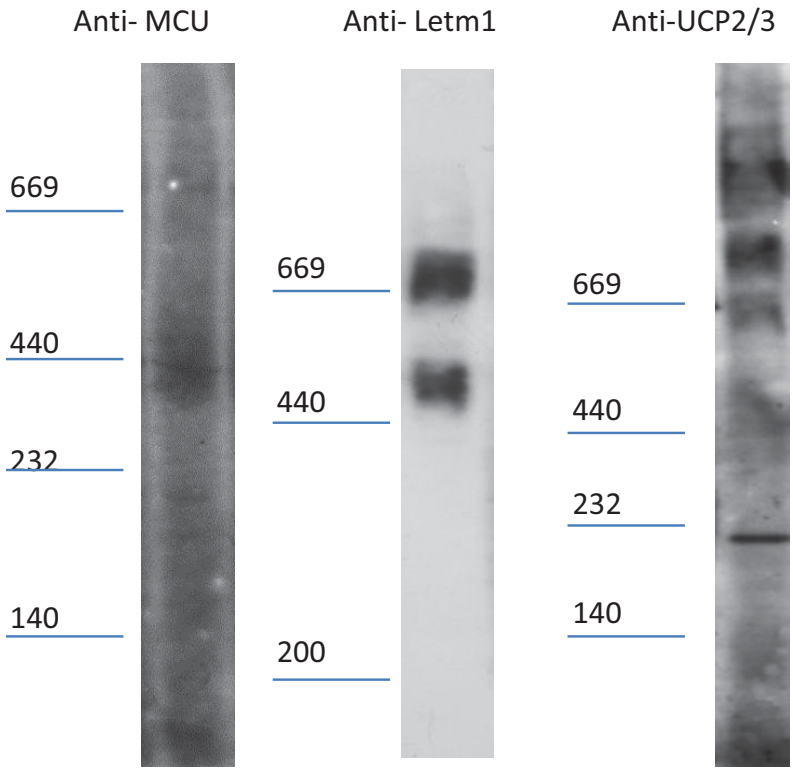

Figure 3.24: Blue native page blotted against MCU, Letm1 and UCP2/3: antibodies against MCU, Letm1 and UCP2/3 detect higher complexes, representative for n=3

As shown above in 3.2.1, Letm1 and UCP2/3 participated in different uptake pathways. MCU was furthermore shown to depend on regulatory proteins. In addition to functional studies on the individual roles of the proteins contributing to mitochondrial Ca^{2+} sequestration, the possibility of dynamic or static interactions due to complexes between the individual protein was assessed via proteomic studies. Blue native page showed larger protein complexes for Letm1, MCU and possibly UCPs, shown in figure 3.24. As known from [23], MCU formed a complex around 400 kDa. Letm1 was shown to be part of a complex around 450 kDa [45] and further showed to form a second higher complex around 650 kDa. Blue native analysis of UCP2 and 3 showed a weak formation of a 450 kDa complex and higher complexes above 650 kDa. Still, these supercomplex signals could be obtained through unspecific antibody binding.

3.3 The mitochondrial organizing system related to mitochondrial Ca^{2+} uptake function

The mitochondrial contact site and cristae organizing system MICOS, former MINOS, involves several proteins along the inner mitochondrial membrane organizing inner and outer membrane contact sites [57]. As the MICOS complex primarily functions in cristae organization, we studied its impact on mitochondrial Ca^{2+} uptake using the example of the newly identified subunit Mic10.

Mic10 was discovered as novel MICOS component through interaction with Mic60 [110]. Its function in human cells has not been cleared yet. Since Mic10 was shown to impact structural integrity of mitochondria in yeast, we performed structural analysis in Hek cells overexpressing Mic10. However, shots from electron microscopy, shown in Figure 3.25, did not point to apparent differences in mitochondrial morphology between the control and the stably transfected cells.

Overexpression of Mic10 did not result in structural differences nor in any significant differences regarding respiratory rates (data not shown). However, Mic10 overexpression affected an increase in mitochondrial Ca^{2+} capacity, shown in Figure 3.26. Silencing Mic10 resulted into slightly increased mitochondrial Ca^{2+} uptake upon Ca^{2+} release from internal stores without any significant differences in Ca^{2+} transfer to Ca^{2+}-starved mitochondria, as demonstrated in Figure 3.27. Overexpression of Mic10, on the other hand, lead to strongly increased maximal Ca^{2+} uptake buffering capacity, demonstrated by an attenuated MPTP formation in permeabilized cells in Figure 3.26. For further characterization, Hek cells overexpressing Mic10 were further analyzed regarding their proteomic profile.

First, Mic10 was checked for its complex formation by size exclusion chromatography. Size dependent flow-throughs were collected as fractions and then blotted against Mic10 as well as control proteins for complex size comparison, shown in figure 3.28. The mitochondrial import receptor subunit TOM70, which was loosely associated with larger TOM complexes around 450 kDa, also migrated as a dimer at 140 kDa. The complex III component RIESKE could be found as a constituent of complex III dimers around 500 kDa and supercomplexes of complex III with complex I and IV between 1000 to 2000 kDa. Anti-Mic10 showed bands mainly in fractions containing larger protein complexes above 700 up to 1500 kDa.

Proteomic immunoprecipitation studies involved analysis through Western Blot as well as mass spectrometry. Western Blot analysis, shown in Figure 3.29, highlights

possible interactions between Mic10 and MCU. Hek cells overexpressing Mic10-FLAG were immunopreciptated using anti-FLAG coupled beads and analyzed against several mitochondrial targets. Corresponding immunoprecipitates exhibited strong accumulation of mitofilin. Furthermore, MCU was present in the Mic10 pull-down fraction but not in the control immunoprecipitate. Whereas, the flowthrough fraction, which represents the unbound protein after incubation with the beads, exhibited a decreased signal of anti-MCU, that supports a assumption of MCU to be part of Mic10 immunoprecipitates.

Further size-dependent analysis of mitochondrial fractions showed MCU not only to be in the pulled down fraction of Mic10 but also to be part of the same or similar sized complex as Mic10, shown in Figure 3.30. Thereby, MCU is shown to accumulate in the same size-range as mitofilin. NADH dehydrogenase ubiquinone 1 beta subcomplex NdufB8 was used as control for the known size of complex I.

Mass spectromic analysis revealed various interaction partners, results shown in table 3.2. Though, Mic10 was discovered by searching for new oligomerization factors to ATP synthase, there was no direct association shown for Mic10 and ATP synthase before [110]. Still, ATP synthase was pulled down in this experiment. VDAC1 was found in the immunoprecipitate analyzed by MS but not through Western Blotting. As the case may be, MCU was pulled-down by the same experimental settings analyzed by Western Blot but not in the MS analysis. Thereby, these co-immunoprecipitated proteins were shown to be weakly bound to MICOS, either as direct neighbors or interaction partners.

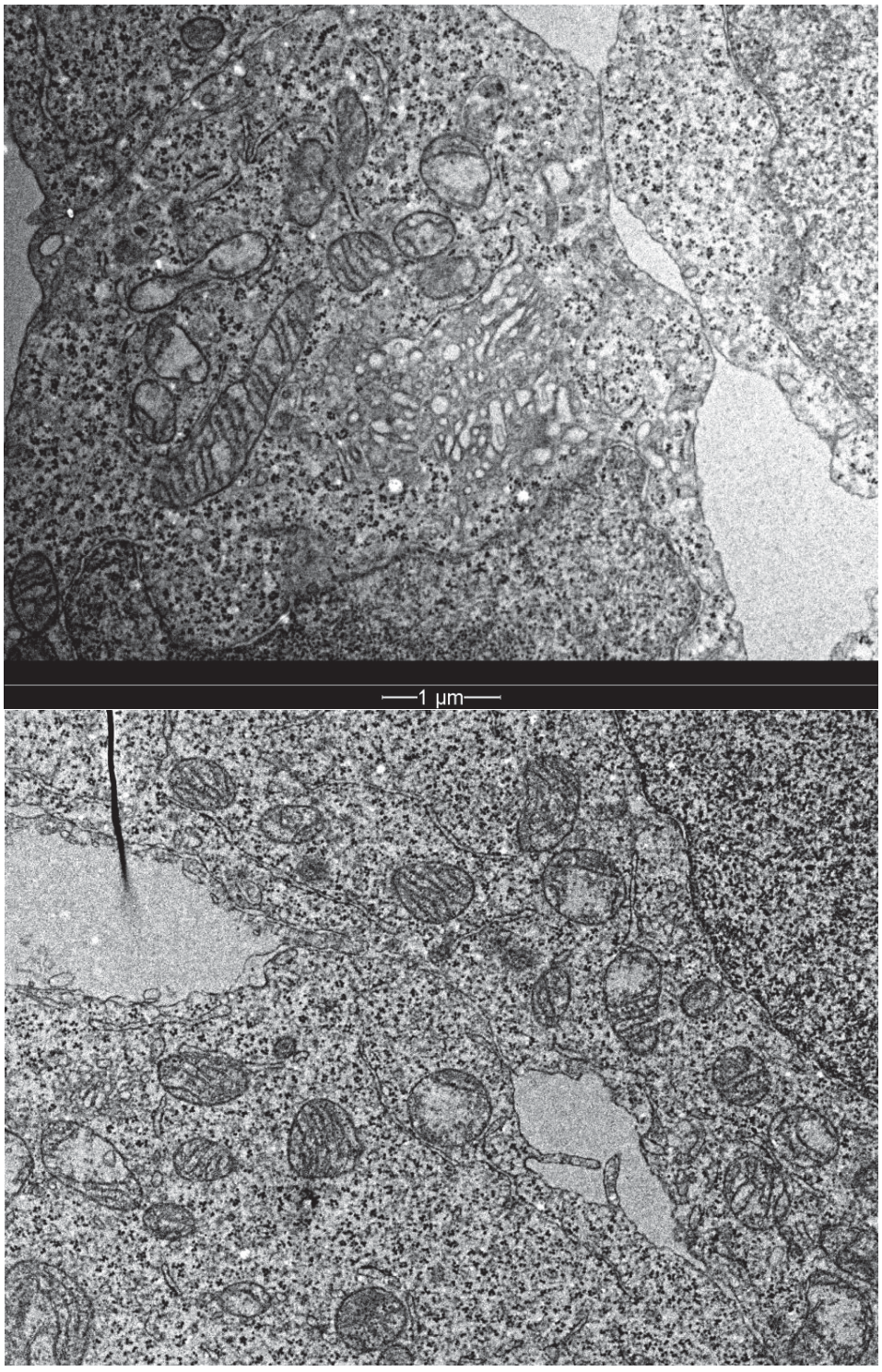

Figure 3.25: Electron Microscopy images of WT Hek cells (lower panel) and Hek cells stably overexpressing Mic10 (top panel), example images recorded by D.Jans at the Department of Nanobiophotonics and Electron Microscopy Facility, Max Planck Institute for Biophysical Chemistry, 37077 Göttingen, Germany

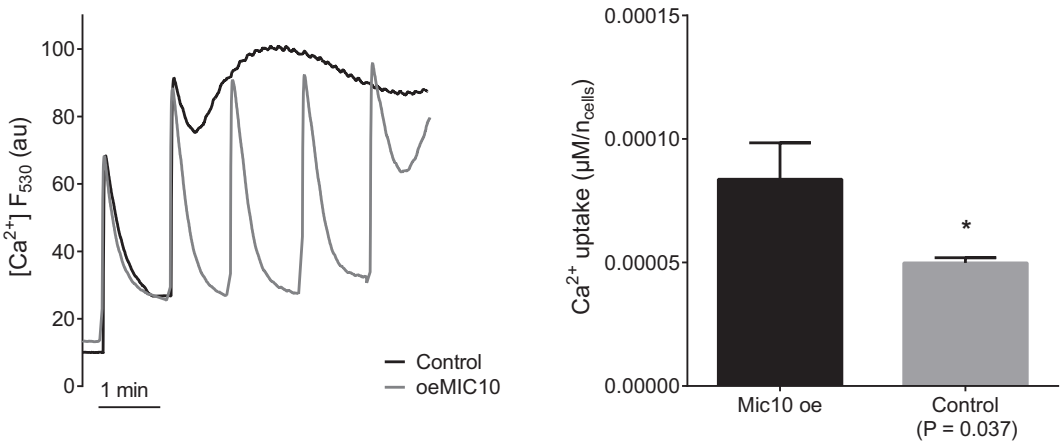

Figure 3.26: Mitochondrial Ca^{2+} uptake upon Mic10 overexpression in Hek cells measured by Calcium Green: representative tracings of time course measurement of fluorescence signal given in ratio between added Ca^{2+} to cell number (left panel), maximum capacity shown in right panel, n=4, * for significant differences according to t-test, $p < 0.05$.

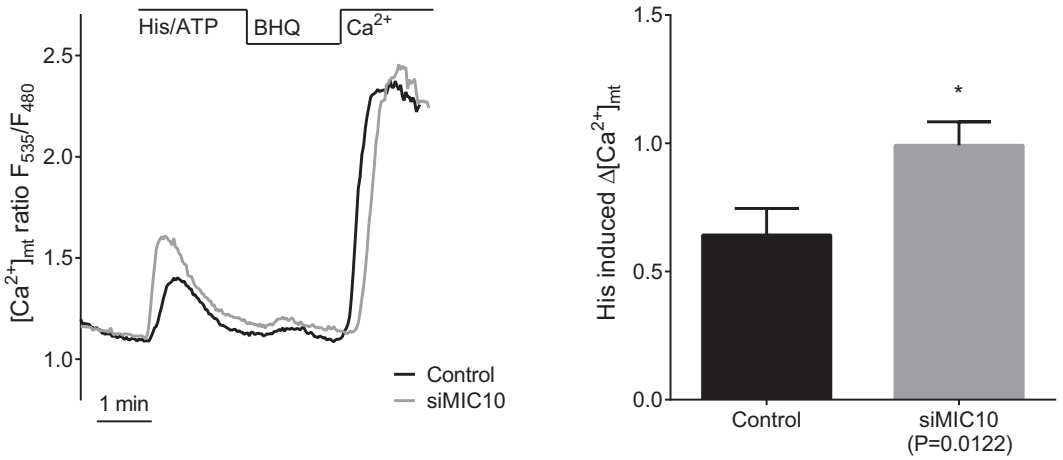

Figure 3.27: Mitochondrial Ca^{2+} uptake upon Mic10 knock-down in HeLa cells measured by 4mtD3cpv: Time course (left panel) of fluorescence signal as ratio and delta of Ca^{2+} uptake after IP3R stimulation compared to basal levels (right panel), n=5, 26-47 cells, * for significant differences according to t-test, $p < 0.05$.

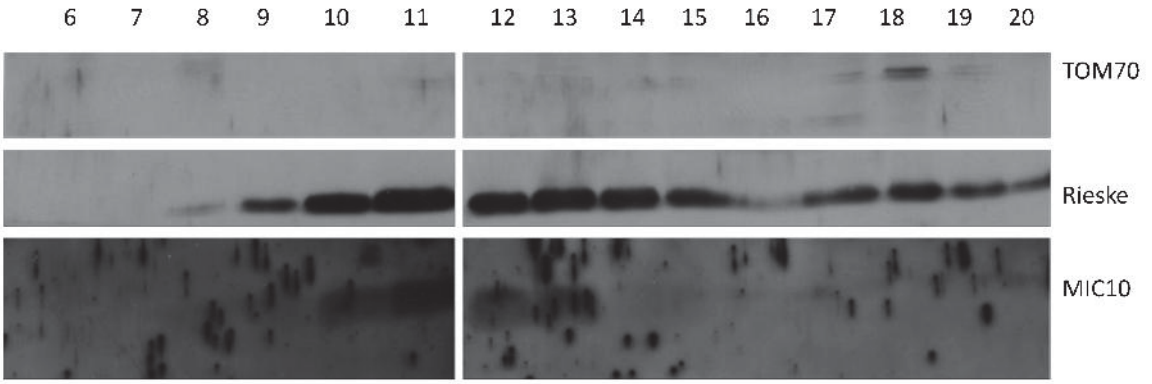

Figure 3.28: Size exclusion analysis showed Mic10 to be part of a supercomplex, SEC fractions were separated on an SDS-gel, left to right from large to small protein sizes; example gels, blotted against Mic10 vs. controls Tom70 and RIESKE.

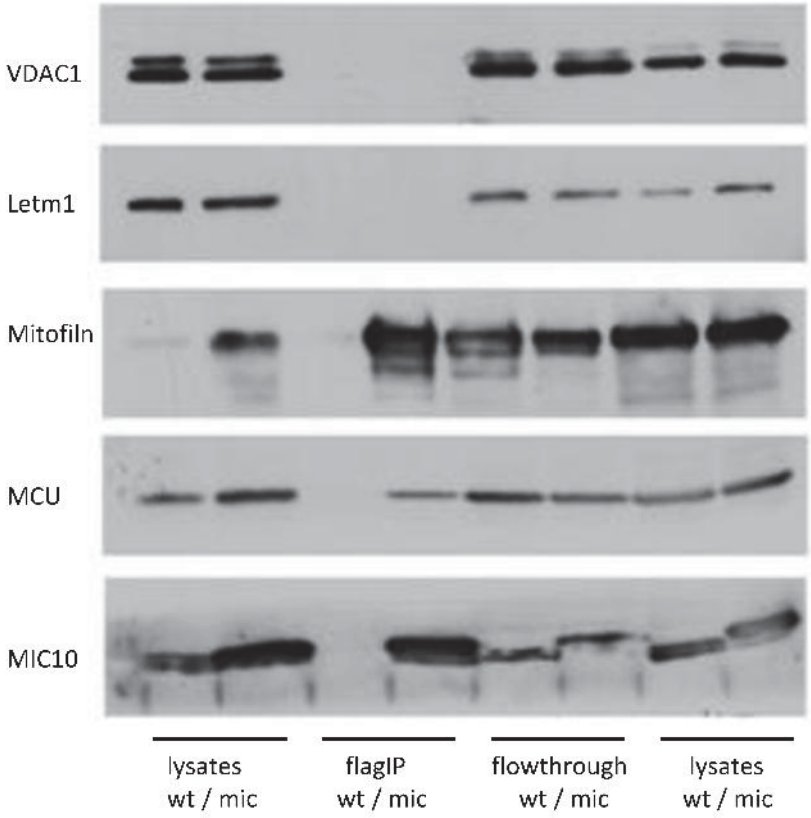

Figure 3.29: Western Blot analysis of Mic10 pull-down: mitochondrial fractions and FLAG immunoprecipitates of WT cells and cells stably overexpressing Mic10-FLAG, blotted against Letm1, VDAC, MCU, control NdufB8 and Mic10, representative for n−3.

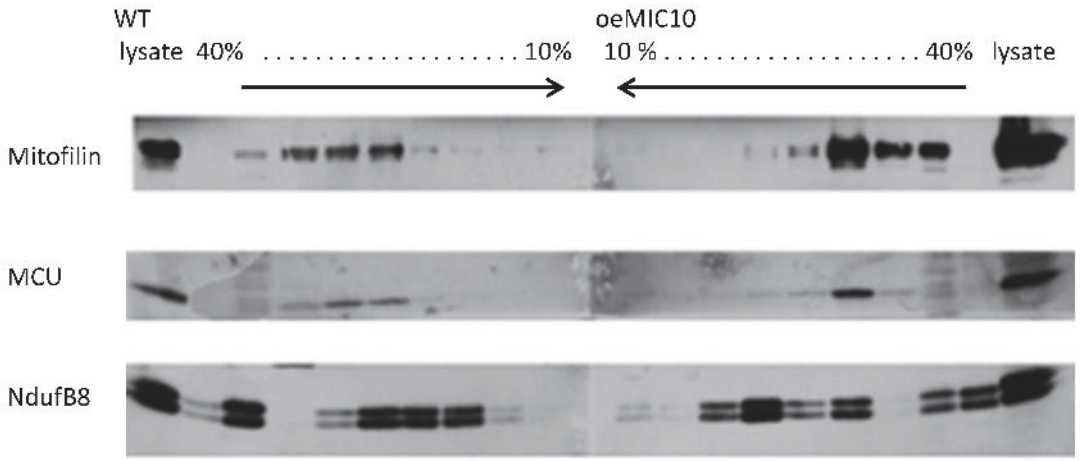

Figure 3.30: Western Blot analysis of size-separated mitochondrial fractions upon Mic10 overexpression: gradient separated fractions of mitochondria from WT cells and cells stably overexpressing Mic10-FLAG; example gel blotted against MCU, control NdufB8 and Mitofilin.

size (kDa)	intensity	IP elements
70-100	medium	IMMT, CCDC160
70-90	weak	IMMT, GRP75, DnaJ-C11, ANM5
60	medium	CHCH3, ZRAB3, MTG16
50-70	medium	ATPase
45	strong	KV201, ASAP2, YG001, I12R2, C10orf88
30	moderate	VDAC1, PHB2, ATPG, NMD3A
25	moderate	ADP/ATP translocase, PHB, ASAP2, Spectrin, NMD3A

Table 3.2: Mass spectrometric analysis of Mic10 pull-down: proteins from cut bands at specified size (kDa), band quantity given as qualified intensity after protein staining, pulled down proteins recognized by MS (IP elements)

4. Discussion

4.1 Assessing mitochondrial Ca^{2+} uptake in mitochondrial populations

There are various methods for assessing Ca^{2+} transfer into mitochondria, altogether exhibiting their respective advantages and disadvantages.

Permeabilization methods offer the possibility to "open" a cell and easily access organelles while maintaining mitochondrial morphology without removing the "natural" surroundings of the organelles. As mentioned before, mitochondria interact with other organelles and in order to fully function they require a more or less intact cellular system. There are multiple permeabilization reagents, regardless of other methods such as electroporation, affecting lipid membranes at different magnitudes depending on the lipid backbones building up the membranes. In general, there are organic solvents which dissolve lipids but denature proteins and there are detergents which for example selectively interact with cholesterol in case of saponins but there are also other more unselective detergents such as triton [118]. Digitonin, as example detergent of the saponin family, has three times the size of cholesterol and disrupts the lipid bilayers by its intercalation into cholesterol-rich cellular membranes. Since the lipid components within the mitochondrial membranes differ from the ones in plasma membranes, the plasma membrane can be primarily targeted for permeabilization without attacking the mitochondria. The ratio of cholesterol to total phospholipids in intracellular membranes is about 0.1 compared to a ratio of 1 for the plasma membrane [119]. Still, the OMM contains higher amounts of cholesterol compared to the IMM and can be more easily disrupted by digitonin after permeabilization of the plasma membrane [120]. After all, digitonin can be utilized for plasma membrane permeabilization but even so for purification treatment after organelle isolation. Yet, one has to keep in mind that a high concentration of the detergent will ultimately lead to intracellular membrane

lysis, too.

Organelle isolation can be readily applied for various samples including primary cells from organs and tissues without having to set up a laborious suitable protocol for permeabilization. However, mitochondrial isolation leads to altered mitochondrial morphology, loss of soluble proteins up to degradation of matrix proteins, and therefore, altered function [121]. Above all, isolated mitochondria have lost their natural environment and interaction to cellular compartments. Still, isolating mitochondria offers the possibility to directly study mitochondrial channel characteristics using the method of mitoplast patch clamping, shortly called mitopatching, as discussed later in section 4.2.

Using sensors outside of mitochondria, as calcium green, represents a method for indirect measurement of mitochondrial Ca^{2+} uptake. Indirect evaluation denotes the procedure of correlating signals to the investigated determinants which are, by that matter, not directly detected. Using the method of calcium green in permeabilized cells or on isolated mitochondria, one has to keep in mind that preparation procedures could affect mitochondrial purity alike mitochondrial function. Moreover, the availability of free Ca^{2+} inside the mitochondrial matrix is subject to mitochondrial phosphate content. Therefore, mitochondrial Ca^{2+} uptake capacity and mitochondrial transition pore opening is also related to the supply of mitochondrial phosphate.

Direct measurement of Ca^{2+} changes within the mitochondrial Ca^{2+} matrix offers the possibility to investigate selected organelles in their natural surroundings involving cellular Ca^{2+} signaling. Next to chemical sensors, the comparison of two different types of protein based biosensors targeted to mitochondria highlights their advantages and disadvantages. Using this method highly sensitive modes of mitochondrial Ca^{2+} uptake could be detected which were not observed before using chemical sensors on isolated mitochondria or permeabilized cells. As shown in figures 3.5 and 3.6, the most sensor sensitivity regarding low Ca^{2+} concentrations could be achieved by combining the procedures of permeabilization and direct mitochondrial Ca^{2+} measurement in single cells via mtRP and high-speed fluorescence microscopy. In case of mtRP the sensor signal early turned saturated at low Ca^{2+} concentration whereas larger Ca^{2+} accumulation could be monitored by calcium green. This comparison between two approaches of measuring mitochondrial Ca^{2+} uptake in permeabilized cells, either on the single cell level or in population, demonstrates the distinct output underlying a specific method.

Certainly, ratiometric pericam mtRP holds the name but, indeed, does not feature ratiometry. In contrast, 4mtD3cpv could be used ratiometrically to determine basal levels of Ca^{2+} within the mitochondrial matrix. Though mtRP was designed to be ratiometric, its second excitation wavelength originally designed to selectively respond to Ca^{2+} changes, could be allocated to simultaneous pH sensing. Besides, mitochondrial cameleon 4mtD3cpv did not feature the same targeting specificity as mtRP even though it possesses more targeting sequences than mtRP. This could be due to size and steric problems of recognition sequences, since cameleons consist of two fluorescent proteins instead of only one permutated fluorescent protein in mtRP.

Mitochondrial Ca^{2+} uptake measured in permeabilized cells either indirectly or directly exhibited distinct sensitivities as well as capacities as shown before in Figures 3.5 and 3.6. These results can be translated as to high and low Ca^{2+} sensitive pathways and distinct mitochondrial Ca^{2+} uptake modes. The question remains whether those pathways are based on a variable set of proteins around a main channel, differently regulated, or distinct channels acting without the other.

Each method comprises its own way of assessing mitochondrial Ca^{2+} signaling. Depending on the actual question of the scientific problem, one given method could be more suitable and preferentially applied over the others. In spite of the above mentioned advantages and disadvantages assessment of mitochondrial Ca^{2+} uptake is preferentially accomplished by multiple methods. Utilization of several methods at once also circumvents possible conflicts within method-specific generated data.

4.2 Distinct channels identified by mitopatching

Using the technique of mitopatching we highlighted distinct amplitudes as the basis for the existence of multiple mitochondrial Ca^{2+} currents in HeLa and Ea.Hy cells. Experiments were executed under Ca^{2+} and Cl^- in the patch pipette and presumably in the mitochondrial matrix. Control experiments using reduced Cl^- levels in patch buffer of pipette solution as well as Cl^- channel blockers, and additionally, K^+ channel inhibitors did not change the observation of multiple conductances, and therefore, underpins the idea of distinct mitochondrial Ca^{2+} currents. As the case may be, two distinct voltage-gated Ca^{2+} channels have been identified before in human cardiomyocytes [122]. However, the different conductances of currents recorded in mitoplast-attached configuration could result from different channels as well as different modes of

one given mitochondrial Ca^{2+} channel [94] and would not necessarily point to multiple channels.

The recorded currents in HeLa cells could be subdivided into the i-MCC, b-MCC and xl-MCC at different rates in occurrence. Additionally, a small current was observed in Ea.Hy cells. Together, mitoplasts from both Ea.Hy and HeLa cells exhibited the most frequently observed intermediate mitochondrial Ca^{2+} current. The i-MCC also supports mitopatch data from other cell-types [122]. The b-MCC was still frequently recorded in mitoplasts from HeLa cells while tracings from the xl-MCC were rarely distinguished. Addition of 1 µM ruthenium red, inhibitor of MCU, affected all observed currents in terms of reduced conductance, and 10 µM ruthenium red largely diminished occurrence of i-MCC and b-MCC and completely abolished xl-MCC, while at a higher concentration of MCU inhibitor at 30 µM there was no single channel activity at all [113].

However, mitoplasts used in patch experiments were not devoid of OMM proteins, as shown in Figure 3.12 . Furthermore, isolation of mitochondria can not provide 100% clean outcome of the single organelles, but rather yields side-contamination of other organelles and membranes. This fact has to be kept in mind during the evaluation of current statistics, since inhomogenities within single experiments could point to channel activity from contaminating membranes stuck to the swollen mitochondria. Further cleaning steps during the isolation and mitoplast formation procedure, as additional actions of washing and centrifugation or even sonication, did not result into different observations during patch experiments but did greatly decrease the yield of mitoplasts. Still, patching mitoplasts required manual selection of the swollen organelle under the microscope and renders a case of targeting other organelles than mitochondria highly unlikely.

The occurrence probability of individual single channel activites in mitoplasts was determined upon MCU knock-down. The number of active patches upon MCU knock-down was greatly reduced which supports the idea of MCU as the core protein for mitochondrial Ca^{2+} uptake. Above all, the occurrence probability of i-MCC channel activity was significantly reduced. Overall, stable knock-down of MCU decreased Ca^{2+} currents in whole-mitoplasts as well as Na^{+} currents, which is in line with the recent finding of MCU to channel Na^{+} in the absence of divalent cations [123]. Thereby, patching mitoplasts from MCU knock-down cells, shown in Figure 3.20 highlights the i-MCC underlying the mitochondrial calcium uniporter protein as the occurrence of i-MCC was greatly reduced. Still, regarding the reduced total single channel activity,

mitoplasts from HeLa cells exhibited an increased occurrence probability of xl-MCC activity upon MCU knock-down. This observation supports the assumption about the existence of multiple Ca^{2+} channeling proteins. The protein underlying xl-MCC could refer to a Ca^{2+} uptake mode independent from MCU. From a physiological point of view, additional Ca^{2+} channeling proteins could compensate a dysfunction of MCU under pathophysiological conditions, since Ca^{2+} signaling and, therefore, mitochondrial Ca^{2+} handling determines cell survival.

Altogether, data obtained from patching mitoplasts indicates a complex machinery behind mitochondrial Ca^{2+} uptake involving multiple modes of mitochondrial Ca^{2+} sequestration.

4.3 Multiple proteins involved in mitochondrial Ca^{2+} uptake

In regard to the contribution of various proteins to mitochondrial Ca^{2+} uptake [103, 96, 94, 95], mitochondria targeted biosensors and fluorescence microscopy were performed on single cells in combination with siRNA-mediated knock-down of the individual proteins. Except for MCU, which was introduced as the main Ca^{2+} channel since its discovery, the investigated proteins were primarily suggested to modulate Ca^{2+} entry into mitochondria. However, as experiments of patching mitoplasts have shown, there are multiple distinct currents within certain cell-types, which were not molecularly uncovered so far [113, 95]. In this regard, we highlighted that reduced expression of UCP2/3 lead to decreased mitochondrial Ca^{2+} uptake upon IP3-mediated release of intracellular Ca^{2+}, which constitutes an important intracellular signaling mechanism. Likewise, siRNA-based knock-down of Letm1 reduced mitochondrial Ca^{2+} uptake upon Ca^{2+} reentry after emptying the cellular Ca^{2+} supply. Letm1 and UCP2/3 were therefore demonstrated to play part in different types of mitochondrial Ca^{2+} uptake routes and furthermore to conduct Ca^{2+} transfer at dissimilar Ca^{2+} concentrations [103]. Notably, overexpression of UCP2/3 increased mitochondrial Ca^{2+} uptake upon both types of Ca^{2+} sequestration while Letm1 overexpression was without any significant effect. Experiments on permeabilized cells provide the possibility to directly adjust cytosolic Ca^{2+} levels and thereby changing from a so-called high to low Ca^{2+} concentration. IP3-mediated Ca^{2+} release from the ER creates Ca^{2+}-rich microdomains at the mitochondrial surface around the respective MAMs which makes UCP2/3 respond to higher

Ca^{2+} levels. Knock-down of UCP2/3 reduced mitochondrial Ca^{2+} uptake at high Ca^{2+} levels, whereas Letm1 knock-down only affected a decrease in Ca^{2+} uptake upon minor Ca^{2+} addition. The response to low Ca^{2+} levels matches buffering at weakly elevated cytosolic Ca^{2+} levels. These data are consistent with overexpression experiments in intact cells. Letm1 is considered to function sensitively at low Ca^{2+} raises, while its overexpression would thereby not lead to significant changes regarding maximal Ca^{2+} uptake rates, which are more likely to be facilitated by UCP2/3.
Furthermore, both Letm1 and UCP2/3 were shown to facilitate Ca^{2+} transfer into mitochondria by MCU [94]. In more detail, the contribution of Letm1 or UCP3 depends on the activity of SERCA or rather the time-dependent supply of extramitochondrial Ca^{2+} and the formation of local Ca^{2+} microdomains. Inhibition of SERCA affects an attenuated Ca^{2+} release which abrogates the before described Ca^{2+} hot spots.

MCU was shown to form a multi-protein complex involving several regulatory proteins. MICU1 was the first protein postulated to regulate mitochondrial Ca^{2+} influx. In line with recent publications, we assessed siRNA-mediated knock-down of MICU1 in HeLa cells which lead to increased basal Ca^{2+} levels within mitochondria. For some time, this impact of MICU1 had not been recognized due to the fact that non-ratiometric sensors were widely used and the evaluation of fluorescence signals were mostly calculated as a ratio to initial fluorescence in order to correct for photobleaching and inhomogeneous signals among single cells. However, the utilization of 4mtD3cpv disclosed the changed mitochondrial Ca^{2+} content upon reduced levels of MICU1, whereat, certain protocols as the application of SERCA inhibitors would also suggest a Ca^{2+} influx modulation by MICU1. Recently, MCU was shown to channel Ca^{2+} into mitochondria by the accessory of EMRE1 only [33]. Thereby, mitochondrial Ca^{2+} uptake does not require the involvement of MICU1/2. However, it was further shown, that these proteins pose important regulators for the fine-tuning of mitochondrial Ca^{2+} sequestration with MICU1 as a gatekeeper and MICU2 as a negative regulator [124]. This regulatory backbone is required to ensure intact metabolism and ATP production and preventing dysregulated Ca^{2+} signaling affected pathophysiological conditions up to cell death.

4.3.1 Assessing mitochondrial Ca^{2+} uptake by means of respiratory rates

Furthermore, next to standard techniques for studying mitochondrial Ca^{2+} uptake, indirect assessment of mitochondrial Ca^{2+} sequestration can be accomplished by measurement of oxygen consumption. This technique is mainly used for determining mitochondrial dysfunction. In order to define the role of the examined proteins, cells were transiently transfected for knocking down Letm1 or UCP2/3. This transient transfection procedure poses the main problem when experimenting on population of cells that can not be distinguished if positively transfected or not. Mitochondrial Ca^{2+} uptake was decreased but was not diminished upon knock-down of the individual proteins. Residual Ca^{2+} uptake was sufficient to induce an increase in oxygen consumption rates. More significant results could be obtained using stably transfected cells or through cell sorting. Still, Ca^{2+} transfer to mitochondria effected by UCPs and Letm1 as shown before, cannot be equated with mitochondrial Ca^{2+} uptake through MCU. UCPs were demonstrated to be mainly involved in Ca^{2+} uptake from Ca^{2+}-rich microdomains and were negated to contribute to Ca^{2+} transfer from cytosol to mitochondria at general raises of cytosolic Ca^{2+} levels. Whereas, Letm1 alone was shown to contribute to Ca^{2+} uptake at low concentrations without high capacity abilities.

4.4 MICOS contributes to mitochondrial Ca^{2+} handling

Mitochondrial dynamics define the networking mitochondrial structure which is fundamental for mitochondrial function. Both mitochondrial function and structure related fission are regulated by Ca^{2+} signaling, and additionally, mitochondrial Ca^{2+} handling is determined by mitochondrial structure [125]. In regard to structure-dependent Ca^{2+} sequestration by mitochondria, the mitochondrial contact site and cristae organizing system was investigated for its participation in the regulation of mitochondrial Ca^{2+} handling. So far, Opa1 was highlighted to modulate mitochondrial Ca^{2+} sequestration and Drp1 was shown to be affected by MCU activity. For that matter, MCU was recently suggested to be involved in mitochondrial fission indirectly by modulating calcineurin activity [9].

Interfering with MICOS protein complexes by changing expression levels of Mic10 lead to altered mitochondrial Ca^{2+} handling. In detail, decreased levels of Mic10 en-

hanced mitochondrial Ca^{2+} uptake upon IP3-mediated Ca^{2+} release from the ER. This phenomenom could involve MICOS in the formation of MAMs at the basis of MICOS interaction to mitochondrial fusion proteins. Notably, increased levels of Mic10 did not significantly change mitochondrial structure and cristae formation. Notwithstanding, though structure did not seem to be effected, mitochondrial capacity was largely increased. This observation integrates Mic10 in the formation of the mitochondrial transition pore. Particularly, proteomic data supports this concept by possible interaction between Mic10 and VDAC. Still, the question remains, if Mic10 is directly involved in mitochondrial Ca^{2+} handling. Next to proteomic analysis of Mic10, as discussed beneath, further functional characterization of Mic10 would be necessary to clarify the details behind.

Mic10 was discovered through an bioinformatic search for regulatory proteins of the ATP synthase. Consecutively, an interaction between those proteins could not be verified. Instead Mic10 was introduced as novel component of the MICOS complex involving the known constituent Mic60 (mitofilin). Notably, our mass spectromic analysis of Mic10 immunoprecipitates included ATPase, that may account for shifting interaction partners underlying mitochondrial dynamics. Furthermore, these Mic10 pull-down experiments indicated MCU or VDAC as part of the immunoprecipitated protein aggregate around MICOS. Still, either MCU or VDAC were detected exclusively. However, ASAP2, a protein interacting with Pyk2, which was recently postulated to induce MCU channel formation, was detected next to VDAC via MS in the Mic10 pull-down sample. Considering data obtained by immunoprecipitation procedures, proteins identified together with the investigated target could be proteins accumulated in the neighborhood or indeed interaction partners or even constituents of one large protein complex. By all means, these possible novel interactions of Mic10 with mitochondrial Ca^{2+} channeling proteins could be alternating depending on the functional needs to ensure intact mitochondrial metabolism and cell survival.

4.5 Conclusion

Within the recent years, we assessed various approaches for studying mitochondrial Ca^{2+} uptake [96]. By using multiple different methods, we have demonstrated several proteins and pathways underlying the Ca^{2+} transfer into mitochondria [103, 94]. In this regard, we have highlighted distinct mitochondrial Ca^{2+} currents [113, 95].

In conclusion, Ca^{2+} sequestration by mitochondria poses a fundamental signaling process that determines the cell's fate in health and disease involving mitochondrial metabolism as well as mitochondrial structure concertedly. Experiments discussed herein indicate multiple Ca^{2+} influx pathways underlying a variable set of individual as well as associated components in regulation of or by this signaling ion. This complex Ca^{2+} signaling machinery will be target of future molecular medicine and therapies against several diseases underlying mitochondrial dysfunction.

Bibliography

[1] Alberts B, Johnson A, Lewis J, Raff M, Roberts K, Walter P. Molecular biology of the cell. vol. 4. Garland Science; 2002.

[2] Kitami T, Logan DJ, Negri J, Hasaka T, Tolliday NJ, Carpenter AE, et al. A chemical screen probing the relationship between mitochondrial content and cell size. PloS one. 2012;7(3):e33755.

[3] Weber NE. Ultrastructural studies of beef heart mitochondria. 3. The inequality of gross morphological change and oxidative phosphorylation. The Journal of cell biology. 1972;55(2):457–70.

[4] Zinser E, Sperka-Gottlieb CD, Fasch EV, Kohlwein SD, Paltauf F, Daum G. Phospholipid synthesis and lipid composition of subcellular membranes in the unicellular eukaryote Saccharomyces cerevisiae. Journal of bacteriology. 1991;173(6):2026–34.

[5] Gohil VM, Greenberg ML. Mitochondrial membrane biogenesis: phospholipids and proteins go hand in hand. The Journal of cell biology. 2009;184(4):469–72.

[6] Osman C, Voelker DR, Langer T. Making heads or tails of phospholipids in mitochondria. The Journal of cell biology. 2011;192(1):7–16.

[7] Vance JE. Phospholipid synthesis in a membrane fraction associated with mitochondria. The Journal of biological chemistry. 1990;265(13):7248–56.

[8] Smirnova E, Griparic L, Shwebsiteand DL, van der Bliek AM. Dynamin-related protein Drp1 is required for mitochondrial division in mammalian cells. Molecular biology of the cell. 2001;12(8):2245–56.

[9] Liang N, Wang P, Wang S, Li S, Li Y, Wang J, et al. Role of mitochondrial calcium uniporter in regulating mitochondrial fission in the cerebral cortexes of living rats. Journal of neural transmission (Vienna, Austria : 1996). 2014;.

[10] Alexander C, Votruba M, Pesch UE, Thiselton DL, Mayer S, Moore A, et al. OPA1, encoding a dynamin-related GTPase, is mutated in autosomal dominant optic atrophy linked to chromosome 3q28. Nature genetics. 2000;26(2):211–5.

[11] Delettre C, Lenaers G, Griffoin JM, Gigarel N, Lorenzo C, Belenguer P, et al. Nuclear gene OPA1, encoding a mitochondrial dynamin-related protein, is mutated in dominant optic atrophy. Nature genetics. 2000;26(2):207–10.

[12] Fülöp L, Szanda G, Enyedi B, Várnai P, Spät A. The effect of OPA1 on mitochondrial Ca^{2+} signaling. PloS one. 2011;6(9):e25199.

[13] Yoon Y, Krueger EW, Oswald BJ, McNiven MA. The mitochondrial protein hFis1 regulates mitochondrial fission in mammalian cells through an interaction with the dynamin-like protein DLP1. Molecular and cellular biology. 2003;23(15):5409–20.

[14] Gandre-Babbe S, van der Bliek AM. The novel tail-anchored membrane protein Mff controls mitochondrial and peroxisomal fission in mammalian cells. Molecular biology of the cell. 2008;19(6):2402–12.

[15] Palou A, Picó C, Bonet ML, Oliver P. The uncoupling protein, thermogenin. The international journal of biochemistry & cell biology. 1998;30(1):7–11.

[16] Rousset S, Alves-Guerra MC, Mozo J, Miroux B, Cassard-Doulcier AM, Bouillaud F, et al. The biology of mitochondrial uncoupling proteins. Diabetes. 2004;53 Suppl 1:S130–5.

[17] Murphy MP. How mitochondria produce reactive oxygen species. The Biochemical journal. 2009;417(1):1–13.

[18] Gunter TE, Gunter KK. Uptake of calcium by mitochondria: transport and possible function. IUBMB life. 2001;52(3-5):197–204.

[19] Trenker M, Malli R, Fertschai I, Levak-Frank S, Graier WF. Uncoupling proteins 2 and 3 are fundamental for mitochondrial Ca^{2+} uniport. Nature Cell Biology. 2007;9(4):445–452.

[20] Jiang D, Zhao L, Clapham DE. Genome-wide RNAi screen identifies Letm1 as a mitochondrial Ca^{2+}/H+ antiporter. Science. 2009;326(5949):144–147.

[21] Palty R, Silverman WF, Hershfinkel M, Caporale T, Sensi SL, Parnis J, et al. NCLX is an essential component of mitochondrial Na+/Ca^{2+} exchange. Proceedings of the National Academy of Sciences. 2010;107(1):436–441.

[22] Perocchi F, Gohil VM, Girgis HS, Bao XR, McCombs JE, Palmer AE, et al. MICU1 encodes a mitochondrial EF hand protein required for Ca^{2+} uptake. Nature. 2010;467(7313):291–296.

[23] Baughman JM, Perocchi F, Girgis HS, Plovanich M, Belcher-Timme CA, Sancak Y, et al. Integrative genomics identifies MCU as an essential component of the mitochondrial calcium uniporter. Nature. 2011;476(7360):341–345.

[24] Raffaello A, De Stefani D, Sabbadin D, Teardo E, Merli G, Picard A, et al. The mitochondrial calcium uniporter is a multimer that can include a dominant-negative pore-forming subunit. The EMBO journal. 2013;32(17):2362–2376.

[25] Plovanich M, Bogorad RL, Sancak Y, Kamer KJ, Strittmatter L, Li AA, et al. MICU2, a paralog of MICU1, resides within the mitochondrial uniporter complex to regulate calcium handling. PLoS One. 2013;8(2):e55785.

[26] Sancak Y, Markhard AL, Kitami T, Kovács-Bogdán E, Kamer KJ, Udeshi ND, et al. EMRE is an essential component of the mitochondrial calcium uniporter complex. Science. 2013;342(6164):1379–1382.

[27] Feng S, Li H, Tai Y, Huang J, Su Y, Abramowitz J, et al. Canonical transient receptor potential 3 channels regulate mitochondrial calcium uptake. Proceedings of the National Academy of Sciences. 2013;110(27):11011–11016.

[28] Mallilankaraman K, Cárdenas C, Doonan PJ, Chandramoorthy HC, Irrinki KM, Golenár T, et al. MCUR1 is an essential component of mitochondrial Ca^{2+} uptake that regulates cellular metabolism. Nature cell biology. 2012;14(12):1336–1343.

[29] Hoffman NE, Chandramoorthy HC, Shanmughapriya S, Zhang XQ, Vallem S, Doonan PJ, et al. SLC25A23 augments mitochondrial Ca^{2+} uptake, interacts with MCU, and induces oxidative stress-mediated cell death. Molecular biology of the cell. 2014;25(6):936–947.

[30] Vasington FD, Gazzotti P, Tiozzo R, Carafoli E. The effect of ruthenium red on Ca^{2+} transport and respiration in rat liver mitochondria. Biochimica et Biophysica Acta (BBA)-Bioenergetics. 1972;256(1):43–54.

[31] Kirichok Y, Krapivinsky G, Clapham DE. The mitochondrial calcium uniporter is a highly selective ion channel. Nature. 2004;427(6972):360–364.

[32] Chaudhuri D, Sancak Y, Mootha VK, Clapham DE. MCU encodes the pore conducting mitochondrial calcium currents. Elife. 2013;2.

[33] Kovács-Bogdán E, Sancak Y, Kamer KJ, Plovanich M, Jambhekar A, Huber RJ, et al. Reconstitution of the mitochondrial calcium uniporter in yeast. Proceedings of the National Academy of Sciences. 2014;p. 201400514.

[34] Uzhachenko R, Ivanov S, Yarbrough WG, Shanker A, Medzhitov R, Ivanova AV. Fus1/Tusc2 is a novel regulator of mitochondrial calcium handling, Ca^{2+}-coupled mitochondrial processes and Ca^{2+}-dependent NFAT-and NFkB-pathways in CD4+ T cells. Antioxidants & redox signaling. 2014;1(20):1533–47.

[35] Pan X, Liu J, Nguyen T, Liu C, Sun J, Teng Y, et al. The physiological role of mitochondrial calcium revealed by mice lacking the mitochondrial calcium uniporter. Nature cell biology. 2013;15(12):1464–72.

[36] Joiner MLA, Koval OM, Li J, He BJ, Allamargot C, Gao Z, et al. CaMKII determines mitochondrial stress responses in heart. Nature. 2012;491(7423):269–73.

[37] O-Uchi J, Jhun BS, XU S, Hurst S, Raffaello A, Liu X, et al. Adrenergic signaling regulates mitochondrial Ca 2+ uptake through Pyk2-dependent tyrosine phosphorylation of the mitochondrial Ca 2+ uniporter. Antioxidants & Redox Signaling;(ja).

[38] Záckova M, Jezek P. Reconstitution of novel mitochondrial uncoupling proteins UCP2 and UCP3. Bioscience reports. 2002;22(1):33–46.

[39] Vozza A, Parisi G, De Leonardis F, Lasorsa FM, Castegna A, Amorese D, et al. UCP2 transports C4 metabolites out of mitochondria, regulating glucose and glutamine oxidation. Proceedings of the National Academy of Sciences. 2014;111(3):960–965.

[40] Liu L, Liu J, Tian XY, Wong WT, Lau CW, Xu A, et al. Uncoupling Protein-2 Mediates DPP-4 Inhibitor-Induced Restoration of Endothelial Function in Hypertension through Reducing Oxidative Stress. Antioxidants & redox signaling. 2013;Epub ahead of print.

[41] Rupprecht A, Sittner D, Smorodchenko A, Hilse KE, Goyn J, Moldzio R, et al. Uncoupling Protein 2 and 4 Expression Pattern during Stem Cell Differentiation Provides New Insight into Their Putative Function. PloS one. 2014;9(2):e88474.

[42] Jia JJ, Zhang X, Ge CR, Jois M. The polymorphisms of UCP2 and UCP3 genes associated with fat metabolism, obesity and diabetes. Obesity reviews. 2009;10(5):519–526.

[43] Endele S, Fuhry M, Pak SJ, Zabel BU, Winterpacht A. LETM1, A Novel Gene Encoding a Putative EF-Hand Ca^{2+} Binding Protein, Flanks the Wolf–Hirschhorn Syndrome (WHS) Critical Region and Is Deleted in Most WHS Patients. Genomics. 1999;60(2):218–225.

[44] Tsai MF, Jiang D, Zhao L, Clapham D, Miller C. Functional reconstitution of the mitochondrial Ca^{2+}/H+ antiporter Letm1. The Journal of general physiology. 2014;143(1):67–73.

[45] Tamai S, Iida H, Yokota S, Sayano T, Kiguchiya S, Ishihara N, et al. Characterization of the mitochondrial protein LETM1, which maintains the mitochondrial tubular shapes and interacts with the AAA-ATPase BCS1L. Journal of cell science. 2008;121(15):2588–2600.

[46] Messina A, Reina S, Guarino F, De Pinto V. VDAC isoforms in mammals. Biochimica et Biophysica Acta (BBA)-Biomembranes. 2012;1818(6):1466–1476.

[47] Colombini M, Blachly-Dyson E, Forte M. VDAC, a channel in the outer mitochondrial membrane. In: Ion channels. Springer; 1996. p. 169–202.

[48] De Pinto V, Reina S, Guarino F, Messina A. Structure of the voltage dependent anion channel: state of the art. Journal of bioenergetics and biomembranes. 2008;40(3):139–147.

[49] Huang H, Hu X, Eno CO, Zhao G, Li C, White C. An Interaction between Bcl-xL and the Voltage-dependent Anion Channel (VDAC) Promotes Mitochondrial Ca^{2+} Uptake. Journal of Biological Chemistry. 2013;288(27):19870–19881.

[50] Zhang CY, Parton LE, Ye CP, Krauss S, Shen R, Lin CT, et al. Genipin inhibits UCP2-mediated proton leak and acutely reverses obesity-and high glucose-induced β cell dysfunction in isolated pancreatic islets. Cell Metabolism. 2006;3(6):417–427.

[51] Kiyonaka S, Kato K, Nishida M, Mio K, Numaga T, Sawaguchi Y, et al. Selective and direct inhibition of TRPC3 channels underlies biological activities of a pyrazole compound. Proceedings of the National Academy of Sciences. 2009;106(13):5400–5405.

[52] Carafoli E, Tiozzo R, Lugli G, Crovetti F, Kratzing C. The release of calcium from heart mitochondria by sodium. Journal of molecular and cellular cardiology. 1974;6(4):361–371.

[53] Scorziello A, Savoia C, Sisalli MJ, Adornetto A, Secondo A, Boscia F, et al. NCX3 regulates mitochondrial Ca^{2+} handling through the AKAP121-anchored signaling complex and prevents hypoxia-induced neuronal death. Journal of cell science. 2013;126(24):5566–5577.

[54] Brenner C, Moulin M. Physiological roles of the permeability transition pore. Circulation research. 2012;111(9):1237–1247.

[55] Miura T, Tanno M. The mPTP and its regulatory proteins: final common targets of signalling pathways for protection against necrosis. Cardiovascular research. 2012;94(2):181–189.

[56] Bootman MD. Calcium signaling. Cold Spring Harbor perspectives in biology. 2012;4(7).

[57] Pfanner N, van der Laan M, Amati P, Capaldi RA, Caudy AA, Chacinska A, et al. Uniform nomenclature for the mitochondrial contact site and cristae organizing system. The Journal of cell biology. 2014;204(7):1083–1086.

[58] Han XJ, Lu YF, Li SA, Kaitsuka T, Sato Y, Tomizawa K, et al. CaM kinase Iα–induced phosphorylation of Drp1 regulates mitochondrial morphology. The Journal of cell biology. 2008;182(3):573–585.

[59] Cereghetti G, Stangherlin A, De Brito OM, Chang C, Blackstone C, Bernardi P, et al. Dephosphorylation by calcineurin regulates translocation of Drp1 to mitochondria. Proceedings of the National Academy of Sciences. 2008;105(41):15803–15808.

[60] Hansford RG. Relation between mitochondrial calcium transport and control of energy metabolism. Springer; 1985.

[61] McMillin JB, Madden MC. The role of calcium in the control of respiration by muscle mitochondria. Medicine and science in sports and exercise. 1989;21(4):406–410.

[62] Cogliati S, Frezza C, Soriano ME, Varanita T, Quintana-Cabrera R, Corrado M, et al. Mitochondrial cristae shape determines respiratory chain supercomplexes assembly and respiratory efficiency. Cell. 2013;155(1):160–171.

[63] Deng Y, Marko M, Buttle KF, Leith A, Mieczkowski M, Mannella CA. Cubic Membrane Structure in Amoeba (Chaos carolinensis) Mitochondria Determined by Electron Microscopic Tomography. Journal of structural biology. 1999;127(3):231–239.

[64] von der Malsburg K, Müller JM, Bohnert M, Oeljeklaus S, Kwiatkowska P, Becker T, et al. Dual role of mitofilin in mitochondrial membrane organization and protein biogenesis. Developmental cell. 2011;21(4):694–707.

[65] Paumard P, Vaillier J, Coulary B, Schaeffer J, Soubannier V, Mueller DM, et al. The ATP synthase is involved in generating mitochondrial cristae morphology. The EMBO journal. 2002;21(3):221–230.

[66] Bohnert M, Wenz LS, Zerbes RM, Horvath SE, Stroud DA, von der Malsburg K, et al. Role of mitochondrial inner membrane organizing system in protein biogenesis of the mitochondrial outer membrane. Molecular biology of the cell. 2012;23(20):3948–3956.

[67] Fülöp L, Szanda G, Enyedi B, Várnai P, Spät A. The effect of OPA1 on mitochondrial Ca^{2+} signaling. PloS one. 2011;6(9):e25199.

[68] Berridge MJ. Cell Signaling Pathways. In: Cell Signaling Biology. Biochemical Journal; 2012. Available from: `http://www.biochemj.org/csb`.

[69] Lodish H, Berk A, Zipursky SL, Matsudaira P, Baltimore D, Darnell J, et al. Intracellular ion environment and membrane electric potential. In: Molecular Cell Biology. 4th ed. New York: WH Freeman; 2000. Available from: `http://www.ncbi.nlm.nih.gov/books/NBK21475`.

[70] Chen LB. Mitochondrial membrane potential in living cells. Annual review of cell biology. 1988;4(1):155–181.

[71] Nichols BJ, Denton RM. Towards the molecular basis for the regulation of mitochondrial dehydrogenases by calcium ions. In: Signal Transduction Mechanisms. Springer; 1995. p. 203–212.

[72] Tarasov AI, Griffiths EJ, Rutter GA. Regulation of ATP production by mitochondrial Ca^{2+}. Cell calcium. 2012;52(1):28–35.

[73] Vygodina T, Kirichenko A, Konstantinov AA. Direct Regulation of Cytochrome c Oxidase by Calcium Ions. PloS one. 2013;8(9):e74436.

[74] Szalai G, Krishnamurthy R, Hajnóczky G. Apoptosis driven by IP3-linked mitochondrial calcium signals. The EMBO journal. 1999;18(22):6349–6361.

[75] Cines DB, Pollak ES, Buck CA, Loscalzo J, Zimmerman GA, McEver RP, et al. Endothelial cells in physiology and in the pathophysiology of vascular disorders. Blood. 1998;91(10):3527–3561.

[76] Groschner LN, Waldeck-Weiermair M, Malli R, Graier WF. Endothelial mitochondria—less respiration, more integration. Pflügers Archiv-European Journal of Physiology. 2012;464(1):63–76.

[77] Herzig S, Maundrell K, Martinou JC. Life without the mitochondrial calcium uniporter. Nature cell biology. 2013;15(12):1398–1400.

[78] Qiu J, Tan YW, Hagenston AM, Martel MA, Kneisel N, Skehel PA, et al. Mitochondrial calcium uniporter Mcu controls excitotoxicity and is transcriptionally repressed by neuroprotective nuclear calcium signals. Nature communications. 2013;4.

[79] Schwartz J, Holmuhamedov E, Zhang X, Lovelace GL, Smith CD, Lemasters JJ. Minocycline and doxycycline, but not other tetracycline-derived compounds, protect liver cells from chemical hypoxia and ischemia/reperfusion injury by inhibition of the mitochondrial calcium uniporter. Toxicology and applied pharmacology. 2013;273(1):172–179.

[80] Hajnóczky G, Csordás G, Das S, Garcia-Perez C, Saotome M, Sinha Roy S, et al. Mitochondrial calcium signalling and cell death: Approaches for assessing the role of mitochondrial Ca^{2+} uptake in apoptosis. Cell calcium. 2006;40(5):553–560.

[81] Abeele FV, Skryma R, Shuba Y, Van Coppenolle F, Slomianny C, Roudbaraki M, et al. Bcl-2-dependent modulation of Ca^{2+} homeostasis and store-operated channels in prostate cancer cells. Cancer cell. 2002;1(2):169–179.

[82] Roderick HL, Cook SJ. Ca2+ signalling checkpoints in cancer: remodelling Ca2+ for cancer cell proliferation and survival. Nature Reviews Cancer. 2008;8(5):361–375.

[83] Kohn EC, Alessandro R, Spoonster J, Wersto RP, Liotta LA. Angiogenesis: role of calcium-mediated signal transduction. Proceedings of the National Academy of Sciences. 1995;92(5):1307–1311.

[84] Lovat F, Valeri N, Croce CM. MicroRNAs in the pathogenesis of cancer. In: Seminars in oncology. vol. 38. Elsevier; 2011. p. 724–733.

[85] Marchi S, Lupini L, Patergnani S, Rimessi A, Missiroli S, Bonora M, et al. Downregulation of the mitochondrial calcium uniporter by cancer-related miR-25. Current Biology. 2013;23(1):58–63.

[86] Esteves P, Pecqueur C, Ransy C, Esnous C, Lenoir V, Bouillaud F, et al. Mitochondrial retrograde signaling mediated by UCP2 inhibits cancer cell proliferation and tumorigenesis. Cancer research. 2014;74:1–12.

[87] Johnson I, Spence M. The molecular probes handbook. A Guide to Fluorescent Probes and Labeling Technologies. 2010;11.

[88] Shimomura O, Johnson FH, Saiga Y. Extraction, purification and properties of aequorin, a bioluminescent protein from the luminous hydromedusan, Aequorea. Journal of cellular and comparative physiology. 1962;59(3):223–239.

[89] Shimomura O. Structure of the chromophore of Aequorea green fluorescent protein. Febs Letters. 1979;104(2):220–222.

[90] Baird GS, Zacharias DA, Tsien RY. Circular permutation and receptor insertion within green fluorescent proteins. Proceedings of the National Academy of Sciences. 1999;96(20):11241–11246.

[91] Ha T, Enderle T, Ogletree D, Chemla D, Selvin P, Weiss S. Probing the interaction between two single molecules: fluorescence resonance energy transfer between a single donor and a single acceptor. Proceedings of the National Academy of Sciences. 1996;93(13):6264–6268.

[92] Truong K, Sawano A, Mizuno H, Hama H, Tong KI, Mal TK, et al. FRET-based in vivo Ca^{2+} imaging by a new calmodulin-GFP fusion molecule. Nature Structural & Molecular Biology. 2001;8(12):1069–1073.

[93] De Michele R, Carimi F, Frommer WB. Mitochondrial Biosensors. The international journal of biochemistry & cell biology. 2014;48:39–44.

[94] Waldeck-Weiermair M, Deak AT, Groschner LN, Alam MR, Jean-Quartier C, Malli R, et al. Molecularly distinct routes of mitochondrial Ca^{2+} uptake are activated depending on the activity of the sarco/endoplasmic reticulum Ca^{2+} ATPase. Journal of Biological Chemistry. 2013;288(21):15367–15379.

[95] Bondarenko AI, Jean-Quartier C, Parichatikanond W, Alam MR, Waldeck-Weiermair M, Malli R, et al. Mitochondrial Ca^{2+} uniporter (MCU)-dependent and MCU-independent Ca^{2+} channels coexist in the inner mitochondrial membrane. Pflügers Archiv-European Journal of Physiology. 2013;p. 1–10.

[96] Jean-Quartier C, Bondarenko AI, Alam MR, Trenker M, Waldeck-Weiermair M, Malli R, et al. Studying mitochondrial Ca^{2+} uptake–A revisit. Molecular and cellular endocrinology. 2012;353(1):114–127.

[97] Edgell C, McDonald CC, Graham JB. Permanent cell line expressing human factor VIII-related antigen established by hybridization. Proceedings of the National Academy of Sciences. 1983;80(12):3734–3737.

[98] Scherer WF, Syverton JT, Gey GO. Studies on the propagation in vitro of poliomyelitis viruses IV. Viral multiplication in a stable strain of human malignant epithelial cells (strain HeLa) derived from an epidermoid carcinoma of the cervix. The Journal of experimental medicine. 1953;97(5):695–710.

[99] Puck T, Fisher H. Genetics of somatic mammalian cells I. Demonstration of the existence of mutants with different growth requirements in a human cancer cell strain (HeLa). The Journal of experimental medicine. 1956;104(3):427–434.

[100] Graham F, Smiley J, Russell W, Nairn R. Characteristics of a human cell line transformed by DNA from human adenovirus type 5. Journal of General Virology. 1977;36(1):59–72.

[101] Biedler JL, Helson L, Spengler BA. Morphology and growth, tumorigenicity, and cytogenetics of human neuroblastoma cells in continuous culture. Cancer research. 1973;33(11):2643–2652.

[102] Asfari M, Janjic D, Meda P, Li G, Halban PA, Wollheim CB. Establishment of 2-mercaptoethanol-dependent differentiated insulin-secreting cell lines. Endocrinology. 1992;130(1):167–178.

[103] Waldeck-Weiermair M, Jean-Quartier C, Rost R, Khan MJ, Vishnu N, Bondarenko AI, et al. Leucine zipper EF hand-containing transmembrane protein 1 (Letm1) and uncoupling proteins 2 and 3 (UCP2/3) contribute to two distinct mitochondrial Ca2+ uptake pathways. Journal of Biological Chemistry. 2011;286(32):28444–28455.

[104] Frezza C, Cipolat S, Scorrano L. Organelle isolation: functional mitochondria from mouse liver, muscle and cultured filroblasts. Nature protocols. 2007;2(2):287–295.

[105] Bradford MM. A rapid and sensitive method for the quantitation of microgram quantities of protein utilizing the principle of protein-dye binding. Analytical biochemistry. 1976;72(1):248–254.

[106] Smith P, Krohn RI, Hermanson G, Mallia A, Gartner F, Provenzano M, et al. Measurement of protein using bicinchoninic acid. Analytical biochemistry. 1985;150(1):76–85.

[107] Schägger H, von Jagow G. Blue native electrophoresis for isolation of membrane protein complexes in enzymatically active form. Analytical biochemistry. 1991;199(2):223–231.

[108] Zerbetto E, Vergani L, Dabbeni-Sala F. Quantification of muscle mitochondrial oxidative phosphorylation enzymes via histochemical staining of blue native polyacrylamide gels. Electrophoresis. 1997;18(11):2059–2064.

[109] Gallagher S, et al. Immunoblotting and immunodetection. Current Protocols in Cell Biology. 2011;p. 6–2.

[110] Alkhaja AK, Jans DC, Nikolov M, Vukotic M, Lytovchenko O, Ludewig F, et al. MINOS1 is a conserved component of mitofilin complexes and required for mi-

tochondrial function and cristae organization. Molecular biology of the cell. 2012;23(2):247–257.

[111] Mick DU, Dennerlein S, Wiese H, Reinhold R, Pacheu-Grau D, Lorenzi I, et al. MITRAC links mitochondrial protein translocation to respiratory-chain assembly and translational regulation. Cell. 2012;151(7):1528–1541.

[112] Shevchenko A, Henrik Tomas JH, Olsen JV, Mann M. In-gel digestion for mass spectrometric characterization of proteins and proteomes. Nature protocols. 2007;1(6):2856–2860.

[113] Bondarenko AI, Jean-Quartier C, Malli R, Graier WF. Characterization of distinct single-channel properties of Ca^{2+} inward currents in mitochondria. Pflügers Archiv-European Journal of Physiology. 2013;465(7):997–1010.

[114] Jans DC, Wurm CA, Riedel D, Wenzel D, Stagge F, Deckers M, et al. STED super-resolution microscopy reveals an array of MINOS clusters along human mitochondria. Proceedings of the National Academy of Sciences. 2013;110(22):8936–8941.

[115] Gnaiger E, Steinlechner-Maran R, Méndez G, Eberl T, Margreiter R. Control of mitochondrial and cellular respiration by oxygen. Journal of bioenergetics and biomembranes. 1995;27(6):583–596.

[116] Kennedy BE, Madreiter CT, Vishnu N, Malli R, Graier WF, Karten B. Adaptations of energy metabolism associated with increased levels of mitochondrial cholesterol in Niemann-Pick type C1-deficient cells. Journal of Biological Chemistry. 2014;289(23):16278–16289.

[117] Waldeck-Weiermair M, Duan X, Naghdi S, Khan MJ, Trenker M, Malli R, et al. Uncoupling protein 3 adjusts mitochondrial Ca^{2+} uptake to high and low Ca^{2+} signals. Cell calcium. 2010;48(5):288–301.

[118] Jamur MC, Oliver C. Permeabilization of cell membranes. In: Immunocytochemical Methods and Protocols. Springer; 2010. p. 63–66.

[119] Van Meer G, Voelker DR, Feigenson GW. Membrane lipids: where they are and how they behave. Nature reviews molecular cell biology. 2008;9(2):112–124.

[120] Cremel G, Filliol D, Jancsik V, Rendon A. Cholesterol distribution in rat liver and brain mitochondria as determined by stopped-flow kinetics with filipin. Archives of biochemistry and biophysics. 1990;278(1):142–147.

[121] Picard M, Taivassalo T, Ritchie D, Wright KJ, Thomas MM, Romestaing C, et al. Mitochondrial structure and function are disrupted by standard isolation methods. PLoS One. 2011;6(3):e18317.

[122] Michels G, Khan IF, Endres-Becker J, Rottlaender D, Herzig S, Ruhparwar A, et al. Regulation of the human cardiac mitochondrial Ca2+ uptake by 2 different voltage-gated Ca2+ channels. Circulation. 2009;119(18):2435–2443.

[123] Fieni F, Lee SB, Jan YN, Kirichok Y. Activity of the mitochondrial calcium uniporter varies greatly between tissues. Nature communications. 2012;3:1317.

[124] Patron M, Checchetto V, Raffaello A, Teardo E, Vecellio Reane D, Mantoan M, et al. MICU1 and MICU2 Finely Tune the Mitochondrial Ca^{2+} Uniporter by Exerting Opposite Effects on MCU Activity. Molecular cell. 2014;53(5):726–737.

[125] Bereiter-Hahn J, Jendrach M. Mitochondrial dynamics. International review of cell and molecular biology. 2010;284:1–65.

A. Abbreviations

4mtD3cpv	mitochondria targeted cameleon
ADP/ATP	adenosine-diphosphate/-triphosphate
AM	acetoymethylester
ASAP2	ArfGAP with SH3 domain, ankyrin repeat and PH domain 2
ATPase	ATP synthase
au	arbitrary units
BHQ	2,5-di(tert-butyl)-1,4-benzohydroquinone
$[Ca^{2+}]_{mt}$	mitochondrial calcium
CaMK	Ca^{2+}/Calmodulin dependent protein kinase
CCDC	coiled-coil domain containing
CFP	cyan fluorescent protein
CL	cardiolipin
CPA	cyclopiazonic acid
CsA	cyclosporin A
DMEM	Dulbecco's modified eagle's medium
DMSO	dimethylsulfoxide
EMRE	essential mitochondrial uniporter regulator
ER	endoplasmic reticulum
ERMES	ER-mitochondrial encounter structures
ETS	electron transport system
F_{wl}	fluorescence at given wavelength
F_0	initial fluorescence at basal level
FA	fatty acid
$FADH_2$	reduced flavine adenine dinucleotide
FCCP	carbonyl cyanide-4-(trifluoromethoxy)phenylhydrazone
FCS	fetal calf serum
FP	fluorescent protein

FRET	Förster resonance energy transfer
GFP	green fluorescent protein
HEK	human embryonic kidney cell-line
HeLa	Henrietta Lacks cervical cancer cell-line
His	histamine
IMM	inner mitochondrial membrane
IMS	inter-membrane space
IP	immunoprecipitation
IP3	inositol-1,4,5-triphosphate
Letm1	Leucine Zipper-EF-hand containing trans-membrane protein
MCC	mitochondrial calcium current
MCU	mitochondrial calcium uniporter
	(alternative nomenclature: CCDC109A)
MCUb	isoform of MCU
	(alternative nomenclature: CCDC109B)
MCUR	mitochondrial calcium uniporter regulator
	(alternative nomenclature: CCDC90A)
Mic60	mitofilin (alternative nomenclature: MFL IMMT, MINOS3)
MICOS	mitochondrial contact site and cristae organizing system
MICU	mitochondrial calcium uptake
MPTP	mitochondrial permeability transition pore
MS	mass spectrometry
mtRP	mitochondria targeted ratiometric pericam
NADH	reduced nicotinamide adeninedinucleotide dehydrogenase
NCX/NCLX	Na^+/Ca^{2+} exchanger
OMM	outer mitochondrial membrane
Opa1	optical atrophy dynamin-line protein
PA	phosphatic acid
PC	phosphatidylcholine
PCR	polymerase chain reaction
PE	phosphatidylethanolamine
PG	phosphatidylglycerol
PI	phosphatidylinositol
PK	proteinase K
PS	phosphatidylserine

PLC	phospholipase C
Pyk2	proline-rich tyrosine kinase 2
RPMI	Roswell Park Memorial Institute medium
UCP	uncoupling protein
ROS	reactive oxygen species
Ru360	ruthenium red 360
RuR/RuRed	ruthenium red
RYR	ryanodine receptor
SD	standard deviation
SEC	size exclusion chromatography
SEM	standard error of mean
SERCA	sarcoplasmic/endoplasmatic reticulum ATPase
siRNA	small interfering ribonucleic acid
SOCE	Store operated Ca^{2+} entry
TCA	tricarboxylic acid cycle
TIM/TOM	transporter of inner/outer mitochondrial membrane
TRPC	transient receptor potential channel
VDAC	voltage-dependent anion channel
WL	wavelength
YFP	yellow fluorescent protein

B. Publications

Published manuscripts during the years of thesis work are listed beneath [103, 96, 113, 94, 95].

Molecular and Cellular Endocrinology 353 (2012) 114–127

Contents lists available at SciVerse ScienceDirect

Molecular and Cellular Endocrinology

journal homepage: www.elsevier.com/locate/mce

Studying mitochondrial Ca^{2+} uptake – A revisit

Claire Jean-Quartier, Alexander I. Bondarenko, Muhammad Rizwan Alam, Michael Trenker, Markus Waldeck-Weiermair, Roland Malli, Wolfgang F. Graier *

Institute of Molecular Biology and Biochemistry, Center of Molecular Medicine, Medical University of Graz, A-8010 Graz, Austria

ARTICLE INFO

Article history:
Available online 11 November 2011

Keywords:
Mitochondrial Ca^{2+} measurements
Mitochondrial Ca^{2+} uptake
Mitochondrial Ca^{2+} uniporter
Mitoplasts
Patch clamp
Pericam

ABSTRACT

Mitochondrial Ca^{2+} sequestration is a well-known process that is involved in various physiological and pathological mechanisms. Using isolated suspended mitochondria one unique mitochondrial Ca^{2+} uniporter was considered to account ubiquitously for the transfer of Ca^{2+} into these organelles. However, by applying alternative techniques for measuring mitochondrial Ca^{2+} uptake evidences for molecularly distinct mitochondrial Ca^{2+} carriers accumulated recently. Herein we compared different methodical approaches of studying mitochondrial Ca^{2+} uptake. Patch clamp technique on mitoplasts from endothelial and HeLa cells revealed the existence of three and two mitoplast Ca^{2+} currents (I_{CaMito}), respectively. According to their conductance, these channels were named small (*s*-), intermediate (*i*-), large (*l*-) and extra-large (*xl*-) mitoplast Ca^{2+} currents (MCC). *i*-MCC was found in mitoplasts of both cell types whereas *s*-MCC and *l*-MCC or *xl*-MCC were/was exclusively found in mitoplasts from endothelial cells or HeLa cells. The comparison of mitochondrial Ca^{2+} signals, measured either indirectly by sensing extra-mitochondrial Ca^{2+} or directly by recording changes of the matrix Ca^{2+}, showed different Ca^{2+} sensitivities of the distinct mitochondrial Ca^{2+} uptake routes. Subpopulations of mitochondria with different Ca^{2+} uptake capacities in intact endothelial cells could be identified using Rhod-2/AM. In contrast, cells expressing mitochondrial targeted pericam or cameleon (4mtD3cpv) showed homogeneous mitochondrial Ca^{2+} signals in response to cell stimulation. The comparison of different experimental approaches and protocols using isolated organelles, permeabilized and intact cells, pointed to cell-type specific and versatile pathways for mitochondrial Ca^{2+} uptake. Moreover, this work highlights the necessity of the utilization of multiple technical approaches to study the complexity of mitochondrial Ca^{2+} homeostasis.

1. Introduction

Mitochondria achieve a multitude of biochemical functions (Graier et al., 2007; McBride et al., 2006) of which the combustion of substrates coupled to the transfer of electrons to molecular oxygen, proton pumping across the inner mitochondrial membrane yielding ATP generation are the best-known examples (Kennedy and Lehninger, 1949). Because of such central role in energy metabolism mitochondria are often referred to as the cell's powerhouses.

The ability of mitochondria to rapidly transform their morphological appearance is an additional remarkable feature of these organelles (Chen, 1988; Koshiba et al., 2004; Liu et al., 2009). Mostly, mitochondria create worm-like structures, which are constantly remodeled by fission, fusion and branching (Bereiter-Hahn and Jendrach, 2010). Moreover, mitochondria are transiently tethered to other cell structures such like the endoplasmic reticulum (ER) (Csordas et al., 1999; de Brito and Scorrano, 2008; Merkwirth and Langer, 2008), the nucleus (Liu and Butow, 2006), other organelles (Stemberger et al., 1984), the plasma membrane (Malli et al., 2003), the cytoskeleton (Ball and Singer, 1982), and linked to motor-proteins for directed movements (Liu and Hajnoczky, 2009).

Another striking feature of mitochondria is their ability to sequester calcium ions (Ca^{2+}), nature's most widely used second messenger (Berridge et al., 2000; Dhalla, 1969; Graier et al., 2007; Malli and Graier, 2010). Mitochondrial Ca^{2+} uptake plays an important role in the cell's physiological and pathological signal transduction (Berridge et al., 2003; Demaurex and Distelhorst, 2003; Duchen et al., 2008). The transfer of Ca^{2+} into mitochondria is assumed to impact cell signaling basically by two processes. *Firstly*, mitochondrial Ca^{2+} uptake shapes the amplitude, the temporal- and spatial pattern of local as well as global extra-mitochondrial Ca^{2+} signals, which considerably impacts on Ca^{2+}-sensitive processes upon cell stimulation (Knot et al., 2005) (i.e. Ca^{2+} buffer function). *Secondly*, elevated mitochondrial Ca^{2+} is crucially important for cellular processes such as respiration and ATP production (Wiederkehr et al., 2011), autophagy (Decuypere et al., 2011),

* Corresponding author. Address: Molecular and Cellular Physiology Research Unit, Institute of Molecular Biology and Biochemistry, Center of Molecular Medicine, Medical University of Graz, Harrachgasse 21/III, A-8010 Graz, Austria. Tel.: +43 316 380 7560; fax: +43 316 380 9615.
E-mail address: wolfgang.graier@medunigraz.at (W.F. Graier).

0303-7207/$ - see front matter © 2011 Elsevier Ireland Ltd. All rights reserved.
doi:10.1016/j.mce.2011.10.033

protein folding (Osibow et al., 2006), gene expression (Cao and Chen, 2009) and, upon excessive Ca^{2+} overload, the initiation of programmed cell death (apoptosis) (Giorgi et al., 2008).

The phenomenon of mitochondrial Ca^{2+} uptake has been discovered in the early 1960s (Deluca and Engstrom, 1961) when it was recognized that isolated mitochondria have a high capacity to sequester Ca^{2+}. In these experiments mitochondrial Ca^{2+} uptake was assessed indirectly by measuring the reduction of the extramitochondrial Ca^{2+} concentration upon repetitive applications of Ca^{2+} portions to isolated, suspended, respiring mitochondria. With such kinds of experiments the enormous capacity of mitochondria to absorb Ca^{2+} was discovered and mitochondrial Ca^{2+} uptake was well characterized as the so-called mitochondrial Ca^{2+} uniport (MCU) (reviewed by Malli and Graier, 2010). It was shown that the MCU is indeed a Ca^{2+} ion channel (Kirichok et al., 2004). More recently, one component of the elusive MCU has been discovered by integrative genomics (Baughman et al., 2011; De Stefani et al., 2011). Remarkably, the MCU of isolated mitochondria exhibited a rather low Ca^{2+} affinity (Gunter et al., 1994). Based on this low Ca^{2+} affinity, mitochondrial Ca^{2+} uptake was considered as physiologically irrelevant, and mitochondria were thought to work as passive Ca^{2+} sinks (reviewed by Santo-Domingo and Demaurex, 2010). However, due to the development of mitochondria targeted luminescent or later on fluorescent protein-based Ca^{2+} sensors that allowed a direct measurement of mitochondrial Ca^{2+} signals, mitochondria were demonstrated to actively contribute to the cells Ca^{2+} homeostasis (Rizzuto et al., 1992; Jiang et al., 2009; Perocchi et al., 2010; Trenker et al., 2008; Miyawaki et al., 1999, 2003; Nagai et al., 2002; Szabadkai et al., 2004). Direct measurements of mitochondrial Ca^{2+} signals in cells using this novel technique revealed distinct modes of mitochondrial Ca^{2+} uptake with high Ca^{2+} sensitivities not seen in isolated mitochondria before (Waldeck-Weiermair et al., 2010a,b). In line with this work, the contribution of two proteins to distinct mitochondrial Ca^{2+} uptake routes in one given cell was described (Waldeck-Weiermair et al., 2011).

In this study different techniques ranging from indirect measurements using isolated, suspended mitochondria to direct recordings of mitochondrial free Ca^{2+} concentration in intact living cells were compared. This comparison highlights the crucial differences of the various techniques and calls for caution for a direct comparison of results obtained by the various methods. In addition, this work provides evidence for molecularly distinct, probably interrelated, pathways for mitochondrial Ca^{2+} sequestration.

2. Materials and methods

2.1. Cell culture

Human umbilical vein endothelial cells (EA.hy926) (Edgell et al., 1983) (passage number > 80) were grown on Dulbecco's modified Eagle's medium (DMEM) supplemented with 10% fetal calf serum (FCS), 1% HAT (5 mM hypoxanthin, 20 μM aminopterin, 0.8 mM thymidine), 50 U/ml penicillin and 50 μg/ml streptomycin (PAA Laboratories, Pasching Austria) at 37 °C, 5% CO_2. HeLa cells were grown on DMEM containing 10% FCS, 50 U/ml penicillin and 50 μg/ml streptomycin. The rat pancreatic cell line (INS-1; 832/13) was cultured in RPMI 1640 medium containing 10% FCS, 10 mM Hepes, 2 mM glutamine, 1 mM Na-pyruvate (PAA Laboratories, Pasching Austria), 0.05 mM 2-mercaptoethanol, 50 U/ml penicillin and 50 μg/ml streptomycin at 37 °C, 5% CO_2. Mouse stromal cells (OP9) were kindly provided by Dr. E. Steyrer (Department of Molecular Biology and Biochemistry, Center for Molecular Medicine, Medical University of Graz, Austria). Cardiac muscle cells derived from mouse cardiomyocyte tumor lineage (HL1) were kindly provided by Dr. K. Groschner (Institute of Pharmaceutical Sciences, University of Graz, Austria). For single-cell analysis cells were grown on glass coverslips, and transiently transfected with the FRET-based mitochondrial sensor 4mtD3cpv using Transfast (Promega, Mannheim, Germany) according to the manufacturer's protocol. Alternatively, EA.hy926 cells were stably transfected with mitochondrial targeted ratiometric pericam (RPmt).

2.2. Isolation of mitochondria and mitoplasts

Mitochondria were freshly isolated by differential centrifugation from wild type yeast (Daum et al., 1982) or liver tissue of mice (Storrie and Madden, 1990) as previously described (Trenker et al., 2008). Isolated mitochondria were suspended in storage buffer composed of 10 mM Hepes, 250 mM sucrose, 1 mM ATP, 0.08 mM ADP, 5 mM succinate, 2 mM KH_2PO_4, 1 mM DTT, pH adjusted to 7.4 with KOH (Lactan, Graz, Austria).

Mitoplasts were prepared from isolated mitochondria of HeLa and a endothelial cell line (Ea.hy926) cells by differential centrifugation steps using both methods of mitochondria isolation kit for cultured cells (Thermo Scientific 89874, USA) and an organelle isolation protocol described by Frezza et al. (2007). Mitoplast formation was achieved by incubation of isolated mitochondria in 4 volumes hypotonic solution (5 mM Hepes, 5 mM sucrose, 1 mM EGTA, pH adjusted to 7.4 with KOH < 10 mM) and equilibrated on ice with 1 volume hypertonic solution (750 mM KCl, 80 mM Hepes, 1 mM EGTA, pH adjusted to 7.4 with KOH < 10 mM) after 15 min.

2.3. Mitoplast patch clamp recordings

All measurements were performed in mitoplast-attached configuration of the patch-clamp technique at room temperature. Gigaohm seals were established on the membrane section opposite to the cap region. Patch pipettes were pulled from glass capillaries using a Narishige puller (Narishige Co., Ltd., Tokyo, Japan), fire-polished and had a resistance of 8–12 MΩ when filled with a solution containing 105 mM $CaCl_2$, 10 mM Hepes, or low chloride solution with 55 mM Ca-methanesulfonate, 50 mM $CaCl_2$, 10 mM Hepes, pH adjusted to 7.2 with Ca(OH). Bath solution contained 150 mM KCl, 1 mM EGTA, 1 mM EDTA, 10 mM Hepes, pH adjusted to 7.2 with KOH. 10 μM Cyclosporin A (Tocris Bioscience, Bristol, UK) and 20 μM CGP-37157 (Ascent Scientific Ltd., Bristol, UK) were added to both the bath and pipette solution. Ruthenium red (RuR) (10 μM) (Merck Chemicals Ltd., Darmstadt, Germany) was added when indicated. Currents were recorded using a patch-clamp amplifier (EPC7, List Electronics, Darmstadt, Germany) at a bandwidth of 3 kHz. Data collection was performed using Clampex software of pClamp (V9.0, Axon Instruments). Signals obtained were low pass filtered at 1 kHz using an eight-pole Bessel filter (Frequency Devices), and digitized with a sample rate of 10 kHz using a Digidata 1200A A/D converter (Axon Instruments, Foster City, CA, USA). Voltage ramps of 1 s duration from −150 and +50 mV were delivered every 10 s from the holding potential 0 mV. Single channel currents were recorded at a fixed holding potential at −160, −150, −140 and −100 mV.

2.4. Indirect measurement of mitochondrial Ca^{2+} uptake of isolated mitochondria and permeabilized cells

Indirect measurement of free mitochondrial Ca^{2+} uptake was performed with Calcium-Green® 5 N. Samples of isolated mitochondria (0.25 mg/ml) and HeLa cells (2.5×10^6 cells/ml, harvested by trypsinization) were suspended in high potassium buffer composed of 110 mM KCl, 500 μM K_2HPO_4, 1 mM $MgCl_2$, 20 mM Hepes, 10 μM EGTA, 5 mM succinate, pH adjusted to 7.3 with KOH. In isolated mitochondria rotenone was supplied to 4 μM, while digitonin (Sigma, Vienna, Austria) was added to

30 μM to permeabilize cells. Calcium-Green® 5 N indicator was added to both samples to a final concentration of 0.25 μM. Ca^{2+} uptake of permeabilized cells and isolated mitochondria in suspension was measured on a fluorescence spectrophotometer (Hitachi F-4500; Hitachi, Inula, Vienna, Austria) at 506 nm for excitation and 532 nm for emission.

2.5. Direct measurement of free mitochondrial Ca^{2+} by chemical fluorophores and mitochondrial targeted biosensors

Single isolated mitochondria were incubated with Fura-2/AM (3.3 μg/ml) in the dark for 1 h at RT. Samples of 20 μl suspended Fura-2/AM-loaded isolated mitochondria were incubated for 8 min on a coverslip until they got attached. Samples were perfused with high potassium buffer for measurement on a Zeiss Axiovert 200 M (Zeiss, Vienna, Austria) at 340 and 380 nm excitation (340HT15, 380HT15, Omega Optical, Brattleborough, VT, USA) and 510 nm emission filter (510WB40, Omega Optical), as described before (Trenker et al., 2008). Intact cells, on glass coverslips, were loaded with 5 μM Rhod-2/AM for 30 min at room temperature, excited at 514 nm (150 mW Ar laser, Laser Physics, USA) and fluorescence was monitored at 570 nm (E570LPv2, Chroma Technology Corp. Rockingham, VT, USA). Single-cell measurements of mitochondrial Ca^{2+} was done in endothelial cells either transfected with RPmt (Nagai et al., 2002) or 4mtD3cpv (Palmer et al., 2006) using a Zeiss Axiovert 200 M (40× oil objective, Zeiss), a polychromator illumination system (VisiChrome High Speed, Xenon lamp, Visitron Systems, Puchheim, Germany) and a thermoelectric-cooled CCD camera (Photometrics Coolsnap HQ, Visitron Systems) or a Nikon Eclipse TE300 (Plan Fluor 40× oil objective, Nikon, Japan), a polychromator lamp (Opti Quip 770, USA) and a liquid-cooled CCD camera (Photometrics Quantix KAF, Roper Scientific, Tucson, AZ, USA). Data acquisition and analysis was done using the MetaMorph or VisiView software (Visitron Systems). Glass coverslips were mounted into an experimental chamber equipped with a perfusion system at a rate around 2 ml/min. Cells were put into resting solution prior to experiments composed of 135 mM NaCl, 5 mM KCl, 2 mM $CaCl_2$, 1 mM $MgCl_2$, 10 mM Hepes, 2.6 mM $NaHCO_3$, 440 μM KH_2PO_4, 340 μM Na_2HPO_4, 10 mM D-glucose, 0.1% vitamins, 0.2% essential amino acids, 1% penicillin/streptomycin, pH adjusted to 7.4 with NaOH. For experiments cells were perfused with Ca^{2+}-free solution, composed of 138 mM NaCl, 5 mM KCl, 1 mM $MgCl_2$, 10 mM D-glucose, 1 mM EGTA, pH adjusted to 7.4 with NaOH. Cells were stimulated by the addition of either 100 μM carbachol, 100 μM ATP or 100 μM histamine and 15 μM BHQ. RPmt was used to simultaneously measure free mitochondrial Ca^{2+} at 410/438 nm excitation and changes in pH at 485 nm excitation, both with emission at 535 nm (433DF15/535AF26, Omega Optical). Excitation of the 4mtD3cpv was applied at 440 ± 10 nm (440AF21, Omega Optical), and emission was recorded at 480 and 535 nm using a beam splitter (Optical Insights, Visitron Systems). Excitation filters were adjusted through a filter-wheel (MAC 6000/5000, Ludl Electronic Products, Hawthorne, NY, USA). Devices were controlled and data was recorded by MetaFluor 4.6r3 software or VisiView 2.0.3 (Universal Imaging, Visitron Systems).

2.6. Confocal imaging of intact cells and mitochondrial preparations

Z-scans were performed on a Nipkow-disk-based array confocal laser-scanning microscope, as described before (Trenker et al., 2008).

3. Results

3.1. Isolated mitoplasts exhibit multiple distinct Ca^{2+} currents that vary depending on the cell type chosen for isolation

Using isolated mitochondria is the most invasive and elaborated method to investigate the phenomenon of mitochondrial Ca^{2+} uptake. However, this technique is certainly a very useful and insightful approach to look at mitochondrial signaling. One powerful feature of using isolated organelles is the possibility to apply the patch clamp technique, which allows the characterization of intracellular Ca^{2+} channels even on the single channel level. We isolated mitochondria from different cell lines and tissues, stained them with MitoTracker®, and imaged them on a fluorescence microscope. Isolated mitochondria always appeared as small spherical structures with diameters ranging from 0.25 to 1.5 μm (Trenker et al., 2008) that tend to aggregate independently from the source used (Fig. 1A). In order to patch the inner mitochondrial membrane (IMM), mitochondria were swelled in hypotonic media, which leads to the rupture of the outer mitochondrial membrane (OMM) obtaining larger objects, the so-called mitoplasts. Mitoplasts from HeLa and endothelial cells were sometimes large in size and frequently contained remnants of the OMM, visible next to the mitotracker-stained particle (Fig. 1B). Non-fluorescent particles are equally attributed to OMM remnants as to disrupted mitochondria, which do not accumulate mitotracker molecules. Mitoplasts were

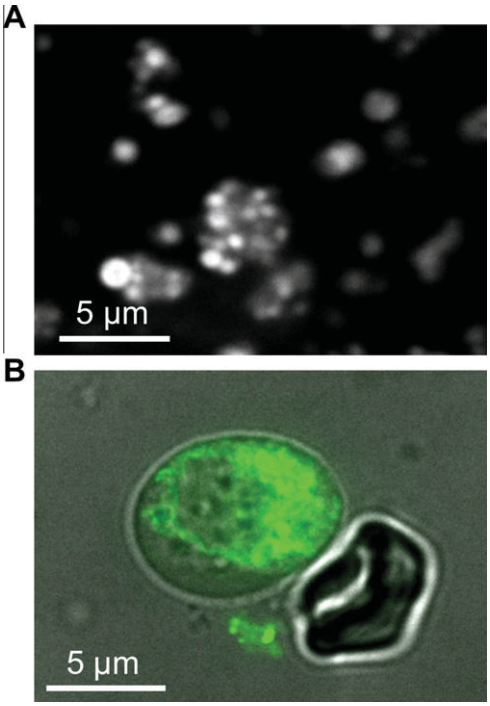

Fig. 1. Ca^{2+} currents and Ca^{2+} uptake in isolated mitochondria. (A) Isolated mitochondria. (B) Mitotracker-stained mitoplasts, prepared from HeLa cells, showing remnants of outer membrane. (C) Representative tracings in mitoplasts-attached mode of membrane currents induced by voltage ramps from −150 to 50 mV in HeLa (n = 6) and Ea.hy 926 cells (n = 3), before (black trace) and after addition of RuR (red trace). (D) Representative tracings of single channel events showing two types of single channel conductances at V_m = −100 and −150 mV in mitoplasts from HeLa cells (n = 10), shown in the right panel, and at V_m = −140 mV and −160 mV for mitoplasts from Ea.hy 926 cells (n = 5), shown in the left panel. (E) Two representative tracings of mitochondrial Ca^{2+} uptake in response to 0.14 μmol Ca^{2+}/mg protein in suspended mitochondria of one given preparation measured by Calcium-Green® 5 N in the bath. (F) Ca^{2+} response in single Fura-2/AM-loaded isolated mitochondria evoked by the addition of 10 μM free Ca^{2+}, three representative curves (n = 22).

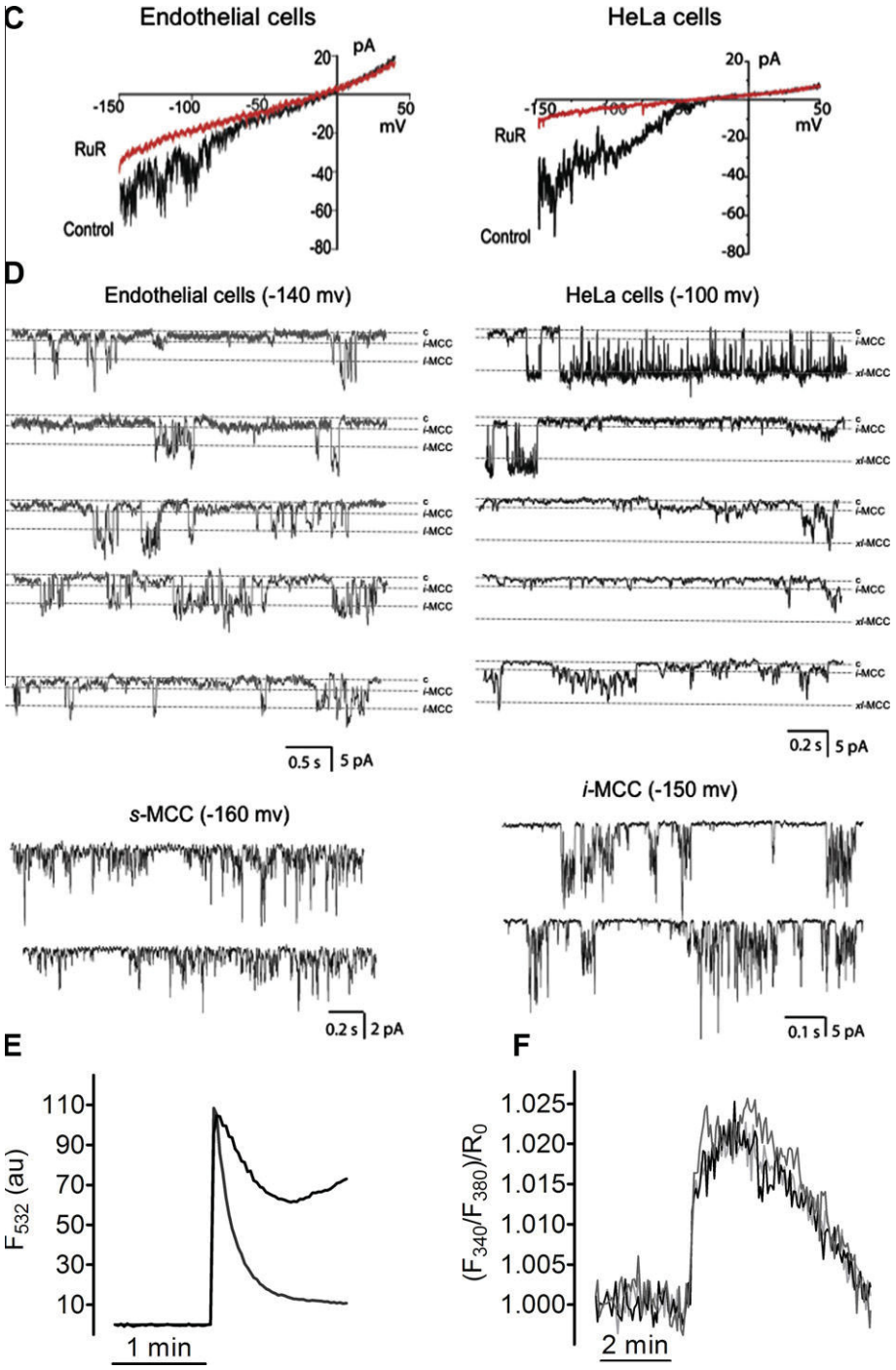

Fig. 1 (*continued*)

used to measure Ca^{2+} currents in the mitoplast-attached configuration. Patch experiments were carried out in buffers containing cyclosporin A for inhibition of mitochondrial permeability transition pore opening and CGP-37157 for blocking mitochondrial Na^+/Ca^{2+} exchanger (Cox and Matlib, 1993; Cox et al., 1993) and Letm1 (Jiang et al., 2009). Moreover, experiments were carried out with low chloride buffer in the pipette, to test whether or not obtained currents are, at least in part, carried by Cl^- outward currents. There were no differences in the observed current conductance and density whether low chloride or high chloride concentration was present in the pipette (data not shown), thus, confirming that the currents measured are carried by Ca^{2+} movements. Experiments with a high Ca^{2+} concentration in the patch pipette revealed strong inward currents at negative potentials (Fig. 1C, black trace), pointing to Ca^{2+} uniporter activities in these mitoplasts. All Ca^{2+} currents (I_{CaMito}) of mitoplasts from HeLa as well as endothelial cells could be blocked by 10 μM RuR in the pipette (Fig. 1C, red trace). Notably, the amplitudes of I_{CaMito} measured were not stable over time. Intermittently different I_{CaMito} responses to voltage ramps in one given mitoplast could be observed. This finding might either point to fluctuations of the activity of one given MCU channel or to the co-existence of more than one distinct current amplitude of single channel events in mitoplasts from endothelial cells (Fig. 1D, left panel) and HeLa cells (Fig. 1D, right

panel). Time-lapsed recordings were taken at holding potentials of either −100, −140, −150 or −160 mV and revealed clear single channel openings in mitoplasts of both cells types. Out of these recordings three and two distinct conductances of I_{CaMito} could be distinguished in endothelial and HeLa cells, respectively (Table 1). These I_{CaMito} were subsequently named as small (*s*-MCC), intermediate (*i*-MCC),large (*l*-MCC) and extra large (*xl*-MCC) mitoplast/mitochondrial Ca^{2+} current (Table 1). Additional biophysical parameters like the current's appearance, mean open time, mean closed time and open probabilities (nPo) are given in Table 1. The *i*-MCC was found in mitoplasts from both cell types. In contrast, *s*-MCC that required high negative voltages and *l*-MCC were only found in endothelial mitoplasts while *xl*-MCC was exclusively found in HeLa cell mitoplasts (Table 1).

3.2. Isolated mitochondria exhibit different Ca^{2+} uptake pathways

A less laborious approach to study mitochondrial Ca^{2+} uptake of isolated mitochondria is to measure the reduction of applied bath Ca^{2+} boluses to suspended mitochondria using a fluorescence Ca^{2+} indicator in the medium. We used Calcium-Green® 5 N for this purpose studying Ca^{2+} uptake of isolated mitochondria from mice liver. Thereby, striking differences in the clearance of added Ca^{2+} could be observed among different experimental approaches, although using isolated mitochondria from the same batch and origin under the same experimental conditions (Fig. 1E). Basically, this finding is in line with the fluctuating activities of mitochondrial Ca^{2+} channels observed in mitoplasts, but might rather point to variances in the stability of the quality of isolated mitochondria from mice liver. Moreover, mitochondrial Ca^{2+} signals, if measured directly by loading Fura-2/AM in isolated organelles, revealed quite homogeneous signals of single isolated mitochondria using fluorescence microscopy (Fig. 1F).

3.3. Mitochondrial Ca^{2+} uptake measured in permeabilized cells unveil high and low Ca^{2+} sensitive pathways

Similar to the signals observed with isolated mitochondria the indirect measurement of mitochondrial Ca^{2+} uptake of digitonin-permeabilized HeLa cells using Calcium-Green® 5 N showed a fast decline in the free extra-mitochondrial Ca^{2+} concentration upon additions of Ca^{2+} portions (Fig. 2). The kinetics of mitochondrial Ca^{2+} uptake in permeabilized cells remained unaltered for several repeats of Ca^{2+} boluses over a considerable period of time, pointing to the high capacity of mitochondria to absorb Ca^{2+} under these conditions. However, after a certain number of cumulative additions of Ca^{2+} to a suspension of permeabilized HeLa cells, the Ca^{2+} concentration of the medium strongly increased, indicating mitochondrial Ca^{2+} overload and opening of a mitochondrial permeability transition pore (Huang et al., 2000; Hunter and Haworth, 1979). The number of the Ca^{2+} pulses that induced mitochondrial Ca^{2+} overload and permeability transition pore opening naturally correlated with the cell number used (Fig. 2A (1.3×10^6 cells) and B (5.9×10^6 cells)).

In line with early results using isolated mitochondria and the Calcium-Green® 5 N method (Eberhard and Erne, 1991) the minimal Ca^{2+} concentration capable of activating mitochondrial Ca^{2+} uptake of suspended permeabilized cells was assessed to be explicitly higher than 3 μM (Fig. 2C). We hypothesized that the low Ca^{2+} affinity of the mitochondrial Ca^{2+} uptake pathway of permeabilized HeLa cells recognized, was overestimated due to the Ca^{2+} buffer capacity of Calcium-Green® 5 N in the medium, which naturally lowers the free Ca^{2+} concentration available on sites of mitochondrial Ca^{2+} uptake. In order to test this assumption, analogous experiments were performed using the high Ca^{2+} sensitive Fura-2 instead of Calcium-Green® 5 N to measure Ca^{2+} in the medium. Using Fura-2 in the medium of the suspension, however, confirmed the low Ca^{2+} affinity of mitochondrial Ca^{2+} uptake of permeabilized HeLa cells (Fig. 2D). Similar data were obtained using permeabilized endothelial cells (data not shown).

For comparison, similar experiments were performed on the single cell level with permeabilized endothelial cells that stably expressed the fluorescence sensor protein mitochondrial targeted pericam (RPmt). In contrast to the experiments above, this approach highlighted clear rises of $[Ca^{2+}]_{mito}$ in permeabilized cells, even at a Ca^{2+} concentration lower than 1 μM (Fig. 2E). Moreover, this experimental approach revealed that the kinetics of mitochondrial Ca^{2+} uptake in one given model (i.e. permeabilized cells) crucially depends on the sensor type and method chosen. Notably, using the rather high-sensitive intraluminal Ca^{2+} sensor pericam already at concentrations of 1 μM bath Ca^{2+} a strong mitochondrial Ca^{2+} sequestration was detected, while the sensor signal got saturated at concentrations > 1 μM bath Ca^{2+}. In contrast, using a Ca^{2+} sensor in the bath (i.e. Calcium-Green® 5 N or Fura-2) bath Ca^{2+} concentrations > 3 μM are essential for measuring a significant mitochondrial Ca^{2+} uptake (Fig. 2F).

Similar to its inhibitory effect on all I_{CaMito} (Fig. 1C), Ruthenium-Red (RuR) inhibited Ca^{2+} uptake in isolated mitochondria and permeabilized cells (Fig. 3). RuR mostly shows inability of passing cellular membranes. Consequently, the usability of RuR in intact cells is limited. The potent uncoupling agent carbonylcyanide-*p*-trifluoro-methoxyphenyl-hydrazone (FCCP) inhibited Ca^{2+} uptake in intact cells and mitochondrial preparations (Fig. 3). Notably, because RuR and FCCP do not impact other Ca^{2+} handling organelles, the inhibition of Ca^{2+} uptake by RuR and FCCP reflects a decreased mitochondrial Ca^{2+} uptake activity. Nevertheless, the impact of RuR and FCCP on the rates of mitochondrial Ca^{2+} uptake differed within the various model/method used. While almost no Ca^{2+} uptake was detectable in presence of both chemical agents in permeabilized cells (Fig. 3C and D), in isolated suspended mitochondria FCCP was more efficient than RuR (Fig. 3B and D). In case of single isolated mitochondria both compounds appeared to be less active in terms of their inhibitory potential on mitochondrial Ca^{2+} uptake (Fig. 3B and D).

Table 1
Gating parameters of mitochondrial Ca^{2+} currents in mitoplasts from endothelial cells (EC) and HeLa cells.

	Density	Conductance (pS)	Mean open time (ms)	Mean closed time (ms)	nPo
EC					
s-MCC	4 out of 14	7.69 ± 1.42	2.44 ± 0.51	19.20 ± 15.88	0.88 ± 1.27
i-MCC	9 out of 14	13.37 ± 2.44	3.14 ± 0.58	11.26 ± 3.82	1.11 ± 0.64
l-MCC	3 out of 14	34.52 ± 4.65	4.57 ± 5.40	52.07 ± 35.87	0.70 ± 0.96
HeLa					
i-MCC	15 out of 22	14.30 ± 2.67	3.6 ± 4.65	13.68 ± 9.62	0.67 ± 0.62
xl-MCC	9 out of 22	74.33 ± 25.7	1.9 ± 0.88	6.08 ± 1.50	1.11 ± 0.66

Abbreviations: number of patches (*n*), small (*s*), intermediate (*i*), large (*l*) and extra large (*xl*) mitochondrial Ca^{2+} current (MCC) in endothelial cells and HeLa cells; open-probability of all channel events (nPo).
Data presented as mean ± standard deviation.

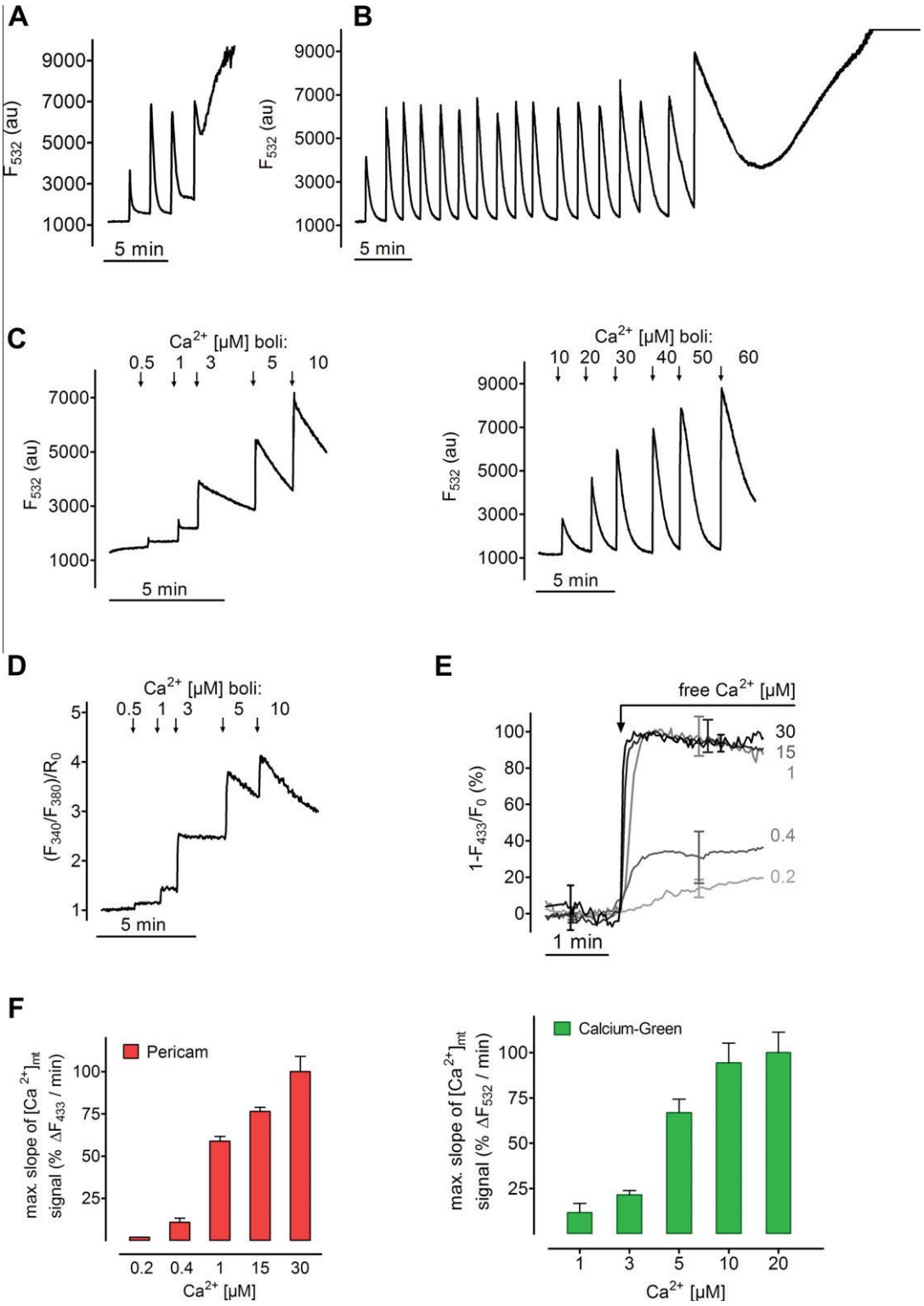

Fig. 2. Variable responses of Ca^{2+} indicators in permeabilized cells. Digitonin-treated HeLa cells were exposed to exogenously added 50 µM Ca^{2+} pulses repeated after 100–200 s and mitochondrial Ca^{2+} uptake was measured with Calcium-Green® 5 N in the bath. Cells show similar rates in uptake, but number of repeats varies in relation to cell quantity, 1.3×10^6 cells (A, $n = 3$) and $5.9*10^6$ cells (B, $n = 3$). (C) Representative tracings of mitochondrial Ca^{2+} uptake in suspended permeabilized cells in response to various Ca^{2+} concentrations in Calcium-Green® containing buffer ($n = 3$). (D) Representative tracings of mitochondrial Ca^{2+} uptake in suspended permeabilized cells in response to various Ca^{2+} concentrations in Fura-2 containing buffer ($n = 3$). (E) Representative tracings of mitochondrial Ca^{2+} uptake in suspended permeabilized cells stably expressing RPmt in response to various Ca^{2+} concentrations. Data was normalized to % max of $1 - (F_{438}/F_0)$ at 1 µM free Ca^{2+} concentration (Waldeck-Weiermair et al., 2010a) and shown as mean ± SEM ($n = 8$–17). (F) Statistical evaluation of the kinetics of mitochondrial Ca^{2+} sequestration presented as % max. slope of mitochondrial $[Ca^{2+}]$ signal of each method upon various Ca^{2+} concentrations in permeabilized cells stably expressing RPmt (left panel; $n = 8$–17) or Calcium-Green® 5 N in the bath (right panel; $n = 3$–5), presented as mean ± SEM.

3.4. Rhod-2 staining reveals distinct subpopulations of mitochondria with different basal Ca^{2+} levels and Ca^{2+} uptake capacity within intact endothelial cells

Rhod-2 is a red fluorescent Ca^{2+} indicator of low molecular weight that is frequently used to study mitochondrial Ca^{2+} signals (Fonteriz et al., 2010). We loaded endothelial cells with the acetoxymethylester of Rhod-2 (Rhod-2/AM) in order to test the suitability of this method. A detectable and consistent staining of all mitochondria with Rhod-2 was observed only if cells were treated for at least 30 min with 1 μM Rhod-2/AM at room temperature (Fig. 4A, left panel). Exposure of these distinctly loaded cells to 514 nm laser light remarkably reduced the selectivity of mitochondrial staining of Rhod-2 within few minutes (Fig. 4A, right panel). In order to reduce such putative phototoxicity, cells were moderately loaded with Rhod-2/AM. Reduction of both the loading time (10 min) and the concentration of Rhod-2/AM (300 nM) yielded a spotty and apparent incomplete staining of mitochondria within one given cell (Fig. 4B, left panel). Notably, most of the mitochondria did not become apparent on the fluorescence microscope using the moderate loading procedure. However, upon stimulation with the IP_3-generating agonist histamine caused a significant flashing of nearly all mitochondrial structures (Fig. 4B, right panel), indicating sufficient Rhod-2 loading to respond to Ca^{2+} rises in almost all mitochondria. The comparison of Rhod-2 signals of mitochondria that exhibited a clear staining already prior to cell stimulation with those which were initially invisible, revealed distinct differences in their capability to respond to cellular Ca^{2+} signals (Fig. 4C and D). In one given cell, mitochondria that initially showed a high Rhod-2 signal under resting conditions, only moderately responded to stimulation with histamine (Fig. 4C and D, red trace). In contrast, the greater subpopulation of mitochondria with very low basal Rhod-2 signals, strongly responded to the IP_3-dependent Ca^{2+} mobilization (Fig. 4C and D, green trace). These findings point to the existence of distinct subpopulations of mitochondria with different basal Ca^{2+} levels and capacities to absorb Ca^{2+}. Moreover, the finding that mitochondria with high basal Rhod-2 signals were almost incompetent to respond to cell stimulation, might point to a negative feedback of Ca^{2+} on the mitochondrial Ca^{2+} uptake pathway.

3.5. Mitochondrial Ca^{2+} and H^+ signals measured with the genetically encoded sensors pericam and cameleon point to FCCP-sensitive mitochondrial Ca^{2+} uptake machineries in intact cells

Mitochondrial targeted ratiometric pericam (RPmt) is a circular permutated fluorescent protein (FP) that was developed by Miyawaki and colleagues in 2001 (Nagai et al., 2001) and exhibits an exceptional targeting efficiency into mitochondria (Fig. 5A) based on a N-terminal targeting sequence of 15 amino acids from the mitochondrial cytochrome *C* oxidase subunit IV (COX IV). This protein-based Ca^{2+} sensor principally consists of a permutated yellow fluorescent protein that is flanked by calmodulin and the Ca^{2+}-calmodulin binding domain M13 (Fig. 5B). Pericam absorbs blue light showing two excitation maxima, particularly in the range of 410–440 nm and 480–490 nm, respectively, while emitting green light at a maximum of approximately 535 nm (Fig. 5C). Ca^{2+} binding to RPmt in intact cells mainly affected the fluorescence of this sensor when excited with 410–440 nm. In contrast, the less Ca^{2+} sensitive fluorescence of pericam at an excitation of 480–490 nm was highly sensitive to changes in pH (Fig. 5C). These properties of pericam offer the possibility to measure changes in Ca^+ and H^+ simultaneously (Fonteriz et al., 2010; Waldeck-Weiermair et al., 2011).

We used an endothelial cell line stably expressing RPmt in order to study the impact of the chemical uncoupler FCCP on the mitochondrial Ca^{2+} and H^+ homeostasis of intact cells (Fig. 5D and E). Cell stimulation with the IP_3-generating agonist histamine triggered a fast and transient increase of mitochondrial Ca^{2+} levels

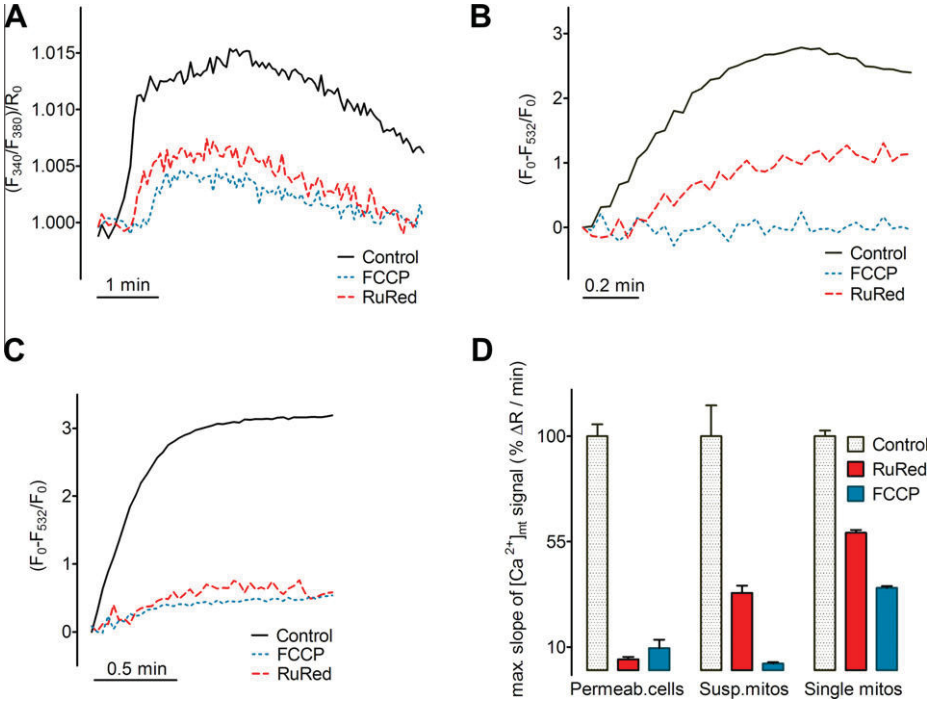

Fig. 3. Differences in the sensitivity of mitochondrial Ca^{2+} uptake to ruthenium red and depolarization depending the mitochondrial preparations. In absence (Control) or presence of either 1 μM RuR or 1 μM FCCP, mitochondrial Ca^{2+} uptake in response to the addition of either 10 μM free Ca^{2+} to Fura-2/AM-loaded single isolated mitochondria (Control: $n = 22$; RuR, $n = 12$; FCCP, $n = 9$) (A), 0.14 μmol Ca^{2+}/mg protein to suspended mitochondria in Calcium-Green® 5 N containing solution (Control: $n = 3$; RuR, $n = 3$; FCCP, $n = 2$) (B) or 50 μM Ca^{2+} to digitonin-permeabilized cells in Calcium-Green® 5 N containing solution (Control: $n = 4$; RuR, $n = 3$; FCCP, $n = 3$) (C). (D) Respective statistical evaluation of the kinetics of mitochondrial Ca^{2+} sequestration presented as % max signal of each method upon Ca^{2+} addition in the absence (Control) or presence of RuR or FCCP.

(Fig. 5D, upper panel), which was subsequently associated with a significant acidification of the mitochondrial matrix (Fig. 5D, lower panel). Addition of FCCP during cell stimulation promptly reduced $[Ca^{2+}]_{mito}$ (Fig. 5D, upper panel) and naturally yielded a

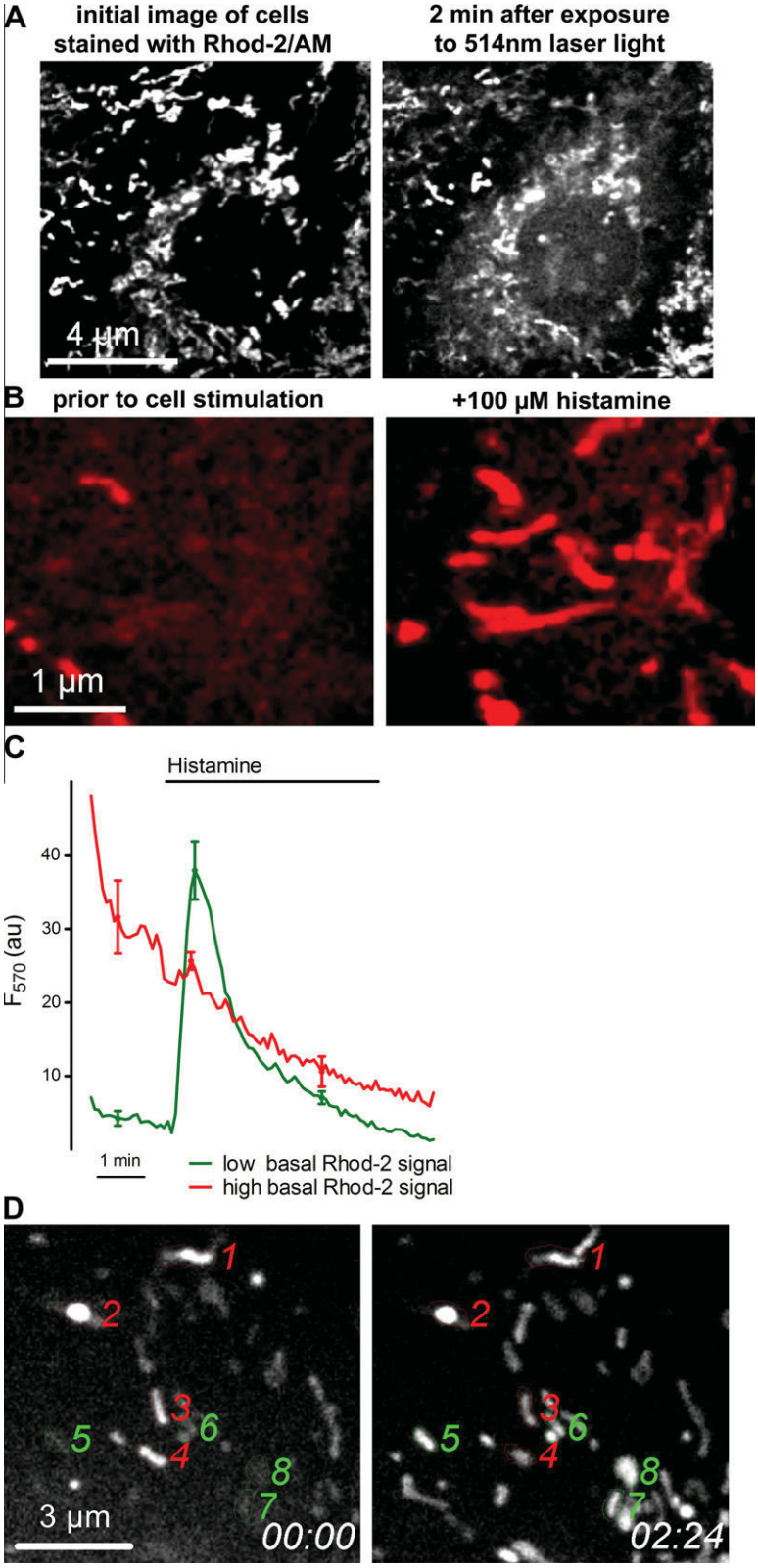

Fig. 4. Different levels of Rhod-2 loading unmask mitochondrial subpopulations. Endothelial cells were treated for 30 min with 1 µM Rhod-2/AM at room temperature (A, left image) and exposed for 2 min at 514 nm (A, right image). Moderately Rhod-2/AM-loaded cells (i.e. 300 nM for 10 min) under resting conditions (B, left panel) and after stimulation with histamine (B, right panel). (C and D) Subpopulations of mitochondria from one cell are shown that exhibited either low basal Rhod-2 signals (green) or high basal Rhod-2 staining (red) prior to cell stimulation. The comparison of those two mitochondrial subpopulations revealed distinct differences in their capability to respond to IP3-dependent Ca^{2+} mobilization (C). Corresponding regions of interest are marked with green and red numbers. Timestamps are given in the right bottom corner in min:sec (D).

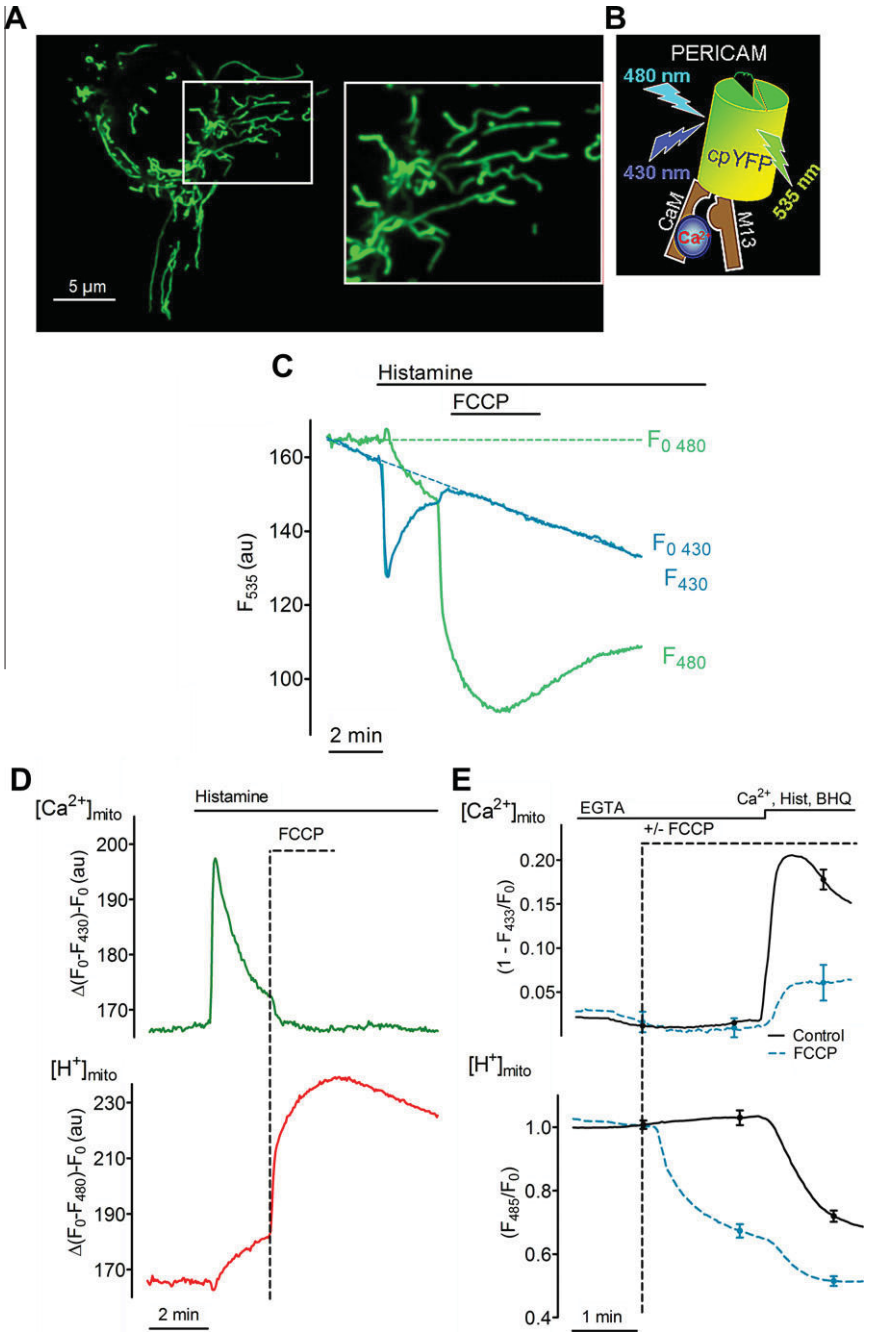

Fig. 5. Close to perfect: mitochondria-targeted ratiometric pericam (RPmt) for monitoring mitochondrial Ca^{2+} uptake. (A) Targeting of RPmt to mitochondria after 24 h of transient transfection in endothelial cells revealed an almost perfect mitochondrial staining. (B) Model with systematic structure of ratiometric pericam. (C) Impact of FCCP on the mitochondrial Ca^{2+} and H^+ concentration in intact endothelial cells visualized using RPmt at either 430 (F_{430}) or 480 (F_{480}) nm excitation and 535 nm emission, respectively. For normalization the respective F_0 curves (F_{430} and F_{480}) were extrapolated from existing basal values using GraphPad® Prism 5. (D) Normalized inverted changes in the fluorescence of RPmt at the Ca^{2+}- and H^+-sensitive wavelength of the sensor in response to application of 100 µM histamine and 2 µM FCCP. (E) Effect of a preincubation with the mitochondrial uncoupler and protonophore FCCP (2 µM) on basal mitochondrial Ca^{2+} (upper graph) and H^+ (lower graph) visualized with RPmt. As indicated 2 mM Ca^{2+}, 100 µM histamine and 15 µM BHQ were added to maximally stimulate mitochondrial Ca^{2+} challenge under these conditions.

pronounced increase of the mitochondrial H^+ concentration (Fig. 5D, lower panel). Removal of FCCP was without any effect on $[Ca^{2+}]_{mito}$ (Fig. 5D, upper panel), but led to a slow recovery of mitochondrial H^+ levels (Fig. 5D, lower panel). In line with these findings, pretreatment of cells with FCCP strongly inhibited mitochondrial Ca^{2+} signals in intact cells (Fig. 5E).

Cameleons are ingenious Ca^{2+} sensors that consist of two different fluorescent proteins, mostly the cyan fluorescent protein (CFP) and the yellow fluorescent protein (YFP), which have overlapping spectral properties (Miyawaki et al., 1997). Ca^{2+} levels in living cells expressing cameleons can be visualized as Ca^{2+} binding to cameleons rapidly changes the conformation of the sensor increasing Förster resonance energy transfer (FRET) from CFP to YFP (Fig. 6A). Cameleons are thus ratiometric Ca^{2+} sensors as the Ca^{2+} induced increase in FRET is naturally associated with a parallel decrease of the CFP fluorescence. Since the introduction of the first cameleon in 1997, several improved derivates of this Ca^{2+} sensor with proper Ca^{2+} sensitivities, higher FRET-efficiencies and increased pH stabilities have been developed (McCombs and Palmer, 2008; Miyawaki et al., 1999). However, probably due to the rela-

tive bulkiness of cameleons, these Ca^{2+} sensors exhibited low targeting specificity. This characteristic could be significantly improved by the introduction of a tandemly duplicated mitochondrial targeting sequence of COX VIII (4mtD3cpv) (Filippin et al., 2005; Palmer et al., 2006). In our experiments, approximately 20% of the endothelial cells expressing 4mtD3cpv exhibited a clear mitochondrial staining of the Ca^{2+} sensor without any mistargeting to the cytosol after 24 h (Fig. 6B, upper panel) and exhibited perfect mirror-like signaling of the donor and the acceptor fluorescence upon cell stimulation (Fig. 6C). Notably, cells with partially mistargeted 4mtD3cpv had often fragmented organelles (Fig. 6B, middle panel) while in cells with high levels of mistargeted cameleon in the cytosol mitochondria appeared highly fragmented (Fig. 6B, lower panel). Overall, these findings may indicate that the expression of 4mtD3cpv potentially impact the morphology of mitochondria. Thus, considering the possibility that mitochondrial Ca^{2+} handling and the morphology of these organelles are interrelated phenomena, the use of this sensor and the interpretation of respective signals should be done with caution.

In order to compare the pH sensitivity of 4mtD3cpv with that of RPmt analogous experiments were performed using FCCP (Figs. 5E vs. 6D). In cells without (Fig. 6D, continuous line) and with mistargeted sensor (Fig. 6D, dotted line), addition of FCCP had only little effects on the fluorescence properties of 4mtD3cpv, pointing to the pH stability of this Ca^{2+} sensor. Mitochondrial Ca^{2+} signals in response to Ca^{2+} mobilization upon histamine and BHQ were clearly inhibited by the chemical uncoupler (Fig. 6D and E). However, in cells with mistargeted sensor, cytosolic Ca^{2+} signals could be measured in parallel (Fig. 6E), confirming the finding that FCCP predominantly impacts the mitochondrial Ca^{2+} homeostasis in this particular cell type.

The usability of 4mtD3cpv for studying mitochondrial Ca^{2+} signals was further tested by imaging IP_3-dependent changes of $[Ca^{2+}]_{mito}$ in various cell types (Fig. 6F). The amount of cells expressing 4mtD3cpv successfully targeted to the mitochondria was approximately 30% in HeLa, 70% in OP-9 cells, 85% in HL-1, and 65% in INS-1 cells. Stimulation of HeLa cells with the IP_3-generating agonists histamine and ATP in the absence of extracellular Ca^{2+} induced a fast and transient increase of $[Ca^{2+}]_{mito}$ in all cells measured, whereas some cells showed an oscillatory mitochondrial Ca^{2+} signal under these conditions (Fig. 6F, left upper panel). Ca^{2+} readdition to prestimulated HeLa cells elevated $[Ca^{2+}]_{mito}$ only in 2 out of 11 cells (Fig. 6F, left upper panel), despite the fact that $[Ca^{2+}]_{cyto}$ was always significantly enhanced in this experimental protocol (data not shown). Both the non excitable mouse stromal cell line OP-9 (Fig. 6F, right upper panel) and the HL-1 mouse cardiomyocytes (Fig. 6F, left lower panel) responded to ATP by a fast increase of $[Ca^{2+}]_{mito}$, which was of higher amplitude in case of the OP-9 cells. Notably, some of the mouse cardiomyocytes showed basal oscillations of $[Ca^{2+}]_{mito}$ probably reflecting the generation of spontaneous action potentials within these excitable

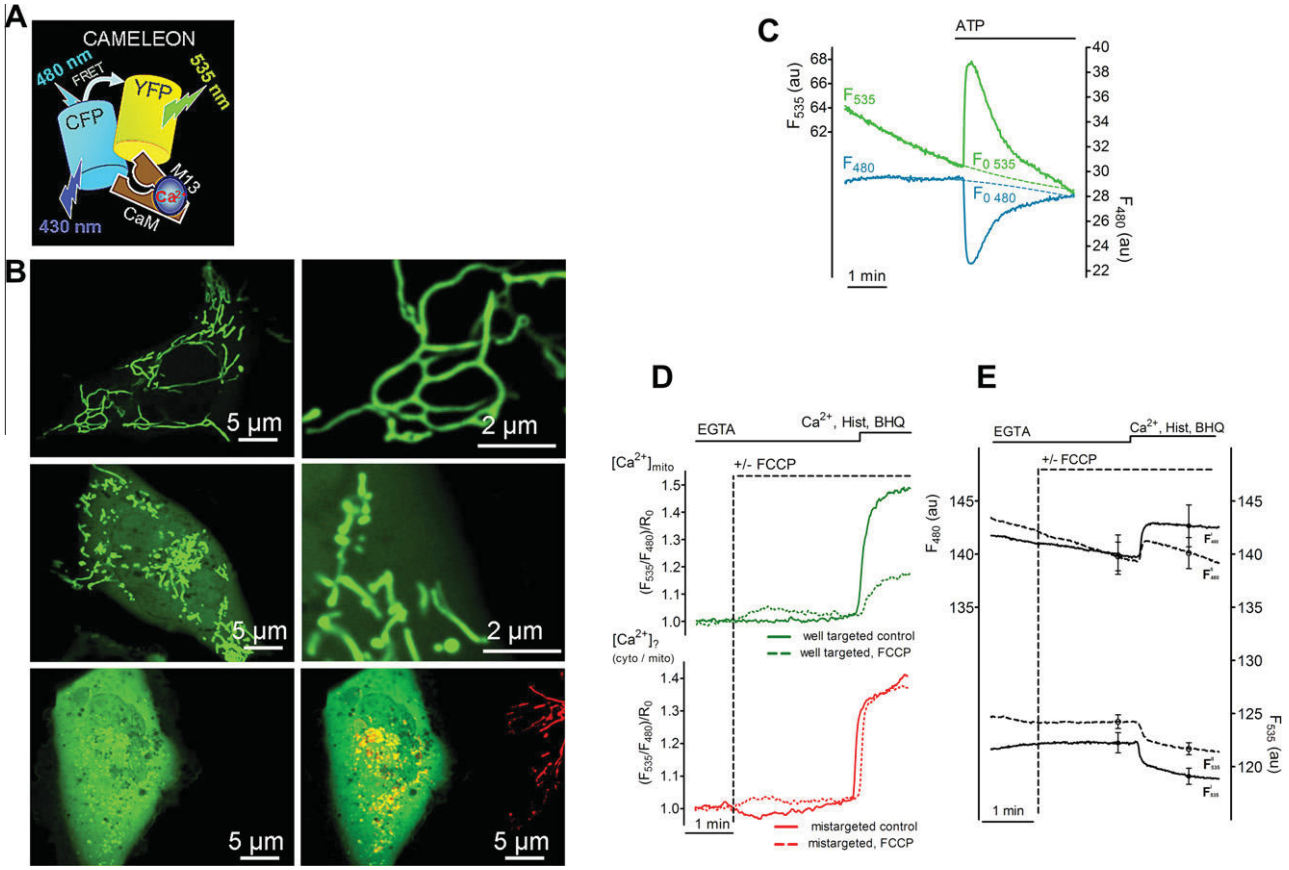

Fig. 6. Close to RTmt but less specific in targeting while essentially ratiometric: mitochondria-targeted cameleon for monitoring mitochondrial Ca^{2+} uptake. (A) Model with systematic structure of mitochondria-targeted cameleons. (B) Targeting of the cameleon 4mtD3cpv to mitochondria after 24 h of transient transfection in endothelial cells revealed few successful targeting to mitochondria (upper panels), cytosolic mistargeting to some degree (middle panel) and high level of mistargeting (lower panels). (C) Original tracings of basal FRET (F_{535}) and the related CFP (F_{480}) fluorescence in endothelial cells transiently expressing 4mtD3cpv. As indicated, cells were stimulated with 100 µM ATP. For normalization the respective F_0 curves (F_{535} and F_{480}) were extrapolated from existing basal values using GraphPad® Prism 5. (D) Impact of 2 µM FCCP on basal mitochondrial Ca^{2+} levels monitored using perfectly targeted (continuous line) and mistargeted (dotted line) 4mtD3cpv. As indicated 2 mM Ca^{2+}, 100 µM histamine and 15 µM BHQ were added to maximally stimulate mitochondrial Ca^{2+} challenge under these conditions (n = 11–13). (E) Individual fluorescence of 4mtD3cpv that correspond to the experiments shown in (D). (F) Original tracings of the effect of IP_3-dependent changes of $[Ca^{2+}]_{mito}$ due to histamine, ATP or carbachol (CCh) in several cell types that were transiently transfected with 4mtD3cpv. Mean represented by bold black line with circles, single responses HeLa n = 11, OP-9 n = 10, HL-1 n = 10, INS-1 n = 8.

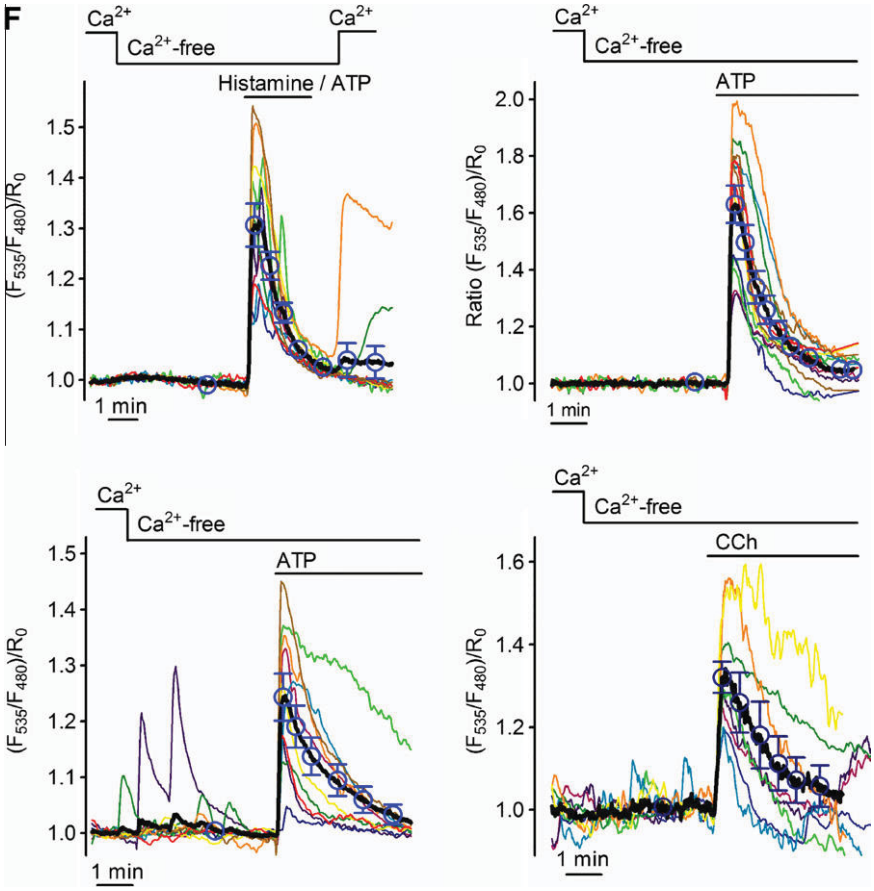

Fig. 6 (*continued*)

cells (Fig. 6F, left lower panel). Oscillations of $[Ca^{2+}]_{mito}$ with a smaller amplitude could be also observed in the β-cell line (INS-1) that showed a fast increase of mitochondrial Ca^{2+} levels upon cell stimulation with carbachol (CCh) (Fig. 6F, right lower panel).

4. Discussion

Mitochondria are able to decode cytosolic Ca^{2+} signals by sequestering these ions and the subsequent activation of Ca^{2+}-dependent processes that, in turn, are crucial for the cell responsiveness and functions (Duchen and Szabadkai, 2010; Graier et al., 2007). Accordingly, mitochondrial Ca^{2+} uptake is considered as an important cellular process that is relevant for both physiological and pathological cell signaling (Duchen et al., 2008).

Events of mitochondrial Ca^{2+} uptake can be studied on isolated organelles with high temporal resolution using the patch camp technique. In addition fluorescent Ca^{2+} sensors that either indirectly indicate the decline of extra-mitochondrial Ca^{2+} upon mitochondrial Ca^{2+} sequestration or directly measure mitochondrial Ca^{2+} signals of the matrix of isolated mitochondria, mitochondria in permeabilized or intact cells are frequently used to study mitochondrial Ca^{2+} signaling. Each method represents a distinct possibility of studying mitochondrial Ca^{2+} uptake whereupon the most appropriate application of one protocol is down to the actual question to be investigated. Our comparison of different experimental approaches and protocols revealed that depending on the techniques used, different properties of mitochondrial Ca^{2+} uptake are unmasked. Notably, caution is necessary in the interpretation of data elaborated with only one technique as discrepancies within data obtained with different techniques might be due to the distinct methodical approaches. Such discrepancies have recently led to controversies regarding the putative function of uncoupling proteins 2 and 3 (UCP2/3) as key components of mitochondrial Ca^{2+} channels (Brookes et al., 2008; De Marchi et al., 2011; Trenker et al., 2008).

The choice of the technique used to study mitochondrial Ca^{2+} uptake appears to be crucial and the decision might base on several considerations: In general, all approaches using isolated mitochondria offer the opportunity to be accessible for cell-impermeable substrates, and are adequate for proteomic studies. Moreover, it offers experiments using the patch clamp technique and, thus, the direct investigation of mitochondrial ion channels. Permeabilization methods require lower sample amount, summarize subsets of mitochondrial populations and do not directly change adjacent cell structure, preserving possible interactions with other organelles (Saks et al., 1998). Still, permeabilization may impede some of the intact cells properties and limits possibilities to studying signal transduction mechanisms due to a loss of cytoplasm. Finally, the undisturbed systemic view on the level of intact cells appears to be the most attractive, if one intends to investigate the complexity of mitochondrial functions in their natural environment and their participation in cellular signal transduction.

4.1. Patching mitoplasts

In this study we show evidence for the existence of two currents of different amplitudes that occurred alternately in a stochastic manner, thus, possibly pointing to different mitochondrial Ca^{2+} channels in mitoplasts prepared from HeLa and endothelial cells.

To our knowledge this is the first time that mitochondrial Ca^{2+} channels have been characterized using the patch clamp technique in this particular cell lines that are frequently used to investigate mitochondrial signaling. Our finding of different mitochondrial Ca^{2+} channels in HeLa and endothelial cells is in line with a recent report that showed distinct mitochondrial Ca^{2+} channels of mitoplasts from human cardiac myocytes (Michels et al., 2009). However, because in the mitoplast-attached configuration used (i.e. high K^+ in the medium) the actual potential of the mitoplast may not entirely be constant, changes of single channel amplitudes may reflect spontaneous alterations of the membrane potential of mitoplasts. Indeed such fluctuations in the membrane potential of the mitoplast might be responsible for the small shifts of the distinct current amplitudes in experiments with a presumably constant holding potential. The different conductances of currents found in our experiments may not necessarily prove the existence of multiple individual channels but different modes of one single channel for mitochondrial Ca^{2+} uptake (Spat et al., 2008; Szanda et al., 2008, 2010). Nevertheless, as individual currents also occur superimposed with rather distinct biophysical characteristics, the distinct ranges of current amplitudes/conductances obtained in mitoplasts of HeLa and endothelial cells, most likely reflect the co-existence of at least two separate inward Ca^{2+} currents. Evidently, these findings support the assumption of the co-existence of multiple and maybe cell type- and species specific mitochondrial Ca^{2+} channels (Michels et al., 2009). Interestingly, with its conductance of 13–14 pS, *i*-MCC that was found to exist in mitoplasts from endothelial and HeLa cells, is strikingly similar to the mCa1 found in non-failing cardiac myocytes (Michels et al., 2009), though the gating parameters were slightly different within the two studies. Moreover, the conductance (7 pS) and gating characteristics of endothelial *s*-MCC, described herein, meets that of the mCa2 in non-failing heart (Michels et al., 2009). In view of the close developmental association of endothelial cells with cardiac myocytes, their similarities in regard of the two mitochondrial Ca^{2+} inward currents might not be surprising and may further point to tissue specificity of the mitochondrial Ca^{2+} uptake machinery.

4.2. Different modes of mitochondrial Ca^{2+} uptake in permeabilized cells

Major differences in Ca^{2+} sensitivity of mitochondrial Ca^{2+} uptake were observed between indirect assessments and direct recordings of mitochondrial Ca^{2+} signals using permeabilized cells. Notably, while in experiments with permeabilized cells expressing RPmt a mitochondrial Ca^{2+} uptake at Ca^{2+} concentrations below 200 nM was measured, this highly Ca^{2+} sensitive uptake pathway/mode could not be observed when mitochondrial Ca^{2+} sequestration was indirectly measured in suspended permeabilized cells using a Ca^{2+} dye in the bath (i.e. "Calcium-Green® 5 N technique"). The actual reason for this difference is not known. However, it has to be considered that the signals obtained, when measuring mitochondrial Ca^{2+} uptake of a population of permeabilized cells indirectly (i.e. "Calcium-Green® 5 N technique"), might reflect the summary of multiple complex Ca^{2+} shuttling events involving the opening of the mitochondrial permeability transition pore as well. This assumption is supported by a recent report demonstrating maximal Ca^{2+} uptake of suspended mitochondria to depend on the mode of Ca^{2+} addition (Chalmers and Nicholls, 2003).

4.3. Mitochondrial Ca^{2+} signals of intact cells

Using FP-based Ca^{2+} sensors targeted to the mitochondria represents the most elegant way to study mitochondrial Ca^{2+} uptake in intact cells (Demaurex, 2005). Very recently, we used this method to assess different modes of mitochondrial Ca^{2+} uptake in endothelial cells (Waldeck-Weiermair et al., 2011). Thereby, the specific contribution of different proteins, that were shown to play important roles in mitochondrial Ca^{2+} uptake, was investigated. In regard to the contribution of uncoupling protein 2 and 3 (UCP2/3) experiments using siRNA mediated knock-down (Trenker et al., 2007; Waldeck-Weiermair et al., 2010a), expression of mutated proteins (Waldeck-Weiermair et al., 2010b), and overexpression of UCP 2/3 (Trenker et al., 2007; Waldeck-Weiermair et al., 2010a) revealed that these proteins fundamentally contribute to mitochondrial uptake of high and low Ca^{2+} signals in intact cells. Notably, under physiological low expression levels of UCP 2/3, these proteins exclusively contributed to mitochondrial Ca^{2+} uptake at sites of ER Ca^{2+} release (Waldeck-Weiermair et al., 2010a,b). In contrast, the leucine zipper EF hand-containing transmembrane protein 1 (Letm1), that was recently identified as a mitochondrial Ca^{2+}/H^+ antiporter (Jiang et al., 2009), entirely accomplished the transfer of entering Ca^{2+} into mitochondria in a UCP 2/3-independent, high Ca^{2+}-sensitive manner (Waldeck-Weiermair et al., 2011). Moreover, we used this method to directly assess the impact of mitochondrial calcium uptake 1 (MICU1), a protein that triggers mitochondrial Ca^{2+} uptake in HeLa cells (Perocchi et al., 2010), on mitochondrial Ca^{2+} signaling in intact endothelial cells. Hence, because siRNA-mediated knock-down (verified on mRNA level) of MICU1 failed to impact mitochondrial Ca^{2+} uptake in the endothelial cell the involvement of MICU1 in mitochondrial Ca^{2+} uptake in this particular cell type can be excluded (Waldeck-Weiermair et al., 2011). The contribution of the ryanodine receptor type 1 (Beutner et al., 2005; Ryu et al., 2010, 2011) and the very recently described mitochondrial Ca^{2+} uniporter protein (Baughman et al., 2011; De Stefani et al., 2011) to mitochondrial Ca^{2+} uptake in endothelial cells awaits investigation. In particular, the question remains, whether or not these proteins contribute to one given conductance/channel/Ca^{2+} entry pathway or achieve distinct Ca^{2+} entry routes into the mitochondria, like it has been recently described for UCP2/3 and Letm1 (Waldeck-Weiermair et al., 2011). Overall, these studies that were mainly based on direct measurements of mitochondrial Ca^{2+} uptake of intact cells using FP-based Ca^{2+} sensors (RPmt and 4mtD3cpv), indicate the co-existence of at least two molecularly distinct mitochondrial Ca^{2+} uptake pathways in one given cell type. These pathways might be necessary in order to properly integrate cytosolic Ca^{2+} signals into mitochondrial responses.

4.4. Conclusion

Here we demonstrate that different experimental approaches yield different views of mitochondrial Ca^{2+} uptake. There is increasing evidence that several different proteins accomplish the transfer of Ca^{2+} across the inner mitochondrial membrane during cell stimulation (Hajnoczky and Csordas, 2010; Malli and Graier, 2010) that may account for either a low Ca^{2+}-sensitive but high capacity or a high Ca^{2+}-sensitive but low capacity mitochondrial Ca^{2+} uptake pathway. Importantly, these different mitochondrial Ca^{2+} uptake routes/modes often become evident or remain undetectable depending on the protocols and techniques used. The scenario gains complexity if one considers multiple ways and mechanisms that may modulate the function of the proteins contributing to mitochondrial Ca^{2+} signaling in intact cells (Koncz et al., 2009; Szanda et al., 2010). Accordingly, mitochondrial Ca^{2+} uptake is still an enigmatic molecular process and to investigate this versatile and complex phenomenon the utilization of multiple techniques and methodical approaches appears necessary.

Acknowledgments

The authors thank Mrs. Anna Schreilechner and Florian Enzinger for their excellent technical assistance, Drs. R. Tsien and

A. Palmer, University of California/San Diego, USA for $D1_{ER}$ and the mito-cameleon (4mtD3cpv), Dr. A. Miyawaki for ratiometric pericam (RP-mt), and Dr. C.J.S. Edgell (University of North Carolina, Chapel Hill, NC, USA) for the EA.hy926 cells. This work was supported by the Austrian Science Funds (FWF, P2081-B05 and P21857-B18 to W.F.G. and P22553-B18 to M.R.) and the Franz-Lanyar-Stiftung, Graz. Claire Jean-Quartier/this work is funded by the FWF (W1226-B18, DKplus Metabolic and Cardiovascular Disease) at the Medical University of Graz. Muhammad Rizwan Alam is funded by the FWF (P21857-B18) within the Doctoral College "Molecular Medicine" at the Medical University of Graz.

References

Baughman, J.M., Perocchi, F., Girgis, H.S., Plovanich, M., Belcher-Timme, C.A., Sancak, Y., Bao, X.R., Strittmatter, L., Goldberger, O., Bogorad, R.L., Koteliansky, V., Mootha, V.K., 2011. Integrative genomics identifies MCU as an essential component of the mitochondrial calcium uniporter. Nature 476, 341–345.

Ball, E.H., Singer, S.J., 1982. Mitochondria are associated with microtubules and not with intermediate filaments in cultured fibroblasts. Proc. Natl. Acad. Sci. USA 79, 123–126.

Bereiter-Hahn, J., Jendrach, M., 2010. Mitochondrial dynamics. Int. Rev. Cell. Mol. Biol. 284, 1–65.

Berridge, M.J., Bootman, M.D., Roderick, H.L., 2003. Calcium signalling: dynamics, homeostasis and remodelling. Nat. Rev. Mol. Cell Biol. 4, 517–529.

Berridge, M.J., Lipp, P., Bootman, M.D., 2000. The versatility and universality of calcium signalling. Nat. Rev. Mol. Cell Biol. 1, 11–21.

Beutner, G., Sharma, V.K., Lin, L., Ryu, S.Y., Dirksen, R.T., Sheu, S.S., 2005. Type 1 ryanodine receptor in cardiac mitochondria: transducer of excitation-metabolism coupling. Biochim. Biophys. Acta 1717, 1–10.

Brookes, P.S., Parker, N., Buckingham, J.A., Vidal-Puig, A., Halestrap, A.P., Gunter, T.E., Nicholls, D.G., Bernardi, P., Lemasters, J.J., Brand, M.D., 2008. UCPs-unlikely calcium porters. Nat. Cell Biol. 10, 1235–1237, author reply 1237–40.

Cao, X., Chen, Y., 2009. Mitochondria and calcium signaling in embryonic development. Semin. Cell Dev. Biol. 20, 337–345.

Chalmers, S., Nicholls, D.G., 2003. The relationship between free and total calcium concentrations in the matrix of liver and brain mitochondria. J. Biol. Chem. 278, 19062–19070.

Chen, L.B., 1988. Mitochondrial membrane potential in living cells. Annu. Rev. Cell Biol. 4, 155–181.

Cox, D.A., Conforti, L., Sperelakis, N., Matlib, M.A., 1993. Selectivity of inhibition of Na(+)-Ca^{2+} exchange of heart mitochondria by benzothiazepine CGP-37157. J. Cardiovasc. Pharmacol. 21, 595–599.

Cox, D.A., Matlib, M.A., 1993. A role for the mitochondrial Na(+)-Ca^{2+} exchanger in the regulation of oxidative phosphorylation in isolated heart mitochondria. J. Biol. Chem. 268, 938–947.

Csordas, G., Thomas, A.P., Hajnoczky, G., 1999. Quasi-synaptic calcium signal transmission between endoplasmic reticulum and mitochondria. EMBO J. 18, 96–108.

Daum, G., Bohni, P.C., Schatz, G., 1982. Import of proteins into mitochondria. Cytochrome *b*2 and cytochrome *c* peroxidase are located in the intermembrane space of yeast mitochondria. J. Biol. Chem. 257, 13028–13033.

De Brito, O.M., Scorrano, L., 2008. Mitofusin 2 tethers endoplasmic reticulum to mitochondria. Nature 456, 605–610.

De Marchi, U., Castelbou, C., Demaurex, N., 2011. Uncoupling protein 3 (UCP3) modulates the activity of sarco/endoplasmic reticulum Ca^{2+}-ATPase (SERCA) by decreasing mitochondrial ATP production. J. Biol. Chem. 286, 32533–32541.

De Stefani, D., Raffaello, A., Teardo, E., Szabo, I., Rizzuto, R., 2011. A forty-kilodalton protein of the inner membrane is the mitochondrial calcium uniporter. Nature 476, 336–340.

Decuypere, J.P., Monaco, G., Bultynck, G., Missiaen, L., De Smedt, H., Parys, J.B., 2011. The IP_3 receptor-mitochondria connection in apoptosis and autophagy. Biochim. Biophys. Acta 1813, 1003–1013.

Deluca, H.F., Engstrom, G.W., 1961. Calcium uptake by rat kidney mitochondria. Proc. Natl. Acad. Sci. USA 47, 1744–1750.

Demaurex, N., 2005. Calcium measurements in organelles with Ca^{2+}-sensitive fluorescent proteins. Cell Calcium 38, 213–222.

Demaurex, N., Distelhorst, C., 2003. Cell biology. Apoptosis – the calcium connection. Science 300, 65–67.

Dhalla, N.S., 1969. Excitation–contraction coupling in heart. I. Comparison of calcium uptake by the sarcoplasmic reticulum and mitochondria of the rat heart. Arch. Int. Physiol. Biochim. 77, 916–934.

Duchen, M.R., Szabadkai, G., 2010. Roles of mitochondria in human disease. Essays Biochem. 47, 115–137.

Duchen, M.R., Verkhratsky, A., Muallem, S., 2008. Mitochondria and calcium in health and disease. Cell Calcium 44, 1–5.

Eberhard, M., Erne, P., 1991. Calcium binding to fluorescent calcium indicators: calcium green, calcium orange and calcium crimson. Biochem. Biophys. Res. Commun. 180, 209–215.

Edgell, C.J., McDonald, C.C., Graham, J.B., 1983. Permanent cell line expressing human factor VIII-related antigen established by hybridization. Proc. Natl. Acad. Sci. USA 80, 3734–3737.

Filippin, L., Abad, M.C., Gastaldello, S., Magalhaes, P.J., Sandona, D., Pozzan, T., 2005. Improved strategies for the delivery of GFP-based Ca^{2+} sensors into the mitochondrial matrix. Cell Calcium 37, 129–136.

Fonteriz, R.I., de la Fuente, S., Moreno, A., Lobaton, C.D., Montero, M., Alvarez, J., 2010. Monitoring mitochondrial [Ca^{2+}] dynamics with rhod-2, ratiometric pericam and aequorin. Cell Calcium 48, 61–69.

Frezza, C., Cipolat, S., Scorrano, L., 2007. Organelle isolation: functional mitochondria from mouse liver, muscle and cultured fibroblasts. Nat. Protoc. 2, 287–295.

Giorgi, C., Romagnoli, A., Pinton, P., Rizzuto, R., 2008. Ca^{2+} signaling, mitochondria and cell death. Curr. Mol. Med. 8, 119–130.

Graier, W.F., Frieden, M., Malli, R., 2007. Mitochondria and Ca^{2+} signaling: old guests, new functions. Pflugers Arch. 455, 375–396.

Gunter, T.E., Gunter, K.K., Sheu, S.S., Gavin, C.E., 1994. Mitochondrial calcium transport: physiological and pathological relevance. Am. J. Physiol. 267, C313–C339.

Hajnoczky, G., Csordas, G., 2010. Calcium signalling: fishing out molecules of mitochondrial calcium transport. Curr. Biol. 20, R888–R891.

Huang, X., Zhai, D., Huang, Y., 2000. Study on the relationship between calcium-induced calcium release from mitochondria and PTP opening. Mol. Cell. Biochem. 213, 29–35.

Hunter, D.R., Haworth, R.A., 1979. The Ca^{2+}-induced membrane transition in mitochondria. III. Transitional Ca^{2+} release. Arch. Biochem. Biophys. 195, 468–477.

Jiang, D., Zhao, L., Clapham, D.E., 2009. Genome-wide RNAi screen identifies Letm1 as a mitochondrial Ca^{2+}/H^{+} antiporter. Science 326, 144–147.

Kennedy, E.P., Lehninger, A.L., 1949. Oxidation of fatty acids and tricarboxylic acid cycle intermediates by isolated rat liver mitochondria. J. Biol. Chem. 179, 957–972.

Kirichok, Y., Krapivinsky, G., Clapham, D.E., 2004. The mitochondrial calcium uniporter is a highly selective ion channel. Nature 427, 360–364.

Knot, H.J., Laher, I., Sobie, E.A., Guatimosim, S., Gomez-Viquez, L., Hartmann, H., Song, L.S., Lederer, W.J., Graier, W.F., Malli, R., Frieden, M., Petersen, O.H., 2005. Twenty years of calcium imaging: cell physiology to dye for. Mol. Interv. 5, 112–127.

Koncz, P., Szanda, G., Fulop, L., Rajki, A., Spat, A., 2009. Mitochondrial Ca^{2+} uptake is inhibited by a concerted action of p38 MAPK and protein kinase D. Cell Calcium 46, 122–129.

Koshiba, T., Detmer, S.A., Kaiser, J.T., Chen, H., McCaffery, J.M., Chan, D.C., 2004. Structural basis of mitochondrial tethering by mitofusin complexes. Science 305, 858–862.

Liu, X., Hajnoczky, G., 2009. Ca^{2+}-dependent regulation of mitochondrial dynamics by the Miro-Milton complex. Int. J. Biochem. Cell Biol. 41, 1972–1976.

Liu, X., Weaver, D., Shirihai, O., Hajnoczky, G., 2009. Mitochondrial 'kiss-and-run': interplay between mitochondrial motility and fusion–fission dynamics. EMBO J. 28, 3074–3089.

Liu, Z., Butow, R.A., 2006. Mitochondrial retrograde signaling. Annu. Rev. Genet. 40, 159–185.

Malli, R., Frieden, M., Osibow, K., Graier, W.F., 2003. Mitochondria efficiently buffer subplasmalemmal Ca^{2+} elevation during agonist stimulation. J. Biol. Chem. 278, 10807–10815.

Malli, R., Graier, W.F., 2010. Mitochondrial Ca^{2+} channels: Great unknowns with important functions. FEBS Lett. 584, 1942–1947.

McBride, H.M., Neuspiel, M., Wasiak, S., 2006. Mitochondria: more than just a powerhouse. Curr. Biol. 16, R551–R560.

McCombs, J.E., Palmer, A.E., 2008. Measuring calcium dynamics in living cells with genetically encodable calcium indicators. Methods 46, 152–159.

Merkwirth, C., Langer, T., 2008. Mitofusin 2 builds a bridge between ER and mitochondria. Cell 135, 1165–1167.

Michels, G., Khan, I.F., Endres-Becker, J., Rottlaender, D., Herzig, S., Ruhparwar, A., Wahlers, T., Hoppe, U.C., 2009. Regulation of the human cardiac mitochondrial Ca^{2+} uptake by 2 different voltage-gated Ca^{2+} channels. Circulation 119, 2435–2443.

Miyawaki, A., Griesbeck, O., Heim, R., Tsien, R.Y., 1999. Dynamic and quantitative Ca^{2+} measurements using improved cameleons. Proc. Natl. Acad. Sci. USA 96, 2135–2140.

Miyawaki, A., Llopis, J., Heim, R., McCaffery, J.M., Adams, J.A., Ikura, M., Tsien, R.Y., 1997. Fluorescent indicators for Ca^{2+} based on green fluorescent proteins and calmodulin. Nature 388, 882–887.

Miyawaki, A., Mizuno, H., Nagai, T., Sawano, A., 2003. Development of genetically encoded fluorescent indicators for calcium. Methods Enzymol. 360, 202–225.

Nagai, T., Ibata, K., Park, E.S., Kubota, M., Mikoshiba, K., Miyawaki, A., 2002. A variant of yellow fluorescent protein with fast and efficient maturation for cell-biological applications. Nat. Biotechnol. 20, 87–90.

Nagai, T., Sawano, A., Park, E.S., Miyawaki, A., 2001. Circularly permuted green fluorescent proteins engineered to sense Ca^{2+}. Proc. Natl. Acad. Sci. USA 98, 3197–3202.

Osibow, K., Frank, S., Malli, R., Zechner, R., Graier, W.F., 2006. Mitochondria maintain maturation and secretion of lipoprotein lipase in the endoplasmic reticulum. Biochem. J. 396, 173–182.

Palmer, A.E., Giacomello, M., Kortemme, T., Hires, S.A., Lev-Ram, V., Baker, D., Tsien, R.Y., 2006. Ca^{2+} indicators based on computationally redesigned calmodulin-peptide pairs. Chem. Biol. 13, 521–530.

Perocchi, F., Gohil, V.M., Girgis, H.S., Bao, X.R., McCombs, J.E., Palmer, A.E., Mootha, V.K., 2010. MICU1 encodes a mitochondrial EF hand protein required for Ca^{2+} uptake. Nature 467, 291–296.

Rizzuto, R., Simpson, A.W., Brini, M., Pozzan, T., 1992. Rapid changes of mitochondrial Ca^{2+} revealed by specifically targeted recombinant aequorin. Nature 358, 325–327.

Ryu, S.Y., Beutner, G., Dirksen, R.T., Kinnally, K.W., Sheu, S.S., 2010. Mitochondrial ryanodine receptors and other mitochondrial Ca^{2+} permeable channels. FEBS Lett. 584, 1948–1955.

Ryu, S.Y., Beutner, G., Kinnally, K.W., Dirksen, R.T., Sheu, S.S., 2011. Single channel characterization of the mitochondrial ryanodine receptor in heart mitoplasts. J. Biol. Chem. 286, 21324–21329.

Saks, V.A., Veksler, V.I., Kuznetsov, A.V., Kay, L., Sikk, P., Tiivel, T., Tranqui, L., Olivares, J., Winkler, K., Wiedemann, F., Kunz, W.S., 1998. Permeabilized cell and skinned fiber techniques in studies of mitochondrial function in vivo. Mol. Cell. Biochem. 184, 81–100.

Santo-Domingo, J., Demaurex, N., 2010. Calcium uptake mechanisms of mitochondria. Biochim. Biophys. Acta 1797, 907–912.

Spat, A., Szanda, G., Csordas, G., Hajnoczky, G., 2008. High- and low-calcium-dependent mechanisms of mitochondrial calcium signalling. Cell Calcium 44, 51–63.

Stemberger, B.H., Walsh, R.M., Patton, S., 1984. Morphometric evaluation of lipid droplet associations with secretory vesicles, mitochondria and other components in the lactating cell. Cell Tissue Res. 236, 471–475.

Storrie, B., Madden, E.A., 1990. Isolation of subcellular organelles. Methods Enzymol. 182, 203–225.

Szabadkai, G., Simoni, A.M., Chami, M., Wieckowski, M.R., Youle, R.J., Rizzuto, R., 2004. Drp-1-dependent division of the mitochondrial network blocks intraorganellar Ca^{2+} waves and protects against Ca^{2+}-mediated apoptosis. Mol. Cell 16, 59–68.

Szanda, G., Halasz, E., Spat, A., 2010. Protein kinases reduce mitochondrial Ca^{2+} uptake through an action on the outer mitochondrial membrane. Cell Calcium 48, 168–175.

Szanda, G., Koncz, P., Rajki, A., Spat, A., 2008. Participation of p38 MAPK and a novel-type protein kinase C in the control of mitochondrial Ca^{2+} uptake. Cell Calcium 43, 250–259.

Trenker, M., Fertschai, I., Mall, R., Graier, W.F., 2008. UCP2/3 – likely to be fundamental for mitochondrial Ca^{2+} uniport. Nat. Cell Biol. 10, 1237–1240.

Trenker, M., Malli, R., Fertschai, I., Levak-Frank, S., Graier, W.F., 2007. Uncoupling proteins 2 and 3 are fundamental for mitochondrial Ca^{2+} uniport. Nat. Cell Biol. 9, 445–452.

Waldeck-Weiermair, M., Duan, X., Naghdi, S., Khan, M.J., Trenker, M., Malli, R., Graier, W.F., 2010a. Uncoupling protein 3 adjusts mitochondrial Ca^{2+} uptake to high and low Ca^{2+} signals. Cell Calcium 48, 288–301.

Waldeck-Weiermair, M., Malli, R., Naghdi, S., Trenker, M., Kahn, M.J., Graier, W.F., 2010b. The contribution of UCP2 and UCP3 to mitochondrial Ca^{2+} uptake is differentially determined by the source of supplied Ca^{2+}. Cell Calcium 47, 433–440.

Waldeck-Weiermair, M., Jean-Quartier, C., Rost, R., Khan, M.J., Vishnu, N., Bondarenko, A.I., Imamura, H., Malli, R., Graier, W.F., 2011. The leucine zipper EF hand-containing transmembrane protein 1 (LETM1) and uncoupling proteins-2 and 3 (UCP2/3) contribute to two distinct mitochondrial Ca^{2+} uptake pathways. J. Biol. Chem. 286, 28444–28455.

Wiederkehr, A., Szanda, G., Akhmedov, D., Mataki, C., Heizmann, C.W., Schoonjans, K., Pozzan, T., Spat, A., Wollheim, C.B., 2011. Mitochondrial matrix calcium is an activating signal for hormone secretion. Cell. Metab. 13, 601–611.

Cell Biology:

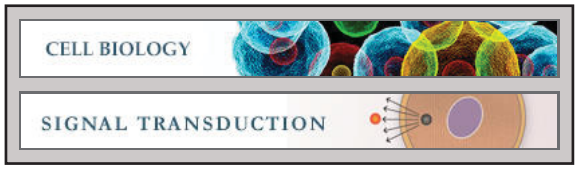

Leucine Zipper EF Hand-containing Transmembrane Protein 1 (Letm1) and Uncoupling Proteins 2 and 3 (UCP2/3) Contribute to Two Distinct Mitochondrial Ca^{2+} Uptake Pathways

Markus Waldeck-Weiermair, Claire Jean-Quartier, Rene Rost, Muhammad Jadoon Khan, Neelanjan Vishnu, Alexander I. Bondarenko, Hiromi Imamura, Roland Malli and Wolfgang F. Graier

J. Biol. Chem. 2011, 286:28444-28455.
doi: 10.1074/jbc.M111.244517 originally published online May 25, 2011

⌘ *Author's Choice*

THE JOURNAL OF BIOLOGICAL CHEMISTRY VOL. 286, NO. 32, pp. 28444–28455, August 12, 2011

Leucine Zipper EF Hand-containing Transmembrane Protein 1 (Letm1) and Uncoupling Proteins 2 and 3 (UCP2/3) Contribute to Two Distinct Mitochondrial Ca^{2+} Uptake Pathways*[S]

Received for publication, March 28, 2011, and in revised form, May 18, 2011 Published, JBC Papers in Press, May 25, 2011, DOI 10.1074/jbc.M111.244517

Markus Waldeck-Weiermair[‡], Claire Jean-Quartier[‡], Rene Rost[‡], Muhammad Jadoon Khan[‡], Neelanjan Vishnu[‡], Alexander I. Bondarenko[‡], Hiromi Imamura[§], Roland Malli[‡], and Wolfgang F. Graier[‡1]

From the [‡]Institute of Molecular Biology and Biochemistry, Molecular and Cellular Physiology Research Unit, Center of Molecular Medicine, Medical University Graz, Harrachgasse 21/III, 8010 Graz, Austria and the [§]Precursory Research for Embryonic Science, Japan Science and Technology Agency, 5 Sanbancho, Chiyoda-ku, Tokyo 102-0075, Japan

Cytosolic Ca^{2+} signals are transferred into mitochondria over a huge concentration range. In our recent work we described uncoupling proteins 2 and 3 (UCP2/3) to be fundamental for mitochondrial uptake of high Ca^{2+} domains in mitochondria-ER junctions. On the other hand, the leucine zipper EF hand-containing transmembrane protein 1 (Letm1) was identified as a mitochondrial Ca^{2+}/H^+ antiporter that achieved mitochondrial Ca^{2+} sequestration at small Ca^{2+} increases. Thus, the contributions of Letm1 and UCP2/3 to mitochondrial Ca^{2+} uptake were compared in endothelial cells. Knock-down of Letm1 did not affect the UCP2/3-dependent mitochondrial uptake of intracellularly released Ca^{2+} but strongly diminished the transfer of entering Ca^{2+} into mitochondria, subsequently, resulting in a reduction of store-operated Ca^{2+} entry (SOCE). Knock-down of Letm1 and UCP2/3 did neither impact on cellular ATP levels nor the membrane potential. The enhanced mitochondrial Ca^{2+} signals in cells overexpressing UCP2/3 rescued SOCE upon Letm1 knock-down. In digitonin-permeabilized cells, Letm1 exclusively contributed to mitochondrial Ca^{2+} uptake at low Ca^{2+} conditions. Neither the Letm1- nor the UCP2/3-dependent mitochondrial Ca^{2+} uptake was affected by a knock-down of mRNA levels of mitochondrial calcium uptake 1 (MICU1), a protein that triggers mitochondrial Ca^{2+} uptake in HeLa cells. Our data indicate that Letm1 and UCP2/3 independently contribute to two distinct, mitochondrial Ca^{2+} uptake pathways in intact endothelial cells.

With the introduction of sophisticated techniques that allowed direct measurements of mitochondrial Ca^{2+} signals in intact cells (1–6), the strong functional and even physical interaction of mitochondria with their cellular environment became evident (7–9). This interaction appeared to be crucial for the organelle's capability to decode and integrate cellular Ca^{2+} signals, which is an essential feature of cell signaling. Notably, convergences between mitochondria and other membrane structures allow the generation of high Ca^{2+} domains at sites of mitochondrial Ca^{2+} uptake (10, 11). It is believed that during physiological cell stimulation such high Ca^{2+} domains enable mitochondria to locally sequester Ca^{2+} via a low Ca^{2+}-sensitive mitochondrial Ca^{2+} uniporter (MCU) that was characterized as a highly selective Ca^{2+} ion channel (12). Notably, besides this low Ca^{2+}-sensitive MCU, modes of high sensitive mitochondrial Ca^{2+} uptake that operate at submicromolar Ca^{2+} ranges have been convincingly reported (13, 14). However it is not clear whether or not mitochondrial Ca^{2+} uptake is accomplished by a unique ubiquitous pathway that works at modes of different Ca^{2+} sensitivities. Alternatively, mitochondria might be equipped with different Ca^{2+} uptake machineries that achieve Ca^{2+} sequestration at different Ca^{2+} concentrations. Although the exact identity of the proteins that actually achieve Ca^{2+} transport into the mitochondrial matrix is still unclear, several recent findings confirm the latter assumption: 1) two different mitochondrial Ca^{2+} influx currents (15) and pathways (16) could be recently identified in one given cell, 2) uncoupling proteins 2 and 3 (UCP2/3)[2] were described to be involved in mitochondrial Ca^{2+} uptake in intact cells (17), 3) with the mitochondrial calcium uptake 1 (MICU1) protein a novel modulator of mitochondrial Ca^{2+} uptake was recently described in HeLa cells (18), and 4) the leucine zipper EF hand-containing transmembrane protein 1 (Letm1) was identified as a mitochondrial Ca^{2+}/H^+ exchanger that achieves a slow but highly sensitive mitochondrial Ca^{2+} loading (19). Moreover, evidence was provided that mitochondrial Ca^{2+} uptake depends on the mode and source of Ca^{2+} mobilization (14, 20, 21).

Based on recent data that indicate that UCP2/3-dependent mitochondrial Ca^{2+} uptake is involved in the rather low Ca^{2+}-

* This work was supported by the Austrian Science Funds (FWF, P20181-B05, P21857-B18, and P22553-B18). C. J.-Q. and N. V. are funded by the FWF (W 1226-B18, DKplus Metabolic and Cardiovascular Disease), and M. J. K. is funded by the FWF within the program Molecular Medicine at the Medical University of Graz.

[S] The on-line version of this article (available at http://www.jbc.org) contains supplemental Figs. S1–S3.

⌘ *Author's Choice*—Final version full access.

[1] To whom correspondence should be addressed: Institute of Molecular Biology and Biochemistry, Molecular and Cellular Physiology Research Unit, Center of Molecular Medicine, Medical University Graz, Harrachgasse 21/III, 8010 Graz, Austria. Tel.: 43-316-380-7560; Fax: 43-316-380-9615; E-mail: wolfgang.graier@medunigraz.at.

[2] The abbreviations used are: UCP2/3, uncoupling protein 2/3; ANT, adenine nucleotide translocase; $[Ca^{2+}]_{mito}$, mitochondrial Ca^{2+} concentration; Letm1, leucine zipper EF hand-containing transmembrane protein 1; MICU1, mitochondrial Ca^{2+} uptake 1; NCX_{mito}, mitochondrial Na^+/Ca^{2+} exchanger; pH_{mito}, mitochondrial pH; SOCE, store-operated Ca^{2+} entry.

sensitive mitochondrial uptake of intracellularly released Ca^{2+} but not that of entering Ca^{2+} (16, 22), and the findings that Letm1 operates as a highly sensitive Ca^{2+} uptake mechanism (19), this study was designed to investigate the particular contribution of Letm1 and UCP2/3 to mitochondrial Ca^{2+} uptake from the two major Ca^{2+} sources (*i.e.* intracellular Ca^{2+} release as well as store-operated Ca^{2+} entry, SOCE) in endothelial cells. Finally, we tested the function of MICU1 to complement an assessment of the individual role of the three most promising putative contributors to mitochondrial Ca^{2+} uptake in endothelial cells.

EXPERIMENTAL PROCEDURES

Materials—Dulbecco's modified Eagle's medium (DMEM), 2,5-di-tert-butylhydrochinone (BHQ), histamine, 2-deoxy-D-glucose, oligomycin, choline chloride, and digitonin were purchased at Sigma-Aldrich (Vienna, Austria). Fetal calf serum and media supplements were obtained from PAA Laboratories (Pasching, Austria). Fura-2/AM was ordered from Molecular Probes Europe (Leiden, Netherlands) and Transfast® reagent from Promega (Mannheim, Germany). All other chemicals were from Roth (Karlsruhe, Germany).

Cell Culture, Constructs, and Transfection—The human umbilical vein endothelial cell line, EA.hy926 passage at ≥45 stably expressing ratiometric pericam-mito (RP-mt) was used for this study. Cells were cultured in DMEM containing 10% FCS, 1% HAT (5 mM hypoxanthin, 20 μM aminopterin, 0.8 mM thymidine), 50 units/ml penicillin, 50 μg/ml streptomycin, and kept at 37 °C in 5% CO_2 atmosphere. 2–4 days before experiments cells were plated on 30 mm glass cover slips. After reaching ~80% of confluence, cells were co-transfected with different plasmids and siRNAs using Transfast® according to the protocol supplied by the manufacturer.

Buffers and Solutions—Cells were loaded with Fura-2/AM and rested prior to experiments in a Hepes-buffered solution containing (in mM): 135 NaCl, 5 KCl, 2 $CaCl_2$, 1 $MgCl_2$, 10 Hepes acid, 2.6 $NaHCO_3$, 0.44 KH_2PO_4, 0.34 Na_2HPO_4, 10 D-glucose, 0.1% vitamins, 0.2% essential amino acids, and 1% penicillin/streptomycin; pH was adjusted to 7.4 with NaOH. For experiments in intact cells the Ca^{2+}-containing experimental buffer (EB) was composed of (in mM): 138 NaCl, 5 KCl, 2 Ca_2Cl, 1 $MgCl_2$, 10 D-glucose, and 10 Hepes acid; pH was adjusted to 7.4 with NaOH. For experiments in Ca^{2+}-free solution, EB containing 1 mM EGTA instead of Ca^{2+} was used. For experiments in partially permeabilized cells, cells were perfused with 3 μM digitonin for 3 min in a high KCl buffer containing (in mM): 110 KCl, 0.5 KH_2PO_4, 1 $MgCl_2$, 20 Hepes acid, 0.03 EGTA, 5 succinate, 10 D-glucose; pH was adjusted to 7.4 with KOH. Mitochondrial Ca^{2+} uptake was triggered by the actual intracellular Ca^{2+} concentration ($[Ca^{2+}]_a$ set to 174 ± 18 nM (n = 17) (referred as "low Ca^{2+}") or to 921 ± 119 nM (n = 17) (referred as "high Ca^{2+}"): $[Ca^{2+}]_a$ was calculated from Fura-2 signals using the following equation as recently described (22): $[Ca^{2+}]_a = 350\ nM^* (F^{Ca} - F^{min})/(F^{max} - F^{Ca})$. To verify the role of the plasma membrane Ca^{2+} ATPase (PMCA), cells were stimulated with 100 μM histamine and 15 μM BHQ in a low sodium buffer (LSB) composed of (in mM): 19 NaCl, 119 choline chloride, 5 KCl, 2 $CaCl_2$ or 1 EGTA, 1 $MgCl_2$, 10 D-glucose, and 10 Hepes acid; pH was adjusted to 7.4 with KOH. For experiments using the perforated patch clamp technique the standard external solution contained (in mM): 145 NaCl, 5 KCl, 1.2 $MgCl_2$, 10 HEPES, 10 D-glucose, 2.4 $CaCl_2$. In Ca^{2+}-free solutions, $MgCl_2$ was increased to 2.2 mM and 1 mM EGTA was added. Patch pipettes were filled with a solution containing (mM): 100 KAsp, 40 KCl, 10 HEPES, 2 $MgCl_2$, 0.2 EGTA.

Isolation of Total RNA and cDNA Synthesis—Total RNA from EA.hy926 cells was isolated with the peqGold Total RNA kit (Peqlab, Erlangen). 2–3 μg of RNA were subsequently reverse transcribed to cDNA using the High Capacity cDNA Reverse Transcription kit (Applied Biosystems, Lincoln, CA).

Gene Verification—Detection of human Letm1 (Letm1, GenBank™ accession no. NM_12318.2) and human MICU1 (MICU1, GenBank™ accession no. NM_006077.2) in EA.hy926 was performed by RT-PCR. Letm1 was identified using a forward primer at position 1082 (5′-AGTTCCTCCAGGACACCATC-3′) and a reverse primer at position 1612 (5′-TCTGCAGTGTGGACTTGAGC-3′). For the verification of MICU1 (GenBank™ accession no. NM_006077.2) the forward primer at position 418 (5′-CCTGGTGAAGCAGAAGTGTT-3′) and the reverse primer at position 1151 (5′-CTCAATGCAGTGTCCACATC-3′) were used.

RNAi Design—According to already published siRNA sense sequences for Letm1 (19) and for MICU1 (18), two different siRNAs were tested in EA.hy926 cells for both genes, Letm1 and MICU1 *versus* a non-functional Control siRNA (Control): AGGUAGUGUAAUCGCCUUGtt; sense sequence for Letm1 siRNA1 (si1-Letm1): UCCACAUUUGAGACUCAGUtt and siRNA2 (si2-Letm1): AUGUUCCAUUUGGCUGCUGtt; sense sequence for MICU1 siRNA1 (si1-MICU1): GCAAUGGCGAACUGAGCAAUAtt and siRNA2 (si2-MICU1): GCAGCUCAAGAAGCACUUCAAtt. Silencing of UCP2/3 was performed using siRNAs as described and validated previously (16, 17).

Validation of siRNAs—Knock-down efficiency of functional siRNAs against human Letm1 (Ambion, Cambridgeshire, UK) or human MICU1 (Microsynth, Balgach, Switzerland) were validated individually and in combination by real-time quantitative-PCR (RTq-PCR) *versus* the Control siRNA (Microsynth, Balgach, Switzerland). 48 h after cell transfection with the respective siRNAs, mRNA was isolated and reverse transcribed. RTq-PCR was performed using specific primer pairs for human Letm1 (5′-TGTTCTTCAAGGCCATCTCC-3′, 5′-TGTTGCTGTGAAGCTCTTCC-3′), for human MICU1 (5′-CAGGTTCAGAGCATCATTCG-3′, 5′-GAACACAAGCCAGACTTGAG-3′), and QuantiTect® Primer Assays (Qiagen, Hilden, Germany), for human UCP2 (Cat. No.: QT00014140) for human UCP3 (Cat. No.: QT00017220) and for human GAPDH (Cat. No.: QT01192646) as housekeeping gene. RTq-PCR was performed with a LightCycler® 480 System (Roche, Basel, Switzerland) using the QuantiFast SYBR Green PCR kit (Qiagen).

Plasmid Constructs—Vectors for Letm1 overexpression were purchased form GeneCopoeia™ (Rockville, MD). For mitochondrial Ca^{2+} measurements the plasmid encoding the untagged Letm1 (Letm1; Cat. No.: EX-W0230-M02) was used for transfection in a ratio 3:1 with a nuclear-targeted GFP (nls-GFP). Visualization of Letm1 was done with a vector expressing

mCherry C-terminally fused to Letm1 (Letm1-mCherry; Cat. No.: EX-W0230-M56). UCP3 overexpression was achieved as previously shown (16). For ATP measurements the novel FRET-based ATP indicator AT1.03 for the cytosolic ATP and its mitochondrial-targeted version mt AT1.03 (23) for mitochondrial ATP were used.

Cytosolic Ca^{2+} and Ba^{2+} Measurements—Changes in $[Ca^{2+}]_{cyto}$ and $[Ba^{2+}]_{cyto}$ were monitored using Fura-2/AM as previously described (24, 25). Addition of Ba^{2+} to SOCE-activated cells was performed with EB using 10 mM $BaCl_2$ instead of 2 mM $CaCl_2$.

Mitochondrial Ca^{2+} and pH Measurements with Ratiometric Pericam-mito—Cells stably expressing ratiometric-pericam-mito (RP-mt) (3) were used to monitor $[Ca^{2+}]_{mito}$ and $[H^+]_{mito}$ simultaneously. RP-mt was excited at either 430 nm or 485 nm with a high-speed polychromator system VisiChrome (Visitron Systems, Puchheim, Germany). Emitted light was recorded at 535 nm using the 535AF26 emission filter from Omega Optical (Brattleboro, VT). $[Ca^{2+}]_{mito}$ was expressed as $1\text{-}F_{430}/F_0$ as previously shown (17, 26). Changes in pH were expressed as $1 - F_{485}/F_0$, where F_{485} is the fluorescence (485 nm excitation) at a given time and F_0 is the mean fluorescence of 30–60 individual measurements collected at the beginning of recordings (27). Experiments were performed at room temperature. Rates of acquisition were between 1.04 and 2.66 s and exposure times were 600–800 ms.

FRET-based Cytosolic and Mitochondrial ATP Measurements—For ATP measurements cells were transiently transfected with the FRET-based ATP indicators AT1.03 or mt AT1.03 to measure changes in cytosolic or mitochondrial ATP levels, respectively (23). The sensor was excited at 430 nm using a high-speed polychromator system VisiChrome (Vistitron Systems, Puchheim, Germany) and emission was collected at 535 and 480 nm (Versatile Filter Wheel Systems, Vistitron Systems, Puchheim, Germany).

Patch Clamp Recordings—Membrane potential was recorded using the perforated patch-clamp technique in a current clamp mode (28–32). For membrane perforation, nystatin (300 μM) was included into the pipette solution. Membrane potential was recorded using a List EPC7 amplifier (HEKA, Lambrecht/Pfalz, Germany). Borosilicate glass pipettes were pulled with a Narishige puller (Narishige Co. Ltd, Tokyo, Japan), fire-polished and had a resistance of 4–6 MΩ. The signals obtained were low pass filtered at 1 kHz, and digitized with a sample rate of 10 kHz using a Digidata 1200A A/D converter (Axon Instruments, Foster City, CA). Data collection and analysis were performed using Clampex and Clampfit software of pClamp 9 (Axon Instruments, Molecular Devices, Sunnyvale, CA).

Confocal Microscopy—High resolution imaging of cells expressing Letm1-mCherry and ratiometric pericam-mito (RP-mt) was performed using a Nipkow-disk-based array confocal laser scanning microscope (ACLSM) as described previously (17, 33). The ACLSM consisted of a Zeiss Axiovert 200 M (Zeiss 100×/1.45 oil objective, Zeiss Microsystems, Jena, Germany), equipped with VoxCell Scan® (VisiTech, Sunderland, UK), and an air-cooled argon ion laser system (series 543, CVI Melles Griot, CA). The laser line 488 nm was used to excite RP-mt, whereas alternatively wavelength 561 nm was used to excite Letm1-mCherry. Emitted light was collected at 535 nm (535AF26; Omega Optical, Brattleboro, VT) for RP-mt or 620 nm (Omega Optical) for Letm1-mCherry using a high resolution CCD camera (Photometrics CoolSNAPfx-HQ, Roper Scientific, Tucson, AZ). Acquisition and analysis were performed with Metamorph 6.2r6 (Universal Imaging, Visitron Systems, Puchheim, Germany).

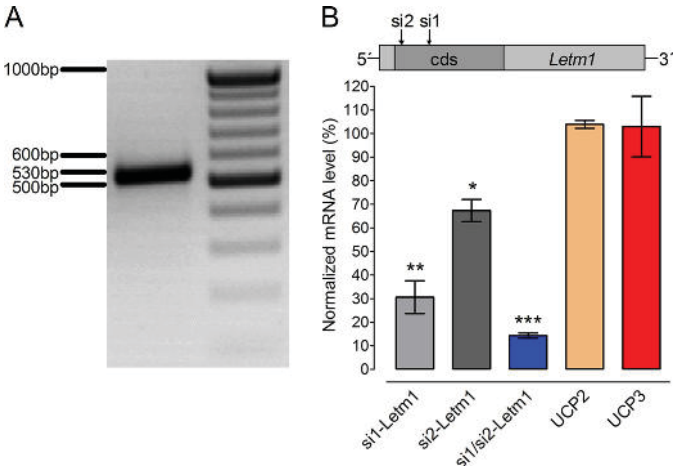

FIGURE 1. **Detection and siRNA validation of human Letm1 on the mRNA level of Ea.hy926 cells.** *Panel A*, RT-PCR using specific primers for Letm1 mRNA (see "Experimental Procedures") yielded a clear 530 bp product amplification. *Panel B*, points of applications of 2 different siRNAs (see "Experimental Procedures") against Letm1 are illustrated within the open reading frame of the mRNA of Letm1. Efficiency of siRNA-mediated Letm1 knock-down was verified by real time quantitative-PCR after transfection of siRNA1 (*si1-Letm1*, $n = 3$) or siRNA2 (*si2-Letm2*, $n = 3$) against Letm1 individually or both in combination (*si1/si2-Letm1*, $n = 3$) *versus* Control siRNA (*Control*, $n = 3$). Data are expressed in % of the maximal response in Control. *, $p = 0.013$; **, $p = 0.0019$; ***, $p < 0.0001$ *versus* Control. mRNA expression levels of either UCP2 or UCP3 were not influenced by the knock-down of Letm1 using the sample that was treated with both siRNAs against Letm1.

Statistics—Statistical data are presented as mean ± S.E. Analysis of variance (ANOVA) and Scheffe's *post hoc* F test were used for evaluation of the statistical significance. $p < 0.05$ was defined significant.

RESULTS

Letm1 Is Expressed in Endothelial Cells and mRNA Levels of Letm1 Can Be Efficiently Reduced by a Combination of Two siRNAs—Using respective primers (see "Experimental Procedures"), the expression of Letm1 was verified in the human umbilical vein endothelial cell line EA.hy926 (Fig. 1*A*). Two siRNA sequences were tested alone and in combination for the knock-down efficiency in human endothelial cells. The siRNAs reduced the mRNA level of Letm1 by 33.6 ± 4.7 ($n = 3$) and 69.4 ± 7.5 ($n = 3$) %, respectively. The combination of both siRNAs achieved the highest knock-down efficiency (85.7 ± 1.1%; $n = 3$), while they had no effect on the expression levels of UCP2 and UCP3 (Fig. 1*B*), thus, this combination was subsequently used for all experiments.

Knock-down of Letm1 and UCP2/3 Exhibit Different Inhibitory Patterns on Mitochondrial Ca^{2+} Uptake—In our previous work using the same type of cells, considerable differences in the contribution of UCP2/3 to mitochondrial Ca^{2+} sequestration were described that basically depend on the source of the Ca^{2+} supply (*i.e.* intracellular Ca^{2+} release from the ER or

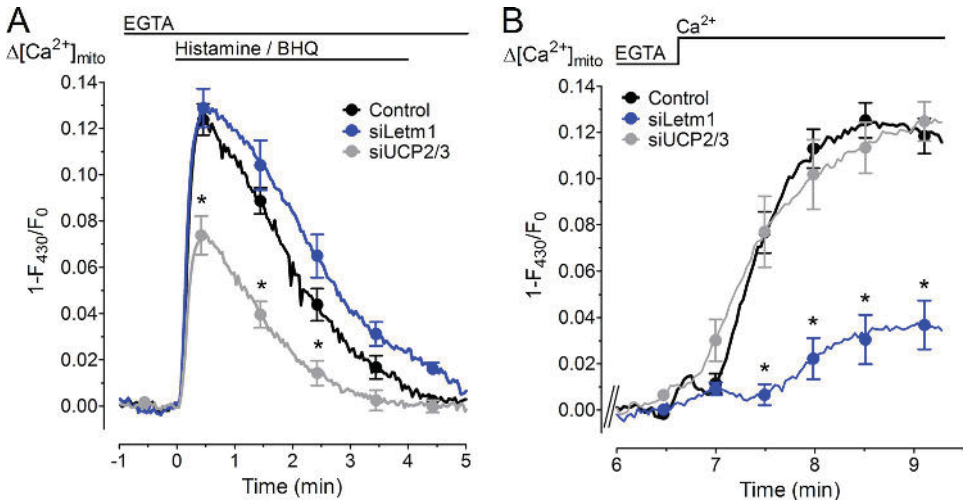

FIGURE 2. **Knock-down of UCP2/3 exclusively reduced the mitochondrial Ca^{2+} uptake from intracellularly released Ca^{2+} whereas Letm1 knock-down strongly diminished mitochondrial Ca^{2+} accumulation only upon SOCE.** Endothelial cells that stably express RP-mt cells were transiently co-transfected with nuclear GFP and either Control siRNA (*Control*: $n = 6$, 14 cells), or siRNA against Letm1 (*siLetm1*: $n = 6$, 12 cells), or siRNA against UCP2 and UCP3 (*siUCP2/3*: $n = 6$, 17 cells). Mitochondrial Ca^{2+} was measured with RP-mt. *Panel A*, knock-down of UCP2/3 but not that of Letm1 diminished mitochondrial Ca^{2+} sequestration in response to intracellular Ca^{2+} release. *, $p < 0.05$ *versus* Control. *Panel B*, knock-down of Letm1 but not that of UCP2/3 blunted mitochondrial uptake of entering Ca^{2+}. *, $p < 0.05$ *versus* Control.

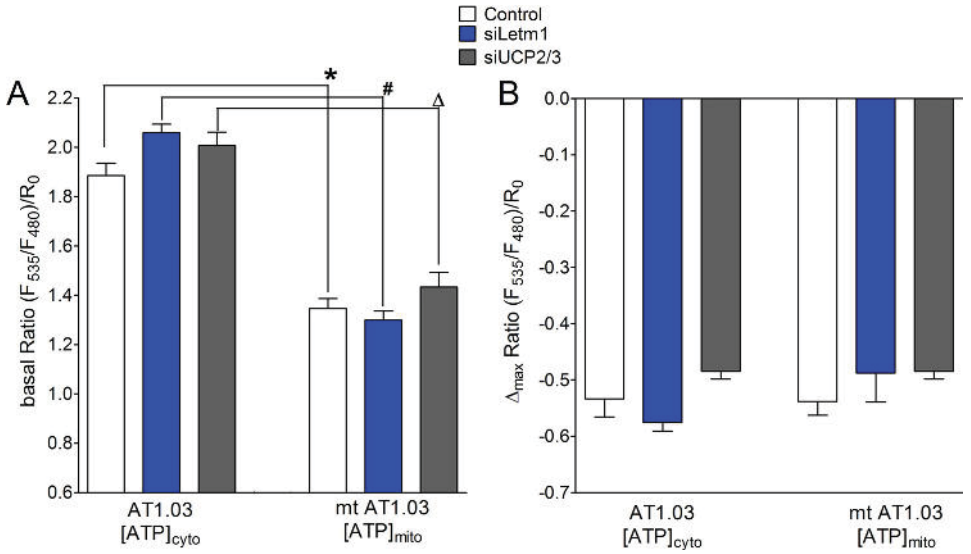

FIGURE 3. **Knock-down of Letm1 did not affect basal cytosolic and mitochondrial ATP levels or the cell's energetic activity.** Endothelial cells were transiently co-transfected with either the cytosolic ATP sensor AT1.03 or with the mitochondrial targeted mt AT1.03 together with the respective siRNAs, control siRNA (*Control*), siRNA against Letm1 (*siLetm1*) or siRNA against UCP2/3 (*siUCP2/3*). *Panel A*, basal cytosolic and mitochondrial ATP levels were neither affected by the knock-down of Letm1 nor by the knock-down of UCP2/3. *Left columns* represent the average ratio (F_{535}/F_{480}) of cytosolic ATP levels ($[ATP]_{cyto}$) at resting conditions for control cells (Control; $n = 20$, 28 cells) and cells transfected with either siRNA against Lemt1 (siLetm1; $n = 14$, 15 cells) or UCP2/3 (siUCP2/3; $n = 9$, 14 cells). *Right columns* show mitochondrial ATP levels ($[ATP]_{mito}$) for control cells ($n = 29$, 32 cells), for siLetm1 ($n = 15$, 15 cells) or siUCP2/3 ($n = 11$, 17 cells). *,#,Δ, $p < 0.05$ between respective cytosolic and mitochondrial [ATP]. *Panel B*, knock-down of Letm1 or UCP2/3 did not influence the cell's energetic activity that was initialized as shown in supplemental Fig. S1. Changes in ATP levels were calculated and expressed as Δ_{max} of Ratio $(F_{535}/F_{480})/R_0$ values representing $\Delta[ATP]_{cyto}$ (*left columns*) for control ($n = 13$, 13 cells), siLetm1 ($n = 6$, 11 cells) or siUCP2/3 ($n = 4$, 7 cells) and of $\Delta[ATP]_{mito}$ (*right columns*) for control ($n = 11$, 11 cells), siLetm1 ($n = 5$, 6 cells), or siUCP2/3 ($n = 5$, 6 cells) upon cell treatment with 10 mM 2-deoxy-D-glucose and 2 μM ologomycin.

entering Ca^{2+}) (16, 22). Therefore, the impact of a knock-down of Letm1 on mitochondrial uptake of intracellularly released Ca^{2+} and Ca^{2+} that is entering the cell via the store-operated Ca^{2+} entry (SOCE) was tested. For comparison, the same type of protocol was performed with cells treated with siRNAs against UCP2/3. Intriguingly, mitochondrial Ca^{2+} signals of cells reduced of either Letm1 or UCP2/3 were very different. In cells that were transiently transfected with siRNA against Letm1, no inhibitory effect on mitochondrial Ca^{2+} sequestration in response to intracellular Ca^{2+} release was found (Fig. 2*A*). The decay of the mitochondrial Ca^{2+} signal in cells treated with siRNA against Letm1 appeared to be slightly but not significantly slower, indicating that knock-down of Letm1 to some extent affects the mitochondrial Ca^{2+} extrusion process. This observation possibly points to the proposed function of mitochondrial Ca^{2+}/H^+ antiport of Letm1, which might secondly contributes to the organelle's Na^+ homeostasis. In contrast knock-down of Letm1 strongly reduced mitochondrial uptake of entering Ca^{2+} by ~80% (Fig. 2*B*). Notably, this inhibitory pattern of knock-down of Letm1 was opposite to that of

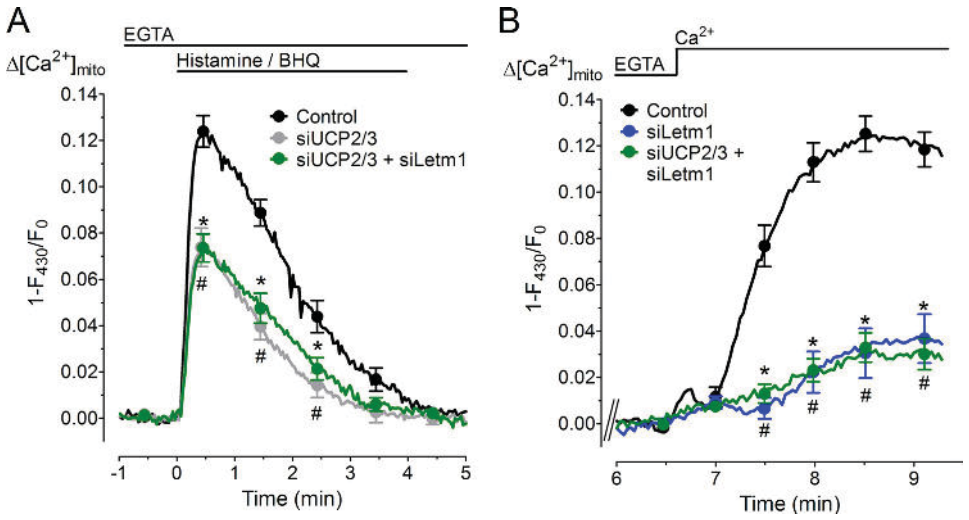

FIGURE 4. **The combined knock-down of Letm1 and UCP2/3 did not further reduce mitochondrial Ca^{2+} uptake.** Stable expressing RP-mt cells were transiently co-transfected with nuclear GFP and either Control siRNA (*Control*: $n = 6$, 14 cells) or siRNA against Letm1 (*siLetm1*: $n = 6$, 12 cells) or siRNA against UCP2 and UCP3 (siUCP2/3: $n = 6$, 17 cells) or both, siRNA against Letm1 and siRNA against UCP2 and UCP3 (siUCP2/3 siLetm1: $n = 6$, 17 cells). *Panel A*, double knock-down of Letm1 and UCP2/3 did not further reduce mitochondrial Ca^{2+} sequestration in response to intracellular Ca^{2+} release compared with that achieved by siRNA against UCP2/3 alone. *,#, $p < 0.05$ *versus* Control. *Panel B*, double knock-down of Letm1 and UCP2/3 exhibit not more inhibitory effect than the siRNA against Letm1 alone. Curves for Control and siUCP2/3 are re-plotted from Fig. 2. *,#, $p < 0.05$ *versus* Control.

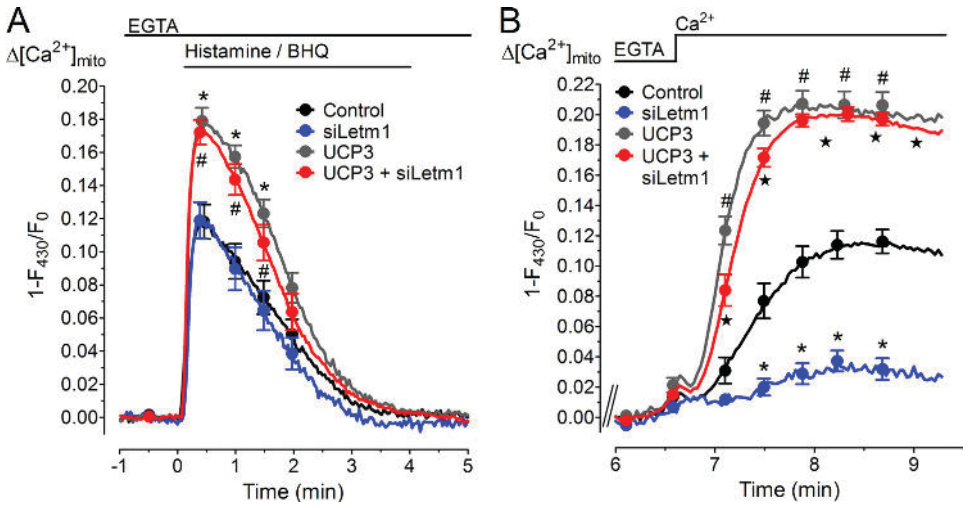

FIGURE 5. **The effect of an overexpression of UCP3 on mitochondrial Ca^{2+} sequestration was not affected by the knock-down of Letm1.** Stable expressing RP-mt cells were transiently co-transfected with nuclear GFP and either Control siRNA (*Control*: $n = 6$, 16 cells), or siRNA against Letm1 (*siLetm1*: $n = 6$, 17 cells). Overexpression of UCP3 was accomplished by co-transfecting the nuclear GFP with a plasmid coding for UCP3 in a ratio 1:3 and either Control siRNA (*UCP3*: $n = 6$, 15 cells), or siRNA against Letm1 (*UCP3 siLetm1*: $n = 6$, 17 cells). Mitochondrial Ca^{2+} was measured with RP-mt. *Panel A*, knock-down of Letm1 did not influence increased mitochondrial Ca^{2+} uptake from intracellular released Ca^{2+} upon UCP3 overexpression. *Panel B*, overexpression of UCP3 induced a strong mitochondrial Ca^{2+} entry via SOCE that was not affected by the knock-down of Letm1. Data are expressed as $1 - F_{430}/F_0$ values. *, #, ≪, $p < 0.05$ *versus* Control.

UCP2/3, which reduced mitochondrial Ca^{2+} uptake of intracellularly released but not entering Ca^{2+} (Fig. 2, *A* and *B*).

Both, Letm1 and UCP2/3-dependent Mitochondrial Ca^{2+} Signals Are Accompanied by an Acidification of the Mitochondrial Matrix—Our data so far indicate that Ca^{2+} released from the ER rapidly enters mitochondria mainly via a UCP2/3-dependent but Letm1-independent Ca^{2+} uniport. In contrast slow mitochondrial sequestration of entering Ca^{2+} appears to be primarily accomplished by Letm1, which was supposed to function as a Ca^{2+}/H^+ antiporter (19). Consequently differences of the mitochondrial proton concentration ($[H^+]_{mito}$) in response to intracellular Ca^{2+} release and Ca^{2+} entry were evaluated by using mitochondrial-targeted pericam that offers the possibility to measure changes of $[Ca^{2+}]_{mito}$ and $[H^+]_{mito}$ simultaneously (19, 26, 27). Mitochondrial Ca^{2+} elevation induced by either ER Ca^{2+} release or Ca^{2+} entry was always accompanied by increase of $[H^+]_{mito}$ (supplemental Fig. S2). These findings are in line with a recent report demonstrating decreases in mitochondrial pH that were triggered by cytosolic Ca^{2+} elevations (34). Notably, during Ca^{2+} entry mitochondrial acidification strictly correlated temporally with the raise of $[Ca^{2+}]_{mito}$, while the increase of $[H^+]_{mito}$ upon ER Ca^{2+} release occurred delayed from the mitochondrial Ca^{2+} signal (supplemental Fig. S2). Knock-down of Letm1 did not affect changes in $[Ca^{2+}]_{mito}$ and $[H^+]_{mito}$ that were induced by ER Ca^{2+} mobilization. However, in line with the data described above, cells treated with siRNA against Letm1 showed

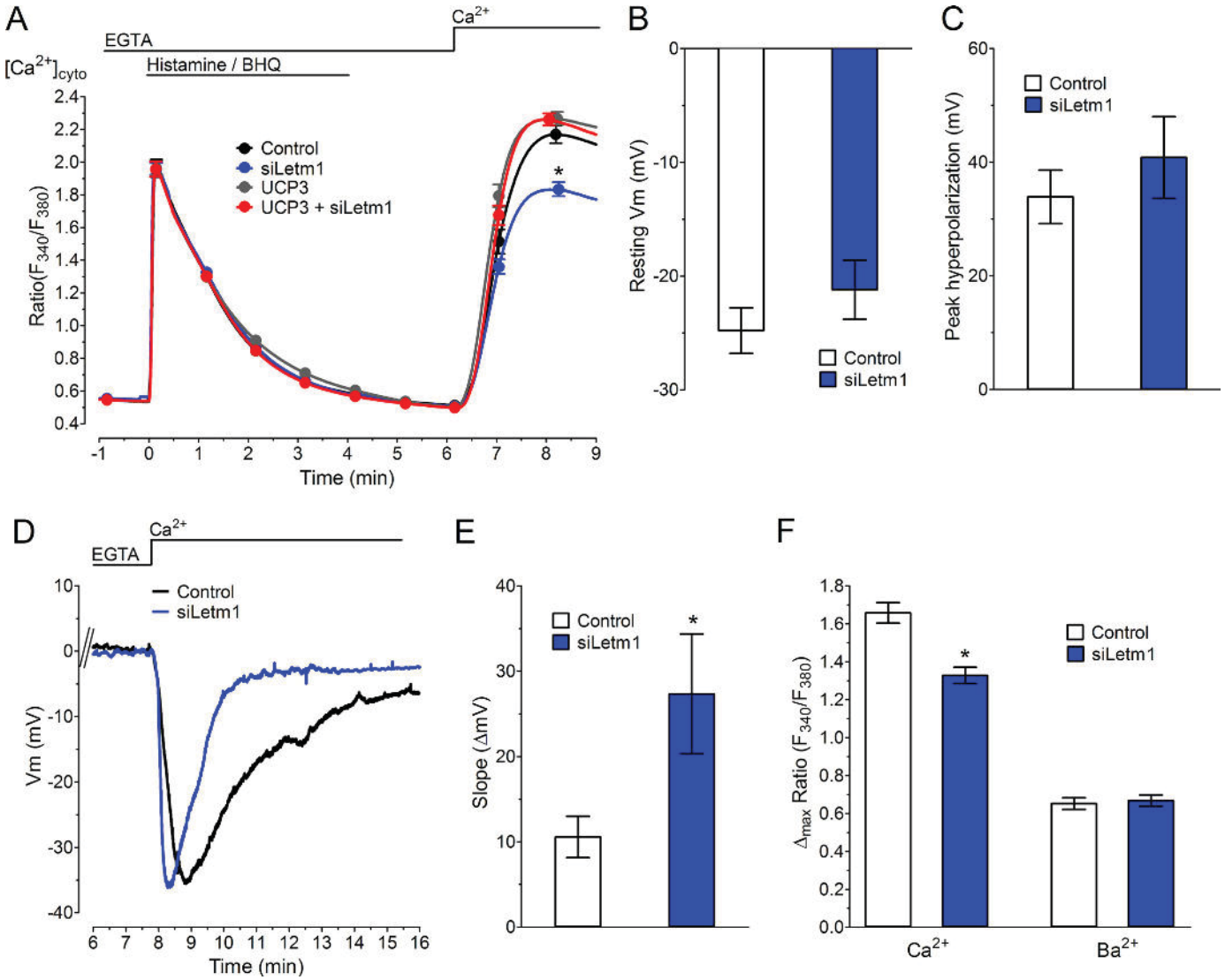

FIGURE 6. **Knock-down of Letm1 reduced the SOCE-induced cytosolic Ca^{2+} elevation that was rescued by the overexpression of UCP3, while Letm1 knock-down did not affect basal membrane potential.** *Panel A*, cells were transiently co-transfected with nuclear GFP and either Control siRNA (*Control*: n = 14, 64 cells) or siRNA against Letm1 (*siLetm1*: n = 14, 66 cells), or together with a plasmid coding for UCP3 in a ratio 1:3 and either Control siRNA (*UCP3*: n = 14, 66 cells) or siRNA against Letm1 (*UCP3 siLetm1*: n = 6, 17 cells). Cytosolic Ca^{2+} was subsequently measured after loading cells with Fura-2/AM. *, $p < 0.05$ *versus* Control. *Panels B–E*, columns and curves representing the average V_m of perforated patch-clamp recordings. *Panel B*, membrane potential at rest was recorded in controls (n = 22) and siLetm1 (n = 16). *Panel C*, peak hyperpolarization was measured after stimulation with 100 μM histamine and 15 μM BHQ in controls (n = 6) or siLetm1 (n = 7). *Panel D*, membrane potential was monitored after readdition of Ca^{2+} in controls (n = 6) or siLetm1 (n = 6). *Panel E*, slope was calculated from Ca^{2+}-induced peak hyperpolarization to 1 min thereafter in controls (n = 6) or siLetm1 (n = 6). *, $p < 0.05$ *versus* control. *Panel F*, cytosolic Ba^{2+} entry was measured in Fura-2/AM-loaded cells after the induction of maximal intracellular Ca^{2+} mobilization with 100 μM histamine and 15 μM BHQ in nominal Ca^{2+}-free solution. Columns represent the average Δ_{max} ratio (F_{340}/F_{380}) in controls (n = 14) or siLetm1 (n = 14) that was induced by addition of 2 mM Ca^{2+} to histamine/BHQ prestimulated cells. Data were analyzed from curves presented in *panel A*, *right columns* represent Δ_{max} ratio (F_{340}/F_{380}) induced by the addition of 10 mM Ba^{2+} to ER Ca^{2+}-depleted cells under control conditions (*Control*; n = 11) or in cells ablated from Letm1 (*siLetm1*; n = 11).

reduced changes in $[Ca^{2+}]_{mito}$ and $[H^+]_{mito}$ during SOCE (supplemental Fig. S2).

The Knock-down of the Mitochondrial Ca^{2+} Transporter Does Not Affect Cytosolic and Mitochondrial Basal ATP Levels—To asses cellular ATP levels, cytosolic, and mitochondrial ATP levels were recorded using FRET-based ATP sensors that are referred to as AT1.03 and mtAT1.03, respectively (23) (supplemental Fig. S1). Basal mitochondrial ATP levels were found to be significantly lower than the cytosolic ATP content in EA.hy926 cells (Fig. 3*A*), which is in line with a recent report introducing AT1.03 and mtAt1.03 investigating ATP levels of HeLa cells (23). Neither the knock-down of Letm1 nor that of UCP2/3 affected basal cytosolic or mitochondrial ATP levels (Fig. 3*A*). Similarly, the energetic activity of the cells that was indicated by the drop of cytosolic and mitochondrial ATP levels in response to 2-deoxy-D-glucose and oligomycin was not affected by knock-down of Letm1 or UCP2/3 (Fig. 3*B*).

Letm1 and UCP2/3 Independently Contribute to Different Mitochondrial Ca^{2+} Uptake Pathways in Endothelial—To test whether or not Letm1 contributes to the same mitochondrial Ca^{2+} uptake machinery than UCP2/3, the expression of these proteins was simultaneously reduced by transient transfection of a mixture of all respective siRNAs. The knock-down of Letm1 did not further reduce mitochondrial Ca^{2+} sequestration of intracellularly released Ca^{2+} in cells with a knock-down of UCP2/3 (Fig. 4*A*). In line with these findings, knock-down of

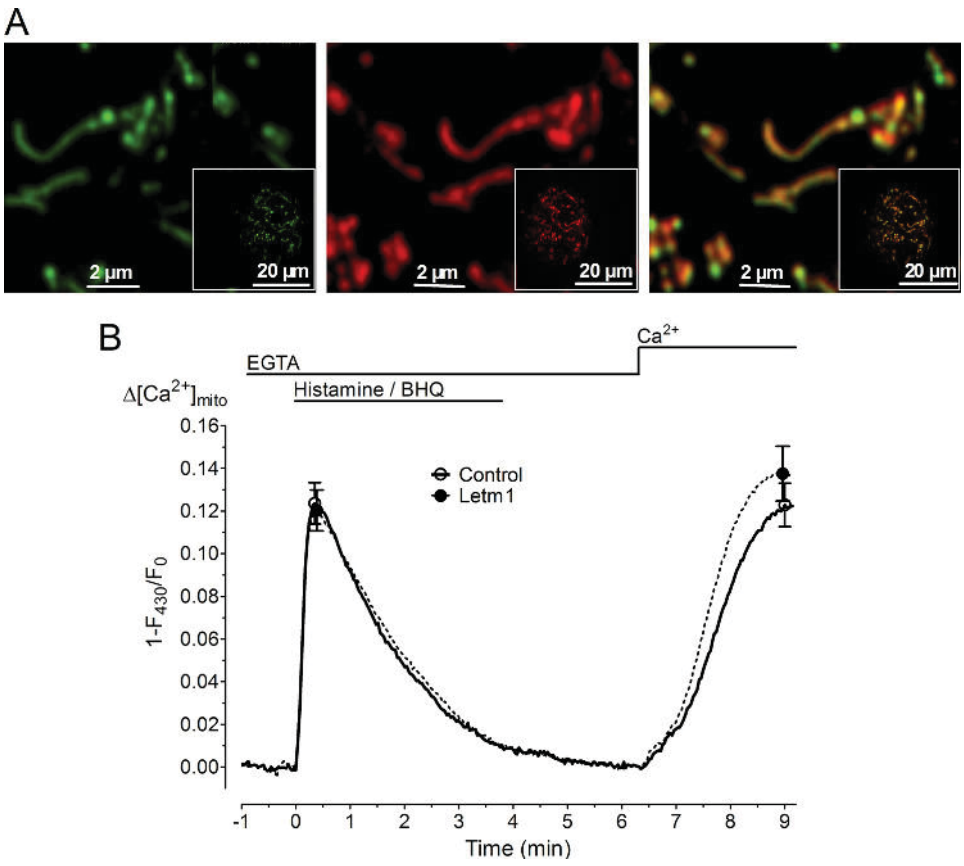

FIGURE 7. **Overexpression of Letm1 co-localized with mitochondria but did not affect mitochondrial Ca^{2+} uptake from any resources.** Plasmids encoding for Letm1-mCherry or Letm1 were transiently transfected in endothelial cells that stably express RP-mt. *Panel A*, mitochondria were visualized using RP-mt (*left panel*), Letm1 that was N-terminally tagged to mCherry was imaged to test protein targeting (*middle panel*). The overlay shows Letm1-mCherry exclusively targeted to the mitochondria (*right panel*). *Panel B*, overexpression of Letm1 did not affect mitochondrial sequestration of either intracellularly released or entering Ca^{2+}. Cells were co-transfected with Letm1 together with a nuclear-targeted GFP in a ratio 3:1 (*Letm1*: $n = 9$, 26 cells) or nuclear-targeted GFP alone (*Control*: $n = 9$, 25 cells).

UCP2/3 failed to further attenuate mitochondrial Ca^{2+} uptake of entering Ca^{2+} in cells lacking Letm1 (Fig. 4*B*).

To test whether or not UCP3 is able to compensate the diminution of Letm1, UCP3 was overexpressed in cells treated with siRNAs against Letm1. Notably, the expected augmentation of mitochondrial uptake of intracellularly released Ca^{2+} in UCP3 overexpressing cells was very robust and was not affected by Letm1 knock-down (Fig. 5*A*). As previously shown an overexpression of UCP3 almost doubled mitochondrial Ca^{2+} uptake of Ca^{2+} that enters the cells via SOCE (Fig. 5*B*). Notably, this increase of $[Ca^{2+}]_{mito}$ in cells overexpressing UCP3 remained unaffected by a knock-down of Letm1 (Fig. 5*B*).

UCP3 Overexpression Rescues a Diminished SOCE in Cells Treated with siRNA against Letm1—Mitochondrial Ca^{2+} uptake was shown to facilitate SOCE (35–39). Thus we examined the impact of Letm1 knock-down on SOCE-induced cytosolic Ca^{2+} signals. Indeed, diminution of Letm1 expression reduced the cytosolic Ca^{2+} elevation in response to SOCE, while the transient increase of $[Ca^{2+}]_{cyto}$ elicited by ER Ca^{2+} mobilization remained unaffected (Fig. 6*A*). Notably, knock-down of Letm1 reduced the SOCE induced cytosolic Ca^{2+} signal by ~20%, while the respective mitochondrial Ca^{2+} signal was reduced by almost 80%. This disparity is in line with a recent report showing that the impact of mitochondrial Ca^{2+} handling on SOCE fades with the strength of Ca^{2+} entry in this particular cell line (40). However, an overexpression of UCP3 in cells treated with siRNA against Letm1, in which an augmented mitochondrial Ca^{2+} load in response to SOCE was observed (Fig. 5*B*), completely restored SOCE-induced elevation of $[Ca^{2+}]_{mito}$ (Fig. 6*A*).

To test whether or not the reduction of SOCE due to Letm1 knock-down was caused by a possible effect on the plasma membrane potential and/or Ca^{2+}-triggered membrane hyperpolarization, electrophysiological recordings were performed. Letm1 knock-down had no effect on either the resting membrane potential (Fig. 6*B*) or peak hyperpolarization in response to Ca^{2+} readdition to histamine/BHQ prestimulated cells (Fig. 6, *C* and *D*). However, in Letm1 knock-down cells plasma membrane hyperpolarization upon Ca^{2+} addition to prestimulated cells was more transient (Fig. 6*D*) and repolarization occurred faster (Fig. 6*E*), thus, indicating that the knock-down of Letm1 yields attenuation of the maintenance of SOCE probably by the lack of the mitochondrial Ca^{2+} buffering capacity.

In agreement with this assumption, diminution of Letm1 had no effect on Ba^{2+}, which serves as Ca^{2+} surrogate for the SOCE but does not exhibit its inhibitory action on the SOC channels (Fig. 6*F*). These data further indicate that Letm1 knock-down had no effect on SOCE activation mechanisms but rather reduced its maintenance by the lack of mitochondrial Ca^{2+} buffering.

Letm1 Knock-down Does Not Affect Plasma Membrane Ca^{2+} ATPase (PMCA) Activity—Though knock-down of Letm1 did not affect cellular ATP levels, changes of cellular Ca^{2+} signals may also occur due to alterations in PMCA activity. Thus, PMCA activity was tested according to a protocol of R. S. Lewis' group that measures the decay of cytosolic Ca^{2+} upon removal of extracellular Ca^{2+} (41). We performed similar experiments in the presence of a the SERCA inhibitor BHQ, the IP3-stimulating agonist histamine, and in low Na^+ concentration to avoid ER Ca^{2+} refilling and Ca^{2+} extrusion via the plasma membrane Na^+/Ca^{2+} exchanger, respectively. These experiments revealed no effect of Letm1 knock-down on PMCA activity (supplemental Fig. S3).

In Contrast to UCP2/3, Letm1 Overexpression Fails to Improve Mitochondrial Ca^{2+} Uptake—As already shown in Fig. 4, overexpression of UCP3 yielded strong elevation in mitochondrial uptake of Ca^{2+} independently from the source it was delivered (*i.e.* intracellular Ca^{2+} release or entering Ca^{2+} via SOCE). In order to test whether an overexpression of Letm1 exhibits similar effects than that of UCP3, two Letm1 overexpression vectors according to that previously published by Jiang *et al.* (19) were designed. To verify targeting of Letm1, a mCherry-fusion construct was used that revealed targeting of overexpressed Letm1 to the mitochondria (Fig. 7*A*). Notably, neither the expression of mCherry fused Letm1 nor that of the wild-type protein had any obvious effect on mitochondrial Ca^{2+} accumulation in response to intracellular Ca^{2+} release and Ca^{2+} influx (Fig. 7*B*).

Letm1 and UCP3 Differ in Terms of Their Ca^{2+} Sensitivity—In view of the data described above that point to a distinct contribution of UCP2/3 and Letm1 to two separate mitochondrial Ca^{2+} uptake routes, the Ca^{2+} sensitivity of Letm1- and UCP2/3-dependent mitochondrial Ca^{2+} uptake was tested in digitonin-permeabilized cells. Under conditions of low Ca^{2+} application (*i.e.* 174 ± 18 nM cytosolic free Ca^{2+}; $n = 17$) (22) knock-down of Letm1 completely abolished mitochondrial Ca^{2+} sequestration, while the knock-down of UCP2/3 had no effect (Fig. 8*A*). In line with the experiments shown in Fig. 4*B*, overexpression of UCP3 boosted mitochondrial Ca^{2+} uptake even under conditions of Letm1 knock-down and established a large Ca^{2+} sequestration that did not differ from the signal in cells expressing Letm1 (Fig. 8*A*).

Challenging the permeabilized cells with a high Ca^{2+} concentration (*i.e.* 921 ± 119 nM cytosolic free Ca^{2+}; $n = 17$) (22) revealed mitochondrial Ca^{2+} uptake that was not affected by Letm1 knock-down but was markedly impaired in cells treated with siRNA against UCP2/3. Overexpression of UCP3 boosted mitochondrial uptake of high Ca^{2+} independently from the expression level of Letm1 (Fig. 8*B*). These data are in line with the findings in intact cells (Figs. 2&4) and confirm the idea of two separate mitochondrial Ca^{2+} uptake pathways: the Letm1-dependent pathway achieves mitochondrial Ca^{2+} sequestration of small capacity at relative low Ca^{2+} concentrations, while the UCP2/3-dependent mitochondrial Ca^{2+} uptake requires higher cytosolic Ca^{2+} concentrations to establish a high capacity Ca^{2+} uptake route into the organelle.

Despite Its Expression in Endothelial Cells, MICU1 Appears Not to Be Involved in Mitochondrial Ca^{2+} Sequestration in This

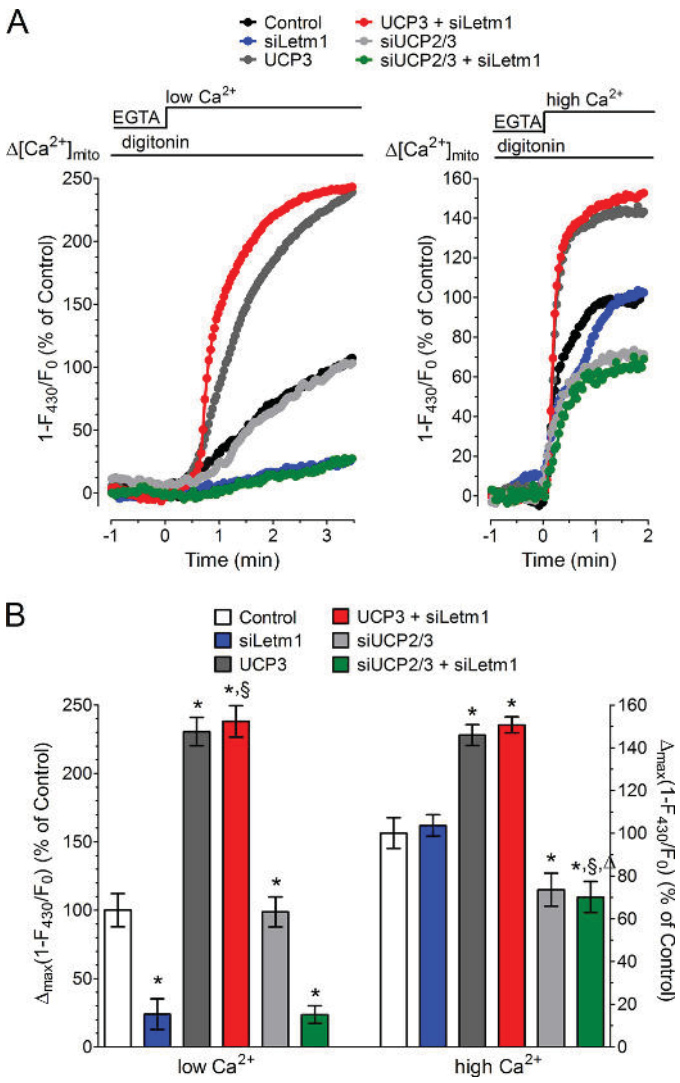

FIGURE 8. **siRNA-mediated knock-down of Letm1 and UCP2/3 had oppositional effects on mitochondrial Ca^{2+} uptake in digitonin-permeabilized cells by applying low and high Ca^{2+} concentrations, while UCP2/3 overexpression rescued mitochondrial Ca^{2+} uptake in cells with Letm1 knock-down.** Stable expressing RP-mt cells were transiently co-transfected with nuclear GFP and either Control siRNA (*Control*), siRNA against Letm1 (*siLetm1*), siRNA against UCP2/3 (*siUCP2/3*), or siRNA against UCP2/3 and Letm1 (*siUCP2/3 + Letm1*). Overexpression of UCP3 was achieved by co-transfecting the nuclear GFP with a plasmid coding for UCP3 in a ratio 1:3 and either Control siRNA (*UCP3*), or siRNA against Letm1 (*UCP3 siLetm1*). Mitochondrial Ca^{2+} was measured with RP-mt. Data are expressed as % of Control under each individual condition. *Panel A*, average curves of mitochondrial Ca^{2+} uptake upon the addition of either low Ca^{2+} concentration or high Ca^{2+} concentration in mild digitonin-permeabilized cells (Control, *black curves*; siLetm1, *blue curves*; UCP3, *light gray curves*; UCP3 + siLetm1, *red curves*; siUCP2/3 *light gray curves*; siUCP2/3 + siLetm1, *green curves*). *Panel B*, maximum mitochondrial Ca^{2+} accumulation according to the average curves of *panel A* was calculated 3.4 min after the application of low Ca^{2+} concentration and 1.8 min after applying high Ca^{2+} concentration. Columns represent the average of mitochondrial Ca^{2+} signals upon the addition of the low Ca^{2+} concentration (Control, *left white column*, $n = 4$, 12 cells; siLetm1, *left blue column*, $n = 4$, 12 cells; UCP3, *left dark gray column*, $n = 4$, 12 cells; UCP3 + siLetm1, *left red column*, $n = 4$, 12 cells; siUCP2/3, *left light gray column*, $n = 4$, 13 cells; siUCP2/3 + siLetm1, *left green column*, $n = 4$, 13 cells), and the high Ca^{2+} concentration (Control, *right white column*, $n = 4$, 10 cells; siLetm1, *right blue column*, $n = 4$, 17 cells; UCP3, *right dark gray column*, $n = 4$, 16 cells; UCP3 + siLetm1, *right red column*, $n = 4$, 13 cells; siUCP2/3, *right light gray column*, $n = 8$, 22 cells; siUCP2/3 + siLetm1, *right green column*, $n = 8$, 30 cells). *, $p < 0.05$ *versus* the respective Control; #, $p < 0.05$ between siLetm1 and UCP3 + siLetm1; §, $p < 0.05$ between siUCP2/3 and siUCP2/3 + siLetm1; and Δ, $p < 0.05$ between siLetm1 and siUCP2/3 + Letm1.

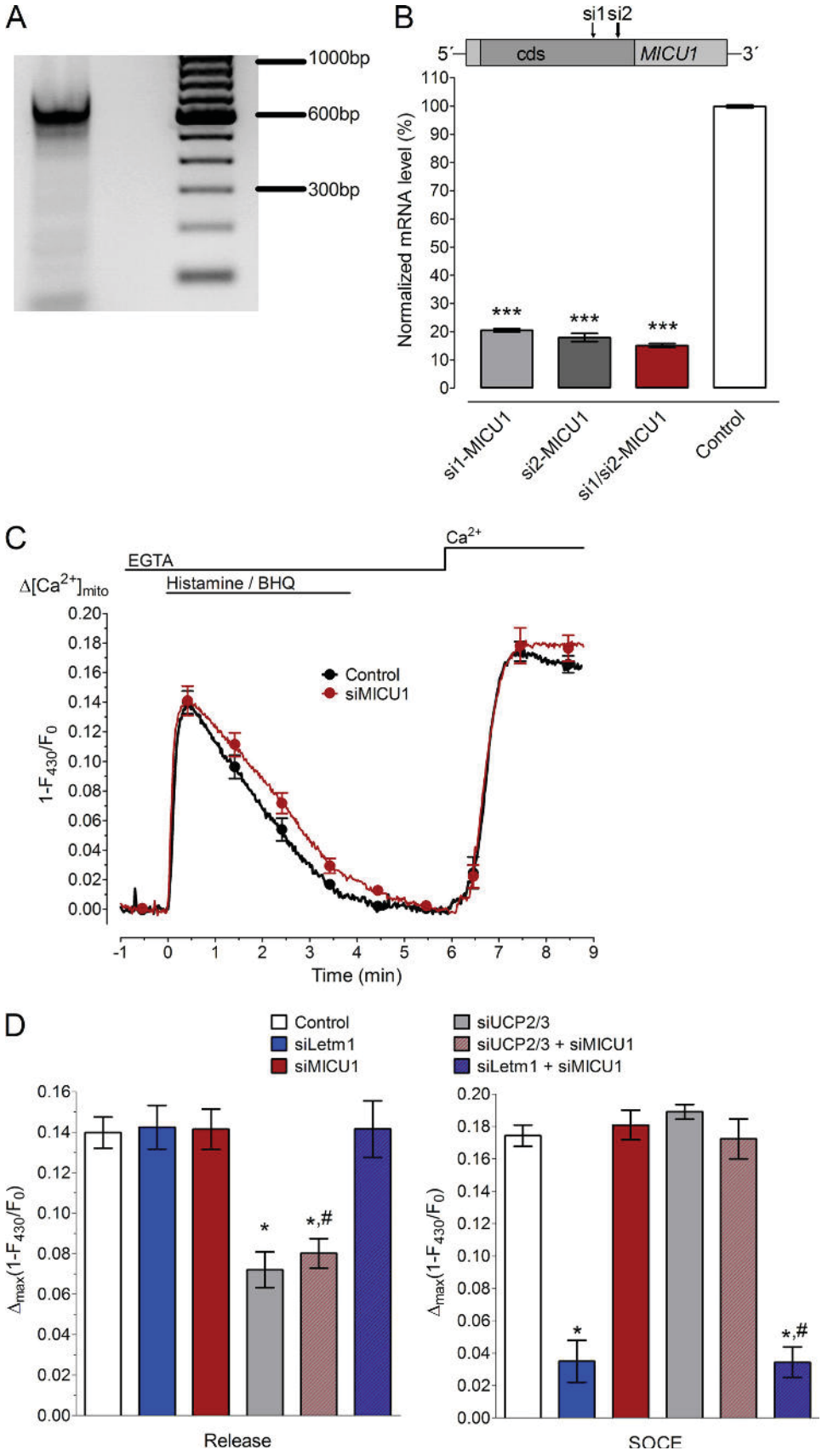

Particular Cell Type—To verify the contribution of MICU1 to mitochondrial Ca^{2+} sequestration in the endothelial cell line used, the expression of MICU1 was tested using RT-PCR (Fig. 9*A*). Hence the efficiencies of the two recently published siRNAs against MICU1 (18) were measured (Fig. 9*B*). Because these experiments revealed best knock-down efficiency by a combination of both siRNAs, such approach was used in all upcoming experiments regarding MICU1 knock-down. In contrast to the knock-down of either Letm1 or UCP2/3, siRNA-mediated diminution of MICU1 mRNA levels had no effect on mitochondrial sequestration of intracellularly released as well as entering Ca^{2+} (Fig. 9*C*). Moreover, the combination of MICU1 knock-down with that of either Letm1 or UCP3 did not have any effect on mitochondrial Ca^{2+} uptake compared with that observed in MICU1-containing cells with the respective knock-down of either Letm1 or UCP2/3 (Fig. 9*D*).

DISCUSSION

Despite intensive investigations over more than a decade, the molecular identity of the mitochondrial Ca^{2+} uniporter could not be resolved entirely so far. During recent years, siRNA-based screening approaches have highlighted basically three proteins that have been found to be essential for or to contribute to mitochondrial Ca^{2+} uptake in intact cells: UCP2/3 (17), Letm1 (19), and MICU1 (18). However, in these studies mitochondrial Ca^{2+} uptake was tested under certain conditions and in distinct cell types like endothelial cells, HeLa cells (17, 18), and *Drosophila* Schneider 2 cells (19). As in other subsequent studies using different cell types and/or approaches these results were challenged, the current consensus suggests that these proteins might modulate mitochondrial Ca^{2+} uptake rather than to contribute directly to this phenomenon (42–45). Importantly, in cardiac myocytes two electrophysiological distinct Ca^{2+} uptake currents could be verified (15) that differ in terms of the Ca^{2+} range they are active, their capacity and sensitivity to ruthenium red. In agreement with this landmark publication, in our previous work, evidence was provided for the co-existence of at least two molecularly distinct mitochondrial Ca^{2+} uptake routes in the endothelial cell line EA.hy926 (16, 22, 46).

As previously published, the siRNA-mediated knock-down of UCP2/3 yielded strong reduction of mitochondrial Ca^{2+} sequestration upon intracellular Ca^{2+} release while no effect was found on mitochondrial uptake of Ca^{2+} that entered the endothelial cells via SOCE (16, 22), thus, pointing to an exclusive contribution of this particular transporter to mitochondrial Ca^{2+} sequestration at ER-mitochondria junctions in wild type endothelial cells. In this study, knock-down of Letm1, had no effect on mitochondrial Ca^{2+} uptake at ER-mitochondria junctions, but strongly diminished mitochondrial sequestration of entering Ca^{2+}, thus, indicating that the UCP2/3- and Letm1-dependent Ca^{2+} signals account for mitochondrial Ca^{2+} uptake from distinct sources (*i.e.* ER-derived intracellular Ca^{2+} release and SOCE). Our findings that the knock-down of Letm1 had no effect on Ba^{2+} entry, PMCA activity, membrane potential or basal ATP levels but diminished cytosolic Ca^{2+} elevation in response to SOCE is in line with previous reports on the considerable contribution of mitochondrial Ca^{2+} uptake/buffering for the activity/maintenance of store-operated Ca^{2+} channels (7, 26, 35–40, 47).

Because the combination of Letm1 and UCP2/3 knock-down just reflected the additive combination of the effects of the individual siRNAs, these particular mitochondrial Ca^{2+} uptake routes appear to be independent from each other. This assumption was further supported by our findings that under conditions of Letm1 knock-down, the effect of UCP3 overexpression remained unaffected. Notably, under such conditions, the overexpression of UCP3 compensated the lack of Letm1 in terms of mitochondrial sequestration of entering Ca^{2+}. These data are in agreement with our previous findings showing that overexpression of UCP2/3 establishes a respective mitochondrial Ca^{2+} uptake route also for entering Ca^{2+}, thus, pointing to the expression level of UCP3 as being the bottleneck for the establishment of a respective mitochondrial Ca^{2+} uptake.

The particular contribution of Letm1- and UCP2/3-dependent mitochondrial Ca^{2+} uptake routes to either entering Ca^{2+} or ER-released Ca^{2+} may indicate that these carriers achieve mitochondrial Ca^{2+} uptake at different Ca^{2+} concentrations. In this respect, the generation of high Ca^{2+} domains in the junction between the ER and the mitochondria to provide sufficient high Ca^{2+} levels to allow mitochondrial Ca^{2+} sequestration via the rather Ca^{2+} insensitive mitochondrial Ca^{2+} uniporter were frequently emphasized (9, 48, 49) and very recently convincingly approved (11, 50). Moreover, considerable differences in the kinetics and capacity of mitochondrial uptake of Ca^{2+} from the two major sources (*i.e.* intracellular

FIGURE 9. **siRNA-mediated knock-down of MICU1 efficiently reduced mRNA levels but had no effect on mitochondrial Ca^{2+} sequestration in endothelial cells.** *Panel A*, RT-PCR using specific primers (see "Experimental Procedures") resulted in a 733 bp product amplification, approving the expression of MICU1 in the human endothelial cell line used in this study. *Panel B*, MICU1 silencing using 2 different siRNA (single and combined). Efficiency of siRNA-mediated MICU1 knock-down was verified by real time quantitative-PCR after transfection of siRNA1 (*si1-MICU1*, $n = 3$) or siRNA2 (*si2-MICU1*, $n = 3$) against MICU1 individually or both in combination (*si1/si2-MICU1*, $n = 3$) *versus* Control siRNA (Control, $n = 3$). Data are expressed in % of Control. ***, $p < 0.0001$ *versus* Control. *Panel C*, mitochondrial Ca^{2+} uptake was not affected by MICU1 knock-down. Stably expressing RP-mt endothelial cells were transiently co-transfected with a plasmid for expression of nuclear-targeted GFP and either a Control siRNA (*Control* $n = 4$, 14 cells) or siRNA against MICU1 (*MICU1* $n = 4$, 14 cells). *Panel D*, knock-down of MICU1 did not affect mitochondrial Ca^{2+} uptake upon intracellular Ca^{2+} release or SOCE. Mitochondrial Ca^{2+} uptake was visualized by RP-mt in endothelial cells transiently expressing nuclear-targeted GFP and the respective siRNAs: Control siRNA (Control, *plain white column*, $n = 4$, 14 cells), siRNAs against Letm1 (siLetm1, *plain blue columns*, $n = 4$, 14 cells); siRNAs against MICU1 (siMICU1, *plain dark red columns*, $n = 4$, 14 cells); siRNAs against UCP2/3 (siUCP2/3, *plain light gray columns*, $n = 4$, 12 cells), siRNAs against UCP2/3 and MICU1 (siUCP2/3 + siMICU1, *dark red-striped light gray columns*, $n = 4$, 15 cells) or siRNA against Letm1 and MICU1 (siLetm1 + siMICU1, *dark red-striped blue columns*, $n = 4$, 16 cells). *Left panel*, maximal intracellular Ca^{2+} mobilization in response to 100 μM histamine and 15 μM BHQ in a nominal Ca^{2+}-free solution. Columns represent the average $\Delta_{max}\ 1-F-F_{430}/F_0$ of mitochondrial Ca^{2+} uptake upon ER Ca^{2+} release. *, $p < 0.05$ *versus* Control and #, $p < 0.05$ between siMICU1 and siUCP2/3 + siMICU1. *Right panel*, columns represent the average $\Delta_{max}\ 1-F_{430}/F_0$ of mitochondrial Ca^{2+} uptake after the addition of 2 mM Ca^{2+} to cells prestimulated with histamine and BHQ. *, $p < 0.05$ *versus* Control and #, $p < 0.05$ between siMICU1 and siLetm1 + siMICU1.

Ca^{2+} release and Ca^{2+} entry via SOCE) in endothelial cells further confirmed these data and emphasized lower Ca^{2+} concentrations at the mitochondria surface under conditions of entering Ca^{2+} than within the ER-mitochondria junction (22). The present experiments using digitonin-permeabilized cells are in agreement with these previous assumptions and indicate that in endothelial mitochondria two Ca^{2+} uptake routes exist that work either at low or high Ca^{2+} concentrations. Our findings that the siRNA-mediated knock-down of Letm1 abolished mitochondrial Ca^{2+} uptake at low but not high Ca^{2+} exposure indicates the Letm1-dependent Ca^{2+} carrier to exclusively account for mitochondrial Ca^{2+} uptake under low Ca^{2+} conditions. Considering the previous reports that entering Ca^{2+} does not generate high Ca^{2+} domains at the mitochondria surface (11, 22) these findings suggest Letm1-dependent mitochondrial Ca^{2+} uptake to account for the organelle's sequestration of Ca^{2+} that enters the cell via the SOCE. In contrast to Letm1, UCP2/3 obviously accounts for mitochondrial Ca^{2+} uptake at high Ca^{2+} concentrations. However, upon overexpression UCP3 is able to compensate the lack of Letm1 even in regard of low Ca^{2+} exposure. It seems likely that even a low active UCP2/3-dependent carrier under low Ca^{2+} load achieves mitochondrial Ca^{2+} load simply because of the largely increased amount of Ca^{2+}-carrying proteins. Notably, while the overexpression of UCP3 (and UCP2) established an increased mitochondrial Ca^{2+} uptake, an overexpression of Letm1 was without effect. Though its localization into the mitochondria was clearly approved, these findings may result from a non-functional Letm1 upon overexpression. However, as both the wild type Letm1 (transfection was controlled by co-expression of nuclear targeted GFP) as well as the FP-fusion construct failed to exhibit any effect on mitochondrial Ca^{2+} signaling, this possibility appears rather unlikely. On the other hand, Letm1 might essentially depend on (a) distinct protein(s) that are the rate-limiting factors for mitochondrial Ca^{2+} uptatke. Such multi-protein complex for mitochondrial Ca^{2+} uptake was also postulated for the UCP2/3-dependent Ca^{2+} uptake route (42, 52).

Considering that both the UCP2/3- and Letm1-dependent mitochondrial Ca^{2+} carriers might be established by a multi-protein complex rather than by the individual proteins alone, a protein that was very recently described to be involved in the regulation of mitochondrial Ca^{2+} uptake in intact cells, MICU1 (18, 43, 53), attracts great attention. However, though mRNA levels from MICU1 could be found in the endothelial cells type used in this study, approved siRNA-mediated MICU1 knock-down did not affect mitochondrial Ca^{2+} sequestration by either Letm1- or UCP2/3-dependent pathways. Accordingly, these data suggest MICU1 to be not involved in Letm1- and UCP2/3-dependent mitochondrial Ca^{2+} transport in this particular cell type. Moreover, in intact and in permeabilized cells, a knock-down of UCP2/3 could not entirely prevent mitochondrial Ca^{2+} sequestration to intracellular Ca^{2+} release and high Ca^{2+} load, respectively. Notably neither knock-down of Letm1 nor that of MICU1 further reduced mitochondrial Ca^{2+} sequestration under these conditions. Though the remaining uptake might be due to an insufficient knock-down of UCP2/3 or a modulator role rather than a carrier function of UCP2/3 in this process (7, 42), the existence of a UCP2/3-, Letm1- and MICU1-independent Ca^{2+} carrier cannot be excluded. In this respect, proteins that may not serve as Ca^{2+} carrier under physiological conditions may allow/facilitate Ca^{2+} influx into the organelle under such artificial Ca^{2+} stress conditions (*e.g.* NCX_{mito} or ANT) (42, 51).

The present findings demonstrate that at least two molecularly distinct mitochondrial Ca^{2+} uptake pathways co-exist in endothelial cells. The distinct mitochondrial Ca^{2+} uptake routes appear to be independent from the recently described modulator protein MICU1 but essentially depend on either Letm1 or UCP2/3. While further studies are necessary to investigate the specific role of each individual Ca^{2+} uptake route in physiology and pathology, this work explains mitochondrial Ca^{2+} uptake to be not a unitary process but to be established by distinct molecules, thus providing the opportunity to verify the particular contribution of each individual mitochondrial Ca^{2+} transporter to distinct physiological and pathological conditions in various cell types.

Acknowledgments—We thank Anna Schreilechner and Florian Enzinger for excellent technical assistance, Dr. A. Miyawaki (Riken, Japan) for the ratiometric pericam, N. Demaurex (University of Geneva, Switzerland) for the NLS-GFP, and Dr. C.J.S. Edgell (University of North Carolina, Chapel Hill, NC) for the EA.hy926 cells.

REFERENCES

1. Rizzuto, R., Bastianutto, C., Brini, M., Murgia, M., and Pozzan, T. (1994) *J. Cell Biol.* **126,** 1183–1194
2. Rizzuto, R., Brini, M., and Pozzan, T. (1994) *Methods Cell Biol.* **40,** 339–358
3. Nagai, T., Sawano, A., Park, E. S., and Miyawaki, A. (2001) *Proc. Natl. Acad. Sci. U.S.A.* **98,** 3197–3202
4. Filippin, L., Abad, M. C., Gastaldello, S., Magalhaes, P. J., Sandona, D., and Pozzan, T. (2005) *Cell Calcium* **37,** 129–136
5. Palmer, A. E., Giacomello, M., Kortemme, T., Hires, S. A., Lev-Ram, V., Baker, D., and Tsien, R. Y. (2006) *Chem. Biol.* **13,** 521–530
6. Palmer, A. E., and Tsien, R. Y. (2006) *Nat. Protoc.* **1,** 1057–1065
7. Demaurex, N., Poburko, D., and Frieden, M. (2009) *Biochim. Biophys. Acta* **1787,** 1383–1394
8. Rizzuto, R., Duchen, M. R., and Pozzan, T. (2004) *Sci. STKE* **2004,** re1
9. Rizzuto, R., Marchi, S., Bonora, M., Aguiari, P., Bononi, A., De Stefani, D., Giorgi, C., Leo, S., Rimessi, A., Siviero, R., Zecchini, E., and Pinton, P. (2009) *Biochim. Biophys. Acta* **1787,** 1342–1351
10. Rizzuto, R., and Pozzan, T. (2006) *Physiol. Rev.* **86,** 369–408
11. Giacomello, M., Drago, I., Bortolozzi, M., Scorzeto, M., Gianelle, A., Pizzo, P., and Pozzan, T. (2010) *Mol. Cell* **38,** 280–290
12. Kirichok, Y., Krapivinsky, G., and Clapham, D. E. (2004) *Nature* **427,** 360–364
13. Pitter, J. G., Maechler, P., Wollheim, C. B., and Spät, A. (2002) *Cell Calcium* **31,** 97–104
14. Szanda, G., Koncz, P., Várnai, P., and Spät, A. (2006) *Cell Calcium* **40,** 527–537
15. Michels, G., Khan, I. F., Endres-Becker, J., Rottlaender, D., Herzig, S., Ruhparwar, A., Wahlers, T., and Hoppe, U. C. (2009) *Circulation* **119,** 2435–2443
16. Waldeck-Weiermair, M., Malli, R., Naghdi, S., Trenker, M., Kahn, M. J., and Graier, W. F. (2010) *Cell Calcium* **47,** 433–440
17. Trenker, M., Malli, R., Fertschai, I., Levak-Frank, S., and Graier, W. F. (2007) *Nat. Cell Biol.* **9,** 445–452
18. Perocchi, F., Gohil, V. M., Girgis, H. S., Bao, X. R., McCombs, J. E., Palmer, A. E., and Mootha, V. K. (2010) *Nature* **467,** 291–296
19. Jiang, D., Zhao, L., and Clapham, D. E. (2009) *Science* **326,** 144–147
20. Spät, A., Fülöp, L., Koncz, P., and Szanda, G. (2009) *Acta Physiol.* **195,**

139–147
21. Spät, A., Szanda, G., Csordás, G., and Hajnóczky, G. (2008) *Cell Calcium* **44,** 51–63
22. Waldeck-Weiermair, M., Duan, X., Naghdi, S., Khan, M. J., Trenker, M., Malli, R., and Graier, W. F. (2010) *Cell Calcium* **48,** 288–301
23. Imamura, H., Nhat, K. P., Togawa, H., Saito, K., Iino, R., Kato-Yamada, Y., Nagai, T., and Noji, H. (2009) *Proc. Natl. Acad. Sci. U.S.A.* **106,** 15651–15656
24. Graier, W. F., Groschner, K., Schmidt, K., and Kukovetz, W. R. (1992) *Biochem. Biophys. Res. Commun.* **186,** 1539–1545
25. Graier, W. F., Paltauf-Doburzynska, J., Hill, B. J., Fleischhacker, E., Hoebel, B. G., Kostner, G. M., and Sturek, M. (1998) *J. Physiol.* **506,** 109–125
26. Malli, R., Frieden, M., Trenker, M., and Graier, W. F. (2005) *J. Biol. Chem.* **280,** 12114–12122
27. Frieden, M., James, D., Castelbou, C., Danckaert, A., Martinou, J. C., and Demaurex, N. (2004) *J. Biol. Chem.* **279,** 22704–22714
28. Bondarenko, A. (2004) *Br. J. Pharmacol.* **143,** 9–18
29. Bondarenko, A. I., Malli, R., and Graier, W. F. (2011) *Pflugers Arch.* **461,** 177–189
30. Bondarenko, A., Waldeck-Weiermair, M., Naghdi, S., Poteser, M., Malli, R., and Graier, W. F. (2010) *Br. J. Pharmacol.* **161,** 308–320
31. Frieden, M., and Graier, W. F. (2000) *J. Physiol.* **524,** 715–724
32. Frieden, M., Malli, R., Samardzija, M., Demaurex, N., and Graier, W. F. (2002) *J. Physiol.* **540,** 73–84
33. Malli, R., Naghdi, S., Romanin, C., and Graier, W. F. (2008) *J. Cell Sci.* **121,** 3133–3139
34. Poburko, D., Santo-Domingo, J., and Demaurex, N. (2011) *J. Biol. Chem.* **286,** 11672–11684
35. Hoth, M., Button, D. C., and Lewis, R. S. (2000) *Proc. Natl. Acad. Sci. U.S.A.* **97,** 10607–10612
36. Hoth, M., Fanger, C. M., and Lewis, R. S. (1997) *J. Cell Biol.* **137,** 633–648
37. Parekh, A. B. (2008) *Cell Calcium* **44,** 6–13
38. Malli, R., Frieden, M., Osibow, K., and Graier, W. F. (2003) *J. Biol. Chem.* **278,** 10807–10815
39. Malli, R., Frieden, M., Osibow, K., Zoratti, C., Mayer, M., Demaurex, N., and Graier, W. F. (2003) *J. Biol. Chem.* **278,** 44769–44779
40. Naghdi, S., Waldeck-Weiermair, M., Fertschai, I., Poteser, M., Graier, W. F., and Malli, R. (2010) *J. Cell Sci.* **123,** 2553–2564
41. Bautista, D. M., and Lewis, R. S. (2004) *J. Physiol.* **556,** 805–817
42. Graier, W. F., Trenker, M., and Malli, R. (2008) *Cell Calcium* **44,** 36–50
43. Hajnóczky, G., and Csordás, G. (2010) *Curr. Biol.* **20,** R888-R891
44. Starkov, A. A. (2010) *The FEBS J.* **277,** 3652–3663
45. Santo-Domingo, J., and Demaurex, N. (2010) *Biochim. Biophys. Acta* **1797,** 907–912
46. Trenker, M., Fertschai, I., Malli, R., and Graier, W. F. (2008) *Nat. Cell Biol.* **10,** 1237–1240
47. Parekh, A. B. (2003) *News Physiol. Sci.* **18,** 252–256
48. Rizzuto, R., Pinton, P., Brini, M., Chiesa, A., Filippin, L., and Pozzan, T. (1999) *Cell Calcium* **26,** 193–199
49. Rizzuto, R., Pinton, P., Carrington, W., Fay, F. S., Fogarty, K. E., Lifshitz, L. M., Tuft, R. A., and Pozzan, T. (1998) *Science* **280,** 1763–1766
50. Csordás, G., Várnai, P., Golenár, T., Roy, S., Purkins, G., Schneider, T. G., Balla, T., and Hajnóczky, G. (2010) *Mol. Cell* **39,** 121–132
51. Graier, W. F., Frieden, M., and Malli, R. (2007) *Pflugers Arch.* **455,** 375–396
52. Malli, R., and Graier, W. F. (2010) *FEBS Lett.* **584,** 1942–1947
53. Collins, S., and Meyer, T. (2010) *Nature* **467,** 283

Pflugers Arch - Eur J Physiol (2013) 465:997–1010
DOI 10.1007/s00424-013-1224-1

ION CHANNELS, RECEPTORS AND TRANSPORTERS

Characterization of distinct single-channel properties of Ca^{2+} inward currents in mitochondria

Alexander I. Bondarenko · Claire Jean-Quartier · Roland Malli · Wolfgang F. Graier

Received: 22 November 2012 / Revised: 21 January 2013 / Accepted: 22 January 2013 / Published online: 9 February 2013

Abstract Previous studies have demonstrated several molecularly distinct players involved in mitochondrial Ca^{2+} uptake. In the present study, electrophysiological recordings on mitoplasts that were isolated from HeLa cells were performed in order to biophysically and pharmacologically characterize Ca^{2+} currents across the inner mitochondrial membrane. In mitoplast-attached configuration with 105 mM Ca^{2+} as a charge carrier, three distinct channel conductances of 11, 23, and 80 pS were observed. All types of mitochondrial currents were voltage-dependent and essentially depended on the presence of Ca^{2+} in the pipette. The 23 pS channel exhibited burst kinetics. Though all channels were sensitive to ruthenium red, their sensitivity was different. The 11 and 23 pS channels exhibited a lower sensitivity to ruthenium red than the 80 pS channel. The activities of all channels persisted in the presence of cylosporin A, CGP 37187, various K^+-channel inhibitors, and Cl^- channel blockers disodium 4,4′-diisothiocyanatostilbene-2,2′-disulfonate and niflumic acid. Collectively, our data identified multiple conductances of Ca^{2+} currents in mitoplasts isolated from HeLa cells, thus challenging the dogma of only one unique mitochondrial Ca^{2+} uniporter.

Keywords Mitochondrial Ca^{2+} channels · Mitoplast · Mitochondria · Ca^{2+} signaling · Patch clamp

Introduction

Mitochondrial functions largely depend on their ability to take up, accumulate and release Ca^{2+}. Thus, mitochondrial Ca^{2+} homeostasis is of pivotal importance for the functions of the organelle as well as the cellular Ca^{2+} signaling and function (for review, see [7, 9]). Isolated mitochondria can rapidly take up a large amounts of Ca^{2+} in a mitochondrial membrane potential-dependent manner via the Ca^{2+} uniporter pathway [14]. Although the mystery of the nature of the mitochondrial Ca^{2+} uniporter has been enlightened by the identification of the so-called mitochondrial Ca^{2+} uniporter (MCU) [3, 6] and its regulator and gatekeeper the mitochondrial calcium uptake 1 (MICU1) [15, 19], our understanding on the properties and characteristics of mitochondrial Ca^{2+} uptake is limited. In a landmark publication, the group of David Clapham described a Ca^{2+} entry current in isolated mitoplasts of which the biophysical characteristics (e.g., ion selectivity and sensitivity) fulfill the features expected from the mitochondrial Ca^{2+} uniporter channel [13]. In another study performed on rat heart mitochondria, four distinct Ca^{2+} channel conductances that were established by mitochondrial ryanodine receptor type 1 (RYR1) were identified [21, 22]. Moreover, the leucine zipper EF hand-containing transmembrane protein 1 (LETM 1) was also described as a putative Ca^{2+} carrier in the inner mitochondrial membrane [12]. Under certain conditions mitochondrial Na^+–Ca^{2+} exchanger (NCX_{mito}) and the novel uncoupling proteins 2 and 3 (UCP2/3) were shown to accomplish the transfer of Ca^{2+} across the inner mitochondrial membrane [26, 27, 29], thus, emphasizing the existence of multiple mitochondrial Ca^{2+} uptake routes. In line with this consideration, more recently, single-channel patch clamp recordings from cardiac mitochondria revealed two different Ca^{2+} channels with distinct gating properties and sensitivity to Ru360 [17], thus questioning the dogma of the existence of one unique channel that exclusively accounts for mitochondrial Ca^{2+} uptake. Notably, distinct Ca^{2+} channels in the inner mitochondrial membrane of one given mitochondrion is not specific for cardiac mitochondria. In our previous work, we described two and three Ca^{2+} inward currents in mitoplasts

A. I. Bondarenko · C. Jean-Quartier · R. Malli · W. F. Graier (✉)
Institute of Molecular Biology and Biochemistry,
Center of Molecular Medicine, Medical University of Graz,
Harrachgasse 21/III,
8010 Graz, Austria
e-mail: wolfgang.graier@medunigraz.at

form HeLa and endothelial cells, respectively [11]. Accordingly, the dogma of a unique and ubiquitously established Ca^{2+} flux through the inner mitochondrial membrane is challenged and the existence of multiple Ca^{2+} entry routes/modes that establish distinct Ca^{2+} currents in one given mitochondria has to be considered.

Notably, a biophysical and pharmacological characterization of these distinct but coexisting Ca^{2+} currents through the inner membrane of mitochondria is missing whilst fundamental for future studies that aim to investigate the individual contribution of the putative candidate proteins (MCU [3, 6], RyR1 [22], LETM 1 [12, 28], and UCP2/3 [25, 26]) that actually accomplish mitochondrial Ca^{2+} uptake. Accordingly, this study was designed to characterize single-channel Ca^{2+} currents in mitoplasts isolated from HeLa cells and to describe the individual biophysical and pharmacological properties of distinct mitochondrial Ca^{2+} channels.

Materials and methods

Cell culture and isolation of mitochondria

HeLa cells were grown on DMEM containing 10 % FCS, 50 U/ml penicillin and 50 μg/ml streptomycin. Mitochondria were freshly isolated as previously described [11] with some modifications. Mitochondria were prepared from HeLa cells by differential centrifugation. Cells were trypsinized, harvested, and washed with PBS. All consecutive steps were carried out at 4 °C according to the protocol described by Frezza et al. [8]. The cell pellet was suspended in a 200-mM sucrose buffer containing 10 mM Tris-MOPS, 1 mM EGTA and protease inhibitor (1:50, P8340 Sigma, Vienna, Austria; pH adjusted to 7.4 with Tris) and homogenized with a glass–Teflon potter (40–50 strokes). Nuclear remnants and cell debris were centrifuged down at 900×*g* for 10 min. Supernatant was centrifuged at 3,000×g for 20 min. The mitochondrial pellet was washed again with IMBc and centrifuged down at 7,000×*g* for 15 min. All fractions were kept on ice until further utilization.

Preparation of mitoplasts

Mitoplast formation was achieved by incubation of isolated mitochondria in hypotonic solution (5 mM HEPES, 5 mM sucrose, and 1 mM EGTA and pH adjusted to 7.4 with KOH) for 8–10 min. Then hypertonic solution (750 mM KCl, 80 mM HEPES, and 1 mM EGTA and pH adjusted to 7.4 with KOH of <10 mM) was added to restore isotonicity. Mitochondrial swelling was monitored as a change of optical density at 540 nm (Schott instruments UviLine 9400) [4, 10, 20]. Isolated mitoplasts appeared as transparent vesicles with attached remnants of the outer membrane. Purity of isolated mitochondria was verified by Western blots labeling plasma membrane and mitochondrial-localized proteins (Orai-1 (H-46:sc-68895 Santa Cruz, Szabo, Vienna, Austria and PSI-1819, Pro-Sci, Szabo, Vienna, Austria) and MCU (E-16:sc-246072 Santa Cruz), respectively).

Table 1 Composition of pipette solutions (PS) used to detect mitoplast Ca^{2+} currents in the mitoplast-attached configuration

	Composition of pipette solution (mM)	Appearance of *i*-MCC	Appearance of *xl*-MCC
PS1	105 $CaCl_2$ 10 HEPES 0.01 CsA 0.01 CGP 37187	Yes	Yes
PS2	65 Ca MeS 40 $CaCl_2$ 10 HEPES 0.01 CsA 0.01 CGP 37187	Yes	Yes
PS3	220 sucrose 35 NMDG-Cl 10 HEPES 2 EGTA 0.1 DIDS 0.01 CsA 0.01 CGP 37187	No	No

The pH of all solutions was adjusted to 7.2 with KOH. In all experiments, bath solution contained (in millimolars): 150 KCl, 1 EGTA, 1 EDTA, 10 HEPES, pH was adjusted to 7.2 with KOH

Mitoplast patch clamp recordings

All measurements were performed in the mitoplast-attached configuration at room temperature. Patch pipettes were

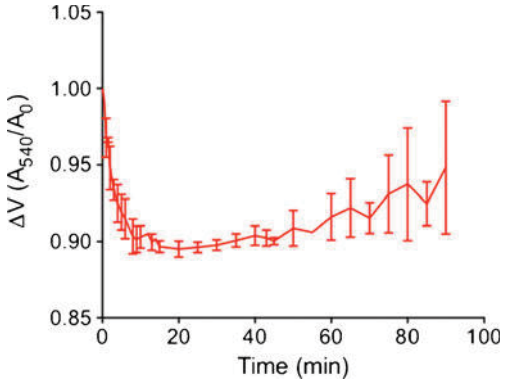

Fig. 1 Time course of mitochondria swelling in hypotonic solution. Isolated mitochondria were suspended in hypotonic solution (5 mM HEPES, 5 mM sucrose, and 1 mM EGTA pH adjusted to 7.4 with KOH) and volume change due to mitochondrial swelling was monitored as decline in absorbance at 540 nm. Data are expressed as ratio between the change in absorbance over time divided by the absorbance at the initial timepoint (mean±SD, n=3)

pulled from glass capillaries using a Narishige puller (Narishige Co., Ltd., Tokyo, Japan), fire-polished and had a resistance of 8–12 MΩ. Experimental buffers contained 105 mM $CaCl_2$ and 10 mM HEPES (pipette solution 1 (PS1)), or low chloride solution with 65 mM Ca-methanesulfonate, 40 mM $CaCl_2$, and 10 mM HEPES (PS2), both pH adjusted to 7.2 with $Ca(OH)_2$. Ca^{2+}-free pipette solution contained (in millimolars): 220 sucrose, 35 *N*-methyl-D-glucamine chloride, 2 EGTA, and 0.1 disodium 4,4′-diisothiocyanatostilbene-2,2′-disulfonate (DIDS; PS3) (Table 1). Bath solution contained 150 mM KCl, 1 mM EGTA, 1 mM EDTA, and 10 mM HEPES, pH was adjusted to 7.2 with KOH. If not otherwise indicated, all pipette solutions contained 10 μM Cyclosporin A (Tocris Bioscience, Bristol, UK) and 10 μM 7-chloro-5-(2-chlorophenyl)-1,5-dihydro-4,1-benzothiazepin-2(3H)-one (CGP 37187, Ascent Scientific Ltd., Bristol, UK) to prevent opening of the permeability transition pore (PTP) and the activity of the mitochondrial Na^+/Ca^{2+} exchanger (NCX_{mito}) as well as LETM1 [12], respectively. Ruthenium red (RuR; 1–30 μM; Merck Chemicals Ltd., Darmstadt, Germany) and DIDS (100 μM) were added as indicated. Currents were recorded using a patch-clamp amplifier (EPC7, List Electronics, Darmstadt, Germany). Data collection was performed using Clampex software of pClamp (V9.0, Axon Instruments). Signals obtained were low pass filtered at 1 kHz using an eight-pole Bessel filter (Frequency Devices), and digitized with a sample rate of 10 kHz using a Digidata 1200A A/D converter (Axon Instruments, Foster

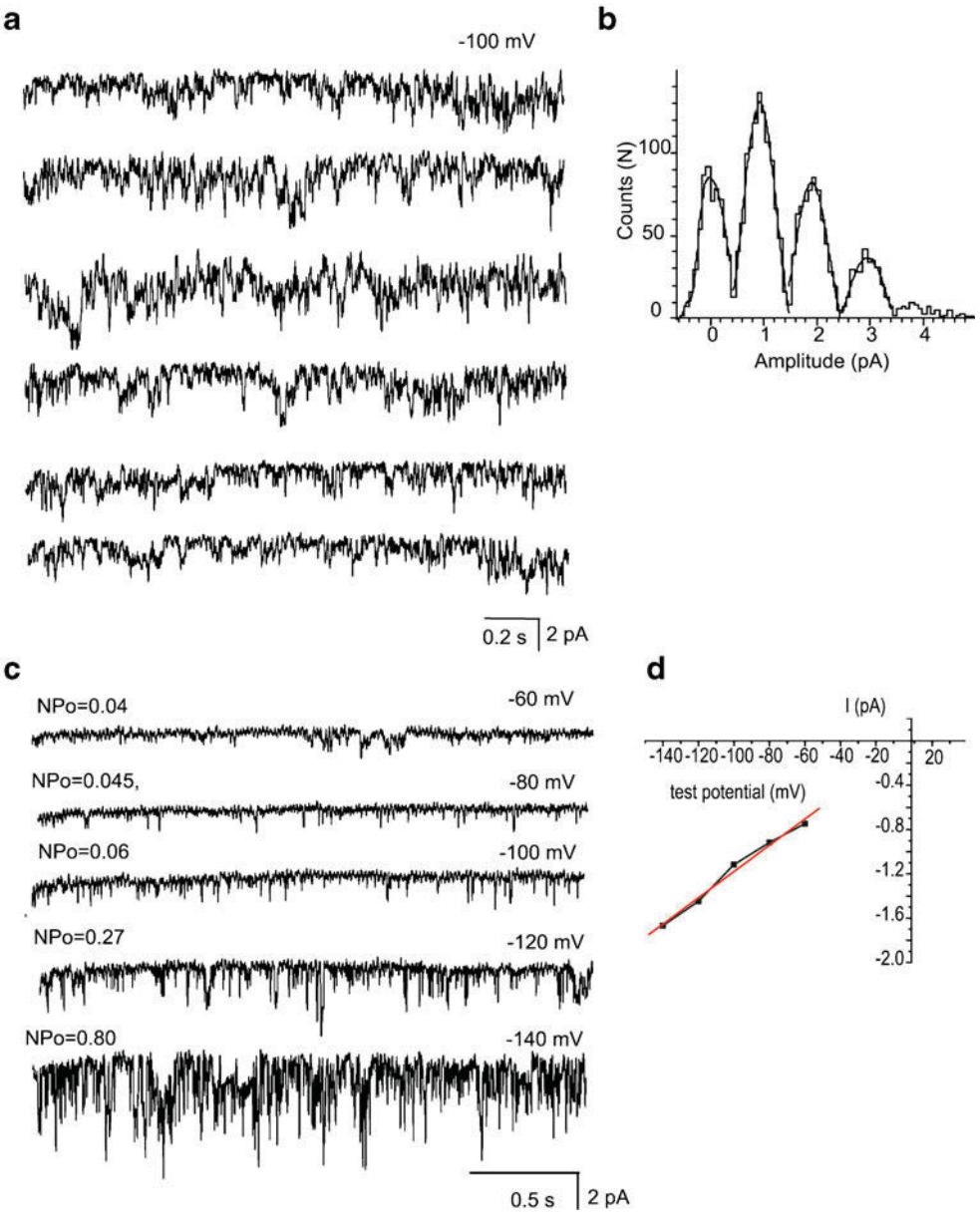

Fig. 2 *i*-MCC are present in mitoplasts isolated from HeLa cells. **a** Exemplary traces of *i*-MCC from HeLa mitochondria at test potential of −100 mV. **b** Corresponding amplitude histogram constructed from traces shown in (**a**). **c** *i*-MCC channel activities at different voltages indicated. **d** Corresponding IV curve of the channel activity shown in (**c**)

City, CA). Voltage ramps of 1 s duration from −150 to + 50 mV were delivered every 10 s from the holding potential 0 mV. Single-channel currents were recorded at a fixed holding potential indicated in the respective figures.

Results

Control of mitoplast preparation

To adjust optimal time of mitochondria incubation in hypotonic medium during mitoplast preparation, we monitored time-dependency of mitochondria swelling. Incubation in hypotonic solution resulted in a gradual decline of the optical density within 8–10 min (Fig. 1), which corresponds to mitochondria swelling and the start of outer membrane rupture and formation of mitoplast [4, 10, 20]. Mitochondria swelling reached a plateau phase within 10 to 20 min, which was followed by a gradual restoration in optical density. Accordingly, for mitoplast preparation from HeLa cells, isolated mitochondria were incubated in hypotonic solution for 7–8 min.

The plasma membrane is comprised of various Ca^{2+} channels that might interfere in our electrophysiological recordings with mitoplasts Ca^{2+} currents. Therefore, in order to assess a

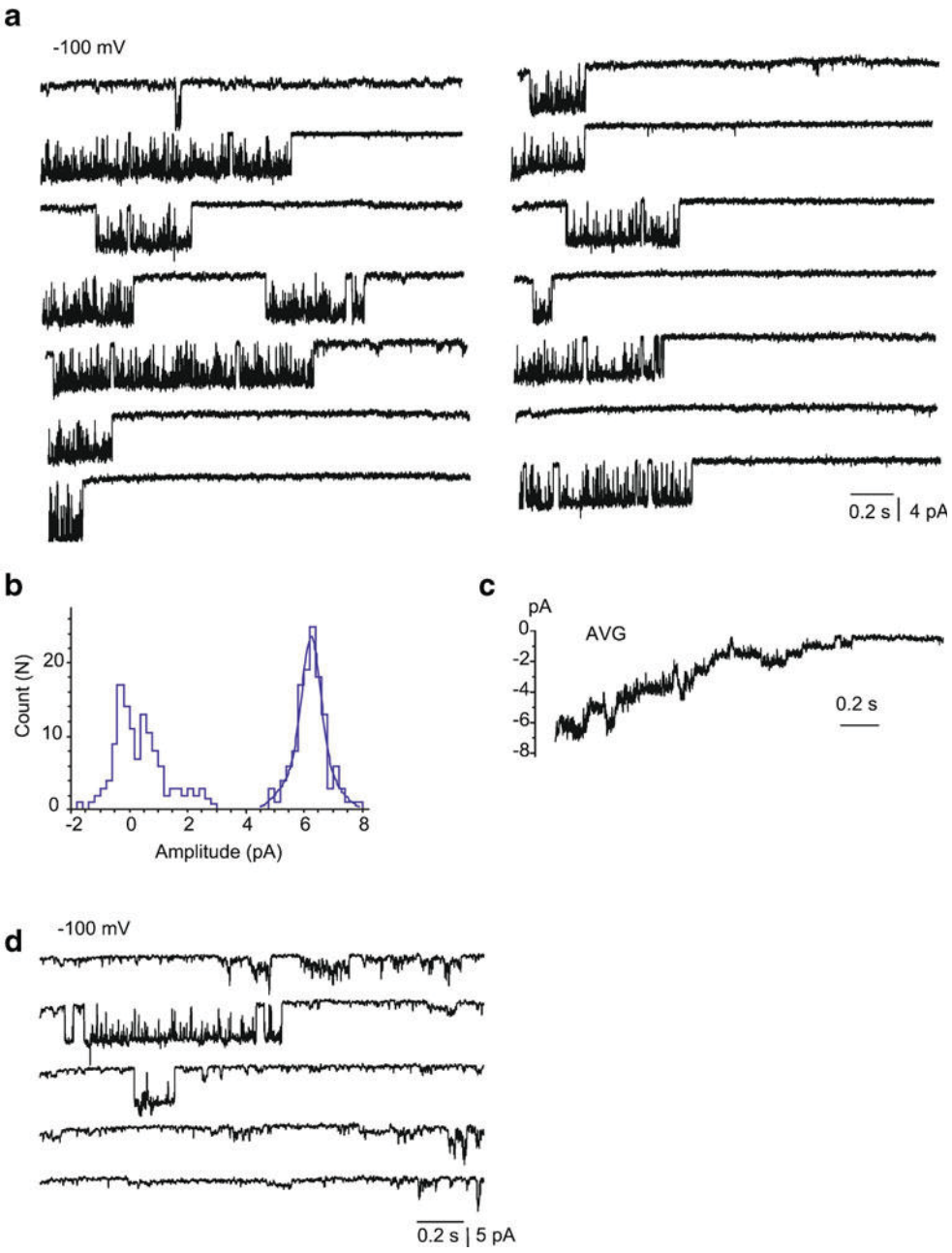

Fig. 3 *xl*-MCC are present in mitochondria from HeLa cells. **a** Representative tracings of single-channel events at a test potential of −100 mV showing activity of *xl*-MCC. **b** Corresponding amplitude histogram constructed from traces shown in (**a**). **c** Average of individual traces shown in (**a**). **d** An exemplary recording from HeLa mitoplast showing coexistence of channels with bursting activity, *i*-MCC and *xl*-MCC in the same patch

potentially contamination of the prepared mitoplasts, we tested for putative plasma membrane particles inside the mitochondrial fraction using Western Blotting. We tested the protein content within organelle fractions for Calcium release-activated calcium channel protein 1 (ORAI-1), as representative plasma membrane protein, and MCU as mitochondrial control protein. Densitometric analyses revealed a 3-fold increase of MCU content in mitochondrial fractions compared with whole cell lysates. Orai-1 was inconsistently present in mitochondrial fractions in approximately 20 times lower amount than in whole cell lysates. Prior electrophysiological measurements, mitoplasts were allowed to settle down to the glass bottom of the recording chamber, gently washed with bath solution, visualized and approached by the patch pipette.

Biophysical characterization of three distinct Ca^{2+} currents in mitoplasts

Recordings in the mitoplast-attached configuration with the use of high Ca^{2+}-containing pipette solution (PS1, Table 1) at test potentials from −100 to −150 mV in high K^+ bath solution revealed several types of single-channel activities. Based on the individual channel conductance and kinetics three distinct Ca^{2+} currents could be discriminated that were observed frequently in the same patch. The most predominant current was a 11.7±0.6-pS (n=14) channel that was referred to as intermediate mitochondrial Ca^{2+} channel (i-MCC) according to our previous report [11]. In high Ca^{2+}-containing pipette solution (PS1) i-MCC was found in about 70 % of patches. Figure 2a shows individual traces of the single-channel activity of i-MCC in a patch held at −100 mV. The channel did not inactivate over time during stepwise voltage shifts. Generally, more than one active channel was present in the patches. The corresponding amplitude histogram indicates the mean single-channel amplitude at −100 mV is approximately 1 pA (Fig. 2b). Representative traces of i-MCC channel at voltages −60 to −140 mV are shown in Fig. 2c. The channel activity starts noticeable at −60 mV. Shifting the holding potential towards more negative values gradually increased the single-channel activity (NPo) and amplitude that showed no rectification at potentials from −60 to −140 mV (Fig. 2d). Because of general instability of patches at voltages more negative than −140 mV in our experiments, we were unable to routinely investigate the channel behavior at −160 mV.

Under our standard experimental conditions (PS1), in 12 % of experiments a high conductance (60–100 pS) single-channel activity with a mean conductance of 80.2± 7.8 pS (n=7) was observed that occurred in addition to the 11 pS i-MCC channel. The channel is characterized by a relatively long-lived open state, during which the channel exhibited bursting behavior. In line with our previous observation [11], this channel is referred to as the extra large conductance mitochondrial Ca^{2+} channel (xl-MCC). Representative traces of the channel activity at −100 mV and the corresponding amplitude histogram are shown in Fig. 3a, b. Generally, only one xl-MCC channel was present in one given patch, thus, pointing to a far lower density of this channel compared with i-MCC. During voltage steps, the xl-MCC channel activity tends to inactivate over time (Fig. 3a) and average of individual traces from the same patch is shown in Fig. 3c. The xl-MCC activity was observed either as a sole Ca^{2+} conductance in the patch (Fig. 3a) or together with i-MCC (Fig. 3d). The activity of xl-MCC started noticeable at −50 mV (Fig. 4a). Similar to i-MCC, single-channel amplitude of xl-MCC channels increased without rectification with increasing voltage as evidenced from the current responses to voltage ramps (Fig. 4a). The activity of xl-MCC channel increased at more negative potentials (Fig. 4b).

In 35 % of the experiments, single-channel activities of either i-MCC or xl-MCC were interrupted by a channel with bursting kinetics and periods of high amplitude and frequency of open-closed transitions separated by silent intervals

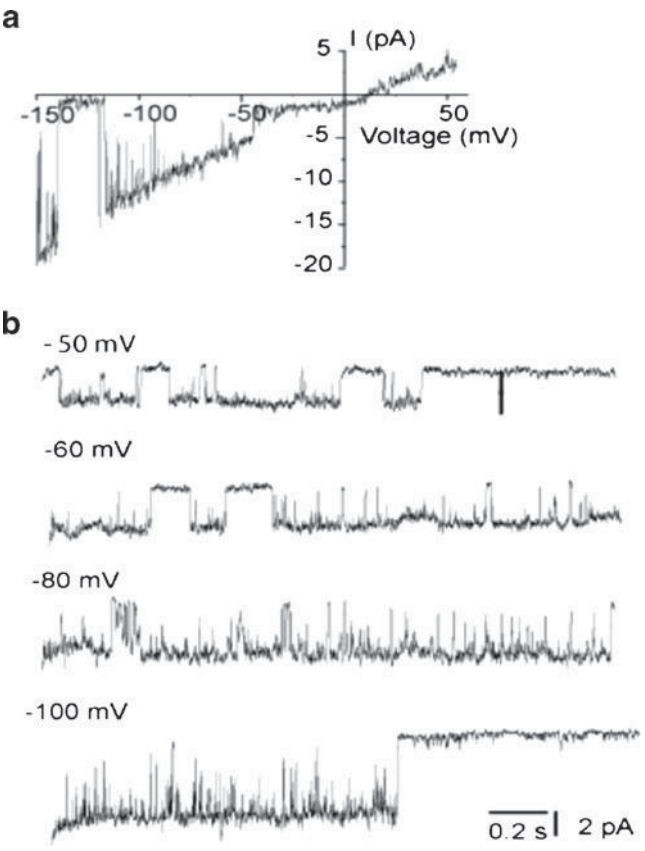

Fig. 4 Voltage dependency of extra-large conductance Ca^{2+} channel. **a** Representative current traces in response to voltage ramps from −150 to +50 mV showing single-channel activity of xl-MCC. The figure depicts the net current obtained after subtraction of the background current obtained from the same patch during nonresponsive sweeps from the xl-MCC current responses. **b** xl-MCC activity at different voltages indicated

(Fig. 5a). Burst activities were observed either simultaneously with *i*-MCC or *xl*-MCC gating or were a sole type of current activity observed in the particular patch (Fig. 5b). The corresponding amplitude histogram showed that the single-channel amplitude of these burst currents (burst mitochondrial Ca^{2+} channel (*b*-MCC)) at −100 mV was 2.3 pA, corresponding to a conductance of 22.5±1.7 pS (n=10) (Fig. 5c). Similar to *i*-MCC and *xl*-MCC, single-channel activity of *b*-MCC channels increased with increasing voltage (Fig. 6a). Single-channel amplitude of *b*-MCC channels showed no rectification within voltage range from −60 to −140 mV (Fig. 6b).

The open probability (Npo) of *i*-MCC and *xl*-MCC were quite similar and exceeded that of the *b*-MCC by 2-fold (Table 2). In terms of open/close kinetics, the mean open time (To_{mean}) and mean closed time (Tc_{mean}) of the *i*-MCC and *b*-MCC were similar. In contrast, To_{mean} and Tc_{mean} for the *xl*-MCC exceeded that of the other two channels by 10- and 2.5-fold, respectively (Table 2).

Ca^{2+} dependence of the distinct mitoplast (Ca^{2+}) inward currents

In the absence of Ca^{2+} in patch pipettes, no channel activity was observed in nine patches tested (data not shown) at voltages −100 to −150 mV. These observations strongly indicate that the observed channel activities are mediated by Ca^{2+} fluxes.

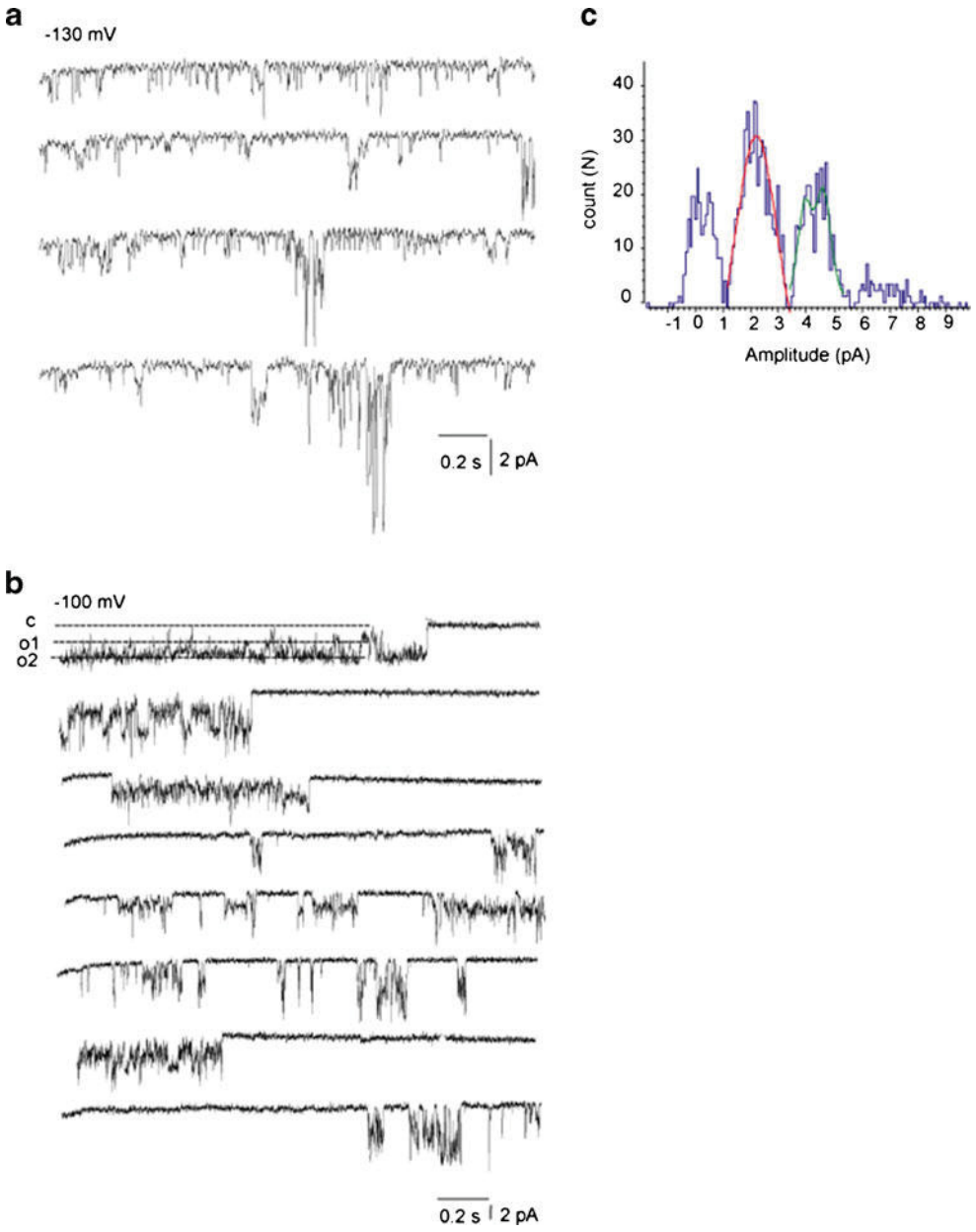

Fig. 5 Channels with *b*-MCC isolated from HeLa cells. **a** Exemplary traces showing the activity of intermediate conductance mitochondrial Ca^{2+} channels together with bursting channel activity in the same patch. **b** Exemplary traces showing the activity of bursting channel as a sole single-channel activity type. **c** Corresponding amplitude histogram constructed from traces shown in (**b**)

Sensitivity of the distinct mitoplast (Ca^{2+}) inward currents to RuR

We next explored the sensitivity of the three distinct single-channel activities to RuR, the golden standard of an inhibitor of the mitochondrial Ca^{2+} uniporter. When 1 μM RuR was present in the pipettes, the occurrences of *i*-MCC and *b*-MCC channels were not altered (13 out of 19 patches). Among these 13 patches, 2 patches exhibited *xl*-MCC activity in the presence of 1 μM RuR, suggesting that the occurrence of *xl*-MCC is also not affected by 1 μM RuR. The conductances of these two *xl*-MCC channels were reduced in the presence of 1 μM RuR in the pipettes to 54 and 48 pS compared with the mean conductance of *xl*-MCC channels of 80.2±7.8 pS (Fig. 7a; Table 3). These observations indicate that the *xl*-MCC conductance, but not

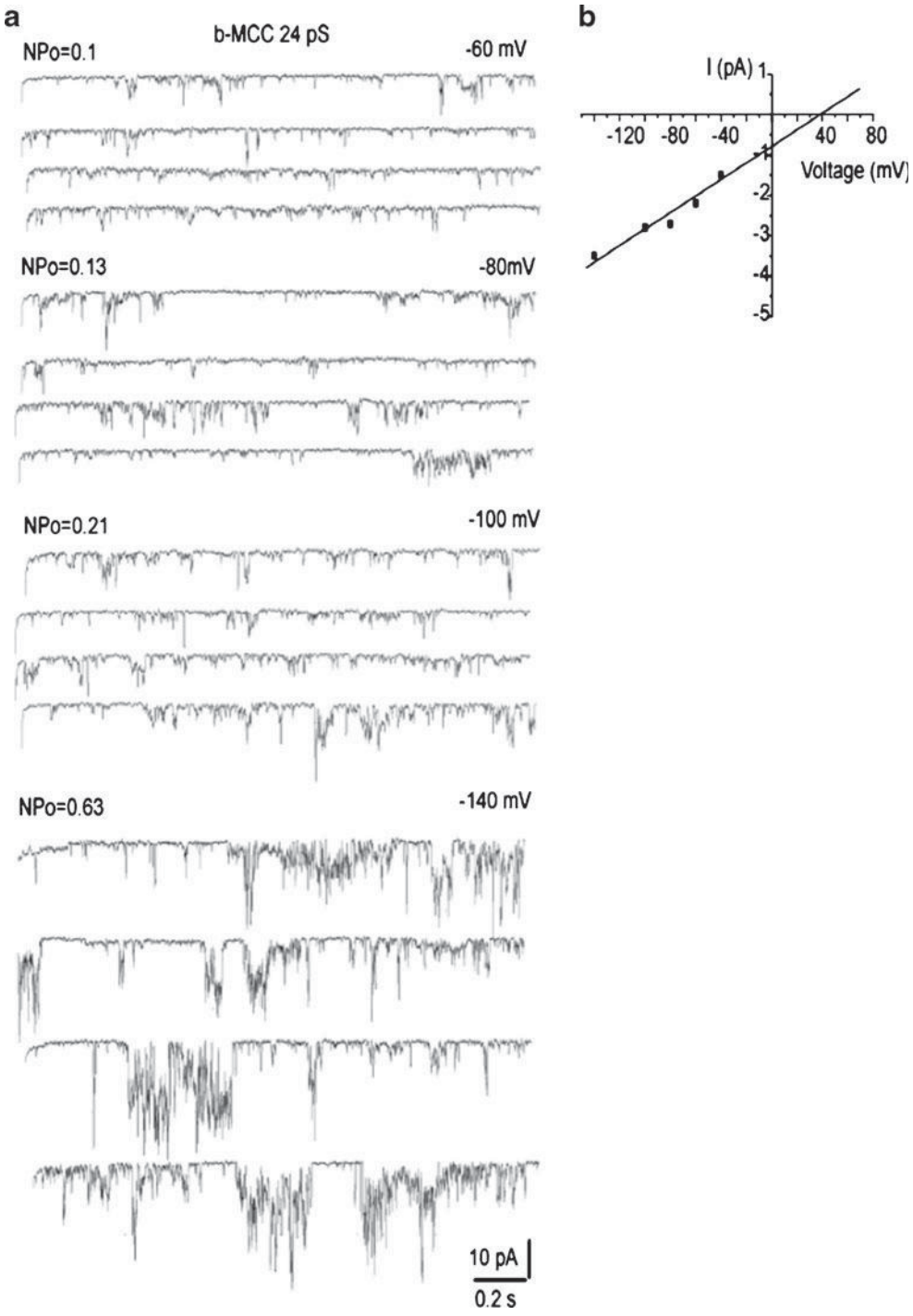

Fig. 6 Bursting Ca channels (*b-MCC*) are voltage dependent. **a** Exemplary single-channel traces of *b*-MCC at different voltages indicated. Note an increase in the *b*-MCC activity at more negative voltages. **b** Corresponding current–voltage relationship of *i*-MCC

Table 2 Gating characteristics of the detected mitoplast Ca^{2+} currents

	NPo(ms)	Tc_{mean}	To_{mean}(ms)	Number
i-MCC	0.61±0.14	3.5±0.5	14.9±2.4	13
xl-MCC	0.77±0.06	45.8±14.3	57.7±15.9	8
b-MCC	0.34±0.08	4.4±0.9	22.6±2.6	5

In all experiments, bath solution contained (in mM): 150 KCl, 1 EGTA, 1 EDTA, and 10 HEPES and pH was adjusted to 7.2 with KOH. Open probability (NPo), mean open time (To_{mean}) and mean close time (Tc_{mean}) of intermediate (*i*-MCC), extra-large mitochondrial Ca^{2+} channel (*xl*-MCC) and burst (*b*-MCC) mitochondrial Ca^{2+} channels are presented as means ± SEM. n, provides the number of individual patches for the respective experiments

occurrence, is reduced in the presence of 1 μM RuR. In the presence of 10 μM RuR in the pipette, the *i*-MCC channel activity was observed in seven out of nine patches tested. Under these conditions, the conductance of *i*-MCC channel was reduced to 7.3±1.1 pS (n=7) (Fig. 7b, c) compared with 11.7±0.6 pS in the absence of RuR. Similar to the *i*-MCC, *b*-MCC conductance was reduced in the presence of 10 μM RuR in the pipette (from 22.6±1.7 pS in the absence of RuR to 16.3±1.8 pS (n=4) in the presence of 10 μM RuR in the pipette) (Table 3). However, among these nine patches tested with 10 μM RuR in the pipette, no *xl*-MCC activity was observed, thus indicating that 10 μM RuR completely prevented *xl*-MCC activity. In the presence of 30 μM RuR in patch pipette, no single-channel activity was observed in 12 patches tested.

We also explored the effect of RuR applied to the bath solution on activities of mitochondria Ca^{2+} channels. When 1 μM RuR was applied to the bath solution the activity but not the conductance of *i*-MCC and *b*-MCC channels was decreased (Fig. 8a). At concentration 10 μM, RuR largely suppressed the single-channel amplitude and open probability (up to 70 %) of both *i*-MCC and *b*-MCC. In two out of six patches, 10 μM RuR applied to the bath completely suppressed the activity of both *i*-MCC and *b*-MCC. The *xl*-MCC activity was largely suppressed by 1 μM RuR and completely inhibited by 10 μM RuR (Fig. 8b). Altogether, these observations may indicate that *i*-MCC and *b*-MCC are less sensitive to RuR than *xl*-MCC (Table 3).

Pharmacological characterization of (Ca^{2+}) inward currents in mitoplasts

As in all experiments described above 10 μM CsA and CGP 37187 were present in the pipette solutions, the observed three mitoplast (Ca^{2+}) currents were obviously not sensitive to inhibition of the PTP, NCX_{mito}, and LETM1.

The inner mitochondrial membrane contains Cl^- channels activated at depolarized but not hyperpolarized voltages [24]. Nevertheless, to exclude the possibility that the observed channel activities were caused by Cl^- conductances, experiments using a pipette solution with a reduced Cl^- concentration (PS2, Table 1) were performed. A decrease of Cl^- concentration either in a pipette (Fig. 9a, b) or a bath (Figs. 8a, b and 9c, d) solution failed to affect inward openings at negative potentials and single-channel conductance. Voltage ramps from −150 to 150 mV revealed single-channel opening events at voltages positive than +30 mV likely corresponding to the activity of Cl^- channels (Fig. 9e). Subsequently, the sensitivity of mitoplast ion currents to well-known Cl^- channel inhibitors has been tested. Neither the presence in the pipette solution of 100 μM niflumic acid, nor 100 μM DIDS prevented the single-channel activities of *xl*-MCC (Figs. 8b and 10a), *i*-MCC and *b*-MCC (Fig. 10b) suggesting that Cl^- channels unlikely account for the observed single-channel activities (Table 3). Incorporation of either paxilline (1 μM), iberiotoxin (100 nM), or glibenclamide (10 μM) into the patch pipette failed to prevent single-channel activities (Table 3; Fig. 10c).

Discussion

In view of the recent progress in the molecular identification of potential contributors to mitochondrial Ca^{2+} uptake (MCU [3, 6], RyR1 [22], LETM 1 [12, 28], and UCP2/3 [25, 26]) and the remaining evaluation of the individual contributions of these proteins to mitochondrial Ca^{2+} signaling in situ, there is an emerging need for a biophysical and pharmacological characterization of these co-existing Ca^{2+} channels of the inner mitochondrial membrane. Our work for the first time provides a clear and transparent basis for studying Ca^{2+} currents of the inner mitochondrial membrane that will help to identify and characterize possible contributors of mitochondrial Ca^{2+} uptake on the molecular level.

Our findings that the currents measured required Ca^{2+} in the pipette indicate that all currents indeed represent Ca^{2+} conductances through the inner mitochondrial membrane. This assumption was further supported by our findings that under conditions in which only Ca^{2+} and Cl^- were present (i.e., PS1) in the pipette/mitoplast matrix, the Cl^- channel blockers DIDS and niflumic acid, and the K^+ channel inhibitors paxilline, iberiotoxin, and glibenclamide did not affect the individual currents. In line with these findings, a reduced Cl^- content of either the pipette or bath buffer did not affect the individual currents. Overall, these data indicate that the three currents described above most likely represent three distinct Ca^{2+} conductances across the inner mitochondrial membrane.

The *xl*-MCC channel activity was observed inconsistently and their occurrence varied between different experimental days. Hence, it was difficult to consistently conduct

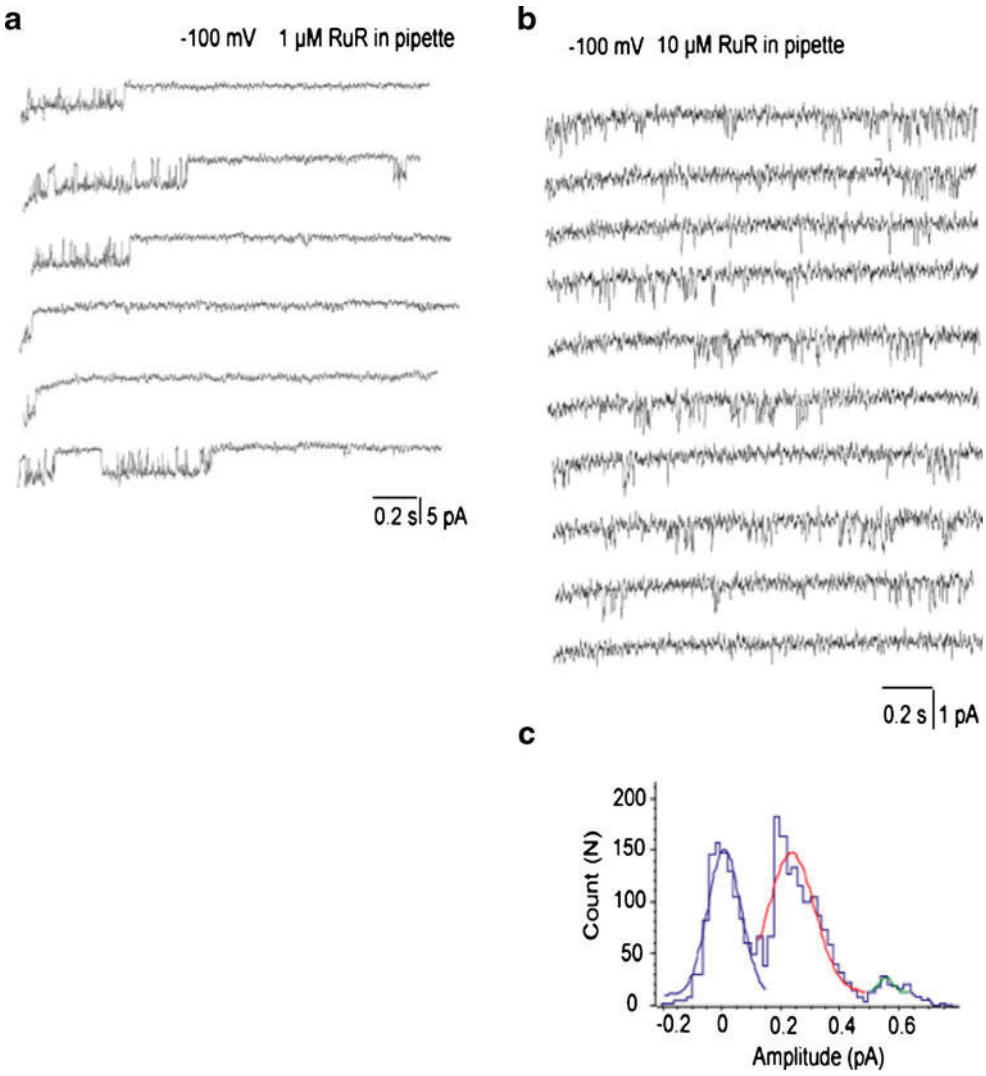

Fig. 7 Pharmacological inhibition of mitochondrial Ca^{2+} channels by ruthenium red (*RuR*). **a** Exemplary traces showing a decreased unitary amplitude of *xl*-MCC channels in the presence of 1 μM RuR in the pipette. Test potential is −100 mV. **b** Exemplary traces showing reduced single-channel amplitude of *i*-MCC channel activity by 10 μM RuR present in the pipette solution. Standard 105 mM $CaCl_2$-containing solutions was supplemented with 100 μM DIDS, 10 μM CsA, 10 μM CGP 37187, and 10 μM RuR. Test potential is −100 mV. **c** Corresponding amplitude histogram of the channel activity shown in (**b**) reveals decreased single-channel amplitude of *i*-MCC in the presence of RuR

experiments specifically on this channel type. In regard of possible channels with similar characteristics to those described above, we cannot completely exclude possible contamination of mitochondrial fractions from the plasma membrane sheets. Cell fractionation has become a standard procedure combining various centrifugation steps and purity

Table 3 Overview on the pharmacological profile of mitoplast Ca^{2+} currents

Target	Compound to be tested (μM)	Concentration	Inhibition of *i*-MCC	Inhibition of *xl*-MCC	Inhibition of *b*-MCC
MCU	Ruthenium red	1	None	Moderate	None
		10	Moderate	Strong	Moderate
		30	Strong	Strong	Strong
NCX_{mito}	CGP 37187	10	None	None	None
PTP	Cyclosporin A	10	None	None	None
(B)K_{Ca}	Paxilline IbTX	1 0.1	None	None	None
			None	None	None
K_{ATP}	Glibenclamide	10	None	None	None
Cl^- channels	DIDS	100	None	None	None
Nonselective cation channels	Niflumic acid	100	None	None	None

The inhibitory potential of the compounds on *i*-MCC, *xl*-MCC, and *b*-MCC were evaluated in experiments using PS1 and PS2 in the pipette. Experiments were performed in mitoplasts of at least five different isolation days. Mitoplasts were isolated from HeLa cells as described under "Materials and methods"

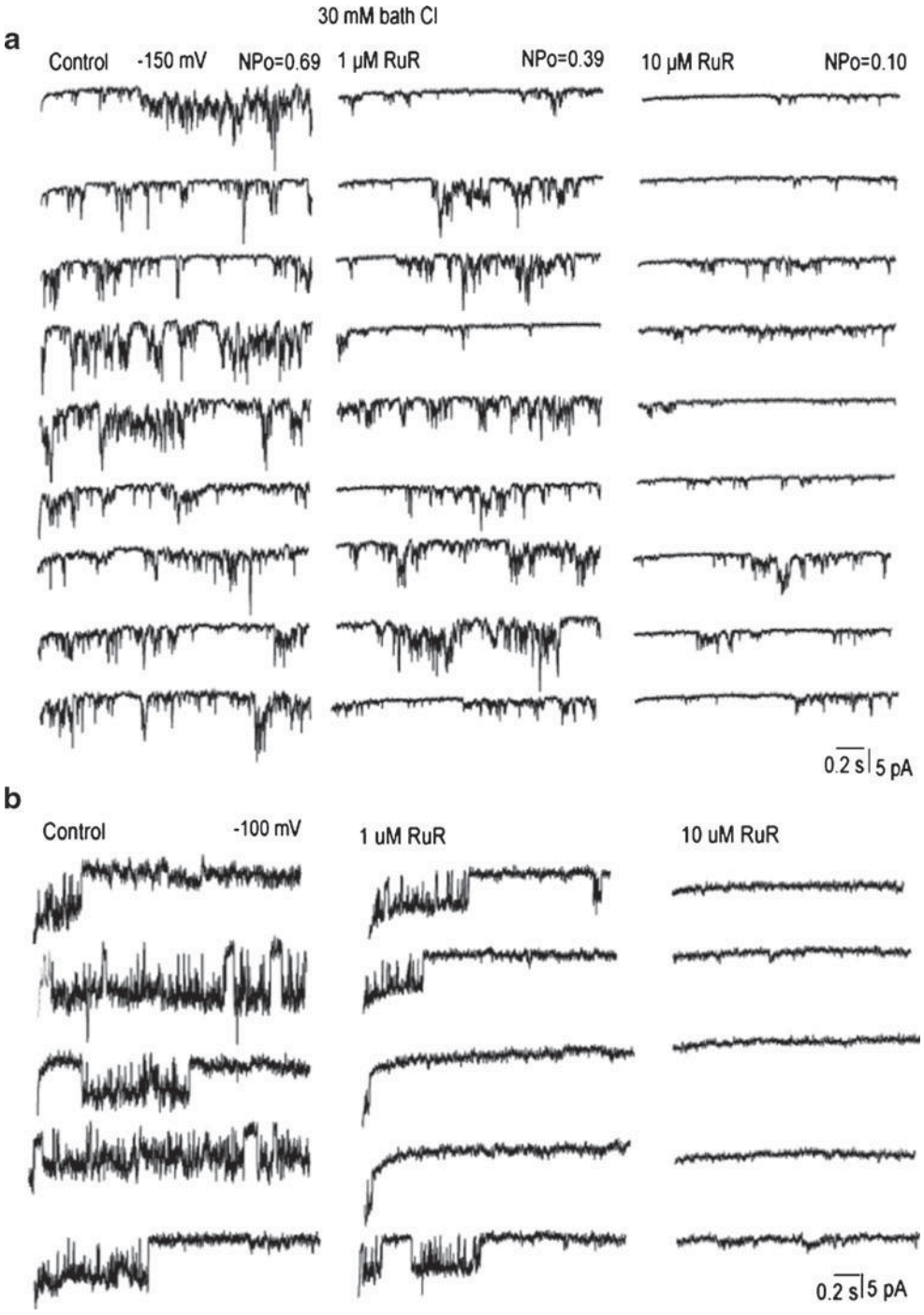

Fig. 8 Ruthenium red suppresses the activities of mitochondrial Ca^{2+} channels. **a**, **b** Representative traces showing the activities of *b*-MCC at test potential of −150 mV (**a**) and *xl*-MCC at test potential of −100 mV (**b**) before (control) and after addition of 1 and 10 μM RuR into the bath solution. Recordings were performed in the bath solution containing 40 mM Cl^- in the absence (**a**) and presence (**b**) of 100 μM DIDS in the pipette solution

of mitoplasts was tested by Western blotting of respective proteins. Moreover, because electrophysiological recordings from mitoplasts were preceded by mitoplast selection and chasing with the patch pipette under visual control, measurements of proteins from other cellular compartments are highly unlikely, although not absolutely excludable.

In the present study we show that under conditions that facilitate Ca^{2+} currents, mitoplasts isolated from HeLa cells exhibit three distinct types of single-channel activity: most frequently an 11 pS channel (*i*-MCC) was observed. In addition, a burst-channel with conductance of 23 pS (*b*-MCC) and a rare, large channel with a conductance of 80 pS (*xl*-MCC) were recorded. The co-existence of *i*-MCC and *xl*-MCC in mitoplasts form HeLa cells is in line with our previous report [11]. Hence, the conductance of *i*-MCC, channel density, and its gating characteristics found in mitoplasts from HeLa cells (this paper) and endothelial cells [11],

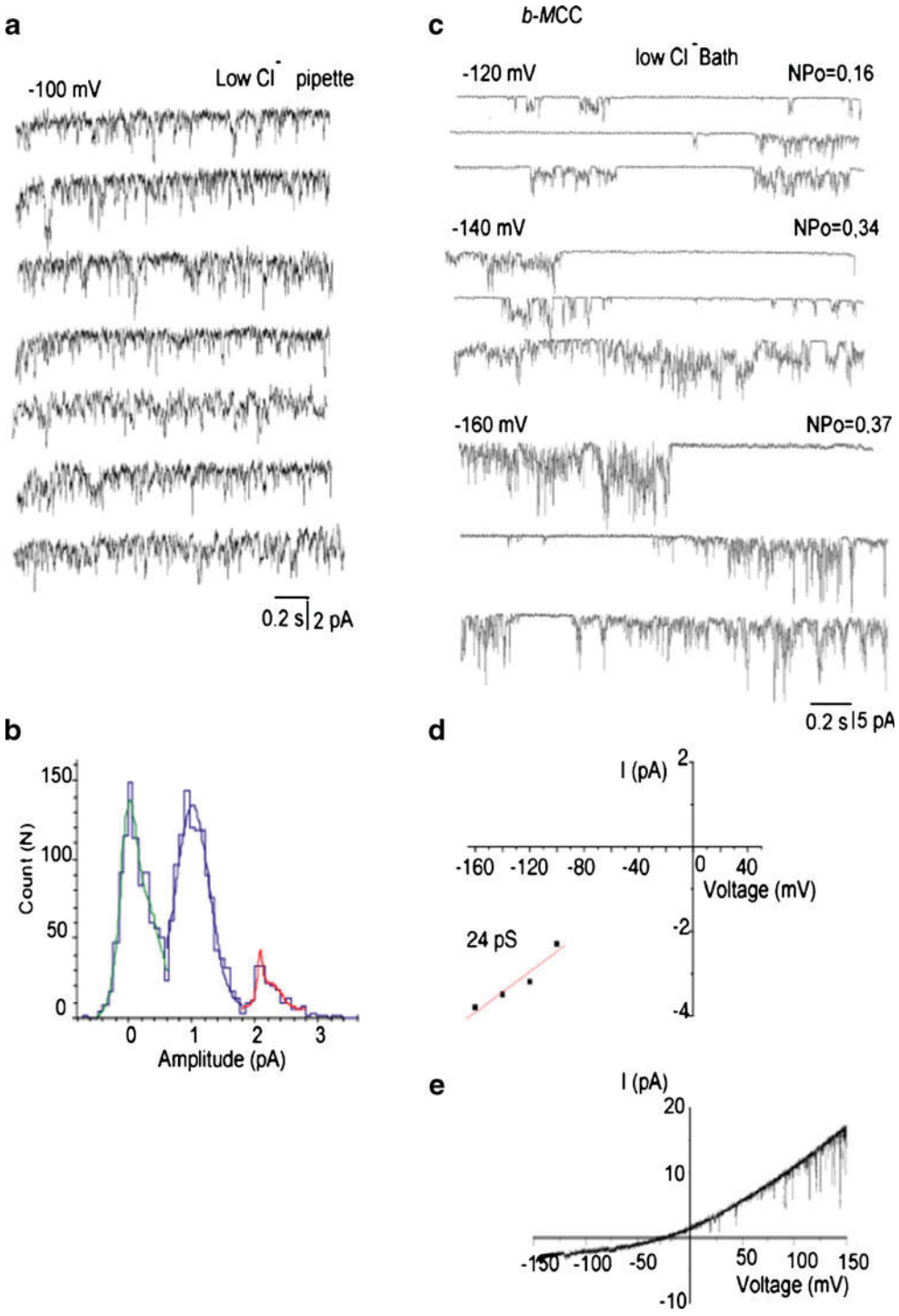

Fig. 9 Effect of manipulation of Cl^- concentrations on (Ca^{2+}) inward currents in mitoplasts. **a** Representative traces of *i*-MCC channel activity recorded with the use of low Cl^- (40 mM Cl^-)-containing pipette solution. Test potential is −100 mV. **b** Amplitude histogram of the channel activity shown in (**a**). **c** Representative traces showing the activity of *b*-MCC at different voltages indicated in the presence of 40 mM bath Cl^-. **d** Corresponding voltage dependency of single-channel amplitudes of single-channel openings shown in (**c**). **e** Representative current responses to a voltage ramps from −150 to +150 mV under our standard recording conditions showing the activity of Cl^- channels at positive potentials

obviously correspond to the mCa1 entitled current recorded in cardiac myocytes [17], thus, pointing to *i*-MCC as to be a likely candidate for an ubiquitous Ca^{2+} channel of the inner mitochondrial membrane. However, with its conductance between 11 and 14 pS, *i*-MCC exceeds that of MCU reconstituted into planar lipid bilayer (6–7 pS) [6], the most promising candidate representing the pore-forming unit of a mitochondrial Ca^{2+} channel [3, 6].

However, a conductance (i.e., 3–8 pS) very similar to that found in planar lipid bilayer with reconstituted MCU was recorded from mitoplasts isolated from COS7 cells [13], cardiac myocytes (mCa2) [17], and endothelial cells (*s*-MCC) [11] but not in HeLa cells (this study and [11]). This

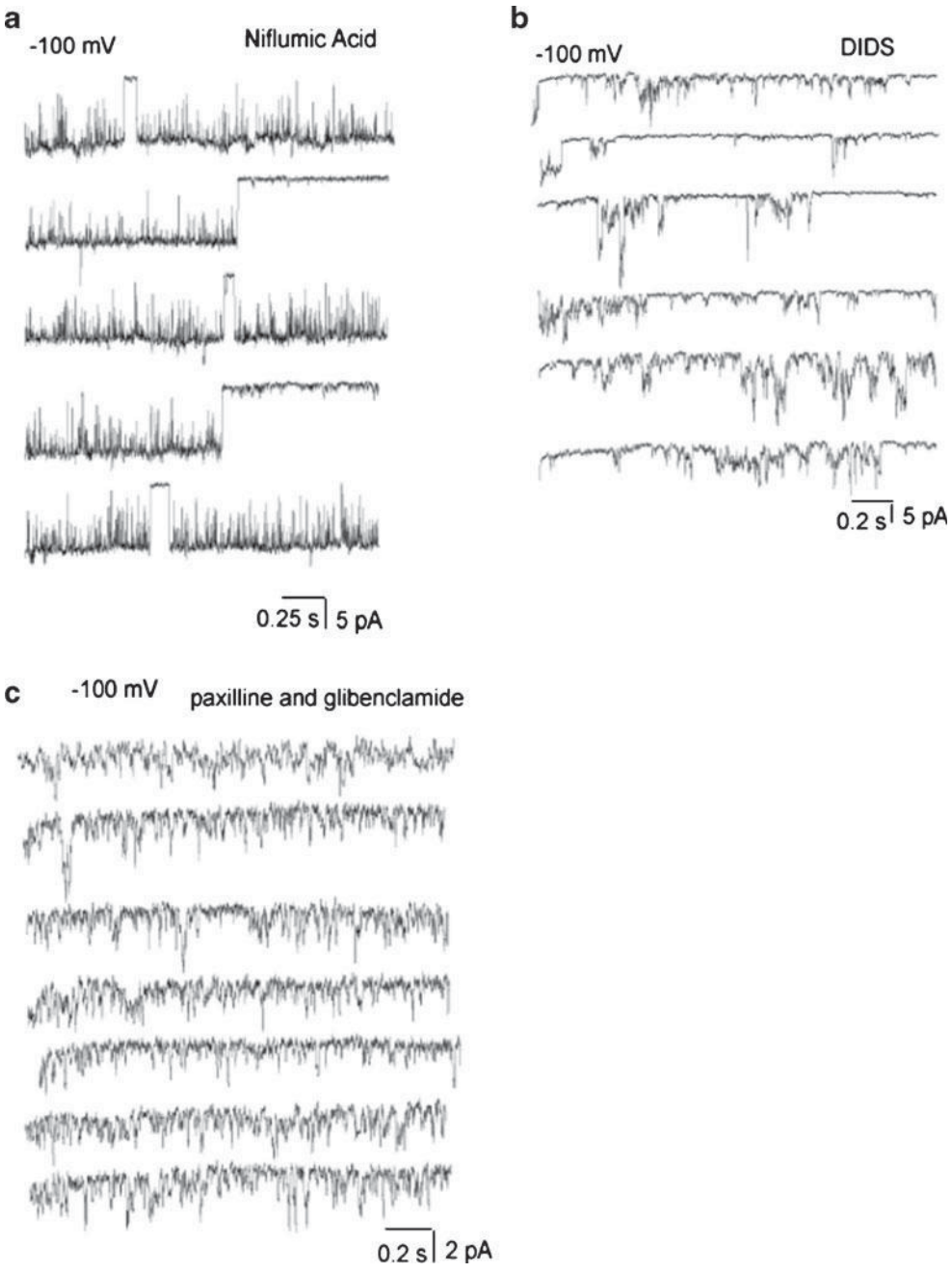

Fig. 10 Pharmacological characterization of (Ca^{2+}) inward currents in mitoplasts. **a** Representative traces showing *xl*-MCC channel activity in the presence of 100 μM niflumic acid in the pipette solution. Test potential is −100 mV. **b** Representative traces showing the activities of *b*-MCC and *i*-MCC in the same patch in the presence of 100 μM DIDS in the pipette solution. Test potential is −100 mV. **c** Representative traces showing the activity of *b i*-MCC in the presence of 1 μM paxilline and 10 μM glibenclamide in the pipette solution. Test potential is −100 mV

is particular notable as MCU is expressed in HeLa cells and was functionally characterized in this particular cell type [3, 6]. Recently, MICU1 [19] was described as a gatekeeping modulator protein regulating the MCU activity [15], thus, this discrepancy might be due to the lack of MICU1 in the in vitro experimental setup, resulting in the channel activity with reduced conductance when measurements are performed from planar lipid bilayer with reconstituted MCU. Accordingly, the individual contribution of MCU and other putative Ca^{2+} channels/carriers of the mitochondrial inner membrane (i.e., Letm1, RyR1, and UCP2/3 [14, 18]) to the three Ca^{2+} currents described herein remains speculative and essentially awaits further investigation.

Moreover, at the current stage, it is unclear whether or not the three distinct types of channel activities we found in the inner mitochondria membrane of HeLa cells correlate with distinct ion carrier proteins of the inner mitochondrial membrane. We also cannot exclude the possibility that during mitoplast preparation procedure certain proteins that normally reside in the outer mitochondrial membrane (e.g., VDAC [2, 23] or mitofusin-2 [1, 5, 16]) interact with the Ca^{2+} channels of the inner mitochondrial membrane and, subsequently, affect their

conductances and biophysical behavior. Hence, the different conductances observed might be either a feature of three distinct Ca^{2+} transport proteins of the inner mitochondrial membrane, or represent different conductance states of one single channel that might be influenced by interactions with proteins of the outer mitochondrial membrane. In this regard, it remains unclear whether or not *b*-MCC indeed represents an independent single-type channel or the burst current activity reflects a not fully open state of the *xl*-MCC channel.

Due to the individual sensitivities to RuR and the different conductances, it is tempting to speculate that *xl*-MCC, *b*-MCC and *i*-MCC are indeed distinct Ca^{2+} channels in one given mitochondrion. Notably, *xl*-MCC was found to be more sensitive to RuR than *i*-MCC and *b*-MCC, thus, pointing to some similarities between *i*-MCC and *b*-MCC. In spite of the huge Ca^{2+} gradient the reversal potential for all three Ca^{2+} currents was quite low, most likely indicating that free Ca^{2+} concentration into the mitochondria matrix was quite high. Importantly, we performed experiments in Na^+ free bath solution, which prevents Ca^{2+} extrusion from mitoplasts via NCX_{mito}.

In the present work, three distinct types of Ca^{2+} currents through the inner mitochondrial membrane have been described that essentially depend on transmembrane Ca^{2+} movements and are neither sensitive to inhibitors of Cl^- and K^+ channels nor susceptible to an inhibition of the PTP, Letm1 and the NCX_{mito}. Based on their individual biophysical characteristics and sensitivity to RuR, these currents are most likely established by three distinct channels/complexes, thus, challenging the view of a unique, ubiquitous mitochondrial Ca^{2+} uniporter. Applying the experimental procedures presented herein, studies on the individual contribution of the reported putative mitochondrial Ca^{2+} channel/carrier proteins to the distinct Ca^{2+} currents across the inner mitochondrial membrane appear feasible.

Acknowledgments We thank Therese Macher, Rene Rost, Ph.D., and Florian Enzinger for their excellent technical assistance. This work was supported by the Austrian Science Funds (FWF, P20181-B05 P21857-B18 and P22553-B18). C.J.-Q. is a fellow of the Doctoral College "Metabolic and Cardiovascular Disease", funded by the Austrian Science Fund (FWF W1226-B18) and the Medical University of Graz, the University of Graz and the Graz University of Technology.

References

1. Bach D, Pich S, Soriano FX, Vega N, Baumgartner B, Oriola J, Daugaard JR, Lloberas J, Camps M, Zierath JR, Rabasa-Lhoret R, Wallberg-Henriksson H, Laville M, Palacin M, Vidal H, Rivera F, Brand M, Zorzano A (2003) Mitofusin-2 determines mitochondrial network architecture and mitochondrial metabolism. A novel regulatory mechanism altered in obesity. J Biol Chem 278:17190–17197
2. Bahamonde MI, Valverde MA (2003) Voltage-dependent anion channel localises to the plasma membrane and peripheral but not perinuclear mitochondria. Pflugers Arch 446:309–313
3. Baughman JM, Perocchi F, Girgis HS, Plovanich M, Belcher-Timme CA, Sancak Y, Bao XR, Strittmatter L, Goldberger O, Bogorad RL, Koteliansky V, Mootha VK (2011) Integrative genomics identifies MCU as an essential component of the mitochondrial calcium uniporter. Nature 476:341–345
4. Bernardi P, Vassanelli S, Veronese P, Colonna R, Szabo I, Zoratti M (1992) Modulation of the mitochondrial permeability transition pore. Effect of protons and divalent cations. J Biol Chem 267:2934–2939
5. de Brito OM, Scorrano L (2008) Mitofusin 2 tethers endoplasmic reticulum to mitochondria. Nature 456:605–610
6. De Stefani D, Raffaello A, Teardo E, Szabò I, Rizzuto R (2011) A forty-kilodalton protein of the inner membrane is the mitochondrial calcium uniporter. Nature 476:336–340
7. Duchen MR (2000) Mitochondria and Ca^{2+} in cell physiology and pathophysiology. Cell Calcium 28:339–348
8. Frezza C, Cipolat S, Scorrano L (2007) Organelle isolation: functional mitochondria from mouse liver, muscle and cultured fibroblasts. Nat Protoc 2:287–295
9. Graier WF, Frieden M, Malli R (2007) Mitochondria and Ca^{2+} signaling: old guests, new functions. Pflugers Arch 455:375–396
10. Hagen T, Lagace CJ, Modica-Napolitano JS, Aprille JR (2003) Permeability transition in rat liver mitochondria is modulated by the ATP-Mg/Pi carrier. Am J Physiol 285:G274–G281
11. Jean-Quartier C, Bondarenko AI, Alam MR, Trenker M, Waldeck-Weiermair M, Malli R, Graier WF (2012) Studying mitochondrial Ca^{2+} uptake—a revisit. Mol Cell Endocrinol 353:114–127
12. Jiang D, Zhao L, Clapham DE (2009) Genome-wide RNAi screen identifies LETM1 as a mitochondrial Ca^{2+}/H^+ antiporter. Science 326:144–147
13. Kirichok Y, Krapivinsky G, Clapham DE (2004) The mitochondrial calcium uniporter is a highly selective ion channel. Nature 427:360–364
14. Malli R, Graier WF (2010) Mitochondrial Ca^{2+} channels: great unknowns with important functions. FEBS Lett 584:1942–1947
15. Mallilankaraman K, Doonan P, Cárdenas C, Chandramoorthy HC, Müller M, Miller R, Hoffman NE, Gandhirajan RK, Molgó J, Birnbaum MJ, Rothberg BS, Mak D-OD, Foskett JK, Madesh M (2012) MICU1 is an essential gatekeeper for MCU-mediated mitochondrial Ca^{2+} uptake that regulates cell survival. Cell 151:630–644
16. Merkwirth C, Langer T (2008) Mitofusin 2 builds a bridge between ER and mitochondria. Cell 135:1165–1167
17. Michels G, Khan IF, Endres-Becker J, Rottlaender D, Herzig S, Ruhparwar A, Wahlers T, Hoppe UC (2009) Regulation of the human cardiac mitochondrial Ca^{2+} uptake by 2 different voltage-gated Ca^{2+} channels. Circulation 119:2435–2443
18. Pan S, Ryu SY, Sheu SS (2011) Distinctive characteristics and functions of multiple mitochondrial Ca^{2+} influx mechanisms. Sci China Life Sci 54:763–769
19. Perocchi F, Gohil VM, Girgis HS, Bao XR, McCombs JE, Palmer AE, Mootha VK (2010) MICU1 encodes a mitochondrial EF hand protein required for Ca^{2+} uptake. Nature 467:291–296
20. Ruiz-Meana M, Garcia-Dorado D, Miró-Casas E, Abellán A, Soler-Soler J (2006) Mitochondrial Ca^{2+} uptake during simulated ischemia does not affect permeability transition pore opening upon simulated reperfusion. Cardiovasc Res 71:715–724
21. Ryu SY, Beutner G, Dirksen RT, Kinnally KW, Sheu S-S (2010) Mitochondrial ryanodine receptors and other mitochondrial Ca^{2+} permeable channels. FEBS Lett 584:1948–1955

22. Ryu SY, Beutner G, Kinnally KW, Dirksen RT, Sheu S-S (2011) Single channel characterization of the mitochondrial ryanodine receptor in heart mitoplasts. J Biol Chem 286:21324–21329
23. Shoshan-Barmatz V, Israelson A, Brdiczka D, Sheu SS (2006) The voltage-dependent anion channel (VDAC): function in intracellular signalling, cell life and cell death. Curr Pharm Des 12:2249–2270
24. Tomaskova Z, Ondrias K (2010) Mitochondrial chloride channels—what are they for? FEBS Lett 584:2085–2092
25. Trenker M, Fertschai I, Malli R, Graier WF (2008) UCP2/3—likely to be fundamental for mitochondrial Ca^{2+} uniport. Nat Cell Biol 10:1237–1240
26. Trenker M, Malli R, Fertschai I, Levak-Frank S, Graier WF (2007) Uncoupling proteins 2 and 3 are fundamental for mitochondrial Ca^{2+} uniport. Nat Cell Biol 9:445–452
27. Waldeck-Weiermair M, Duan X, Naghdi S, Khan MJ, Trenker M, Malli R, Graier WF (2010) Uncoupling protein 3 adjusts mitochondrial Ca^{2+} uptake to high and low Ca^{2+} signals. Cell Calcium 48:288–301
28. Waldeck-Weiermair M, Jean-Quartier C, Rost R, Khan MJ, Vishnu N, Bondarenko AI, Imamura H, Malli R, Graier WF (2011) The leucine zipper EF hand-containing transmembrane protein 1 (LETM1) and uncoupling proteins-2 and 3 (UCP2/3) contribute to two distinct mitochondrial Ca^{2+} uptake pathways. J Biol Chem 286:28444–28455
29. Waldeck-Weiermair M, Malli R, Naghdi S, Trenker M, Kahn MJ, Graier WF (2010) The contribution of UCP2 and UCP3 to mitochondrial Ca^{2+} uptake is differentially determined by the source of supplied Ca^{2+}. Cell Calcium 47:433–440

Signal Transduction:

Molecularly Distinct Routes of Mitochondrial Ca^{2+} Uptake Are Activated Depending on the Activity of the Sarco/Endoplasmic Reticulum Ca^{2+} ATPase (SERCA)

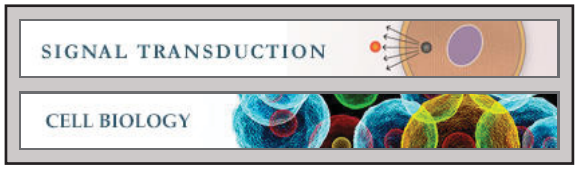

Markus Waldeck-Weiermair, András T. Deak, Lukas N. Groschner, Muhammad Rizwan Alam, Claire Jean-Quartier, Roland Malli and Wolfgang F. Graier

J. Biol. Chem. 2013, 288:15367-15379.
doi: 10.1074/jbc.M113.462259 originally published online April 16, 2013

THE JOURNAL OF BIOLOGICAL CHEMISTRY VOL. 288, NO. 21, pp. 15367–15379, may 21, 2013

Molecularly Distinct Routes of Mitochondrial Ca^{2+} Uptake Are Activated Depending on the Activity of the Sarco/Endoplasmic Reticulum Ca^{2+} ATPase (SERCA)*[S]

Received for publication, February 15, 2013, and in revised form, April 4, 2013 Published, JBC Papers in Press, April 16, 2013, DOI 10.1074/jbc.M113.462259

Markus Waldeck-Weiermair[1], András T. Deak[1,2], Lukas N. Groschner, Muhammad Rizwan Alam[3], Claire Jean-Quartier, Roland Malli, and Wolfgang F. Graier[4]

From the Institute of Molecular Biology and Biochemistry, Center of Molecular Medicine, Medical University of Graz, 8010-Graz, Austria

Background: Mitochondria may utilize different proteins to decode high and low cytosolic Ca^{2+}.
Results: Inhibition of SERCA shifts mitochondrial Ca^{2+} uptake from being UCP3-dependent to Letm1-dependent.
Conclusion: Depending on the mode of intracellular Ca^{2+} release, two different mitochondrial Ca^{2+} uptake pathways are engaged.
Significance: The dissection of two molecularly distinct mitochondrial Ca^{2+} uptake routes depending on SERCA activity points to the complexity of the mitochondrial Ca^{2+} uptake machinery.

The transfer of Ca^{2+} across the inner mitochondrial membrane is an important physiological process linked to the regulation of metabolism, signal transduction, and cell death. While the definite molecular composition of mitochondrial Ca^{2+} uptake sites remains unknown, several proteins of the inner mitochondrial membrane, that are likely to accomplish mitochondrial Ca^{2+} fluxes, have been described: the novel uncoupling proteins 2 and 3, the leucine zipper-EF-hand containing transmembrane protein 1 and the mitochondrial calcium uniporter. It is unclear whether these proteins contribute to one unique mitochondrial Ca^{2+} uptake pathway or establish distinct routes for mitochondrial Ca^{2+} sequestration. In this study, we show that a modulation of Ca^{2+} release from the endoplasmic reticulum by inhibition of the sarco/endoplasmatic reticulum ATPase modifies cytosolic Ca^{2+} signals and consequently switches mitochondrial Ca^{2+} uptake from an uncoupling protein 3- and mitochondrial calcium uniporter-dependent, but leucine zipper-EF-hand containing transmembrane protein 1-independent to a leucine zipper-EF-hand containing transmembrane protein 1- and mitochondrial calcium uniporter-mediated, but uncoupling protein 3-independent pathway. Thus, the activity of sarco/endoplasmatic reticulum ATPase is significant for the mode of mitochondrial Ca^{2+} sequestration and determines which mitochondrial proteins might actually accomplish the transfer of Ca^{2+} across the inner mitochondrial membrane. Moreover, our findings herein support the existence of distinct mitochondrial Ca^{2+} uptake routes that might be essential to ensure an efficient ion transfer into mitochondria despite heterogeneous cytosolic Ca^{2+} rises.

The ability of mitochondria to respond to cytosolic Ca^{2+} elevations is fundamental for cell signaling (1). An accumulation of Ca^{2+} within mitochondria impacts the rate of oxidative phosphorylation (2) and shapes cytosolic Ca^{2+} signals (3, 4). Notably, since excessive Ca^{2+} uptake into mitochondria alters the morphology of the organelle and triggers cell death pathways (5), a proper control of mitochondrial Ca^{2+} sequestration is essential to maintain mitochondrial and cellular homeostasis (6).

Whereas the phenomenon of mitochondrial Ca^{2+} uptake is well characterized as to be accomplished by the so-called mitochondrial Ca^{2+} uniporter, the identification of the actual protein(s) that establish mitochondrial Ca^{2+} uptake is/are still not entirely completed. Moreover, though early patch-clamp studies revealed one Ca^{2+} current in mitoplasts (7), recent reports point to the existence of several distinct mitochondrial Ca^{2+} currents across the inner mitochondrial membrane (IMM)[5] (8–10), thus, challenging the concept of one sole, ubiquitous, mitochondrial Ca^{2+} uniporter. In agreement with these findings several proteins of the IMM have been identified as putative mitochondrial Ca^{2+} carriers and/or components of mitochondrial Ca^{2+} uptake sites (6, 11). Among these molecules, a 40 kDa protein initially referred to as CCDC109A and then renamed to "mitochondrial calcium uniporter" (MCU) (12, 13) appears to be a promising candidate for a mitochondrial Ca^{2+}

* This work was supported by the Austrian Science Funds (FWF, P20181-B05, P21857-B18, and P22553-B18).
⌘ *Author's Choice*—Final version full access.
[S] This article contains supplemental Figs. S1—S3.
[1] Both authors contributed equally to this work.
[2] Funded by the FWF within the PhD program Neuroscience at the Medical University of Graz.
[3] Funded by the FWF within the PhD program MolMed of the Medical University of Graz.
[4] To whom correspondence should be addressed: Institute of Molecular Biology and Biochemistry, Molecular and Cellular Physiology Research Unit, Center of Molecular Medicine, Medical University Graz, Harrachgasse 21/III, Graz, Austria. Tel.: +43-316-380-7560; Fax: +43-316-380-9615; E-mail: wolfgang.graier@medunigraz.at.

[5] The abbreviations used are: IMM, inner mitochondrial membrane; $[Ca^{2+}]_{cyto}$, cytosolic free Ca^{2+} concentration; Letm1, leucine zipper EF hand-containing transmembrane protein 1; MCUR1, mitochondrial calcium uniporter regulator 1; MICU1, mitochondrial Ca^{2+} uptake 1; $[Ca^{2+}]_{mito}$, mitochondrial Ca^{2+} concentration; SERCA, sarco/endoplasmic reticulum Ca^{2+}-ATPase; SOCE, store-operated Ca^{2+} entry; UCP2/3, uncoupling protein 2 and 3.

channel (6). MCU, which was suggested to represent the Ca^{2+} conducting pore in the IMM, was shown to accomplish mitochondrial Ca^{2+} uptake independently from the source of Ca^{2+}. In contrast, the leucine zipper-EF-hand containing transmembrane protein 1 (Letm1), which was initially described as a K^+/H^+ exchanger in the IMM (14), was also shown to function as a mitochondrial Ca^{2+}/H^+ antiporter (15) that mainly achieved mitochondrial Ca^{2+} accumulation as a result of slow cytosolic Ca^{2+} rises, such as those induced by Ca^{2+} entry via the store-operated Ca^{2+} entry (SOCE) pathway in endothelial and HeLa cells (16). In the same cell types, however, the novel uncoupling proteins 2 and 3 (UCP2/3) were found to contribute primarily to the instant transfer of intracellularly released Ca^{2+} into mitochondria while UCP2/3 did not appear to be engaged in mitochondrial Ca^{2+} uptake upon activation of SOCE (17–19). Such distinct contribution of Letm1 and UCP2/3 to mitochondrial Ca^{2+} uptake might explain the versatility of mitochondria to decode the various patterns of the cytosolic Ca^{2+} signal (20), while the actual molecular function of these proteins remain elusive (6, 21). However, a recent study reports that inhibition of the sarco/endoplasmatic reticulum ATPase (SERCA) abrogates the contribution of UCP3 to mitochondrial Ca^{2+} uptake in HeLa cells (22). Although these findings confirm our previous report, in which mitochondrial Ca^{2+} uptake following SERCA inhibition was shown to be independent of UCP3 (23), the individual interpretation of these data are very different. On one hand, based on their measurements of cytosolic ATP, De Marchi *et al.* concluded that UCP3 is not engaged in mitochondrial Ca^{2+} uptake, but affects the transfer of Ca^{2+} into mitochondria by impacting the SERCA activity via the modulation of mitochondrial ATP generation (22). On the other hand, our group provided experimental evidence, that the contribution of UCP2/3 is independent of the organelles ATP production (17). Hence, upon SERCA inhibition mitochondrial Ca^{2+} uptake is accomplished by a CGP37157-sensitive Ca^{2+} exchanger (23). However, as the potential contribution of a mitochondrial Ca^{2+} exchanger to mitochondrial Ca^{2+} uptake under SERCA inhibition was not evaluated by De Marchi *et al.*, the controversial conclusions remain and await clarification.

Therefore, the present study was designed to solve this controversy. Thus, we employed the same cell model (HeLa cells) and evaluated the contribution of UCP3, Letm1 and MCU to mitochondrial and cytosolic Ca^{2+}signaling using a recently developed, mitochondrially targeted red-shifted Ca^{2+} sensor (24) and fura-2/am. This technique allowed us to follow simultaneously respective Ca^{2+} signals in both compartments.

EXPERIMENTAL PROCEDURES

Chemicals and Buffer Solutions—Cell culture materials were obtained from PAA laboratories (Pasching, Austria). Thapsigargin was purchased from Abcam® (London, UK), Histamine and EGTA were from Sigma (Vienna, Austria). Prior to experiments cells were washed and maintained for 20 min in a HEPES buffered solution composed of (in mM): 138 NaCl, 5 KCl, 2 $CaCl_2$, 1 $MgCl_2$, 1 HEPES, 2.6 $NaHCO_3$, 0.44 KH_2PO_4, 0.34 Na_2HPO_4, 10 D-glucose, 0.1% vitamins, 0.2% essential amino acids, and 1% penicillin/streptomycin; pH adjusted to 7.4 with NaOH. During the experiments cells were continuously perfused with a Ca^{2+} containing buffer, which consisted of (in mM): 145 NaCl, 5 KCl, 2 $CaCl_2$, 1 $MgCl_2$, 10 D-glucose, and 10 HEPES; pH adjusted to 7.4 with NaOH. In experiments where a Ca^{2+}-free solution was applied to the cells, the $CaCl_2$ was replaced with 1 mM EGTA.

siRNAs and Approval of Their Respective Knock-down Efficiency—The siRNAs against human MCU, UCP2/3 and Letm1 were obtained from Microsynth (Balgach, Switzerland) and their nucleotide sequences (5′-3′) were as follows: si1-hMCU: GCCAGAGACAGACAAUACUtt; si2-hMCU: GGAAAGGGAGCUUAUUGAAtt; si1-hLetm1: UCCACAUUUGAGACUCAGUtt; si2-hLetm1: AUGUUCCAUUUGGCUGCUGtt; si-hUCP2: GCACCGUCAAUGCCUACAAtt; si-hUCP3: GGAACUUUGCCCAACAUCAtt.

For controls, a scrambled siRNA was used: UUCUCCGAACGUGUCACGUtt. Although all siRNAs used in this study have been previously approved to exhibit reliable gene knock-down efficiency (16), their efficiency was again verified by quantitative RT-PCR in HeLa as previously described (25).

Total RNA was isolated from control and target siRNA treated HeLa cells using a RNA isolation kit (PEQLAB Biotechnologie GmbH, Erlangen, Germany). Reverse transcription was carried out using a cDNA synthesis kit from Applied Biosystems. The efficiency of siRNA was validated by performing Real time PCR using QuantiFast SYBR Green RT-PCR kit (Qiagen, Hilden, Germany) on LightCycler 480 (Roche Diagnostics, Vienna, Austria). RNA polymerase II (RPOL2) was used as housekeeping control. Primers for RPOL2, UCP2, UCP3, MCU, and LETM1 were obtained from Invitrogen (Vienna, Austria) and there sequences (5′-3′) are as follows: RPOL2 for: CATTGACTTGCGTTTCCACC, RPOL2 rev: ACATTTTGTGCAGAGTTGGC, UCP2 for: TCCTGAAAGCCAACCTCATG, UCP2 rev: GGCAGAGTTCATGTATCTCGTC, UCP3 for: AGAAAATACAGCGGGACTATGG, UCP3 rev: CTTGAGGATGTCGTAGGTCAC, MCU for: TTCCTGGCAGAATTTGGGAG, MCU rev: AGAGATAGGCTTGAGTGTGAAC, Letm1 for: TGTTCTTCAAGGCCATCTCC, Letm1 rev: TGTTGCTGTGAAGCTCTTCC. The expression data were analyzed by ΔΔCt method as described previously (25). Knockdown efficiency was in the same range than previously reported for endothelial cells (16).

Cell Culture and Transfection—HeLa cells were cultured as described previously (24). Briefly, cells were grown in Dulbeccos´s Modified Eagle Medium (Sigma, Vienna, Austria) containing 10% fetal bovine serum, 100 units/ml penicillin, and 100 μg/ml streptomycin and were plated on 30-mm glass coverslips. At 60–80% confluency, cells were transfected with 2 μg (per 30-mm well) of plasmid DNA encoding 4mtD1GO-Cam (24) alone or in combination with 100 μM siRNA using 4 μg/well TransFast™ transfection reagent (Promega, Madison, WI) in 0.5 ml of serum and antibiotic-free transfection medium. Cells were maintained in a humidified incubator (37 °C, 5% CO_2, 95% air) for 16–20 h before changing back to complete RPMI 1640 medium. All experiments were performed either 48 h or 72 h after transfection.

Simultaneous Cytosolic and Mitochondrial Ca^{2+} Measurements—4mtD1GO-Cam (24) transfected HeLa cells were loaded with 2

μM fura-2/AM (TEFLabs, Austin, TX) for 45 min prior to the experiments. Co-imaging of fura-2 and the 4mtD1GO-Cam was achieved with a digital wide field imaging system, the Till iMIC (Till Photonics Graefelfing, Germany) using a 40× objective (alpha Plan Fluar 40×, Zeiss, Göttingen, Germany). For illumination of fura-2 and the 4mtD1GO-Cam an ultra fast switching monochromator, the Polychrome V (Till Photonics) equipped with an excitation filter (E500spuv, Chroma Technology Corp., Rockingham, Vermont) and a dichroic filter (495dcxru, Chroma Technology Corp) was used. fura-2 was excited alternatively at 340 nm and 380 nm and the red-shifted mitochondrial-targeted cameleon was excited at 477 nm, respectively. Emitted light was simultaneously collected at 510 nm (fura-2 and GFP of GO-Cam) and at 560 nm (FRET-channel of GO-Cam) using a single beam splitter design (Dichrotome, Till Photonics) that was equipped with a dual band emission filter (59004m ET Fitc/Tritc Dual Emitter, Chroma Technology Corp.) and a second dichroic filter (560dcxr, Chroma Technology Corp.). Images were recorded with a charged-coupled device (CCD) camera (AVT Stringray F145B, Allied Vision Technologies, Stadtroda, Germany). For the data acquisition and the control of the digital fluorescence microscope the live acquisition software (LA) version 2.0.0.12 (Till Photonics) was used. Post-acquisition image analysis was performed on MetaMorph 7.7.0.0 (Visitron Systems, Puchheim, Germany).

Statistics—Data shown represent the mean ± S.E., where n reflects the number of cells. Statistical analyses were performed with unpaired Student's t test, and $p < 0.05$ was considered to be significant.

RESULTS

SERCA Inhibition Slows Down the IP_3-mediated Transfer of Ca^{2+} into Mitochondria—$[Ca^{2+}]_{cyto}$ and $[Ca^{2+}]_{mito}$ were simultaneously measured using Fura-2/AM-loaded cells that transiently expressed 4mtD1GO-Cam, a recently developed red shifted genetically encoded Ca^{2+} probe targeted to the mitochondrial matrix (Fig. 1*A*). This approach allowed an accurate temporal correlation of changes in $[Ca^{2+}]_{cyto}$ with $[Ca^{2+}]_{mito}$. Stimulation with the IP_3-generating agonist histamine in the absence of extracellular Ca^{2+} induced a fast increase of both cytosolic and mitochondrial Ca^{2+} levels (Fig. 1*B*, *left panel*), indicating an efficient transfer of Ca^{2+} from the endoplasmic reticulum (ER) into mitochondria. The Ca^{2+} signal in the cytosol occurred slightly faster than the respective Ca^{2+} elevation within mitochondria of same single individual cells (Fig. 1, *B*, *left panel* & *C*). Pretreating the cells with the SERCA inhibitor thapsigargin 40 s prior to the addition of histamine, enhanced the cytosolic Ca^{2+} elevation (Fig. 1, *B*, *right panel* & *C*). Notably, in the presence of thapsigargin, $[Ca^{2+}]_{cyto}$ started to increase slowly, indicating Ca^{2+} leakage from the ER. This weak thaspsigargin-induced cytosolic Ca^{2+} signal was not accompanied by a significant elevation in $[Ca^{2+}]_{mito}$ (Fig. 1*B*, *right panel*). Subsequent addition of histamine evoked a further pronounced rise of both $[Ca^{2+}]_{cyto}$ and $[Ca^{2+}]_{mito}$. However, these signals increased with a slower kinetics compared with respective Ca^{2+} elevations in the absence of the SERCA inhibitor (Fig. 1, *B* & *C*). In addition, the time gap between the histamine induced rise of $[Ca^{2+}]_{cyto}$ and the respective mitochondrial Ca^{2+} signal was considerably extended in the presence of thapsigargin (Fig. 1, *B* & *C*), indicating that SERCA inhibition decelerates the transfer of Ca^{2+} into mitochondria upon IP_3-mediated Ca^{2+} release. A correlation between changes of $[Ca^{2+}]_{cyto}$ and respective Ca^{2+} signals within mitochondria showed that in the presence of thapsigargin almost twice as much cytosolic Ca^{2+} was elevated, until mitochondrial Ca^{2+} uptake was activated (Fig. 1*D*).

These protocols that illustrate the distinct kinetics of the compartmental Ca^{2+} rises and coupling between $[Ca^{2+}]_{cyto}$ and $[Ca^{2+}]_{mito}$ were subsequently used to investigate the contribution of the individual proteins that have been proposed to be involved in mitochondrial Ca^{2+} uptake (*i.e.* UCP3, Letm1, and MCU).

SERCA Inhibition Switches Mitochondrial Ca^{2+} Uptake from a UCP3-dependent into a Letm1-dependent Mode—We speculated that the SERCA-dependent differences in the kinetics of mitochondrial Ca^{2+} signals probably reflect the involvement of distinct mitochondrial Ca^{2+} uptake routes. Therefore, we performed experiments, in which the contribution of the mitochondrial proteins UCP2/3, Letm1 and MCU to mitochondrial Ca^{2+} uptake in various protocols was investigated by diminution of these proteins with a transient transfection of the respective siRNA. The siRNAs against UCP2/3, Letm1, and MCU have already been validated to specifically and significantly reduce mRNA level of the respective proteins (16).

In line with previous studies (17, 18, 22), a transient knock-down of UCP3 significantly reduced the histamine-induced mitochondrial Ca^{2+} signal, while the respective cytosolic Ca^{2+} elevation was only minimally affected (Fig. 2, *A*, *left panel* & *B*). As recently demonstrated (22), SERCA inhibition with thapsigargin, which was added shortly before histamine, abolished the effect of UCP3 knock-down on $[Ca^{2+}]_{mito}$ (Fig. 2, *A*, *right panel* & *B*).

Next we performed analogous experiments with cells, in which Letm1 was silenced (Fig. 2, *C* & *D*). Mitochondrial Ca^{2+} sequestration upon IP_3-mediated Ca^{2+} mobilization in the absence of thapsigargin was not affected in cells that were treated with siRNA against Letm1 (Fig. 2, *C*, *left panel* & *D*). In contrast, if SERCA activity prior to the addition of the agonist was blocked, diminution of Letm1 strongly reduced the histamine-induced mitochondrial Ca^{2+} signal (Fig. 2, *C*, *right panel* & *D*). Notably, the siRNA-mediated knock-down of UCP2/3, Letm1, and MCU neither affected the mitochondrial membrane potential (supplemental Fig. S1), nor the capacity of mitochondria to extrude Ca^{2+} (supplemental Fig. S2). These data indicate that SERCA inhibition switches the mode of mitochondrial Ca^{2+} uptake from a Letm1-independent to a Letm1-dependent one and, hence, explain the lacking contribution of UCP2/3 to mitochondrial Ca^{2+} uptake under conditions of SERCA inhibition.

MCU Contributes to Mitochondrial Ca^{2+} Uptake Independently from SERCA Activity and, Hence, the Mode of Ca^{2+} Mobilization—To investigate the participation of MCU in the transfer of intracellularly released Ca^{2+} into mitochondria, respective experiments were performed with MCU-depleted cells. The knock-down of MCU negligibly altered cytosolic Ca^{2+} signals in response to cell stimulation (Fig. 3*A* & Fig. 5*B*).

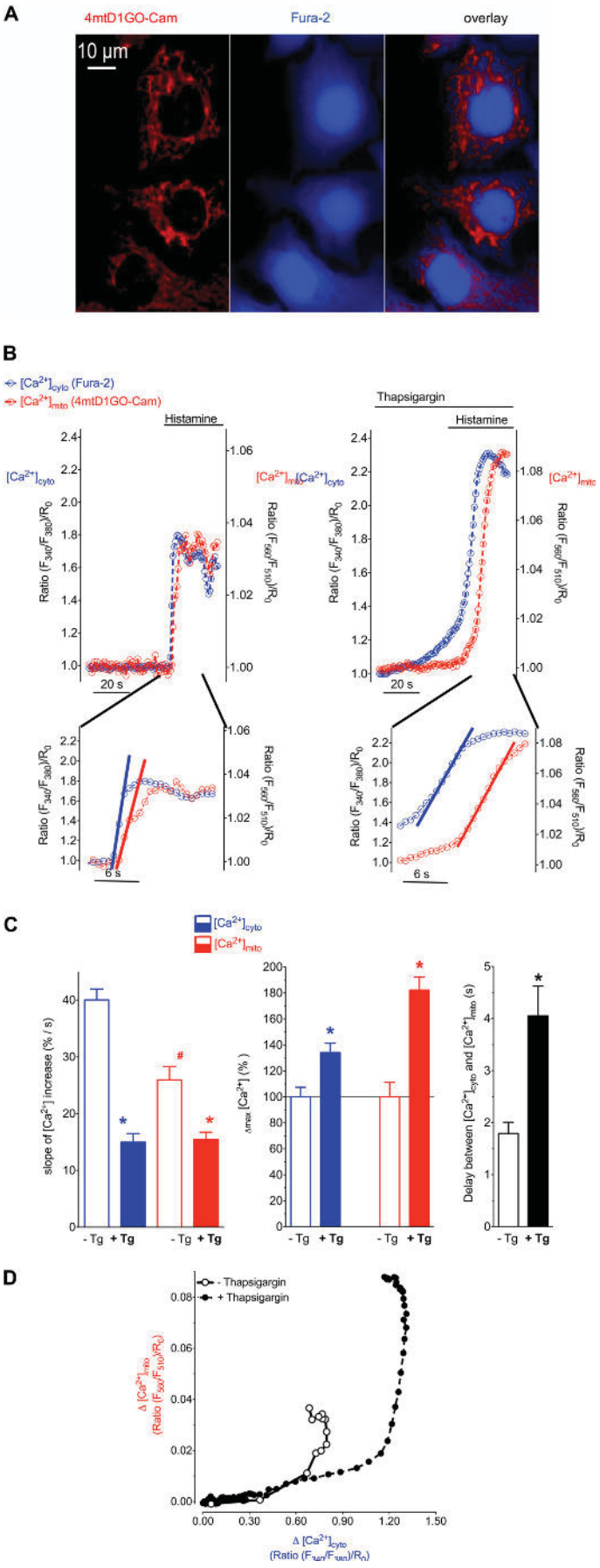

However, respective mitochondrial Ca^{2+} signals were strongly diminished in cells depleted of MCU (Fig. 3, *A* & *B*). Notably, the inhibitory effect of MCU knock-down on mitochondrial Ca^{2+} accumulation was independent of the absence or presence of thapsigargin (Fig. 3), indicating that MCU facilitates mitochondrial Ca^{2+} uptake independently of SERCA activity and, hence, the mode of Ca^{2+} mobilization.

A simultaneous knock-down of either MCU and UCP2/3 or MCU and Letm1 did not further reduce mitochondrial Ca^{2+} uptake under the various conditions (Fig. 3, *C* and *D* & supplemental Fig. S3), thus, pointing to a functional interaction between these putative contributors of mitochondrial Ca^{2+} uptake.

SERCA Inhibition Following IP_3-mediated Ca^{2+} Release Increases SOCE and Also Abrogates the Contribution of UCP2/3 to MCU-mediated Mitochondrial Ca^{2+} Uptake, While Letm1 Gets Involved—SERCA inhibition prior to cell stimulation with histamine partially emptied the internal Ca^{2+} store that results in a decelerated, but higher cytosolic Ca^{2+} signal and a greater delay of the Ca^{2+} transfer into the mitochondria (Fig. 1*B*, *right panel*) suggesting a shift in the mode/route of mitochondrial Ca^{2+} uptake.

To test whether or not this change in mitochondrial Ca^{2+} uptake mode/route also occurs under condition in which the cell is already stimulated by an IP_3-generating agonist, we performed different experimental protocols, in which thapsigargin was added after histamine. If cells were continuously exposed to the IP_3 generating agonist in the absence of extracellular Ca^{2+}, the subsequent SERCA inhibition transiently elevated $[Ca^{2+}]_{cyto}$ (Fig. 4*A*). This transient thapsigargin-induced increase of cytsolic Ca^{2+} levels evoked only small changes of $[Ca^{2+}]_{mito}$. In contrast, SERCA inhibition following IP_3-mediated Ca^{2+} release in the presence of extracellular Ca^{2+}-induced prominent, longer-lasting elevations of both $[Ca^{2+}]_{cyto}$ and $[Ca^{2+}]_{mito}$ (Fig. 4*B*), thus, highlighting the involvement of SOCE that promotes mitochondrial Ca^{2+} accumulation. The latter protocol was further used to test the contribution of UCP3, Letm1, and MCU to mitochondrial Ca^{2+} sequestration under these conditions of Ca^{2+} mobilization.

Consistent with our previous work and the experiments in the absence of extracellular Ca^{2+} (Fig. 2, *B* and *D*) cells depleted of UCP3 showed greatly reduced mitochondrial Ca^{2+} accumulation in response to histamine (Fig. 5*A*). The subsequent addition of thapsigargin evoked a substantial rise of $[Ca^{2+}]_{mito}$ that was not affected by the diminution of UCP3.

In contrast, knock-down of Letm1 negligibly influenced mitochondrial Ca^{2+} uptake that was elicited by histamine, whereas $[Ca^{2+}]_{mito}$ was significantly reduced in response to a subsequent SERCA inhibition (Fig. 5*A*). These findings demonstrated that in protocols in which SERCA was blocked after the initiation of IP_3-mediated Ca^{2+} release, mitochondrial Ca^{2+} uptake also switched from an UCP3-reliant to a Letm1-dependent mode.

Consistent with previous experiments, cells that were treated with siRNA against MCU showed attenuated mitochondrial Ca^{2+} signals in response to histamine and to the subsequent addition of thapsigargin (Fig. 5*A*). Notably, the initial cytosolic Ca^{2+} peak and the thapsigargin induced rise remained unaffected under all conditions (Fig. 5*B*).

DISCUSSION

Our present data reveal that IP_3-mediated, rapid Ca^{2+} rises, that are associated with the generation of high Ca^{2+} microdomains at the surface of mitochondria (26) were transferred into these organelles via an UCP3- and MCU-dependent but Letm1-independent pathway (Fig. 6*A*). However, if the mode of Ca^{2+} mobilization was decelerated by SERCA inhibition, which increased ER Ca^{2+} leakage and, thus, probably attenuated the inter-organelle Ca^{2+} micro-domains, mitochondria slowly accumulated Ca^{2+} via an UCP3-independent, but Letm1- and MCU-reliant route (Fig. 6*B*).

Basically, our current findings indicate that a modification of the IP_3-mediated Ca^{2+} release by SERCA inhibition significantly alters the molecular characteristics of mitochondrial Ca^{2+} uptake. At first glance, these findings are not surprising, considering the central role of ER Ca^{2+} pumps in the control of the cellular Ca^{2+} homeostasis (27, 28). Virtually, in all cells, SERCA activity is necessary to maintain high Ca^{2+} levels within the ER by counteracting Ca^{2+} leakage and to restore Ca^{2+} upon events of ER Ca^{2+} release (29, 30). In line with these reports, our measurements show that a combination of the SERCA inhibitor with the IP_3-generating agonist boosts the total increases in global cytosolic and mitochondrial Ca^{2+} signals, thus, further supporting the hypothesis that during IP_3-mediated ER depletion, SERCA activity counteracts cytosolic Ca^{2+} rises under control conditions (31).

One possible explanation for this obvious switch in the mode of mitochondrial Ca^{2+} uptake is an attenuation of high Ca^{2+} micro-domains in the inter-organelle gap between the ER and mitochondria upon inhibition of SERCA. High Ca^{2+} micro-

FIGURE 1. **SERCA inhibition prior to IP_3-mediated Ca^{2+} release impacts the kinetics of Ca^{2+} signals and coupling between $[Ca^{2+}]_{cyto}$ and $[Ca^{2+}]_{mito}$.** *A*, HeLa cells expressing the mitochondrial Ca^{2+} sensor 4mtD1GO-Cam (*red*) were loaded with fura-2/AM (*blue*). Images were taken with a fully automated fluorescence microscope using a camera binning of 4. *B*, *upper panels:* representative traces of cytosolic (*blue curves*) and mitochondrial (*red curves*) Ca^{2+} signals in HeLa cells upon stimulation with 100 μM histamine in the absence of Ca^{2+} (*left upper panel*). SERCA inhibition was achieved by using 1 μM thapsigargin that was added 40 s prior to cell treatment with histamine (*right upper panel*). Data are expressed as normalized ratios: $(F_{340}/F_{380})/R_0$ for $[Ca^{2+}]_{cyto}$ and $(F_{560}/F_{510})/R_0$ for$[Ca^{2+}]_{mito}$. R_0 was calculated from basal ratio values for each individual cell respectively. *Lower panels:* zoom-in of *upper panels* showing which part was used for calculating the slope of Ca^{2+} increase. Following onset, each curve was fitted with linear regression (*bold lines*) to assess maximal slope of cytosolic and mitochondrial $[Ca^{2+}]$ elevations. *C*, statistical evaluation of the Ca^{2+} signals presented in *panel B*. *Left panel:* columns represent the maximal slopes of $[Ca^{2+}]_{cyto}$ (*blue columns*) and $[Ca^{2+}]_{mito}$ (*red columns*) increases upon histamine stimulation in the absence (*white columns*, $n = 18$) or presence of thapsigargin pretreatment (*filled columns*, $n = 15$). *Middle panel:* columns represent the average of maximum delta ratios in the absence (*white columns*) or prescence of thapsigargin preincubation (*filled columns*). Cytosolic and mitochondrial $[Ca^{2+}]$ elevation in response to cell treatment with 100 μM histamine was defined as 100%, respectively (*B*, *left panel*). *Right panel:* lag times in seconds between cytosolic and respective mitochondrial Ca^{2+} rises in the absence of thapsigargin (*white column*, $n = 18$) and upon pretreatment with thapsigargin (*black column*, $n = 15$). *, $p < 0.05$ *versus* in the absence of thapsigargin (−Tg), #, $p < 0.05$ *versus* $[Ca^{2+}]_{cyto}$ in the absence of thapsigargin (−Tg). *D*, representative temporal correlations between histamine-induced (100 μM) changes of $[Ca^{2+}]_{cyto}$ (*x* axis) and $[Ca^{2+}]_{mito}$ (*y* axis) in the absence of thapsigargin (continuous line with *open circles*) and upon pretreatment with the SERCA inhibitor (*dotted line with filled circles*).

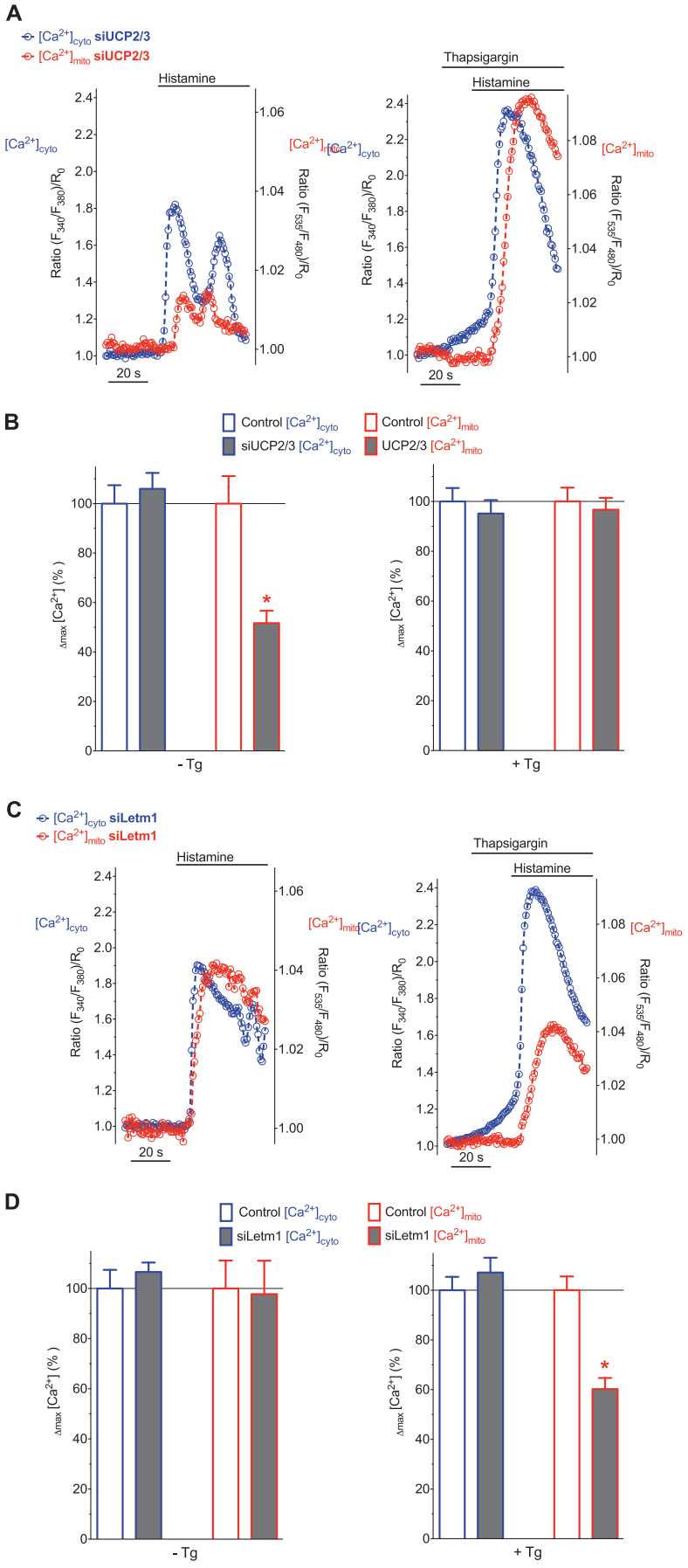

domains at ER-mitochondria contact sites were supposed to be fundamental for the activation of the low Ca^{2+} sensitive mitochondrial Ca^{2+} uniport upon IP_3-mediated ER Ca^{2+} release (32–34). In sophisticated studies the existence of such high Ca^{2+} micro-domains, also referred to as Ca^{2+} hot spots, on sites of mitochondrial Ca^{2+} uptake has been recently demonstrated (26, 35). Although we did not measure local Ca^{2+} hot spots, based on the clear effects of the SERCA activity on global cytosolic Ca^{2+} signals we reported herein, it is likely that an acute deactivation of ER Ca^{2+} pumps prior to or during the activation of the IP_3-mediated pathway also considerably impedes the formation of such local Ca^{2+} domains. In agreement with this assumption, our data demonstrate that a loss of SERCA activity in HeLa cells instantly increases a leak of Ca^{2+} from the ER resulting in a slow and moderate cytosolic Ca^{2+} elevation that is accompanied with a tiny but measurable increase in $[Ca^{2+}]_{mito}$. Due to the slightly lower Ca^{2+} affinity of the cameleon probe used for measuring $[Ca^{2+}]_{mito}$ (1.53 μM, (24)) than that of fura-2 (224 nM, (36)), the mitochondrial Ca^{2+} elevation upon thapsigargin might be underestimated. However, these data clearly show that despite the massive and pronounced ER depletion and its associated slow, but considerable cytosolic Ca^{2+} elevation, mitochondrial Ca^{2+} elevation remains small. Accordingly, the ER Ca^{2+} leakage might be locally facilitated by neighboring mitochondria that sequester and buffer the leaked Ca^{2+} from the inter-organelle gap and, thus, maintain the great Ca^{2+} gradient. Consequently, such phenomenon might result in an accelerated local ER Ca^{2+} depletion in ER regions that are in the vicinity of mitochondria. Such scenario would explain the decelerated cytosolic Ca^{2+} rise in response to IP_3-mediated Ca^{2+} mobilization upon the short preincubation with a SERCA inhibitor. Under such conditions, the IP_3-triggered formation of inter-organelle Ca^{2+} hot spots is hampered, thus, a mitochondrial Ca^{2+} carrier such as UCP3 that, might require high Ca^{2+} domains to be activated due to its low Ca^{2+} sensitivity (19) is inactive.

In addition, the increased Ca^{2+} leak from the ER upon SERCA inhibition might *per se* impact the transfer of Ca^{2+} into mitochondria. Such a scenario is feasible, as it was shown that an increased ER Ca^{2+} leakage in cells expressing an inactive truncated version of SERCA1 inhibited mitochondrial movements and increased ER-mitochondria contact sites, which consequently led to mitochondrial Ca^{2+} overload (37). However, our data showed that the thapsigargin induced Ca^{2+} leak in HeLa cells is only slowly and moderately transferred into mitochondria. Nevertheless, the increased Ca^{2+} leak upon SERCA inhibition might indeed affect the local organization and architecture of ER-mitochondria contact sites and, thus, the mode of mitochondrial Ca^{2+} uptake (38–41). Notably, using genetically encoded linker proteins that allowed a definite tethering of the ER to mitochondria indicated that the distance of the gap between both organelles is determent for the ability of mitochondria to sense Ca^{2+} hot spots upon ER Ca^{2+} release (42).

Irrespective of high local Ca^{2+} signals at inter-organelle junctions between mitochondria and the ER, mitochondria have been shown to accomplish also the uptake of smooth, moderate cytosolic Ca^{2+} elevations (18, 32–34). The coexistence of both rapid mitochondrial uptake of high Ca^{2+} microdomains and mitochondrial Ca^{2+} sequestration of global slow rising Ca^{2+} signals is consistent with our data presented in this study. Moreover, our findings highlight a clear delay between cytosolic and respective mitochondrial Ca^{2+} signals, particularly if the IP_3-mediated cytosolic Ca^{2+} elevation was decelerated by SERCA inhibition. Accordingly, we assumed that the slow and delayed mitochondrial Ca^{2+} accumulation in the presence of the SERCA inhibitor exhibits a specific mode of Ca^{2+} transfer across the IMM, which is distinct from mitochondrial Ca^{2+} uptake during fast IP_3-mediated ER Ca^{2+} release. This "slow" presumably highly sensitive type of mitochondrial Ca^{2+} accumulation in the presence of thapsigargin might be comparable with mitochondrial uptake of Ca^{2+} entering the cell via the SOCE pathway (19). Notably, it was shown that mitochondria in HeLa cells are not exposed to Ca^{2+} hot spots in response to SOCE (26). These findings are also consistent with our previous study using endothelial cells, which showed a diffusion dependent and, hence, slow mode of mitochondrial Ca^{2+} sequestration if Ca^{2+} was mobilized via the SOCE pathway (18). In this endothelial cell model we unveiled that the slow mode of mitochondrial Ca^{2+} sequestration upon SOCE especially requires Letm1, while UCP2/3 contributed exclusively to fast mitochondrial uptake of Ca^{2+} that was mobilized via the IP_3 pathway (16). These findings are in line with the observed switch of mitochondrial Ca^{2+} uptake from an UCP3-dependent to a Letm1-dependent mode upon SERCA inhibition in HeLa cells, we reported herein.

Letm1 as well as UCP2/3 were described to accomplish the transfer of Ca^{2+} into mitochondria, while their functioning and contribution to mitochondrial Ca^{2+} uptake is debated (6, 11, 21, 43, 44). Despite strong functional data, the concerns against the idea that Letm1 and UCP2/3 indeed accomplish a transfer of Ca^{2+} across the IMM, are primarily based on the postulation of a unique, ubiquitous Ca^{2+} uniporter being a low sensitive Ca^{2+} channel protein that is activated exclusively by high Ca^{2+}

FIGURE 2. **Depending on the SERCA activity either UCP2/3 or Letm1 contribute to mitochondrial Ca^{2+} uptake.** *A*, representative recordings of $[Ca^{2+}]_{cyto}$ (*blue*) and $[Ca^{2+}]_{mito}$ (*red*) in single individual HeLa cells transfected with siRNAs against UCP2/3. Cells were treated with 100 μM histamine alone (*left panel*) or together with 1 μM thapsigargin (*right panel*). *B*, column statistics of histamine-evoked cytosolic (*blue-bordered columns*) and mitochondrial (*red-bordered columns*) Ca^{2+} signals in HeLa cells transfected either with scrambled siRNA (control, *white columns*) or with siRNA against UCP2/3 (UCP2/3, *gray columns*). Experiments were performed in the absence (*left panel*, $n = 18$ for control and $n = 19$ for siUCP2/3) or in the presence of 1 μM thapsigargin pretreatment (*right panel*, $n = 15$ for control and $n = 17$ for siUCP2/3). The delta maximum of normalized cytosolic and mitochondrial Ca^{2+} signals were defined as 100% under control conditions (*i.e.* cells transfected with scrambled siRNA as shown in Fig. 1*C*) both in the absence (*left panel*) and presence (*right panel*) of thapsigargin, *, $p < 0.05$ *versus* Control $[Ca^{2+}]_{mito}$ *C*, simultaneous, representative recordings of $[Ca^{2+}]_{cyto}$ (*blue*) and $[Ca^{2+}]_{mito}$ (*red*) in HeLa cells transfected with siRNA against Letm1. Ca^{2+} signals were evoked with 100 μM histamine in the absence (*left panel*) or presence (*right panel*) of 1 μM thapsigargin. *D*, column statistics of cytosolic and mitochondrial Ca^{2+} signals in HeLa cells transfected with siRNA against Letm1 (*gray columns*) without thapsigargin (*left panel*, $n = 19$) and upon pretreatment with thapsigargin (*right panel*, $n = 17$). *White columns* represent control conditions as indicated in *panel B*. *, $p < 0.05$ *versus* Control $[Ca^{2+}]_{mito}$.

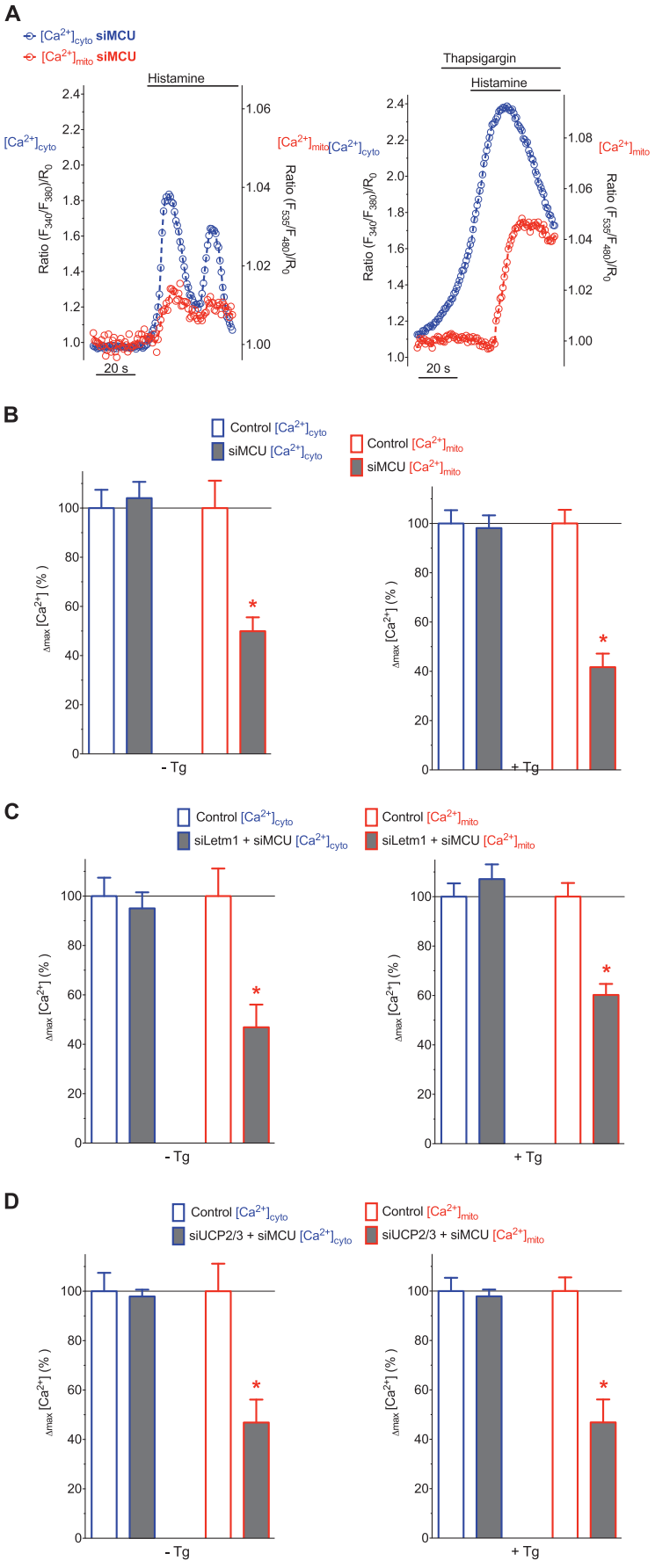

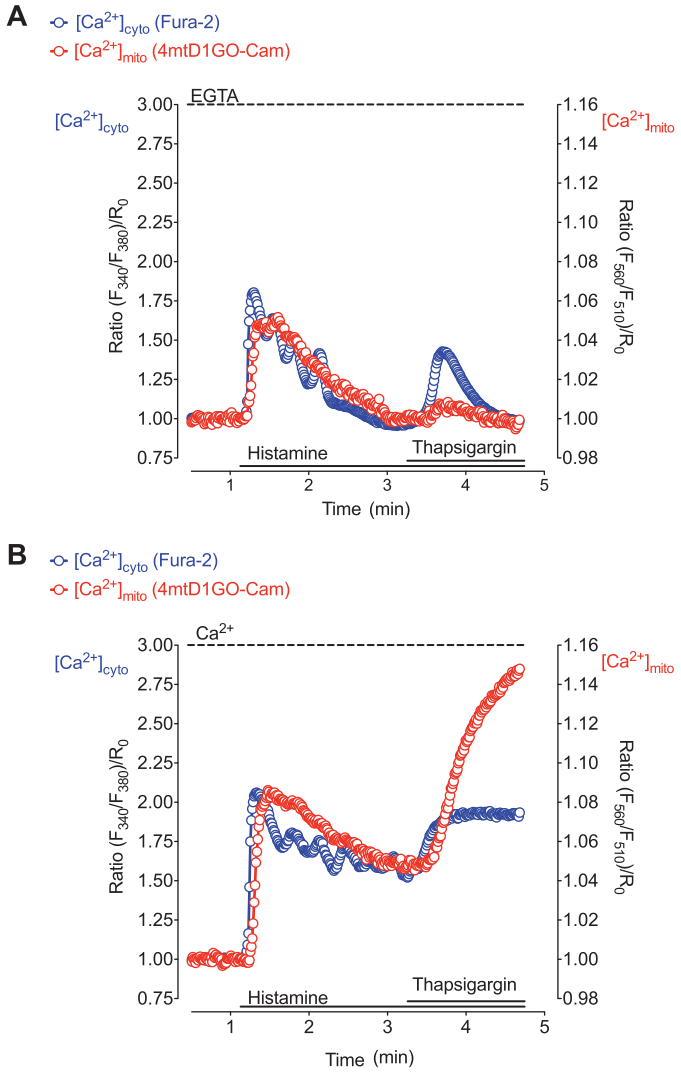

FIGURE 4. **SERCA inhibition during cell stimulation with an IP_3-generating agonist enhances $[Ca^{2+}]_{cyto}$ and $[Ca^{2+}]_{mito}$.** Representative curves demonstrating simultaneous measurement of $[Ca^{2+}]_{cyto}$ (*blue*) and $[Ca^{2+}]_{mito}$ (*red*) in HeLa cells loaded with fura-2/AM and transiently transfected with 4mtD1GO-Cam. *A*, cells were treated with 100 μM histamine for 2 min before the addition of 1 μM thapsigargin in the absence of extracellular Ca^{2+}. *B*, cells were treated with 100 μM histamine for 2 min before the addition of 1 μM thapsigargin in the presence of 2 mM Ca^{2+} in the extracellular medium.

signals. A recently identified protein of the IMM, referred to as MCU, was shown to fulfill some of the criteria that have been expected for a protein that accomplishes mitochondrial Ca^{2+} uniport (12, 13). In agreement with these landmark publications, siRNA-mediated knock-down of MCU attenuated mitochondrial Ca^{2+} signals independently from the mode of Ca^{2+} mobilization in the present study. These observations indicate that MCU is activated over a large range of Ca^{2+} concentration and, hence, contributes to mitochondrial uptake of high and low cellular Ca^{2+} signals, which is, however, in disagreement with the low Ca^{2+} sensitivity of the mitochondrial Ca^{2+} uniport phenomenon (45, 46).

Notably, in several reports elimination of the mitochondrial Ca^{2+} buffering increases cytosolic Ca^{2+} peak and accelerates its decline (13, 47, 48). However, our findings are in agreement with other reports using the same cell type (HeLa) (17, 49, 50) where inhibition of mitochondrial Ca^{2+} uptake failed or only slightly affected cytosolic Ca^{2+} elevation upon stimulation, while the kinetics of decline remained unchanged. Accordingly, these data may indicate that in the cell type used herein, mitochondria have a rather low Ca^{2+} buffer capacity and do not accumulate large proportions of released Ca^{2+}, thus, resulting in the lack of strong changes in cytosolic Ca^{2+} signaling by MCU knock-down.

The contribution of the MCU, to mitochondrial Ca^{2+} uptake was shown to be tightly regulated by an associated protein, referred to as mitochondrial calcium uptake 1 (MICU1) (51) that, in contrast to MCU, has Ca^{2+} binding domains. Initially, it was reported that MICU1 facilitates MCU-dependent mitochondrial Ca^{2+} uptake in HeLa (51) and clonal pancreatic beta-cells (25) but not endothelial cells (16). However, in a very recent study a contrary function of MICU1 in HeLa and endothelial cells acting as a gatekeeper and, thus, preventing MCU-dependent mitochondrial Ca^{2+} loads was unveiled (52), thus, indicating that further studies are necessary to understand the definite role of MICU1 in the control of mitochondrial Ca^{2+} uptake. Nevertheless, the intricate regulation of the MCU activity by MICU1 and other associated proteins such as the recently identified mitochondrial calcium uniporter regulator 1 (MCUR1) (53) might explain why the MCU catalyzes mitochondrial Ca^{2+} uptake of both high and low Ca^{2+} signals. From this point of view our data might also indicate that depending on the SERCA activity either UCP2/3 or Letm1 contribute to mitochondrial Ca^{2+} uptake by modulating the activity of MICU1, MCUR1, and/or the MCU. This assumption is further supported by our observation that a double knock-down of either MCU and UCP2/3 or MCU and Letm1 did not further impact mitochondrial Ca^{2+} accumulation. The lack of any further reduction of mitochondrial Ca^{2+} uptake in MCU depleted cells by an additional knock-down of either UCP2/3 or Letm1 also suggest that these proteins might function as upstream regulators of the MCU. However, whether or not the remaining uptake under such conditions indicates a so far unknown additional mitochondrial Ca^{2+} carrier or is due

FIGURE 3. **Transient knock-down of MCU results in a diminished mitochondrial Ca^{2+} uptake independently from SERCA activity.** *A*, representative curves of $[Ca^{2+}]_{cyto}$ (*blue*) and $[Ca^{2+}]_{mito}$ (*red*) in HeLa cells transfected with siRNA against MCU that were treated with 100 μM histamine in the absence of thapsigargin (*left panel*) and upon pretreatment with the SERCA inhibitor (*right panel*). *B*, column statistics of cytosolic (*blue border columns*) and mitochondrial Ca^{2+} (*red-bordered columns*) signals in control HeLa cells (*white columns*) and cells transfected with siRNA against MCU (*gray columns*) without thapsigargin (*left panel*, $n = 24$) and upon pretreatment with thapsigargin (*right panel*, $n = 14$). *White columns* represent control conditions (defined as 100%) as indicated in Fig. 2. *, $p < 0.05$ *versus* Control $[Ca^{2+}]_{mito}$. *C*, HeLa cells transfected with siRNA against Letm1 and MCU were stimulated with histamine in the absence (*left panel*, $n = 18$) and presence (*right panel*, $n = 14$) of thapsigargin in experimental conditions indicated in *panel A*. *D*, HeLa cells transfected with siRNA against UCP2/3 and MCU were stimulated with histamine in the absence (*left panel*, $n = 27$) and presence (*right panel*, $n = 14$) of thapsigargin in experimental conditions indicated in *panel A*.

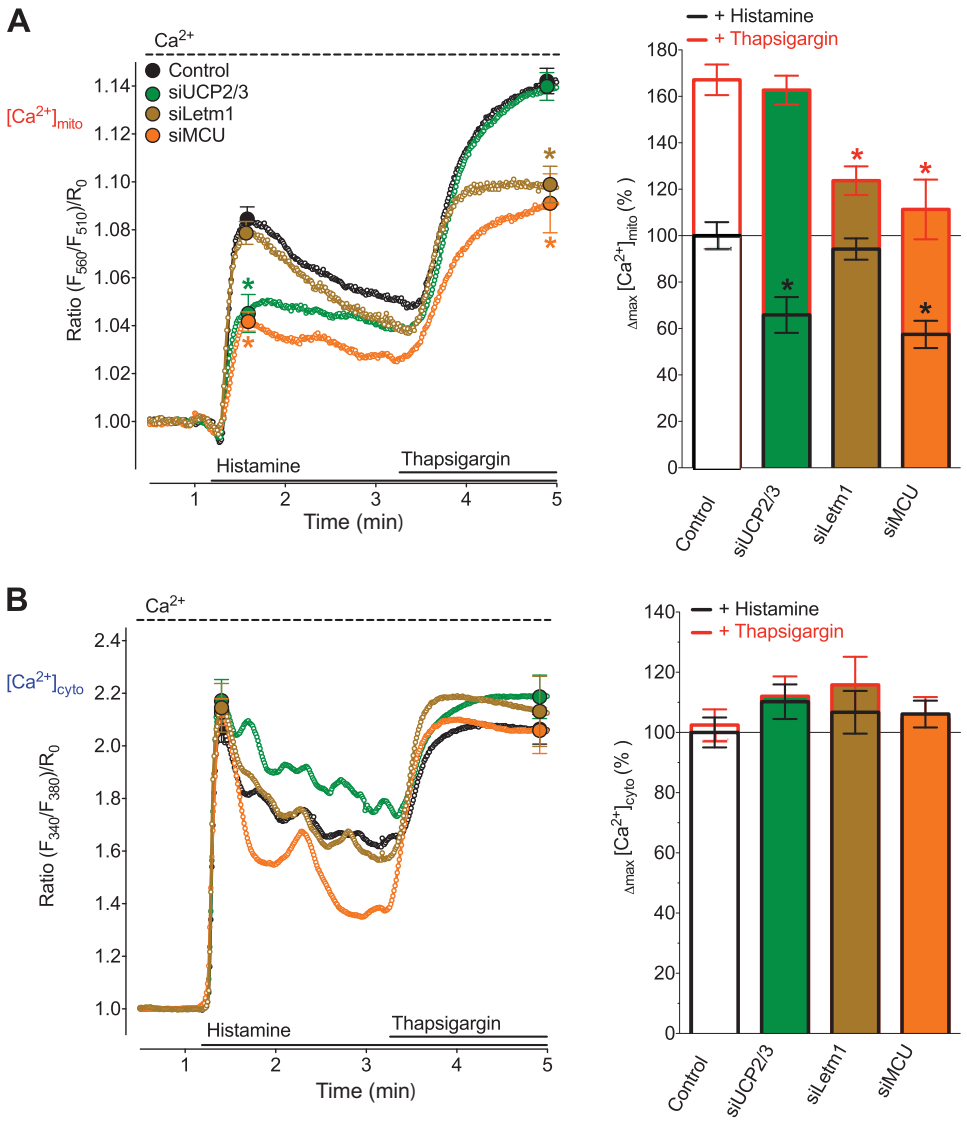

FIGURE 5. **SERCA inhibition during cell stimulation with histamine switches mitochondrial Ca^{2+} uptake from being UCP2/3 and MCU dependent to an UCP2/3 independent, but Letm1 and MCU-dependent mode.** HeLa cells were either transfected with an inoperative Control siRNA (*black curves* and *white columns*, $n = 18$), or siRNAs against UCP2 and UCP3 (*green curves* and *green columns*, $n = 18$), or Letm1 (*brown curves* and *brown columns*, $n = 20$) or MCU (*orange curves* and *orange columns*, $n = 19$). *A*, average curves (*left panel*) and statistical data (*right panel*) of $[Ca^{2+}]_{mito}$ signals measured with 4mtD1GO-Cam upon cell treatment with 100 μM histamine and the subsequent addition of 1 μM thapsigargin in the presence of 2 mM Ca^{2+}. *, $p < 0.05$ *versus* respective Controls (*B*). Respective cytosolic Ca^{2+} curves (*left panel*) and statistical analysis of Δmax $[Ca^{2+}]_{cyto}$ values (*right panel*) from Fura-2 signals of HeLa cells that were treated as indicated in Fig. 1*A*.

to incomplete diminution of the proteins by the siRNA remains unclear.

The findings that SERCA inhibition abrogates the contribution of UCP3 to mitochondrial Ca^{2+} uptake in HeLa cells was recently interpreted as an indication that UCP3 do not accomplish mitochondrial Ca^{2+} uniport or directly modulate a mitochondrial Ca^{2+} channel (22). The authors suggested that UCP3 reduces SERCA activity by limiting mitochondrial ATP generation, which increases the amount of Ca^{2+} at sites of mitochondrial Ca^{2+} uptake. However such interpretation is in contradiction to the reported lack of uncoupling activity of UCP2/3 (54), findings that overexpression of UCP2/3 boosts mitochondrial ATP generation upon Ca^{2+} mobilization and UCP2/3 contributed to mitochondrial Ca^{2+} uptake also under conditions in which mitochondrial ATP production was prevented (17).This is further supported by the observation that silencing of UCP2/3 failed to hyperpolarize mitochondrial membrane potential (supplemental Fig. S1) However, the present findings confirm the assumption of Demaurex's group and demonstrate that SERCA activity affects mitochondrial Ca^{2+} uptake.

Overall the present study demonstrates that the inhibition of SERCA affects the kinetics of IP_3-triggered intracellular Ca^{2+} release, and, subsequently, shifts the mode of mitochondrial Ca^{2+} uptake from an UCP3- and MCU-dependent and Letm1-independent toward a Letm1- and MCU-dependent but UCP3-independent route (Fig. 6). These observations indicate that SERCA activity is a crucial determinant for the mode of mitochondrial Ca^{2+} uptake and appoints which proteins of the IMM actually contribute to the transfer of Ca^{2+} into mitochondria.

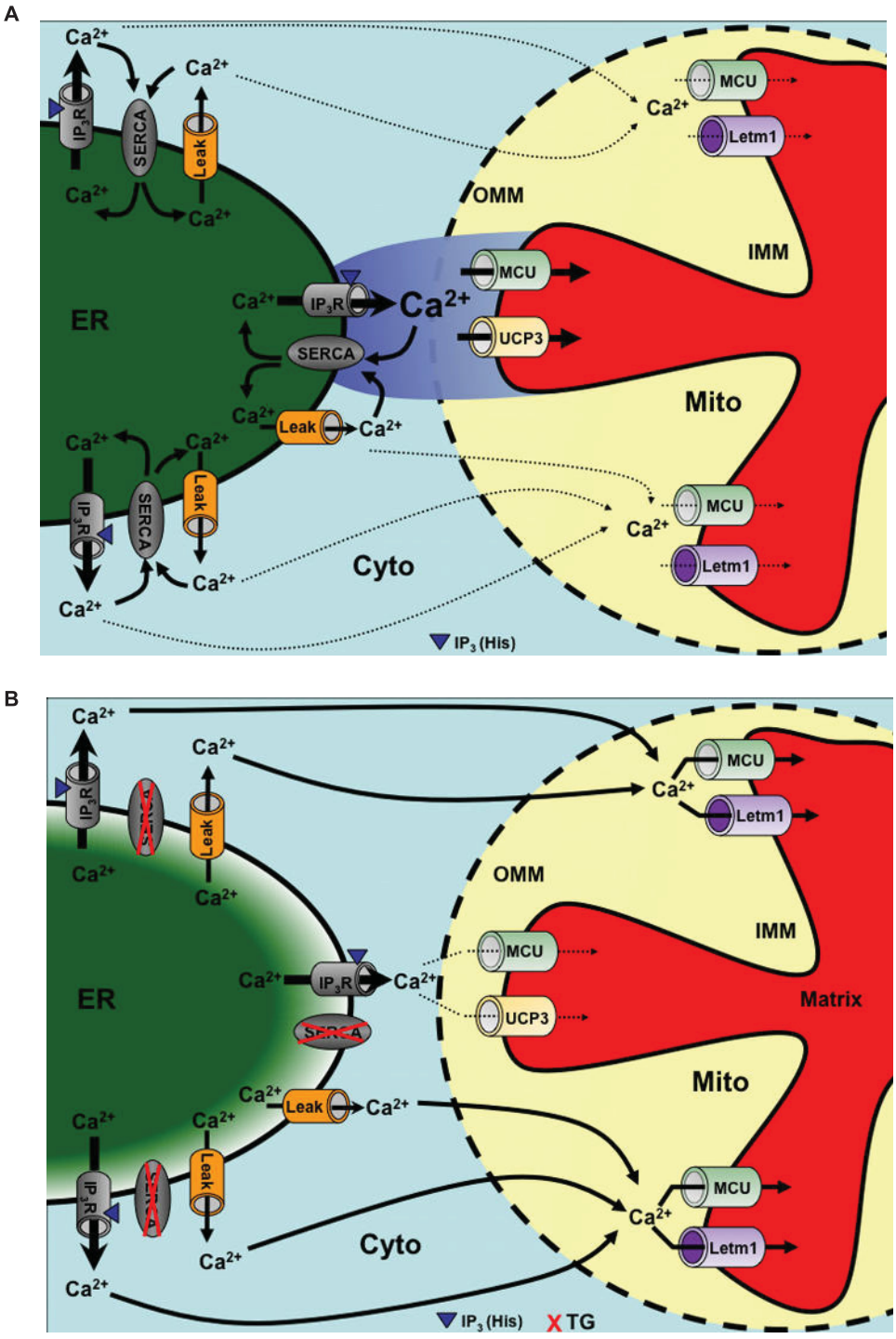

FIGURE 6. **Schematic illustration of a hypothetical switch of mitochondrial Ca^{2+} uptake by SERCA inhibition upon IP_3-mediated Ca^{2+} release.** *A*, SERCA activity counteracting ER Ca^{2+} leakage and recycling Ca^{2+} into the ER supports the generation of high Ca^{2+} micro-domains upon IP_3-mediated ER Ca^{2+} release. Under these conditions Ca^{2+} hot spots at close sites of mitochondrial Ca^{2+} uptake are sensed by UCP2/3 and MCU, which accomplish the transfer of Ca^{2+} across the IMM. *B*, impaired SERCA activity yields partial ER Ca^{2+} depletion counteracting the generation of high Ca^{2+} micro-domains at mitochondrial contact sites. Under these conditions the global slow cytosolic Ca^{2+} elevation is partially transferred into mitochondria by Letm1 and MCU. *Arrows* indicate Ca^{2+} fluxes.

Acknowledgments—We thank Sandra Blass, Therese Macher, Florian Enzinger, and Dr. Rene Rost for excellent technical assistance.

REFERENCES

1. Duchen, M. R. (2000) Mitochondria and Ca^{2+} in cell physiology and pathophysiology. *Cell Calcium* **28,** 339–348
2. Jouaville, L. S., Pinton, P., Bastianutto, C., Rutter, G. A., and Rizzuto, R. (1999) Regulation of mitochondrial ATP synthesis by calcium: evidence for a long-term metabolic priming. *Proc. Natl. Acad. Sci. U.S.A.* **96,** 13807–13812
3. Szabadkai, G., Simoni, A. M., Bianchi, K., De Stefani, D., Leo, S., Wieckowski, M. R., and Rizzuto, R. (2006) Mitochondrial dynamics and Ca^{2+} signaling. *Biochim. Biophys. Acta* **1763,** 442–449
4. Graier, W. F., Frieden, M., and Malli, R. (2007) Mitochondria and Ca^{2+}

signaling: old guests, new functions. *Pflugers Arch.* **455,** 375–396
5. Rimessi, A., Giorgi, C., Pinton, P., and Rizzuto, R. (2008) The versatility of mitochondrial calcium signals: From stimulation of cell metabolism to induction of cell death. *Biochim. Biophys. Acta* **1777,** 808–816
6. Pizzo, P., Drago, I., Filadi, R., and Pozzan, T. (2012) Mitochondrial Ca^{2+} homeostasis: mechanism, role, and tissue specificities. *Pflugers Arch.* **464,** 3–17
7. Kirichok, Y., Krapivinsky, G., and Clapham, D. E. (2004) The mitochondrial calcium uniporter is a highly selective ion channel. *Nature* **427,** 360–364
8. Ryan, T., Sharma, P., Ignatchenko, A., MacLennan, D. H., Kislinger, T., and Gramolini, A. O. (2011) Identification of Novel Ryanodine Receptor 1 (RyR1) Protein Interaction with calcium homeostasis endoplasmic reticulum protein (CHERP). *J. Biol. Chem.* **286,** 17060–17068
9. Jean-Quartier, C., Bondarenko, A. I., Alam, M. R., Trenker, M., Waldeck-Weiermair, M., Malli, R., and Graier, W. F. (2012) Studying mitochondrial Ca^{2+} uptake - A revisit. *Mol. Cell. Endocrinol.* **353,** 114–127
10. Bondarenko, A. I., Jean-Quartier, C., Malli, R., and Graier, W. F. (2013) Characterization of distinct single-channel properties of Ca^{2+} inward currents in mitochondria. *Pflugers Arch.* 2013 (in press) DOI: 10.1007/s00424-013-1224-1
11. Ryu, S. Y., Beutner, G., Dirksen, R. T., Kinnally, K. W., and Sheu, S. S. (2010) Mitochondrial ryanodine receptors and other mitochondrial Ca^{2+} permeable channels. *FEBS Lett.* **584,** 1948–1955
12. Baughman, J. M., Perocchi, F., Girgis, H. S., Plovanich, M., Belcher-Timme, C. A., Sancak, Y., Bao, X. R., Strittmatter, L., Goldberger, O., Bogorad, R. L., Koteliansky, V., and Mootha, V. K. (2011) Integrative genomics identifies MCU as an essential component of the mitochondrial calcium uniporter. *Nature* **476,** 341–345
13. De Stefani, D., Raffaello, A., Teardo, E., Szabò, I., and Rizzuto, R. (2011) A forty-kilodalton protein of the inner membrane is the mitochondrial calcium uniporter. *Nature* **476,** 336–340
14. Nowikovsky, K., Froschauer, E. M., Zsurka, G., Samaj, J., Reipert, S., Kolisek, M., Wiesenberger, G., and Schweyen, R. J. (2004) The LETM1/YOL027 gene family encodes a factor of the mitochondrial K^+ homeostasis with a potential role in the Wolf-Hirschhorn syndrome. *J. Biol. Chem.* **279,** 30307–30315
15. Jiang, D., Zhao, L., and Clapham, D. E. (2009) Genome-wide RNAi screen identifies Letm1 as a mitochondrial Ca^{2+}/H^+ antiporter. *Science* **326,** 144–147
16. Waldeck-Weiermair, M., Jean-Quartier, C., Rost, R., Khan, M. J., Vishnu, N., Bondarenko, A. I., Imamura, H., Malli, R., and Graier, W. F. (2011) The leucine zipper EF hand-containing transmembrane protein 1 (LETM1) and uncoupling proteins-2 and -3 (UCP2/3) contribute to two distinct mitochondrial Ca^{2+} uptake pathways. *J. Biol. Chem.* **286,** 28444–28455
17. Trenker, M., Malli, R., Fertschai, I., Levak-Frank, S., and Graier, W. F. (2007) Uncoupling proteins 2 and 3 are fundamental for mitochondrial Ca^{2+} uniport. *Nat. Cell Biol.* **9,** 445–452
18. Waldeck-Weiermair, M., Malli, R., Naghdi, S., Trenker, M., Kahn, M. J., and Graier, W. F. (2010) The contribution of UCP2 and UCP3 to mitochondrial Ca^{2+} uptake is differentially determined by the source of supplied Ca^{2+}. *Cell Calcium* **47,** 433–440
19. Waldeck-Weiermair, M., Duan, X., Naghdi, S., Khan, M. J., Trenker, M., Malli, R., and Graier, W. F. (2010) Uncoupling protein 3 adjusts mitochondrial Ca^{2+} uptake to high and low Ca^{2+} signals. *Cell Calcium* **48,** 288–301
20. Szanda, G., Koncz, P., Várnai, P., and Spät, A. (2006) Mitochondrial Ca^{2+} uptake with and without the formation of high-Ca^{2+} microdomains. *Cell Calcium* **40,** 527–537
21. Malli, R., and Graier, W. F. (2010) Mitochondrial Ca^{2+} channels: Great unknowns with important functions. *FEBS Lett.* **584,** 1942–1947
22. De Marchi, U., Castelbou, C., and Demaurex, N. (2011) Uncoupling protein 3 (UCP3) modulates the activity of Sarco/endoplasmic reticulum Ca^{2+}-ATPase (SERCA) by decreasing mitochondrial ATP production. *J. Biol. Chem.* **286,** 32533–32541
23. Trenker, M., Fertschai, I., Malli, R., and Graier, W. F. (2008) UCP2/3-likely to be fundamental for mitochondrial Ca^{2+} uniport. *Nat. Cell Biol.* **10,** 1237–1240
24. Waldeck-Weiermair, M., Alam, M. R., Khan, M. J., Deak, A. T., Vishnu, N., Karsten, F., Imamura, H., Graier, W. F., and Malli, R. (2012) Spatiotemporal Correlations between Cytosolic and Mitochondrial Ca^{2+} Signals Using a Novel Red-Shifted Mitochondrial Targeted Cameleon. *PLoS ONE* **7,** e45917
25. Alam, M. R., Groschner, L. N., Parichatikanond, W., Kuo, L., Bondarenko, A. I., Rost, R., Waldeck-Weiermair, M., Malli, R., and Graier, W. F. (2012) Mitochondrial Ca^{2+} Uptake 1 (MICU1) and Mitochondrial Ca^{2+} Uniporter (MCU) Contribute to Metabolism-Secretion Coupling in Clonal Pancreatic β-Cells. *J. Biol. Chem.* **287,** 34445–34454
26. Giacomello, M., Drago, I., Bortolozzi, M., Scorzeto, M., Gianelle, A., Pizzo, P., and Pozzan, T. (2010) Ca^{2+} hot spots on the mitochondrial surface are generated by Ca^{2+} mobilization from stores, but not by activation of store-operated Ca^{2+} channels. *Mol. Cell* **38,** 280–290
27. Carafoli, E., and Brini, M. (2000) Calcium pumps: structural basis for and mechanism of calcium transmembrane transport. *Curr. Opin Chem. Biol.* **4,** 152–161
28. Brini, M., Bano, D., Manni, S., Rizzuto, R., and Carafoli, E. (2000) Effects of PMCA and SERCA pump overexpression on the kinetics of cell Ca^{2+} signalling. *EMBO J.* **19,** 4926–4935
29. Camello, C., Lomax, R., Petersen, O. H., and Tepikin, A. V. (2002) Calcium leak from intracellular stores-the enigma of calcium signalling. *Cell Calcium* **32,** 355–361
30. Bakowski, D., and Parekh, A. B. (2001) Sarcoplasmic/endoplasmic-reticulum-Ca^{2+}-ATPase-mediated Ca^{2+} reuptake, and not $Ins(1,4,5)P_3$ receptor inactivation, prevents the activation of macroscopic Ca^{2+} release-activated Ca^{2+} current in the presence of physiological Ca^{2+} buffer in rat basophilic leukaemia-1 cells. *Biochem. J.* **353,** 561–567
31. Csordás, G., and Hajnóczky, G. (2001) Sorting of calcium signals at the junctions of endoplasmic reticulum and mitochondria. *Cell Calcium* **29,** 249–262
32. Spät, A., Fülöp, L., Koncz, P., and Szanda, G. (2009) When is high-Ca^{2+} microdomain required for mitochondrial Ca^{2+} uptake? *Acta Physiol.* **195,** 139–147
33. Spät, A., Szanda, G., Csordás, G., and Hajnóczky, G. (2008) High- and low-calcium-dependent mechanisms of mitochondrial calcium signalling. *Cell Calcium* **44,** 51–63
34. Spät, A. (2006) Calcium microdomains and the fine control of cell function: an introduction. *Cell Calcium* **40,** 403–404
35. Csordás, G., Várnai, P., Golenár, T., Roy, S., Purkins, G., Schneider, T. G., Balla, T., and Hajnóczky, G. (2010) Imaging interorganelle contacts and local calcium dynamics at the ER-mitochondrial interface. *Mol. Cell* **39,** 121–132
36. Grynkiewicz, G., Poenie, M., and Tsien, R. Y. (1985) A new generation of Ca^{2+} indicators with greatly improved fluorescence properties. *J. Biol. Chem.* **260,** 3440–3450
37. Chami, M., Oulès, B., Szabadkai, G., Tacine, R., Rizzuto, R., and Paterlini-Bréchot, P. (2008) Role of SERCA1 truncated isoform in the proapoptotic calcium transfer from ER to mitochondria during ER stress. *Mol. Cell* **32,** 641–651
38. Kornmann, B., and Walter, P. (2010) ERMES-mediated ER-mitochondria contacts: molecular hubs for the regulation of mitochondrial biology. *J. Cell Sci.* **123,** 1389–1393
39. Merkwirth, C., and Langer, T. (2008) Mitofusin 2 builds a bridge between ER and mitochondria. *Cell* **135,** 1165–1167
40. de Brito, O. M., and Scorrano, L. (2008) Mitofusin 2 tethers endoplasmic reticulum to mitochondria. *Nature* **456,** 605–610
41. Csordás, G., Thomas, A. P., and Hajnóczky, G. (1999) Quasi-synaptic calcium signal transmission between endoplasmic reticulum and mitochondria. *EMBO J.* **18,** 96–108
42. Csordás, G., Renken, C., Várnai, P., Walter, L., Weaver, D., Buttle, K. F., Balla, T., Mannella, C. A., and Hajnóczky, G. (2006) Structural and functional features and significance of the physical linkage between ER and mitochondria. *J. Cell Biol.* **174,** 915–921
43. Santo-Domingo, J., and Demaurex, N. (2010) Calcium uptake mechanisms of mitochondria. *Biochim. Biophys. Acta* **1797,** 907–912
44. Pan, S., Ryu, S. Y., and Sheu, S.-S. (2011) Distinctive characteristics and functions of multiple mitochondrial Ca^{2+} influx mechanisms. *Sci. China Life Sci.* **54,** 763–769

45. Bernardi, P. (1999) Mitochondrial transport of cations: channels, exchangers, and permeability transition. *Physiol. Rev.* **79,** 1127–1155
46. Azzolin, L., Basso, E., Argenton, F., and Bernardi, P. (2010) Mitochondrial Ca^{2+} transport and permeability transition in zebrafish (*Danio rerio*). *Biochim. Biophys. Acta* **1797,** 1775–1779
47. Raffaello, A., De Stefani, D., and Rizzuto, R. (2012) The mitochondrial Ca^{2+} uniporter. *Cell Calcium* **52,** 16–21
48. Poburko, D., Potter, K., van Breemen, E., Fameli, N., Liao, C.-H., Basset, O., Ruegg, U. T., and van Breemen, C. (2006) Mitochondria buffer NCX-mediated Ca^{2+}-entry and limit its diffusion into vascular smooth muscle cells. *Cell Calcium* **40,** 359–371
49. Rizzuto, R., Bastianutto, C., Brini, M., Murgia, M., and Pozzan, T. (1994) Mitochondrial Ca^{2+} homeostasis in intact cells. *J. Cell Biol.* **126,** 1183–1194
50. Marchi, S., Lupini, L., Patergnani, S., Rimessi, A., Missiroli, S., Bonora, M., Bononi, A., Corrà, F., Giorgi, C., De Marchi, E., Poletti, F., Gafà, R., Lanza, G., Negrini, M., Rizzuto, R., and Pinton, P. (2013) Downregulation of the Mitochondrial Calcium Uniporter by Cancer-Related miR-25. *Current Biology*, **23,** 58–63
51. Perocchi, F., Gohil, V. M., Girgis, H. S., Bao, X. R., McCombs, J. E., Palmer, A. E., and Mootha, V. K. (2010) MICU1 encodes a mitochondrial EF hand protein required for Ca^{2+} uptake. *Nature* **467,** 291–296
52. Mallilankaraman, K., Doonan, P., Cárdenas, C., Chandramoorthy, H. C., Müller, M., Miller, R., Hoffman, N. E., Gandhirajan, R. K., Molgó, J., Birnbaum, M. J., Rothberg, B. S., Mak, D.-O., Foskett, J. K., and Madesh, M. (2012) MICU1 is an essential gatekeeper for MCU-mediated mitochondrial Ca^{2+} uptake that regulates cell survival. *Cell* **151,** 630–644
53. Mallilankaraman, K., Cárdenas, C., Doonan, P. J., Chandramoorthy, H. C., Irrinki, K. M., Golenár, T., Csordás, G., Madireddi, P., Yang, J., Müller, M., Miller, R., Kolesar, J. E., Molgó, J., Kaufman, B., Hajnóczky, G., Foskett, J. K., and Madesh, M. (2012) MCUR1 is an essential component of mitochondrial Ca^{2+} uptake that regulates cellular metabolism. *Nat. Cell Biol.* **14,** 1336–1343
54. Nedergaard, J., and Cannon, B. (2003) The 'novel' "uncoupling" proteins UCP2 and UCP3: what do they really do? Pros and cons for suggested functions. *Exp. Physiol.* **88,** 65–84

Pflugers Arch - Eur J Physiol (2014) 466:1411–1420
DOI 10.1007/s00424-013-1383-0

ION CHANNELS, RECEPTORS AND TRANSPORTERS

Mitochondrial Ca^{2+} uniporter (MCU)-dependent and MCU-independent Ca^{2+} channels coexist in the inner mitochondrial membrane

Alexander I. Bondarenko · Claire Jean-Quartier · Warisara Parichatikanond · Muhammad Rizwan Alam · Markus Waldeck-Weiermair · Roland Malli · Wolfgang F. Graier

Received: 15 July 2013 / Revised: 10 October 2013 / Accepted: 12 October 2013 / Published online: 27 October 2013

Abstract A protein referred to as CCDC109A and then renamed to mitochondrial calcium uniporter (MCU) has recently been shown to accomplish mitochondrial Ca^{2+} uptake in different cell types. In this study, we investigated whole-mitoplast inward cation currents and single Ca^{2+} channel activities in mitoplasts prepared from stable MCU knockdown HeLa cells using the patch-clamp technique. In whole-mitoplast configuration, diminution of MCU considerably reduced inward Ca^{2+} and Na^{+} currents. This was accompanied by a decrease in occurrence of single channel activity of the intermediate conductance mitochondrial Ca^{2+} current (*i*-MCC). However, ablation of MCU yielded a compensatory 2.3-fold elevation in the occurrence of the extra large conductance mitochondrial Ca^{2+} current (*xl*-MCC), while the occurrence of bursting currents (*b*-MCC) remained unaltered. These data reveal *i*-MCC as MCU-dependent current while *xl*-MCC and *b*-MCC seem to be rather MCU-independent, thus, pointing to the engagement of at least two molecularly distinct mitochondrial Ca^{2+} channels.

Keywords Mitochondrial Ca^{2+} channels · Mitochondrial Ca^{2+} uniporter · MCU · Ca^{2+} signaling

Introduction

Ca^{2+} uptake by mitochondria stimulates metabolic processes and can also initiate cell death pathways (for review, see [5, 8]). Accordingly, mitochondrial Ca^{2+} channels represent promising molecular targets for future therapeutic modulation of mitochondria functions. A precise understanding of the molecular mechanisms of mitochondrial Ca^{2+} uptake, molecular structure, and function of mitochondrial Ca^{2+} channels is required. Therefore, identification and electrophysiological characterization of mitochondrial Ca^{2+} channels and especially pinpointing specific channel activity to specific proteins will provide invaluable insight into actual processes that accomplish mitochondrial Ca^{2+} uptake.

Although several proteins have been identified to contribute to mitochondrial Ca^{2+} uptake, such like the mitochondrial Ca^{2+} uptake 1 (MICU1) [18], uncoupling proteins 2 and 3 [22, 23], ryanodine receptors [20, 21], mitochondrial Ca^{2+} uniporter regulator 1 (MCUR1) [14], and the canonical transient receptor potential 3 channel [6], the mitochondrial Ca^{2+} uniporter, MCU, a transmembrane protein in the inner mitochondrial membrane, has been proposed to be dominantly responsible for mitochondrial Ca^{2+} uptake [1, 4]. Recent advancement of the patch-clamp approach using mitoplasts allowed to identify mitochondrial Ca^{2+} uniport as a highly Ca^{2+}-selective ion channel [13] that was dependent on the presence of MCU [3]. Moreover, MCU-established currents were sensitive to ruthenium red, which has been assumed to be a classic feature of the mitochondrial Ca^{2+} uniport. A point mutation in the putative pore domain of MCU decreased the sensitivity of the respective Ca^{2+} current to ruthenium red without changing the current magnitude [3]. However, integral Ca^{2+} currents through whole mitoplasts presented in the study of Chaudhuri et al. do not enable to discriminate between contributions of different single channel conductances [3]. Single channel recordings allowed to characterize more than one ruthenium red-sensitive Ca^{2+} inward current in mitoplasts isolated from cardiac myocytes

A. I. Bondarenko · C. Jean-Quartier · W. Parichatikanond · M. R. Alam · M. Waldeck-Weiermair · R. Malli · W. F. Graier (✉)
Institute of Molecular Biology and Biochemistry, Center of Molecular Medicine, Medical University of Graz, Harrachgasse 21/III, 8010 Graz, Austria
e-mail: wolfgang.graier@medunigraz.at

(mitochondrial Ca^{2+} currents 1 and 2; mCa1, mCa2) [17], mitochondrial ryanodine receptor channel activity [21], endothelial cells [small mitochondrial Ca^{2+} currents, intermediate mitochondrial Ca^{2+} currents (*i*-MCC), and large mitochondrial Ca^{2+} currents (*l*-MCC)] [9], and HeLa cells [*i*-MCC and the extra large mitochondrial Ca^{2+} current (*xl*-MCC)] [2, 9], thus challenging the concept of MCU being the one and only Ca^{2+} channel in the inner mitochondrial membrane. The present study was designed to characterize the impact of MCU knockdown on different Ca^{2+} currents in mitoplasts isolated from HeLa cells by applying electrophysiological recordings in whole-mitoplast and mitoplast-attached configurations. These experiments were complemented with fluorescent mitochondrial Ca^{2+} measurements in the respective wild type and MCU knockdown (MCU-KD) HeLa cells. We show that in divalent-free conditions, Na^+ readily permeates ruthenium red (RuR)-sensitive Ca^{2+} channels and downregulation of MCU protein results in suppression of whole-mitoplast inward Na^+ and Ca^{2+} currents and a decreased occurrence probability of *i*-MCC that was associated with a partial increase in occurrence of the *xl*-MCC [2].

Materials and methods

Design and production of stably MCU knockdown HeLa cells and their corresponding control cells

HeLa MCU-KD and HeLa control cells have been produced upon request and supplied by TeBu-bio® (Tebu-bio SAS, Le Perray-en-Yvelines Cedex, France). HeLa cells with stable MCU knockdown and the respective scrambled control cells were produced by applying the SilenciX® technology (Tebu-bio, www.tebu-bio.com, Le Perray-en-Yvelines, France) using the following 5′-3′shRNA sequence against MCU: GGTGCAA TTTATCTTTATA.

Cell culture and isolation of mitochondria

All cells were grown on DMEM containing 10 % FCS, 50 U/ml penicillin, and 50 μg/ml streptomycin. Mitochondria were freshly isolated as previously described [2]. Mitochondria were prepared from HeLa cells by differential centrifugation. Cells were trypsinized, harvested, and washed with PBS. The cell pellet was suspended in a 200-mM sucrose buffer containing 10 mM Tris-MOPS, 1 mM EGTA and protease inhibitor (1:50, P8340 Sigma, Vienna, Austria) (pH adjusted to 7.4 with TRIS), and homogenized with a glass–Teflon potter (40–50 strokes). Nuclear remnants and cell debris were centrifuged down at 900 g for 10 min. The supernatant was centrifuged at 3,000*g* for 20 min. The mitochondrial pellet was washed and centrifuged down at 7,000*g* for 15 min. All fractions were kept on ice until further utilization.

Preparation of mitoplasts

Isolation and preparation of mitoplasts (mitochondria devoid of outer membrane) from HeLa cells was performed as recently described [2]. Briefly, mitoplast formation was achieved by incubation of isolated mitochondria in hypotonic solution (5 mM HEPES, 5 mM sucrose, 1 mM EGTA, pH adjusted to 7.4 with KOH) for 8 min. Then, hypertonic solution (750 mM KCl, 80 mM HEPES, 1 mM EGTA, pH adjusted to 7.4 with KOH) was added to restore isotonicity.

Mitoplast patch-clamp recordings

Single channel measurements were performed in the mitoplast-attached configuration as previously described [2, 9]. In brief, patch pipettes were pulled from glass capillaries using a Narishige puller (Narishige Co., Ltd., Tokyo, Japan), fire-polished, and had a resistance of 8–12 MΩ. Mitoplasts were bathed in the solution containing (in millimolars): 145 KCl, 1 EGTA, HEPES, and pH adjusted to 7.2 with KOH. For single channel recordings, the pipette solution contained 105 mM $CaCl_2$ and 10 mM HEPES, 10 μM cyclosporin A (Tocris Bioscience, Bristol, UK) and 10 μM 7-chloro-5-(2-chlorophenyl)-1,5-dihydro-4,1-benzothiazepin-2(3*H*)-one (CGP 37157, Ascent Scientific Ltd., Bristol, UK) to prevent opening of the permeability transition pore, and the activity of the mitochondrial Na^+/Ca^{2+} exchanger (NCX_{mito}), respectively. pH was adjusted to 7.2 with $Ca(OH)_2$. Single channel currents were recorded at a fixed holding potential indicated in the respective figures. For whole-mitoplast recordings, pipette solution contained (in millimolars): 120 Cs methanesulfonate, 30 CsCl, 1 EGTA, 110 sucrose, 2 gluconic acid, and pH by TEAOH to 7.2. For obtaining whole-mitoplast configuration, voltage steps of 300–600 mV and 20–50 ms duration were applied. Voltage ramps of 1 s duration from −160 to +50 mV were delivered every 5 or 10 s from the holding potential 0 mV. Currents were recorded using a patch-clamp amplifier (EPC7, List Electronics, Darmstadt, Germany). Data collection was performed using Clampex software of pClamp (V9.0, Molecular Devices, Sunnyvale, CA, USA). Signals obtained were low pass filtered at 1 kHz using an eight-pole Bessel filter (Frequency Devices) and digitized with a sample rate of 10 kHz using a Digidata 1200A A/D converter (Molecular Devices, Sunnyvale, CA, USA). All measurements were performed at room temperature. For recording cationic currents via whole mitoplasts, bath solution contained (in millimolars): 150 TRIS HCl, 1 EGTA, 1 EDTA, 10 HEPES with pH 7.2. For I_{Na} recording, NaCl was substituted for TRIS HCl. Ca^{2+}-containing bath solution for I_{Ca} recording

contained (in millimolars): 140 TRIS HCl, 3 $CaCl_2$, 10 HEPES, and pH 7.2

Single cell Ca^{2+} imaging and data acquisition

Imaging mitochondrial targeted cameleon 4mtD3cpv was performed on a digital wide field imaging system, the Till iMIC (Till Photonics Graefelfing, Germany) using a 40× objective (alpha Plan Fluar 40×, Zeiss, Göttingen, Germany). For illumination of the cameleon, an ultrafast switching monochromator, the Polychrome V (Till Photonics), was used for excitation light at 430 nm. Emission light was collected at 480 and 535 nm using a single beam splitter design (Dichrotome, Till Photonics). Images were recorded with a charged-coupled device camera (AVT Stringray F145B, Allied Vision Technologies, Stadtroda, Germany). For the data acquisition and the control of the digital fluorescence microscope, the live acquisition software version 2.0.0.12 (Till Photonics) was used. Experiments were performed at the same day than the isolation, purification, and electrophysiological measurements of the respective mitoplasts.

Experimental buffers for Ca^{2+} measurements

Ca^{2+} measurements in HeLa cells were performed by stimulating cells in Ca^{2+}-containing environment. Cells were superfused by a Ca^{2+}-containing buffer, which was composed of (in millimolars): 138 NaCl, 5 KCl, 2 CaCl2, 1 MgCl2, 10 D-glucose and 10 HEPES, and pH adjusted to 7.4 with NaOH. Stimulation was performed using 100 μM of the IP_3-generating agonist histamine.

Western blot

HeLa cells that were washed with ice-cold PBS or isolated mitochondria were lysed with RIPA buffer containing protease inhibitor cocktail (Sigma-Aldrich, Vienna, Austria). The protein concentration was measured using the BCA protein assay (Thermo Fisher Scientific Inc., Vienna, Austria). Forty micrograms of protein were separated by SDS-PAGE and transferred to a nitrocellulose membrane. The membrane was incubated with the primary antibody at 4 °C overnight and the primary antigen–antibody complex was detected by incubating the blot with a horseradish peroxidase-conjugated secondary antibody at room temperature for 2 h. The membrane was further developed with the ECL Plus Western blotting detection system (GE Healthcare, Vienna, Austria). To control the equal amount of protein loading of whole cell lysates and isolated mitochondria, MCU expression (sc-246071; Santa Cruz, Vienna, Austria) were densitometrically normalized to β-actin (sc-47778; Santa Cruz) and VDAC (sc-32063 and sc-32059; Santa Cruz), respectively.

Real-time PCR

RNA was isolated from HeLa cells using a Total RNA isolation kit (PEQLAB Biotechnologie GmbH, Erlangen, Germany), and it was reverse transcribed using a High Capacity cDNA Reverse Transcription Kit (Applied Biosystems, USA). The analysis of the expression of the target genes was performed by conventional polymerase chain reaction (PCR) using GoTaq Green master mix (Promega, Madison, WI, USA) and real-time PCR using QuantiFast SYBR Green RT-PCR kit (Qiagen, Hilden, Germany) on LightCycler 480 (Roche Diagnostics, Vienna, Austria). RNA polymerase II (RPOL2) was used as a housekeeping control [12, 16, 24]. Primers for RPOL2 and MCU were obtained from Invitrogen (Vienna, Austria) and their sequences (5′–3′) were as follows: RPOL2: CATTGACTTGCGTTTCCACC, RPOL2 rev: ACATTTTGTGCAGAGTTGGC, MCU: TTCCTGGCAGAATTTGGGAG, and MCU rev: AGAGATAGGCTTGAGTGTGAAC.

Statistical analysis

The occurrence probability was calculated as a fraction of patches displayed specific channel activity relative either to the total number of patches studied or the number of active patches displayed any type of the channel activity. Single channel analysis was performed using Clampfit 9.2 (Molecular Devices, Sunnyvale, CA, USA). Data are expressed as means with standard error. Statistical comparisons were conducted with a two-tailed unpaired *t* test. Values of $p<0.05$ (*) were taken as statistically significant. Statistical analysis was performed by Graph Pad Software version 5.01 (La Jolla, CA, USA).

Results

Stably knockdown of MCU strongly reduced mitochondrial Ca^{2+} sequestration in intact HeLa cells

Diminution in MCU gene expression by stably expression of the respective shRNA in HeLa cells (MCU-KD cells) was confirmed by quantitative real-time PCR. In MCU-KD cells, the level of MCU mRNA expression was significantly depressed and amounted 36±10 % ($n=3$, $p<0.005$) of the level detected in control cells (Fig.1a). Hence, Western blot analysis revealed that the cellular MCU protein content was attenuated to 33±6 % ($n=2$, $p<0.08$) of the level detected in control cells (Fig.1b). In line with these findings, in MCU-KD cells, histamine-induced mitochondrial Ca^{2+} elevation was reduced to 19 % of the level attained in control cells (Fig.1c, d).

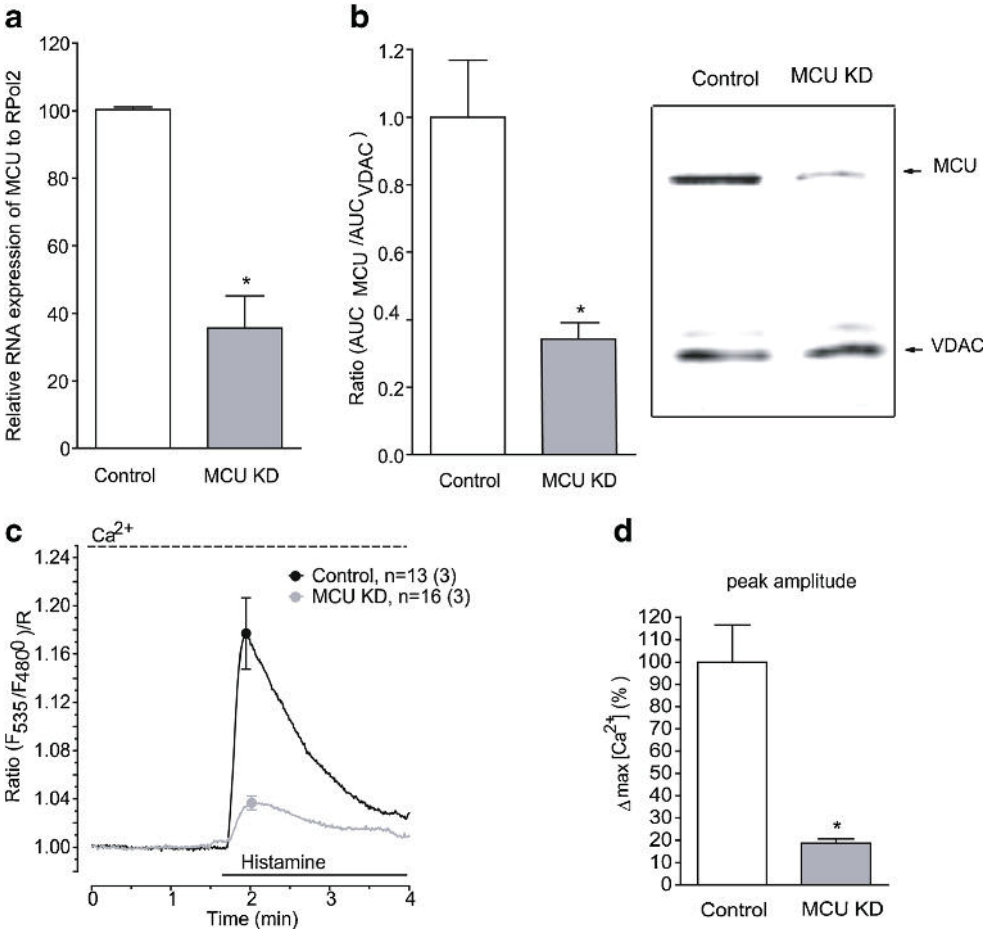

Fig. 1 MCU knockdown impairs intramitochondrial Ca^{2+} rise during cell stimulation. **a** Relative RNA expression of control and MCU-KD cells, **b** MCU protein expression in control and MCU-KD cells. Representative bands for MCU and VDAC protein expression. **c** Averaged traces of mitochondrial Ca^{2+} signals upon stimulation with 100 μM histamine of intact control HeLa cell (*black trace*, $n=13$ cells from three coverslips) and MCU-KD HeLa cells (*gray trace*, $n=16$ cells from three coverslips). Mitochondrial Ca^{2+} signals were measured using cells expressing 4mtD3cpv. **d** Quantitative expression of intramitochondrial Ca^{2+} rise during cell stimulation with 100 μM histamine in MCU-KD cells relative to the rise in control cells

Knockdown of MCU strongly reduced whole-mitoplast Ca^{+} currents

In whole-mitoplast configuration, switching from Ca^{2+}-free to Ca^{2+}-containing (3 mM) solution during voltage ramps from −160 to +50 mV resulted in an inward current at negative potentials (Fig.2a) that was sensitive to RuR (Fig.2b, c). In mitochondria isolated from MCU-KD cells, the current elicited by Ca^{2+} addition was strongly reduced (Fig.2d) to 17 % of the level attained in control cells, while it remained sensitive to RuR (Fig.2e, f). In control group, at −155 mV, the Ca^{2+} current amplitude averaged −251.4±55.8 pA ($n=11$), while in mitoplasts isolated from MCU-KD cells, the current averaged −43.5±18.4 pA ($n=5$) (Fig.2g). These results are very similar to that published very recently by the group of Clapham [3] and demonstrate that diminution of MCU results in a pronounced suppression of RuR-sensitive transmitochondrial inward I_{Ca} accompanied by potent reduction of intramitochondrial Ca^{2+} rise in intact cells exposed to supramaximal concentrations of histamine (Fig.1c).

Diminution of MCU strongly reduced whole-mitoplast Na^{+} currents in the absence of Ca^{2+}

In whole-mitoplast configuration, switching from Na^{+}-free to Na^{+}-containing divalent-free solution resulted in a development of a pronounced inward current at negative potentials (Fig.3a). The current amplitude was a function of the applied membrane voltage. A mean current amplitude at −155 mV averaged 706±142 pA ($n=8$). The current rapidly terminated upon removal of bath Na^{+} and was inhibited by 10 μM RuR (Fig.3a–c). These observations indicate that in the absence of Ca^{2+}, external Na^{+} readily permeates the RuR-sensitive channel(s), and the amplitude of transmitochondrial Na^{+} current (I_{Na}) is higher than that generated by Ca^{2+} influx, an observation that is in line with previous studies [7, 13].

Stable knockdown of MCU resulted in a marked suppression of whole-mitoplast inward Na^{+} current (I_{Na}) elicited by voltage ramps to 170.4±21.0 pA ($n=8$) that equals a reduction by 76 % (Fig.3d–g). These results demonstrate that MCU downregulation results in a pronounced suppression of transmitochondrial inward RuR-sensitive I_{Na}.

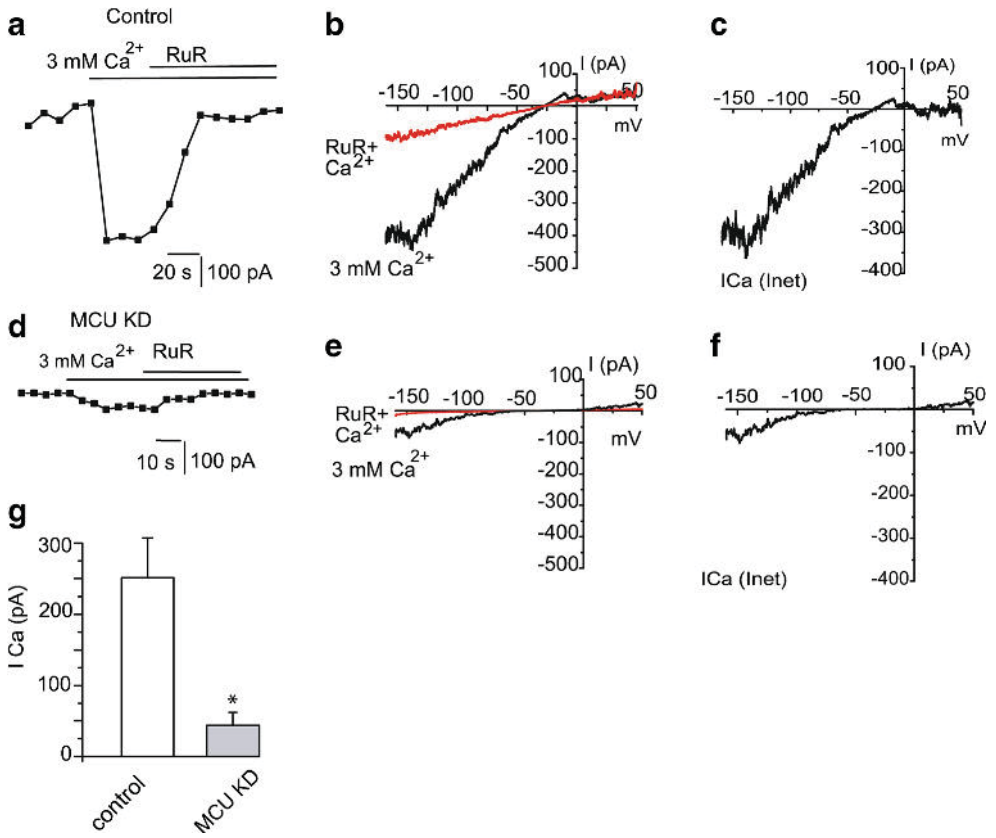

Fig. 2 MCU knockdown suppresses whole-mitoplast Ca^{2+} current. **a** Exemplary time course of the whole-mitoplast current at −155 mV before and after addition of 3 mM Ca^{2+} followed by addition of 10 μM RuR ($n=4$). Recording from mitoplast isolated from control cells. Voltage ramps were applied every 10 s. **b** Corresponding Ca^{2+} current responses to voltage ramps before and after addition of 10 μM RuR in the presence of 3 mM Ca^{2}. **c** Net I_{Ca} obtained after subtraction of RuR-insensitive current. **d** Representative time course of whole-mitoplast currents at −155 mV induced by addition of 3 mM Ca^{2+} to the bath followed by addition of 10 μM RuR. Recoding from mitoplast isolated from MCU-KD cells. Voltage ramps were applied every 5 s. **e** Corresponding Ca^{2+} current responses to voltage ramps before and after addition of 10 μM RuR in the presence of 3 mM Ca^{2+} ($n=3$). **f** Net I_{Ca} obtained after subtraction of RuR-insensitive current. **g** Mean amplitudes of mitochondrial C_a from control ($n=11$) and MCU-KD ($n=5$) mitoplasts

Stable knockdown of MCU reduces the occurrence of active single channels per patch

We next characterized the probability of occurrence of any single channel activities of mitochondrial Ca^{2+} channels in the mitoplast-attached configuration [2] under conditions of MCU knockdown. Among 67 patches tested in mitochondrial from MCU-KD cells, only 35 patches displayed single channel activity, providing 52 % occurrence. In mitoplasts isolated from control cells, single channel activity was detected more frequently in 71 out of 103 patches tested, providing an occurrence probability of 69 %. For statistical processing, we analyzed the occurrence probability of the channel activity for each individual experimental day and calculated the mean values and statistics out of the individual values from all experimental days (N^D). In the control group, the occurrence probability of single channel activities amounted 71±6 % ($N^D=32$), while in MCU-KD group, the occurrence probability of single channel activities was significantly ($p<0.05$) less and averaged 47±8.0 % ($N^D=13$). Similar to mitoplasts from control group, in mitoplasts isolated from MCU-KD cells, we observed all three types of the channel activities described by us earlier [2].

Stable knockdown of MCU reduces the occurrence of *i*-MCC

We next analyzed the proportion of each individual channel activity in the total number of patches tested and to the number of active patches, which would give an indication on the density of individual channel type in the overall population of Ca^{2+} channels.

In mitochondria isolated from control cells, the most predominant channel was the 11 pS channel (intermediate conductance mitoplast Ca^{2+} channel, *i*-MCC) [2]. Exemplary traces of this type of activity in control and MCU-KD mitoplasts occasionally interrupted with bursting activity are depicted in Fig. 4a, b, respectively. Under control conditions, *i*-MCC activity was observed in 43 out of 103 patches tested

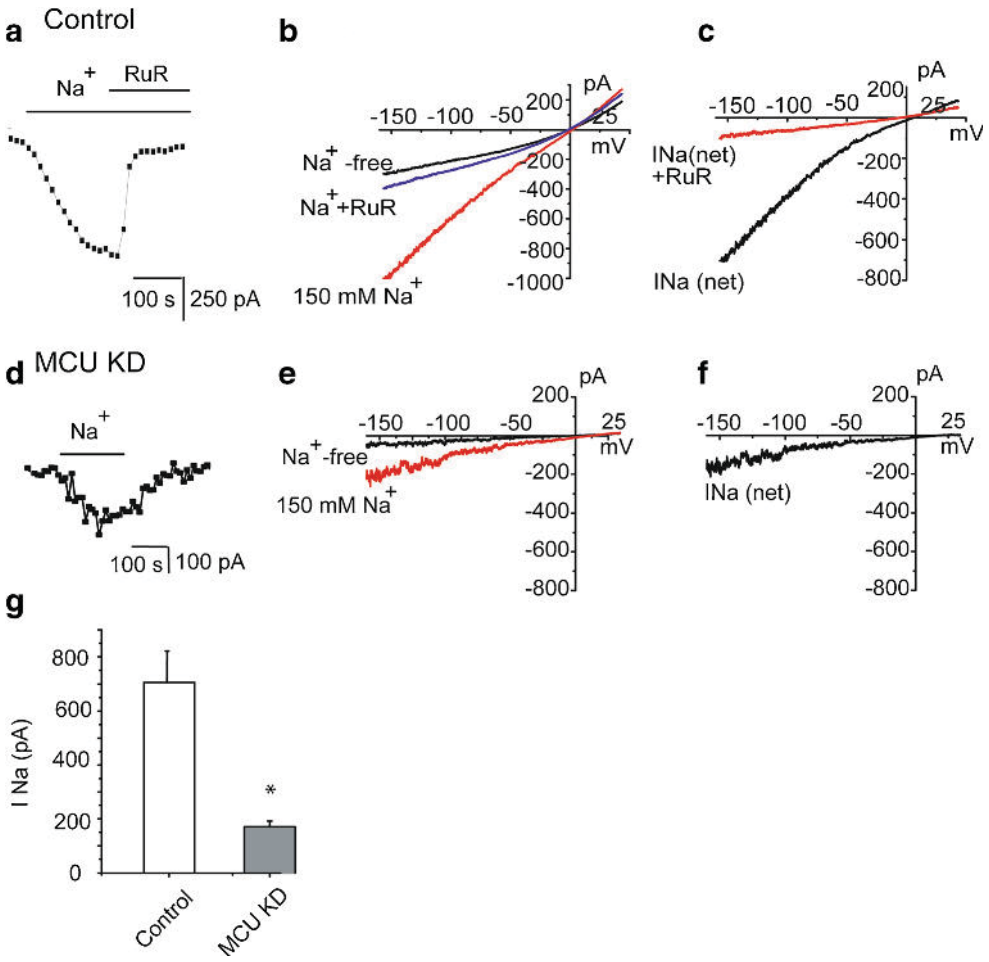

Fig. 3 MCU knockdown suppresses whole-mitoplast Na^+ current. **a** Exemplary time course of the whole-mitoplast current recorded from mitoplast isolated from control cells ($n=8$) at −155 mV. The current was elicited by replacement of bath TRIS for Na^+ in divalent-free conditions and was measured during voltage ramps applied every 10 s. **b** Corresponding current responses to voltage ramps before (Na^+ free) and after addition of 150 mM Na^+ either alone or in the presence of 10 μM RuR. **c** Net $I_{Na(Control)}$ obtained after subtraction of the background current obtained in Na^+ and divalent-free solution. **d** Representative time course of the whole-mitoplast current recorded from the mitoplast isolated from MCU-KD cells ($n=8$) and measured at −155 mV during voltage ramps applied every 10 s before and after replacement of bath TRIS for Na^+ in divalent-free solution ($n=8$). **e** Corresponding current responses to voltage ramps before (Na^+ free) and after application of 150 mM Na^+ to MCU-KD mitoplast. **f** Net $I_{Na\ (MCU-KD)}$ obtained after subtraction of background current. **g** Mean amplitudes of mitochondrial I_{Na} from control and MCU-KD groups

(occurrence probability 42±7 %, $N^D=29$) (Fig.4c) and its individual contribution to active channels ($n=71$) was 61±8 % (Fig.4d). In mitochondria from MCU-KD cells, the occurrence probability of this channel was strongly reduced compared to controls: the *i*-MCC channel activity was detected in 11 out of 67 patches tested (occurrence probability 14±6 %, $N^D=11$) (Fig.4c) and its individual contribution to active channels ($n=35$) was 28±12 % (Fig.4d). In MCU-KD group, the *i*-MCC conductance (11.5±0.5 pS, $n=6$) was not different from that observed in mitoplasts isolated from control cells (11.9±0.6 pS, $n=15$). Gating characteristics of *i*-MCC were slightly affected by MCU knockdown and revealed a tendency for reduced open probability (NPo) and mean open time (To_{mean}) while mean closed time (Tc_{mean}) was prolonged (Table 1).

Stable knockdown of MCU had no effect on the occurrence of the *b*-MCC

Similar to mitoplasts isolated from control cells (Fig.5a), the second type of the channel activity studied in mitoplasts isolated from MCU-KD cells was the bursting activity (Fig.5b). According to our previous reports, we refer to this channel as bursting mitochondrial Ca^{2+} channel (*b*-MCC) [2]. Neither occurrence nor conductance of *b*-MCC was altered in mitochondria isolated from MCU-KD cells. In control cells, this channel was observed in 23 out of 103 patches tested. The probability of occurrence of this channel activity was 25±6 % ($N^D=32$) in control group and 23±9 % ($N^D=13$) in the MCU-KD group in respect to all patches tested (Fig.5c). Within mitoplasts from MCU-KD cells, the *b*-MCC activity was

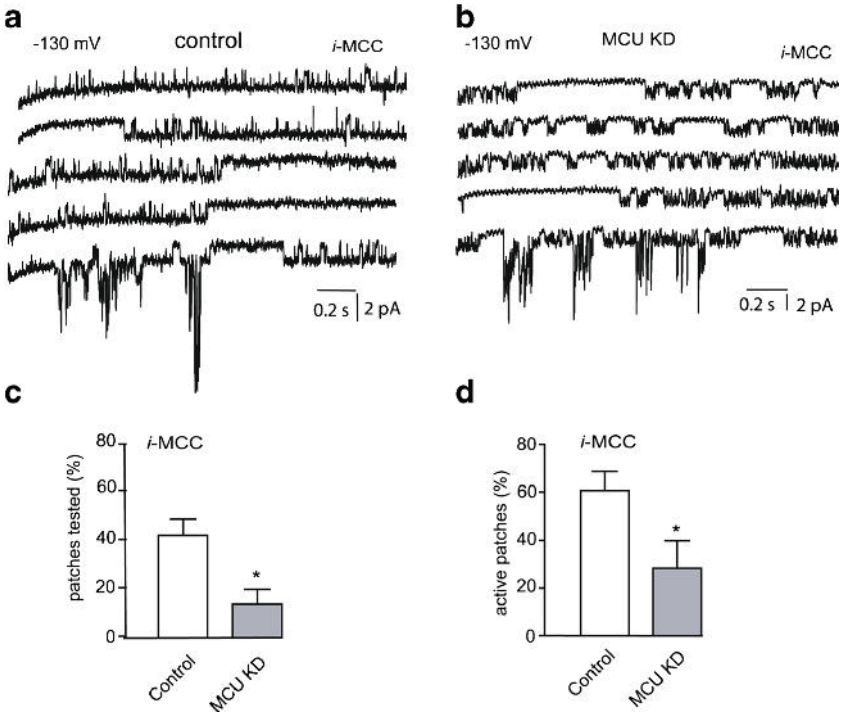

Fig. 4 The occurrence probability of *i*-MCC channel is largely decreased in the inner mitochondria membrane from MCU-KD HeLa cells. **a** Representative single channel recording of *i*-MCC activity interrupted with *b*-MCC at a holding voltage of −130 mV in mitoplast isolated from control cells. **b** Representative recording of *i*-MCC interrupted with *b*-MCC at a holding voltage of −130 mV in mitoplast isolated from MCU-KD cells. **c** *Bars* represent the occurrence of *i*-MCC activity in mitoplasts from control and MCU-KD HeLa cells in respect to the total number of patches tested. **d** The same as in **c** but in respect to the number of active patches with any MCC activity

detected in 16 out of 67 patches tested (35 active patches) and the occurrence probability in respect to active patches was slightly higher (45±13 %, N^D=11) compared to the control group (33±7 %, N^D=29) (Fig.5d). In mitoplasts isolated from control cells, mean conductance of *b*-MCC channel was 25.7±1.3 pS (n=8), and in MCU-KD mitoplasts, the channel conductance was unaltered and averaged 26.0±1.8 pS (n=9) (Table 1).

Stable knockdown of MCU increased the occurrence of the *xl*-MCC

Both in control (Fig.6a) and MCU-KD group (Fig.6b), we also identified a third type of activity that we define as *xl*-MCC [2, 9]. In the control HeLa cells, *xl*-MCC conductance was 74.8±7.9 pS (n=8), thus, comparable to that previously reported [2]. Diminution of MCU did not affect significantly (p>0.05) *xl*-MCC conductance 70.7±5.9 pS (n=6) (Table 1). Remarkably, in the control group, this type of activity was the least frequent and was observed in 8 out of 103 patches tested, while in MCU-KD mitoplasts, this type of channel activity was observed in 10 out of 67 patches tested. The occurrence probability of this channel in respect to all patches studied was 6±2 % (N^D=32) in the control group and 13±5 % (N^D=13) in MCU-KD group, indicating a 2.3-fold increase in the occurrence probability of *xl*-MCC in MCU-KD mitoplasts (Fig.6c). When compared with respect to the number of active patches, the occurrence probability of *xl*-MCC in the MCU-KD group showed 4.3-fold increase from 9±4 % (N^D=29) in the controls to 38±14 % (N^D=11) in the MCU-KD group (Fig.6d). Gating characteristics of *xl*-MCC were also affected by MCU knockdown and revealed a significant reduction in NPo, To_{mean}, while Tc_{mean} was not significantly altered (Table 1).

Table 1 The effect of MCU knockdown on gating characteristics of mitochondrial Ca^{2+} currents (*i*-MCC and *xl*-MCC)

	Conductance (pS)	NPo	To_{mean} (ms)	Tc_{mean} (ms)	n
i-MCC control	11.9±0.5	0.60±0.13	3.4±0.5	14.2±2.1	15
i-MCC MCU-KD	11.5±0.6	0.36±0.05	4.6±0.8	17.3±2.3	6
p value	0.70	0.26	0.17	0.42	
b-MCC control	25.7±1.3	0.39±0.08	2.7±0.4	27.7±4.9	8
b-MCC MCU-KD	26.0±1.8	0.40±0.13	1.6±0.3*	12.5±2.6*	9
p value	0.89	0.98	0.04	0.01	
xl-MCC control	74.8±7.9	0.74±0.08	31.2±5.0	50.0±14.4	6
xl-MCC MCU-KD	70.7±5.9	0.40±0.14*	12.1±1.6*	44.7±16.1	6
p value	0.690	0.002	0.006	0.248	

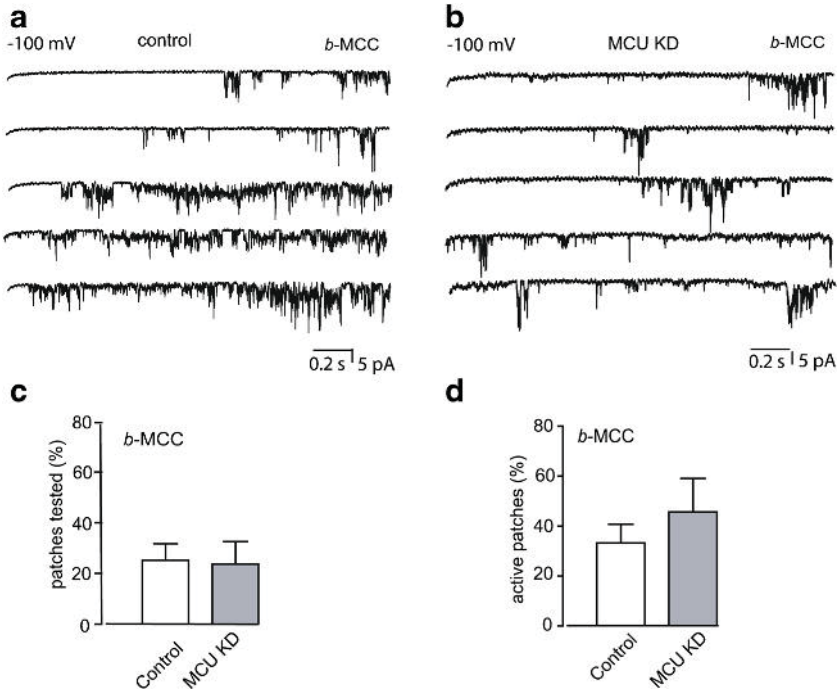

Fig. 5 MCU knockdown does not affect the occurrence probability of *b*-MCC. **a** Representative single channel recording of *b*-MCC activity at a holding voltage −100 mV in mitoplast isolated from control cells. **b** Representative *b*-MCC recording from mitoplast isolated from MCU-KD HeLa cells. **c** *Bars* represent the occurrence of *b*-MCC activity in mitoplasts from control and MCU-KD HeLa cells in respect to the total number of patches. **d** The same as in **c** but in respect to the number of active patches with any MCC activity

Discussion

MCU has recently been identified as the ion-conducting pore in the mitochondrial inner membrane [1, 4]. However, several other studies have pointed for alternative putative channels/carriers for mitochondrial Ca^{2+} influx including mitochondrial ryanodine receptors [20, 21], the Ca^{2+}/H^{+} antiporter leucine zipper EF hand-containing transmembrane protein 1 [10, 11, 25], the uncoupling proteins 2 and 3 [22, 23, 26], and the canonical transient receptor potential 3 channel [6]. Moreover, so far, two regulator proteins for mitochondrial Ca^{2+} uptake, the MICU1 [15, 18] and the MCUR1 [14], have been

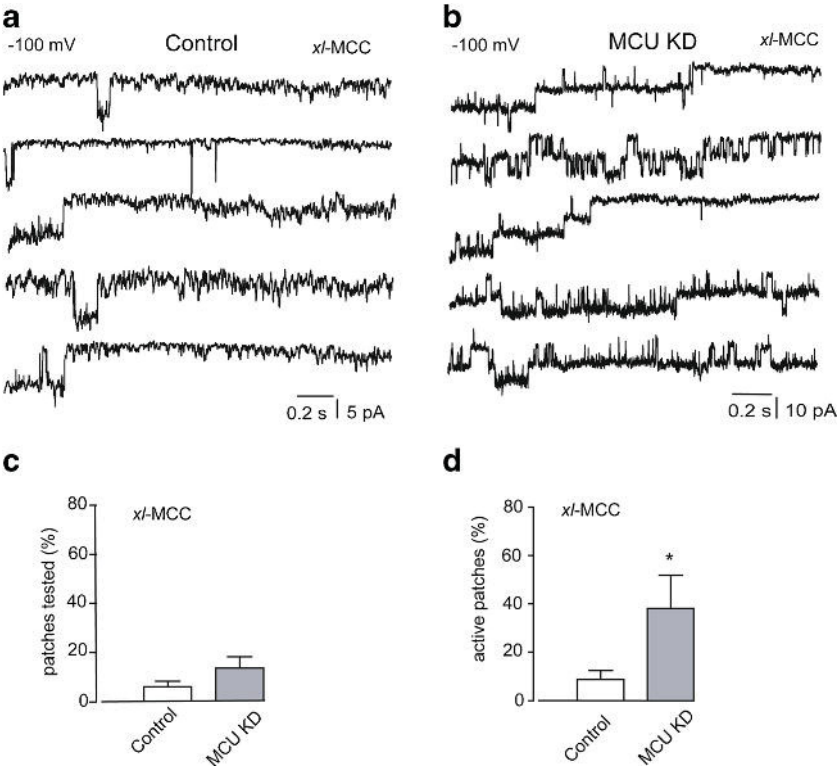

Fig. 6 Effect of MCU knockdown on the occurrence of *xl*-MCC activity. **a** and **b** Representative single channel recording of *xl*-MCC activity at a holding voltage −100 mV in mitoplasts isolated from control (**a**) and MCU-KD cells (**b**). **c** *Bars* represent the occurrence of *xl*-MCC activity in mitoplasts from control and MCU-KD HeLa cells in respect to the total number of patches tested. **d** The same as in (**c**) but in respect to the number of active patches with any MCC activity

described, thus supporting the concept of a multiprotein complex being responsible to establish the mitochondrial Ca^{2+} uniporter phenomenon [8, 19]. While single channel measurements of mitochondrial Ca^{2+} channels in the mitoplast-attached configuration recently confirmed the existence of multiple mitochondrial Ca^{2+} entry pathways [2, 9, 17, 21], the actual proteins that account for the individual channels are unknown. Therefore, in the present study, we explored the effect of MCU knockdown on the occurrence probability of distinct types of single channel activities in the inner mitochondria membrane of HeLa cells and the amplitude of whole-mitoplast inward Ca^{2+} and Na^{+} currents.

In whole-mitoplast configuration, diminution of MCU considerably reduced the inward Ca^{2+} current, an observation similar to that published previously [3]. Applying voltage ramps in divalent-free conditions produced a development of a linear inward current upon switching from Na^{+}-free to Na^{+}-containing solution. The current was sensitive to ruthenium red and had higher amplitude than the current developed when Ca^{2+} was added to the bath in the absence of Na^{+}, indicating that in the absence of Ca^{2+}, the channels permeate Na^{+}, an observation consistent with the previous ones [7, 13]. We used this intrinsic property of mitochondrial Ca^{2+} permeable channel(s) to better discriminate the consequences of MCU silencing on electrical signaling of mitoplasts. Here, we show that MCU knockdown effectively suppresses transmitochondrial currents carried by Ca^{2+} and Na^{+}. The degree of I_{Ca} and I_{Na} suppression upon MCU knockdown corresponded well to the degree of suppression of mitochondrial Ca^{2+} accumulation in intact cells upon histamine exposure. These findings confirm a very recent report that describes a large reduction of ruthenium red-sensitive whole-mitoplast currents of HEK293 cells with RNAi-mediated knockdown of the MCU [3].

In addition to the evaluation on the knockdown of MCU on ruthenium red-sensitive whole-mitoplast currents, we also explored whether MCU knockdown affects the occurrence probability of the individual and distinct single channel activities previously reported in HeLa mitoplast [2]. We found that the occurrence probability of active patches has been largely reduced in MCU-KD mitoplasts, thus supporting the concept of MCU being the main conducting pore of mitochondrial Ca^{2+} currents. However, we found that this reduction is mostly due to reduced occurrence probability of *i*-MCC channel that represents one (i.e., *i*-MCC; app. 14.3 pS) [9] out of three Ca^{2+} currents (*i*-MCC, *b*-MCC, *and xl*-MCC) in mitoplasts isolated from HeLa cells [2]. Although it was shown that purified MCU shows channel activity in lipid bilayers where under symmetrical 100 mM Ca^{2+} conditions the channel conductance was reported to be 6–7 pS [4], one can speculate that in its natural environment and under asymmetrical Ca^{2+} conditions, the MCU conductance may differ, possibly due to the formation of hetero-multimers. This assumption is in line with other reports on native mitoplasts isolated from cardiac myocytes and endothelial cells where two different channels with the conductance of app.13-14 and 7–8 pS have been discriminated under asymmetrical Ca^{2+} conditions [9, 17]. Accordingly, the selective decrease in occurrence probability of *i*-MCC upon MCU knockdown observed in the present study suggests that this type of activity is indicative for the MCU-established current.

The other observation of the present study is that MCU knockdown yielded an increased occurrence probability of *xl*-MCC channel activity in respect to active channels. This observation indicates that *xl*-MCC (app. 74–77 pS) [2, 9] is independent from the presence of MCU protein and mitochondrial Ca^{2+} channels other that MCU play a compensatory role under functional MCU diminution. Notably, our statistical analysis regarding the individual gating characteristics of *i*-MCC and *xl*-MCC revealed a decrease in the mean NPo and To_{mean} of both channels in mitoplasts from MCU-KD cells. However, in view of the rather large variances in these measurements, caution is necessary in the interpretation of these changes. Nevertheless, these data further support the concept of a rather complex mitochondrial Ca^{2+} uptake machinery that might consist from MCU-dependent and MCU-independent pathways that are functionally interrelated to meet the versatile Ca^{2+} demand of the organelle under different conditions of high and low metabolic and ion fluxes.

It is still unclear whether *b*-MCC and *xl*-MCC represent distinct or the same channel protein. However, because of observation that *b*-MCC could turn into *xl*-MCC activity, it is reasonable to suggest that a single channel pore protein accomplishes two distinct activities. Because the pipette solution for single channel recordings in the present study contained CGP37157, an inhibitor of NCX_{mito}, which partially inhibits pH-dependent Ca^{2+} transport (Letm1), and because *xl*-MCC is a channel, mitochondrial Na^{+}/Ca^{2+} exchanger(s) and Letm1 can be excluded from being responsible for *xl*-MCC current. Thus, further studies are needed to identify the molecular player(s) governing the *xl*-MCC activity.

Overall, the present study addressed the role of MCU in transmitochondrial Ca^{2+} fluxes using the direct patch-clamp approach on mitoplasts isolated from HeLa cells with diminished MCU expression and respective controls. Our current study shows that MCU knockdown results in a strong decrease in whole-mitoplast current and the number of active patches with Ca^{2+} channel behavior. Notably, this decrease is exclusively due to a decrease in the number of active recently identified *i*-MCC but not *b*-MCC or *xl*-MCC of which the latter one seems to play a compensatory role under conditions of MCU knockdown. Nevertheless, as gating characteristics for *i*-MCC and *xl*-MCC were affected by diminution of MCU, our findings point to a modulatory interaction between

the two independent Ca^{2+} currents the nature of which awaits to be identified.

Acknowledgments We thank Rene Rost, PhD. for his excellent technical assistance. This work was supported by the Austrian Science Funds (FWF, P20181-B05 P21857-B18 and P22553-B18). C.J.-Q. is a fellow of the Doctoral College "Metabolic and Cardiovascular Disease" funded by the Austrian Science Fund (W1226-B18) and the Medical University of Graz, the University of Graz and the Graz University of Technology. W.P. is supported by the Austrian academic exchange services (ÖAD).

References

1. Baughman JM, Perocchi F, Girgis HS, Plovanich M, Belcher-Timme CA, Sancak Y, Bao XR, Strittmatter L, Goldberger O, Bogorad RL, Koteliansky V, Mootha VK (2011) Integrative genomics identifies MCU as an essential component of the mitochondrial calcium uniporter. Nature 476:341–345
2. Bondarenko AI, Jean-Quartier C, Malli R, Graier WF (2013) Characterization of distinct single-channel properties of Ca^{2+} inward currents in mitochondria. Pflugers Arch 465:997–1010
3. Chaudhuri D, Sancak Y, Mootha VK, Clapham DE (2013) MCU encodes the pore conducting mitochondrial calcium currents. eLife 2: e00704–e00704
4. De Stefani D, Raffaello A, Teardo E, Szabò I, Rizzuto R (2011) A forty-kilodalton protein of the inner membrane is the mitochondrial calcium uniporter. Nature 476:336–340
5. Duchen MR (2000) Mitochondria and Ca^{2+} in cell physiology and pathophysiology. Cell Calcium 28:339–348
6. Feng S, Li H, Tai Y, Huang J, Su Y, Abramowitz J, Zhu MX, Birnbaumer L, Wang Y (2013) Canonical transient receptor potential 3 channels regulate mitochondrial calcium uptake. Proc Natl Acad Sci U S A 110:11011–11016
7. Fieni F, Bae Lee S, Jan YN, Kirichok Y (2012) Activity of the mitochondrial calcium uniporter varies greatly between tissues. Nat Comms 3:1317
8. Graier WF, Frieden M, Malli R (2007) Mitochondria and Ca^{2+} signaling: old guests, new functions. Pflugers Arch 455:375–396
9. Jean-Quartier C, Bondarenko AI, Alam MR, Trenker M, Waldeck-Weiermair M, Malli R, Graier WF (2012) Studying mitochondrial Ca^{2+} uptake—a revisit. Mol Cell Endocrinol 353:114–127
10. Jiang D, Zhao L, Clapham DE (2009) Genome-wide RNAi screen identifies Letm1 as a mitochondrial Ca^{2+}/H^{+} antiporter. Science 326: 144–147
11. Jiang D, Zhao L, Clish CB, Clapham DE (2013) Letm1, the mitochondrial Ca^{2+}/H^{+} antiporter, is essential for normal glucose metabolism and alters brain function in Wolf-Hirschhorn syndrome. Proc Natl Acad Sci U S A 110:E2249–E2254
12. Kim I, Yang D, Tang X, Carroll JL (2011) Reference gene validation for qPCR in rat carotid body during postnatal development. BMC Res Notes 4:440
13. Kirichok Y, Krapivinsky G, Clapham DE (2004) The mitochondrial calcium uniporter is a highly selective ion channel. Nature 427:360–364
14. Mallilankaraman K, Cárdenas C, Doonan PJ, Chandramoorthy HC, Irrinki KM, Golenár T, Csordás G, Madireddi P, Yang J, Müller M, Miller R, Kolesar JE, Molgó J, Kaufman B, Hajnóczky G, Foskett JK, Madesh M (2012) MCUR1 is an essential component of mitochondrial Ca2+ uptake that regulates cellular metabolism. Nat Cell Biol 14:1336–1343
15. Mallilankaraman K, Doonan P, Cárdenas C, Chandramoorthy HC, Müller M, Miller R, Hoffman NE, Gandhirajan RK, Molgó J, Birnbaum MJ, Rothberg BS, Mak D-OD, Foskett JK, Madesh M (2012) MICU1 is an essential gatekeeper for MCU-mediated mitochondrial Ca^{2+} uptake that regulates cell survival. Cell 151: 630–644
16. Mehta R, Birerdinc A, Hossain N, Afendy A, Chandhoke V, Younossi Z, Baranova A (2010) Validation of endogenous reference genes for qRT-PCR analysis of human visceral adipose samples. BMC Mol Biol 11:39
17. Michels G, Khan IF, Endres-Becker J, Rottlaender D, Herzig S, Ruhparwar A, Wahlers T, Hoppe UC (2009) Regulation of the human cardiac mitochondrial Ca^{2+} uptake by 2 different voltage-gated Ca^{2+} channels. Circulation 119:2435–2443
18. Perocchi F, Gohil VM, Girgis HS, Bao XR, McCombs JE, Palmer AE, Mootha VK (2010) MICU1 encodes a mitochondrial EF hand protein required for Ca^{2+} uptake. Nature 467:291–296
19. Pizzo P, Drago I, Filadi R, Pozzan T (2012) Mitochondrial Ca^{2+} homeostasis: mechanism, role, and tissue specificities. Pflugers Arch 464:3–17
20. Ryu SY, Beutner G, Dirksen RT, Kinnally KW, Sheu S-S (2010) Mitochondrial ryanodine receptors and other mitochondrial Ca^{2+} permeable channels. FEBS Lett 584:1948–1955
21. Ryu SY, Beutner G, Kinnally KW, Dirksen RT, Sheu S-S (2011) Single channel characterization of the mitochondrial ryanodine receptor in heart mitoplasts. J Biol Chem 286:21324–21329
22. Trenker M, Fertschai I, Malli R, Graier WF (2008) UCP2/3 - likely to be fundamental for mitochondrial Ca^{2+} uniport. Nat Cell Biol 10: 1237–1240
23. Trenker M, Malli R, Fertschai I, Levak-Frank S, Graier WF (2007) Uncoupling proteins 2 and 3 are fundamental for mitochondrial Ca^{2+} uniport. Nat Cell Biol 9:445–452
24. Waldeck-Weiermair M, Deak AT, Groschner LN, Alam MR, Jean-Quartier C, Malli R, Graier WF (2013) Molecularly distinct routes of mitochondrial Ca^{2+} uptake are activated depending on the activity of the sarco/endoplasmic reticulum Ca^{2+} ATPase (SERCA). J Biol Chem 288:15367–15379
25. Waldeck-Weiermair M, Jean-Quartier C, Rost R, Khan MJ, Vishnu N, Bondarenko AI, Imamura H, Malli R, Graier WF (2011) The leucine zipper EF hand-containing transmembrane protein 1 (LETM1) and uncoupling proteins- 2 and 3 (UCP2/3) contribute to two distinct mitochondrial Ca^{2+} uptake pathways. J Biol Chem 286: 28444–28455
26. Waldeck-Weiermair M, Malli R, Naghdi S, Trenker M, Kahn MJ, Graier WF (2010) The contribution of UCP2 and UCP3 to mitochondrial Ca^{2+} uptake is differentially determined by the source of supplied Ca^{2+}. Cell Calcium 47:433–440